

HOPPING CONDUCTIVITY AND CHARGE TRANSPORT IN
LOW DENSITY POLYETHYLENE

by

Jerilyn Brunson

A dissertation submitted in partial fulfillment
of the requirements for the degree

of

DOCTOR OF PHILOSOPHY

in

Physics

Approved:

John R. Dennison
Major Professor

D. Mark Riffe
Committee Member

David Peak
Committee Member

Bela G. Fejer
Committee Member

Stephen Bialkowski
Committee Member

Byron R. Burnham
Dean of Graduate Studies

UTAH STATE UNIVERSITY
Logan, Utah

2010

Copyright © Jerilyn Brunson 2010

All Rights Reserved

ABSTRACT

Hopping Conductivity and Charge Transport
in Low Density Polyethylene

by

Jerilyn Brunson, Doctor of Philosophy

Utah State University, 2010

Major Professor: Dr. John R. Dennison
Department: Physics

The properties and behaviors of charge transport mechanisms in highly insulating polymers are investigated by measuring conduction currents through thin film samples of low density polyethylene (LDPE). Measurements were obtained using a constant voltage method with copper electrodes inside a chamber adapted for measurements under vacuum and over a wide range of temperatures and applied fields. Field-dependent behaviors, including Poole-Frenkel conduction, space charge limited current (SCLC), and Schottky charge injection, were investigated at constant temperature. These field-dependent mechanisms were found to predict incorrect values of the dielectric constant and the field dependence of conductivity in LDPE was not found to be in agreement with SCLC predicted behavior. A model of thermally assisted hopping was a good fit at low applied fields and produced activation energies within the accepted range for LDPE. Low applied field measurements over the range of 213 K to 338 K were used to investigate two prominent hopping conduction mechanisms: thermally assisted hopping and variable range hopping. The observed temperature dependence of LDPE was found to be consistent with both thermally assisted hopping and variable range hopping. Activation energies determined for the range of temperatures were consistent with values reported in the literature for

LDPE under similar conditions. A third aspect of charge transport behavior is a bulk response with time dependence. Conductivity behavior is examined in relation to transient current behavior, long time decay currents, and electrostatic discharge. Comparing charging and discharging cycles allowed qualitative separation of polarization and multiple trapping behaviors.

(217 pages)

DEDICATION

In loving memory of my grandfather, Austin Loveless.

ACKNOWLEDGMENTS

I am grateful to the Seeley-Hinckley Scholarship Foundation and the Rocky Mountain Space Grant Consortium for their generous fellowship and support throughout my graduate work. I am indebted to my advisor, J. R. Dennison, for his patience and encouragement throughout my research, even when it seemed impossible. Particular thanks must go to Ryan Hoffmann, Justin Dekany, Steven Hart, Alec Sim, Amberly Evans, and other members of the Materials Physics Group, who have each given their time and effort into making this work possible.

It is only through the support of family and friends that this work is possible. My grandmother, Geniel Loveless, has served as daily inspiration, through her personal strength and character, and her passionate dedication to my academic success. My parents, Peter and Annette Brunson, and my siblings, Jennifer Delgado and Paul Brunson, have provided emotional support as well as sanctuary. Thanks to Lara Anderson, for being a wonderful lab partner and fellow adventurer in physics, for assuring me it was okay to have typos in my dissertation, and for continually pushing me to believe that I can accomplish anything. Thanks to Nick “Hero” West, who gave me the strength and courage to stand my ground. Many good friends have supported me and suffered with me in the pursuit of this goal; Julie Frost, Mark DeVries, Maure Smith, Ann Wilde, Justin Nafziger, and countless others who have been there to cheer me on and support me through the difficult times.

I am especially thankful to the Physics Department, both faculty and staff, for taking me under their wing when I first arrived here at Utah State. Deborah Reece, Karalee Ransom, Shelley Williams, and Sharon Pappas, who kept me sane and balanced throughout my academic career; Dr. Wheeler, Dr. Riffe, Dr. Fejer, and many others, who took an interest in a terrified grad student who was too shy to ask questions in class. I would like to thank Dr. Peak, without whom I would not have remained in physics.

Finally, I would like to thank Joshua Hodges, for his selfless support and enormous personal sacrifice over the past two years that made it possible for me to recover my health and finish my degree. A wonderful man, an invaluable partner, and the love of my life; I will be forever in his debt.

Jerilyn Brunson

CONTENTS

	Page
ABSTRACT.....	iii
DEDICATION	v
ACKNOWLEDGMENTS	vi
LIST OF TABLES.....	x
LIST OF FIGURES	xi
NOMENCLATURE	xiv
CHAPTER	
1. INTRODUCTION.....	1
1.1. Polyethylene and Low Density Polyethylene Characteristics	2
1.2. Spacecraft Charging	6
1.3. Research Objectives	9
2. THEORY AND BACKGROUND IN POLYMERS.....	14
2.1. Conductivity and Charge Carriers	16
2.1.1. Identification of Charge Carriers	19
2.1.2. Charge Injection.....	23
2.2. Conduction Mechanisms of Individual Carriers.....	26
2.2.1. Poole-Frenkel Conduction	28
2.2.2. Space Charge Limited Current Conduction.....	31
2.2.3. Thermally Assisted Hopping Conduction.....	34
2.2.4. Variable Range Hopping Conduction.....	36
2.3. Conduction Mechanisms of Distributions of Carriers	40
2.3.1. Dispersive Transport.....	41
2.3.2. Polarization	42
3. EXPERIMENTAL DETAILS	46
3.1. Samples and Sample Characterization.....	46
3.2. Constant Voltage Chamber.....	54
3.2.1. Instrumentation Overview	55

	ix
3.2.2. Applied Field Dependence Measurements	64
3.2.3. Temperature Dependence Measurements	69
3.3. Summary of Measured Data	72
3.3.1. Summary of Electric Field Dependence Data.....	72
3.3.2. Summary of Temperature Dependence Data.....	73
3.3.3. Summary of Electrostatic Discharge Measurements	73
4. ELECTRICAL PROPERTIES OF LOW DENSITY POLYETHYLENE.....	78
4.1. Influence of Applied Electric Field on Conductivity.....	79
4.1.1. Electric Field Dependent Conduction Models.....	82
4.1.1.1. Poole-Frenkel Conduction	82
4.1.1.2. Space Charge Limited Current Conductivity	84
4.1.1.3. Thermally Assisted Hopping Conductivity.....	86
4.1.2. Charge Injection.....	88
4.2. Influence of Temperature on Conductivity.....	90
4.2.1. Activation Energies.....	95
4.2.2. Thermally Assisted Hopping Conductivity	100
4.2.3. Variable Range Hopping Conductivity.....	107
4.3. Influence of Time of Measurement on Conductivity	113
4.3.1. Time-Dependent Conduction.....	113
4.3.2. Charging and Discharging Behavior.....	117
4.3.3. Electrostatic Breakdown	120
5. SUMMARY AND CONCLUSIONS.....	123
5.1. Charge Carriers and Carrier Mobilty.....	123
5.2. Hopping Conductivity Models	125
5.3. Time Dependent Phenomena and Electrostatic Discharge in LDPE.....	127
5.4. Summary and Future Work	128
REFERENCES	130
APPENDICES	138
APPENDIX A – CVC instrumentation	139
APPENDIX B – Electronic diagrams and schematics.....	144
APPENDIX C –Instrumental resolution.....	153
APPENDIX D – Details of data collection.....	171
CURRICULUM VITAE.....	200

LIST OF TABLES

Table		Page
3.1	Current error and sensitivity of Keithley 616 electrometer	67
3.2	Summary of applied field data used in analysis	74
3.3	Summary of temperature data used in this analysis.....	75
3.4	Measured electrostatic breakdown values	77
3.5	Measured electrostatic breakdown values with temperature	77
4.1	Comparison of determined activation energies with values of activation energy reported in literature.....	99

LIST OF FIGURES

Figure		Page
1.1	Chemical structure of polyethylene	2
1.2	Typical fractional mass distribution of polyethylene	3
1.3	Structure of LDPE	4
1.4	Resistivity and charge decay times relevant to spacecraft charging.....	8
2.1	Illustration of localized electron wave function	15
2.2	Illustration of hopping conduction.....	18
2.3	Illustration of random resistor network percolation	27
2.4	Localized state with distorted potential barriers	28
2.5	Ideal space charge limited current behavior	34
2.6	Temperature and field dependence of thermally assisted hopping conductivity	37
2.7	Temperature and field dependence of variable range hopping conductivity	39
3.1	Bakeout profile for LDPE.....	48
3.2	Reflectance spectra of LDPE and residuals.....	50
3.3	Reflectance of LDPE as a function of photon energy and wavelength	51
3.4	Transmission spectra of LDPE and residuals	52
3.5	Photograph of inside of ESD chamber	53
3.6	First constant voltage apparatus	55
3.7	Constant voltage chamber	56
3.8	CVC experimental plate stack	56
3.9	CVC voltage half-plate with sample.....	57
3.10	CVC copper electrode plate assembly	58
3.11	CVC experimental plate stack without radiation shield	59

		xii
3.12	Coaxial signal wire interface at CVC face plate.....	61
3.13	Screenshot of user interface of the LabVIEW program	64
3.14	Illustration of regions of observed current behavior.....	66
3.15	Example of repeated applied field runs	68
3.16	Temperature vs time plot for cryogenic region	70
3.17	Temperature vs time plot for high-temperature region.....	71
3.18	Change in temperature rates over full temperature range.....	71
3.19	Measured electrostatic field strength of LDPE.....	76
4.1	Conductivities for applied field data sets.....	80
4.2	Conductivities for applied field data sets at or below 3.6×10^6 V/m	81
4.3	Poole-Frenkel conduction plots for electric field dependence of measured current.....	83
4.4	Space charge limited current plot for electric field dependence of current density.....	84
4.5	Thermally assisted hopping model fit for electric field data	87
4.6	Schottky charge injection plots for electric field dependence of current density	89
4.7	Measured current over one thermal cycle at 1000 V	92
4.8	Measured current over one thermal cycle at 2500 V	93
4.9	Arrhenius plot for conductivity at 100 V, 1000 V, and 2500 V	97
4.10	Arrhenius plots for conductivity at 100 V, 1000 V, and 2500 V at high and low temperatures	98
4.11	Temperature dependent conductivity at 100 V with thermally assisted hopping model fit	104
4.12	Temperature dependent conductivity at 1000 V with thermally assisted hopping model fit	105
4.13	Temperature dependent conductivity at 2500 V with thermally assisted hopping model fit	106
4.14	Temperature dependent conductivity at 100 V with variable range hopping model fit	110
4.15	Temperature dependent conductivity at 1000 V with variable range hopping model	

	fit.....	xiii 111
4.16	Temperature dependent conductivity at 100 V with thermally assisted hopping conductivity and variable range hopping conductivity model fits.....	112
4.17	Current decay at 100 V for 22 hours	113
4.18	Initial currents at low applied fields	114
4.19	Peak initial current values for 30 V to 1000 V data set	115
4.20	Current decay at 100 V for 22 hours with power law fit	116
4.21	Charging and discharging conductivities.....	118
4.22	Physical effects of electrostatic breakdown.....	122
B.1	CVC computer system block diagram.....	145
B.2	CVC vacuum chamber block diagram.....	146
B.3	CVC AC power system wiring diagram.....	147
B.4	CVC chamber block diagram	147
B.5	CVC LabVIEW VI flowchart.....	148
B.6	CVC LabVIEW VI flowchart - Configuration Mode.....	149
B.7	CVC LabVIEW VI flowchart - Manual Mode	150
B.8	CVC temperature control system block diagram.....	151
B.9	CVC vacuum pumping system block diagram	152
C.1	Components in the CVC measurement system	154
C.2	Total current error for the Keithley 616 electrometer.....	156
C.3	Voltage as a function of elapsed time for a constant voltage data set	158
C.4	Voltage as a function of elapsed time for a constant voltage data set	161
C.5	Constant Voltage Chamber electrode assembly.	164
C.6	Example of errors introduced in binning of time varying data.....	167
C.7	Flow chart of the dynamic bin selection algorithm.	168

NOMENCLATURE

a	= average nearest neighbor trap separation.
α	= real space decay constant of the localized state wave function.
β_A	= the ratio of field energy to thermal energy for thermally activated hopping conductivity.
β_V	= the ratio of field energy to thermal energy for variable range hopping conductivity.
D_n	= Fick's diffusion coefficient for electrons.
D_o	= unspecified diffusion coefficient.
E_b	= energy difference between top of conduction band and the steady-state Fermi level due to irradiation.
E_C	= energy of the bottom of the conduction band.
E_F	= energy of the dark current Fermi level.
E_F'	= energy of the steady-state Fermi level due to irradiation.
E_{gap}	= band gap energy, energy difference between top of conduction band and the top of the valence band.
E_o	= energy difference between top of conduction band and the dark current Fermi level.
E_V	= energy of the top of the valence band.
E	= electric field.
E_A	= thermally activated hopping reduced E-field scaling factor.
E_{ESD}	= electrostatic breakdown field strength.
E_V	= variable range hopping reduced E-field scaling factor.
ΔH	= energy separation of trapped states for hopping conductivity.
m_e^*, m_h^*	= electron and hole effective masses.
n_c	= density of free carriers.
n_e	= density of free electrons.

n_D	= density of occupied localized states that may act as donor states.
N_D	= density of empty localized states that may act as donor states.
$p(t)$	= time dependent spatial charge carrier density.
ϕ_{eff}	= effective barrier height.
q_c	= charge per carrier.
q_e	= charge per electron.
R	= variable range separation of trapped states.
s	= capture cross section of conduction electrons by fixed holes.
σ	= the conductivity (the ratio of current density to electric field).
σ_{diff}	= diffusive conductivity.
σ_P	= polarization conductivity.
σ_{TAH}	= thermally activated hopping (TAH) conductivity.
σ_{TAHo}	= thermally activated hopping reduced conductivity scaling factor.
σ_{VRH}	= variable range hopping (VRH) conductivity.
σ_{VRHo}	= variable range hopping reduced conductivity scaling factor.
T	= temperature.
T_A	= thermally activated hopping reduced temperature scaling factor.
T_V	= variable range hopping reduced temperature scaling factor.
$t_{transit}$	= time for drifting carriers to travel from one electrode to another.
μ_c	= carrier mobility.
μ_e	= electron mobility.
ν_{TAC}	= hopping frequency for thermally activated hopping conductivity.
ν_{VRH}	= hopping attack frequency for variable range hopping conductivity.
ν_o	= frequency of carrier escapes.
v	= velocity of electron.

z = depth of sample.

CHAPTER 1

INTRODUCTION

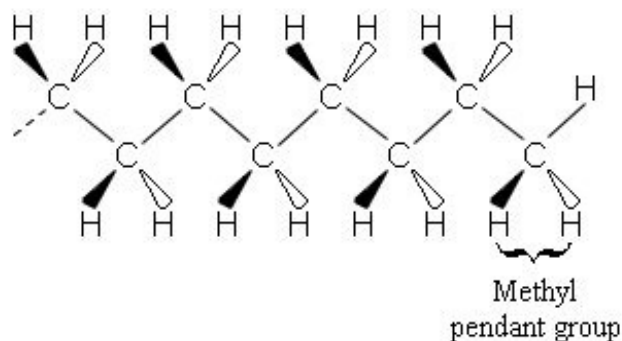
Polymer research and development is a relatively young discipline that spans the fields of physics, chemistry, electrical engineering, and beyond. It is one of the most interdisciplinary endeavors of modern science. From practical beginnings in the vulcanization of rubber to the designer polymers of today, such as Kevlar™ and Teflon™, the study of polymers continues to provide a rich variety of technological solutions and scientific challenges. Basic understanding of these macromolecules has advanced significantly from the early theory of small groups of molecules bound together by an unknown intermolecular force, but many questions remain. In many applications, polymers behave much differently than other solid materials. Attempting to explain these differences in behavior has vexed the scientific polymer community for decades and has driven much of the investigation into disordered systems. This study does not attempt to explain all of the unique behavior observed in the hundreds of different polymers available for investigation. Rather, it is necessary to focus on the electrical properties of a specific polymer. The observations and data obtained in the course of this research further the understanding of charge transport mechanisms in many polymers. In addition, the results of this study add to our ability to anticipate electrical behavior of polymers in application.

The first step in this research was the selection of a suitable polymer. Desirable qualities included mechanical toughness, inertness to common laboratory chemicals, a relatively low value of resistivity, and availability as a high-quality thin film. Once a polymer was chosen, it was then necessary to carefully measure its electrical properties under a range of experimental conditions and determine ways to tie the measurements to the physical structure of LDPE. This is most commonly done through calculations of dielectric constant, average activation energy, and transitions between regions of distinct electrical behaviors that can be tied to physical transitions, including phase transitions.

1.1 Polyethylene and Low Density Polyethylene Characteristics

A relatively simple molecule of polymerized ethylene (C_2H_4), polyethylene (PE) is primarily made up of covalently bonded carbon atoms with hydrogen or methyl (CH_3) pendants. The most stable conformation of the polymer chain is a planar zigzag, depicted in Fig. 1.1 with a methyl pendant group, with chain branches spaced approximately 30 to 100 monomers along the chains (Peacock, 2000). Deviations in the chains, such as unsaturated sites, branching, and residual chemicals from the polymerization process, decrease the degree of crystallinity and influence material behavior (Zallen, 1983). Below a certain chain length and molecular weight, PE is found in vapor or liquid form and chain lengths of a few hundred to a few hundred thousand are required to obtain the most commonly sought after properties (Peacock, 2000). Average molecular weights, closely tied to chain lengths and branching distributions, determine much of

a) Planar Zigzag Chain



b) Single Monomer

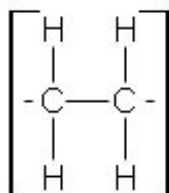


FIG. 1.1. Chemical structure of polyethylene. The simplest, most stable conformation of the PE chain is a) a planar zigzag with hydrogen or methyl pendant groups and b) a single monomer of PE consists of two carbon atoms and four hydrogen atoms.

the behavior of the final product. There is a broad distribution of chain lengths in a sample of PE, from a few ethylene molecules to chains that are millions of ethylene molecules long. Chain lengths can be correlated to molecular weights and determined using size elution chromatography (Peacock, 2000). Precise determination of the properties of the resin could be obtained if each branch and group could be known and characterized; the enormity of this task requires determination of characteristics based on averages of molecular weight and branching distributions. Statistical averaging of the numbers of chains and their respective molecular weights gives a typical fractional mass distribution for a PE resin; illustrated in Fig. 1.2.

One common class of PE is low density polyethylene (LDPE), contains significant amounts of branching on the polyethylene chains, as illustrated in Fig. 1.3a. Branches are primarily ethyl ($-C_2H_5$) and butyl ($-C_4H_9$) functional groups, but can be much longer chains with

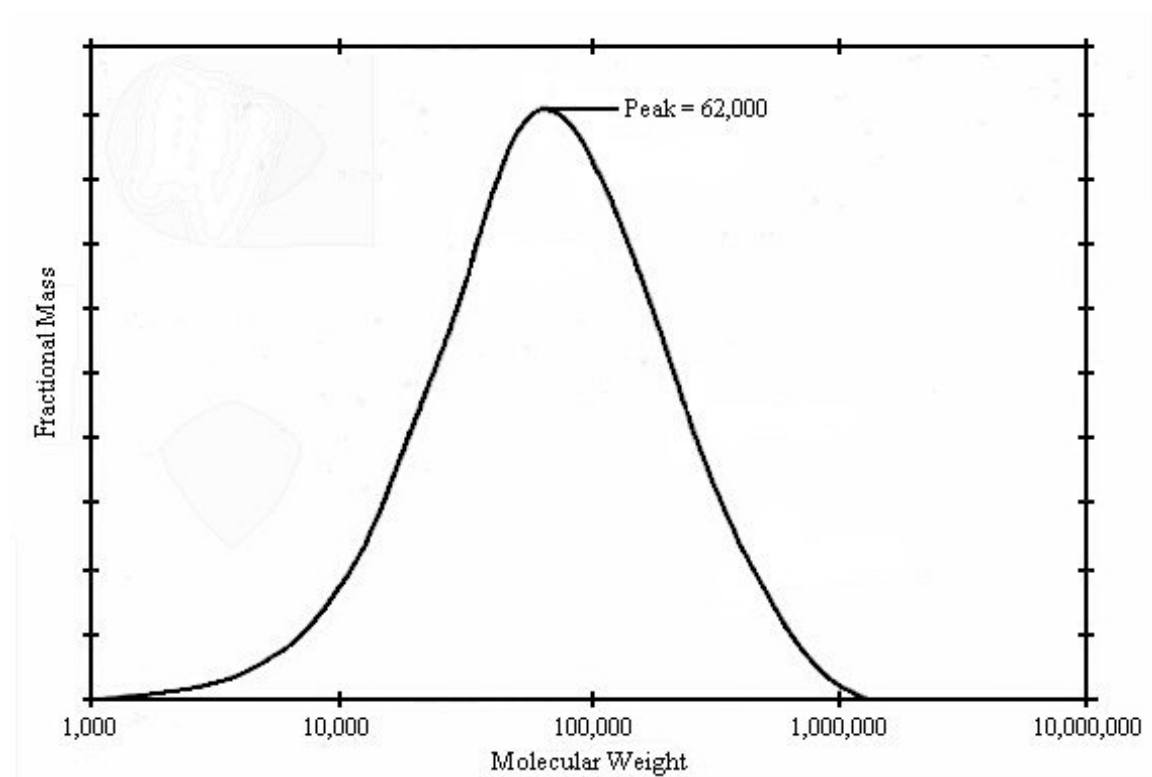


FIG. 1.2. Typical fractional mass distribution of polyethylene. This information is commonly obtained using size elution chromatography, with a typical peak fractional mass of 62,000.

secondary branches and functional groups. These common functional groups are depicted in Fig. 1.3b. The branches inhibit the ability of the resin to crystallize, resulting in decreased overall crystallinity and lower density, with some physical properties sensitive to the amount of short or long chain branching. Commercial LDPE has a typical density of 0.90-0.94 g/cm³ and a percent crystallinity of 42% to 62% (Peacock, 2000). In comparison, high density polyethylene (HDPE) has tightly packed chains with fewer branches and can have a percent crystallinity of up to 85%. LDPE is a semi-crystalline polymer; it is less crystalline than the polytetrafluoroethylenes (PTFE), which can be polymerized with as much as 98% crystallinity, but more crystalline than a polyimide (such as Kapton™), which typically has up to 40% percent crystallinity (Salamone, 1996).

LDPE morphology consists of three phases: crystalline, non-crystalline, and interfacial

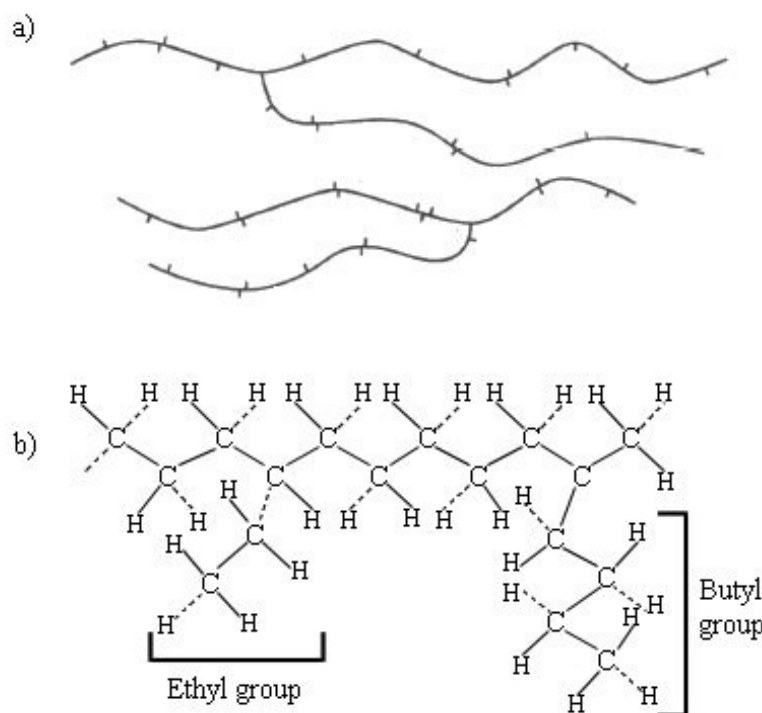


FIG. 1.3. Structure of LDPE. a) Long and short branches and b) illustration of common small functional groups, ethyl and butyl groups.

regions. Sections of close-packed chains form ordered regions called crystallites that are embedded in the non-crystalline regions. Under most circumstances, the crystalline regions form orthorhombic crystals as the unit cell, consisting of one complete ethylene molecule and segments of adjacent ethylene molecules (Peacock, 2000). Within these localized regions of ordered crystals, the traditional approach to crystal structure and transport, including band theory, can be applied with suitable approximations. The crystalline regions can adopt a variety of formations; ribbon-like crystallites (lamellae) that may be curved or fragmented and large-scale, spherical structures, called spherulites, that consist of bundles of lamellae growing outward from a central core. Typical lamellae are 50-200 Å thick with their length varying from a few hundred angstroms to several millimeters (Peacock, 2000). Extended chain lengths allow for individual chains to transverse the amorphous region and act as part of multiple crystallites. The degree of connectivity of these crystalline regions via the interconnecting extended chains plays a determining role in the physical properties of the material (Dissado and Fothergill, 1992; Peacock, 2000; Sperati *et al.*, 1953).

With respect to the electrical properties of LDPE, charge carriers are believed to move preferentially along individual chains rather than transferring from chain to chain (Zallen, 1983) and a greater degree of interconnectivity increases the mobility of a carrier by increasing the likelihood of long-range connectivity between crystalline regions. Interfacial regions between the crystalline and non-crystalline regions are partially ordered and have mixed properties, exhibiting a blend of crystalline and amorphous behaviors that is not well understood or characterized (Zallen, 1983). The majority of carrier traps that play an active role in charge transport are believed to lie within these interfacial regions (Davies, 1972; Fowler, 1956; Lida *et al.*, 1992). Known to be a vital component in the mechanical properties of LDPE, the investigation and theoretical modeling of the electrical properties of the interfacial regions is an emerging focus in the study of polymers. When determining the ratio of crystallinity, the interfacial and non-

crystalline regions are typically considered together and broadly referred to as the amorphous region.

While LDPE is one of the simplest of the commercially available polymers today, its very simplicity also removes signature behavior that proves useful in examining the electrical behavior of polymers. It lacks strongly polar, aromatic, or unique functional groups that are often easily targeted experimentally and which frequently control the rate of charge transport. The branched nature of LDPE gives it a reduced percentage of crystallinity in comparison with other forms of PE, such as HDPE and linear low density polyethylene (LLPE), and when compared to strongly crystalline polymers like PTFE. This decreased crystallinity increases the dependence of electrical behavior on the non-crystalline and interfacial regions.

Despite these difficulties, LDPE remains a prime choice for experimental work for two primary reasons. First, and foremost, the structural simplicity of LDPE allows for the ability to obtain high-quality, high-purity samples at a relatively low cost from a wide variety of manufacturers. This reduces the dependence of sample behavior on the manufacturing process and environment, impurities, and sample handling prior to its use in the laboratory. It is widely available in nearly any form imaginable, from thin films to cables and thick, insulating blocks. Secondly, the relatively low resistivity of 10^{15} - 10^{18} Ω -cm at room temperature means it is measurable using standard constant voltage methods and laboratory equipment. This relative ease of measurement has led to an enormous wealth of literature and experimental data dedicated to the study of LDPE, which is available for comparison to the current research.

1.2 Spacecraft Charging

Although polymers were developed early in the twentieth century, it was not until World War II that they began to emerge as a material of choice in nearly every area of industry. Polyethylene played a key role in insulating radar electronics during the War (Peacock, 2000) and

its use has continued to rapidly expand. Today, highly insulating polymers like LDPE are ubiquitous in use, easily tailored to address specific chemical and physical requirements, and endless in their possible applications in new technology. While the use of LDPE to create milk containers or kitchen garbage bags may not have lead to further scientific interest, its use as an insulating material in high-voltage transmission lines, sensitive electronics, and on spacecraft gave a new importance to understanding its electrical properties.

The space environment includes a dynamic mix of particle species, charged and neutral, plasmas, electric and magnetic fields, radiation, and physical debris (Hastings and Garrett, 1996). Effects of interaction with this environment can include physical damage to the spacecraft, degradation of the electronic components, and unwanted electrical behavior (Leach and Alexander, 1995). Small, integrated circuits and the microelectronics found on board modern spacecraft make them ever more susceptible to accumulating charge and electrostatic discharges (Dennison *et al.*, 2003a, 2003b, 2005a, 2005b; Hastings and Garrett, 1996).

Spacecraft charging is a deceptively simple issue of being able to predict and control the effects within materials as the spacecraft interacts with the space environment. Modeling and understanding the complex relationships between the spacecraft and its surroundings is fundamentally based on a detailed knowledge of how individual materials store and transport charge. The low charge mobility of insulators causes charge to accumulate where deposited, preventing even redistribution of charge and creating inhomogeneous local electric fields and potentials. Effects of these inhomogeneous potentials can range from systematic errors in the electrical components to complete system failure due to electrostatic breakdown of the material (Frederickson and Benson, 2001; Frederickson and Dennison, 2003; Hastings and Garrett, 1996). Long-term accumulation of charge can cause degradation of exterior surfaces, enhance contamination, and deteriorate protective coatings on sensitive components. The history of the sample becomes important as the behavior of the material is modified with further charging

(Brunson and Dennison, 2006; Frederickson and Benson, 2001). Fig. 1.4 illustrates the basic connection between conductivity and charge dissipation and decay times relevant for spacecraft charging (Dennison *et al.*, 2006).

Increasing the versatility and reliability of spacecraft charging models and expanding the database of information for the electronic properties of insulating materials can assist spacecraft designers in accommodating and mitigating these harmful effects (Dennison *et al.*, 2003a; Frederickson and Benson, 2001). Improving the design models requires a better understanding of the physics of materials, particularly with respect to the increasingly complex insulating polymers that cannot be accurately modeled with standard solid state methods. The conductivity of the material is a key transport parameter in determining how deposited charge will distribute across the spacecraft, how rapidly charge imbalances will dissipate, and what equilibrium potential will

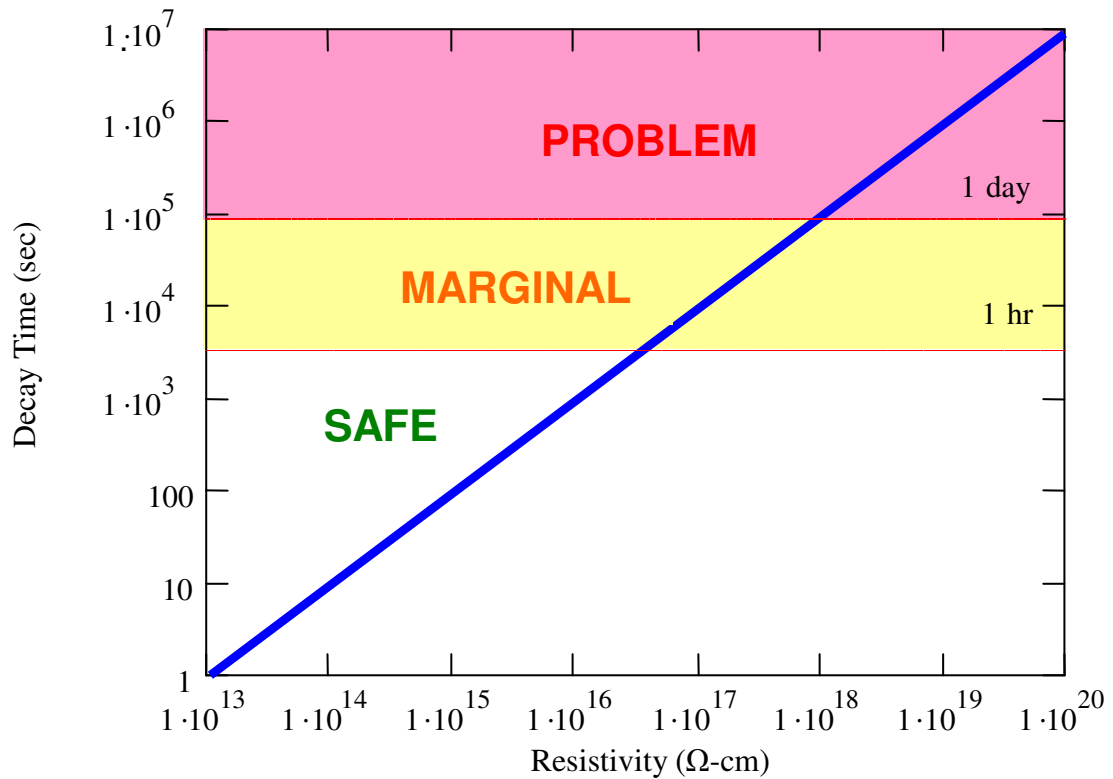


FIG. 1.4. Resistivity and charge decay times relevant to spacecraft charging.

be established under given environmental conditions (Dennison *et al.*, 2005b; Frederickson and Dennison, 2003). Hence, it is critical for reliable spacecraft charging models to use appropriate values of conductivity for thin film insulators to determine the correct charge storage decay times for the materials. The bulk conductivity values of commonly used insulators have most often been found using standard ASTM prescribed methods (ASTM D 257-99), utilizing a parallel plate capacitor geometry. These methods need further modification and in some cases, are not strictly applicable to common situations encountered in spacecraft charging (Frederickson and Dennison, 2003; Coelho *et al.*, 1989).

The first experimental step taken in this study was to more closely approximate the space environment. Through the development of a chamber that houses a constant voltage apparatus, it was possible to perform measurements under vacuum conditions. Additionally, the low temperatures of the space environment required adaptation of the constant voltage chamber (CVC) to allow measurements of temperature dependent conductivity. Also developed was the automated control of applied voltage, experiment duration and sequencing, and temperature control of the chamber. Exposure to repetitive and varying applied fields was used to investigate the charging and discharging cycles of the insulating materials under constant temperature conditions.

1.3 Research Objectives

The immediate application of this study is to further the investigation into the electrical properties of polymers, in particular LDPE, within the framework of parameters relevant to spacecraft charging. Three primary parameters relevant to spacecraft charging and the space environment are applied electric field, temperature, and duration of experiment. For each of these relevant parameters, careful investigation and measurement of leakage currents¹ can identify

¹ Leakage current is simply defined as the current measured due to conduction through the material.

probable charge transport mechanisms. Both temperature and the duration of experiment are relevant to the space environment and can approximate the thermal and charging cycles that a spacecraft undergoes as it orbits the Earth. Varying the applied field provides information about the charge storage characteristics of the material and how its conductivity changes with exposure to an electric field or accumulated charge. This information can be used to increase reliability of spacecraft charging models and further understanding of the electrical behavior of polymers in a wide variety of applications.

Determining the conduction properties of LDPE requires careful examination of the complex response of the sample to the test conditions. Continued research into electrical conduction in polymers has yielded a rich variety of theoretical and experimental work, but it has also exposed limitations in the crystalline and amorphous modeling approaches to conduction in polymers. Polymers are dynamic materials, with molecules in constant, if limited, motion that can alter the location, depth, and type of carrier traps (Adamec and Calderwood, 1978; Boudou and Guastavino, 2000; Jones *et al.*, 2005; Lewis, 2002). The interfacial regions where crystalline regions join amorphous regions have emerged as an important part of the conduction process (Davies, 1972; Lida *et al.*, 1992). It has also become apparent that the time evolution of the polymer morphology is a significant factor in determining conduction behavior (Adamec and Calderwood, 1978; Lewis, 2002). Over time, and with exposure to an applied field or thermal energy, even a simple polymer like LDPE can undergo conformational changes along the polymer chains. This evolution is not well understood, but is frequently treated as an aging² phenomenon and is known to have mechanical, electrical, and thermal components (IEC 505, 1975). Electrical aging is a broad term associated with a variety of undesirable electrical phenomena, including breakdown, discharge, treeing, interactions with charges, etc. A series of relaxation processes

² Aging is most clearly defined in IEC Publication 505 as “irreversible deleterious change to the service ability of insulation systems. Such changes are characterized by a failure rate which increases with time.”

have been found to occur in LDPE with exposure to charging and thermal cycles (Adamec and Calderwood, 1978; Griffiths *et al.*, 1998; Ieda, 1980; Ieda *et al.*, 1988), with irreversible effects on both crystalline and amorphous regions. Several of these relaxation processes have been correlated to physical transition points and deep carrier trap levels via experiments in thermoluminescence and thermally stimulated currents (Ieda, 1980; Ieda *et al.*, 1988; Peacock, 2000). This abundance of information can be difficult to collect and apply to new research, especially since the experimental data are spread across multiple scientific fields.

Investigating the nature of charge transport begins with looking for information that sheds light on the nature, identity, spatial and energy distribution, and mobility of the charge carriers. The questions that must be addressed about the nature of the carriers include their identity, the source of available carriers, and how carriers move through a polymer material. Careful investigation of the conductivity of LDPE can provide insight into these questions and provide possible answers.

High quality, thin film sheets of LDPE were obtained from Goodfellow Cambridge Ltd. and baked to remove water content introduced during manufacturing and handling. Individual samples were then placed into a vacuum chamber developed by the USU Materials Physics Group. Section 3.1 provides details of sample properties and characterization. Measurements reported in this dissertation were made in a custom, high-vacuum test chamber described in Section 3.2, using a constant voltage method with parallel plate capacitor geometry. This is the simplest and most reproducible method available for measuring the conductivity of thin films using standard laboratory equipment.

The samples were pressed between grounded copper or aluminum plates and copper electrodes and the leakage current through the sample was measured with sensitive electrometers. Two types of primary measurements were taken: constant room temperature measurements with a varying applied electric field and constant applied field measurements while the temperature of

the sample changed. Summaries of data utilized in analysis are found in Section 3.3. For constant temperature measurements, the samples were exposed to a wide range of applied fields, from less than 1% of the predicted breakdown field to near breakdown. For variable temperature measurements, the chamber and samples were cooled using liquid nitrogen and allowed to return to room temperature without external aid while the leakage currents were measured. Resistance heating strips in direct contact with the outside of the chamber proved to be the most reliable method of heating the chamber and samples, resulting in the most consistent heating rates. Samples were then allowed to slowly return from high temperatures to room temperature as leakage currents through the samples were measured. Further experimental details, including technical details of the CVC apparatus, test methods, and the data obtained, are provided in Appendices A, B, C, and D.

Measurements of leakage current at room temperature with a varying applied field were used to obtain the field dependence of the conductivity of LDPE, discussed in Section 4.1. Determination of field dependence allows the investigation of conduction models such as Poole-Frenkel conduction and space charge limited current conduction, as well as the evaluation of carrier injection mechanisms such as Schottky injection. To determine the validity of these models, their results are compared to accepted values of the dielectric constant for LDPE. It is impossible to discuss field dependence without touching on electrostatic discharge (ESD) and breakdown phenomena. The concepts of endurance time and the nature of ESD will be qualitatively discussed in Section 4.3.3 and as relevant to the field dependence of conductivity in LDPE.

Measurements of leakage current as sample temperature varies provide additional verification of physical parameters, such as average activation energies. Determination of temperature dependence also allows verification of prominent hopping conduction mechanisms; results of those measurements are discussed in Section 4.2. Two mechanisms of interest are

thermally assisted hopping (multiple trapping) and variable range hopping (tunneling), both of which are expected to show distinct temperature dependent behavior. A mathematical framework is introduced in Section 2.2 and further developed in Sections 4.1 and 4.2 to evaluate both transport mechanisms with reduced temperature and applied field variables, as well as fitting parameters immediately relatable to physical and structural properties of LDPE.

Finally, the conduction mechanisms and material responses that are tied to the changes in carrier density and time-dependent charge transport must be addressed in relation to transient and long time behaviors, including dispersive transport and polarization. These mechanisms are discussed in Section 4.3.

CHAPTER 2

THEORY AND BACKGROUND IN POLYMERS

The complexity and adaptability of polymers make it relatively easy to tailor their properties to suit a specific purpose, but this adaptability also creates challenges in measuring and determining their intrinsic properties. In particular, the electrical properties prove difficult to accurately measure due to the highly resistive nature of the materials. Despite this extreme insulating nature, low-level conduction is found to occur in all known polymers (Adamec and Calderwood, 1978; Dissado and Fothergill, 1992). Rather than a single, dominant conduction mechanism described by band theory, as is often the case for conductors and semiconductors, there may be multiple interdependent or competing mechanisms occurring simultaneously. Separating these charge transport mechanisms and determining the contribution and relevant regime of each mechanism is quite difficult both in theory and experimentally. Determining how charge transport occurs within a given polymer requires knowledge of the nature, density, and mobility of available charge carriers, as well as how the mobility of the carrier is dependent on experimental conditions such as applied field, temperature, and deposited charge or energy. This information is also heavily influenced by morphology, crystallinity, impurities, structural defects, sample history, and even the processing method used to create the individual polymer sample. Both the micro- and macro-structures of polymers are sensitive to thermal, mechanical, and electrical history (Boudou and Guastavino, 2000, 2002; Lewis, 2002; Parpal *et al.*, 1997).

The crystal structure and well-developed mathematical formalism based on Bloch's theorem is the foundation of understanding the properties and behavior of solid materials. For conducting materials with crystalline morphology, a calculation of conduction bands and other properties has led to a successful methodology for understanding charge transport, but this approach is based on periodicity and long-range order. The primary transport mechanism for

conductors involves intraband excitations of electrons from filled extended states to empty extended states at only slightly higher energy states within the same conduction band. This mechanism is not available in insulators since there are no empty states within the valence band and insulators are largely populated by localized states rather than extended states. Bloch function extended-state solutions are dependent on long-range order and on delocalization of electron wave functions, which is largely absent in amorphous materials. Without long-range order, the wave function of the electron is concentrated in a small region and falls off exponentially with distance, as illustrated in Fig. 2.1.

The band structure methods and developed mathematics for conducting materials can also be extended, with suitable approximations, to semiconducting materials. Charge transport in intrinsic semiconductors is primarily via thermally activated interband excitation of electrons from states in the valence band to states in the conduction band with the activation energy equal to the band gap energy. However, this conduction mechanism is negligible in insulators at reasonable working temperatures. A primary distinction between semiconductors and insulators is that thermally activated transitions between extended states are highly improbable in insulators,

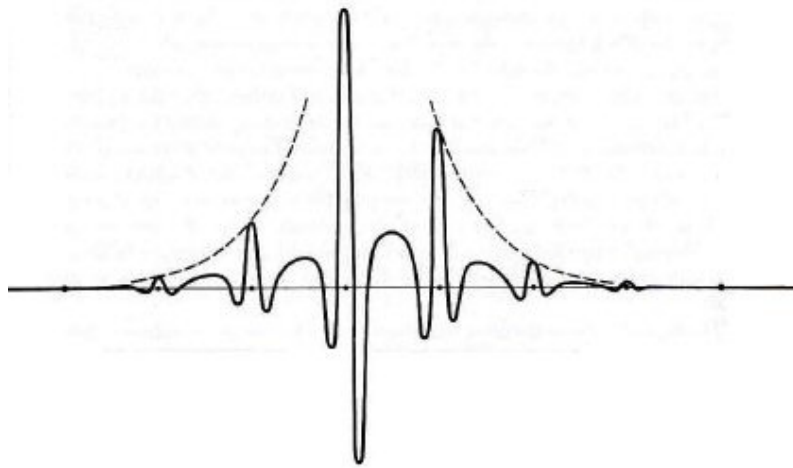


FIG. 2.1. Illustration of a localized electron wave function. The wave function falls off exponentially with distance in the absence of long-range order.

because the band gap energy separating the conduction and valence bands is much larger than the average thermal energy of the electrons. In intrinsic semiconductors, the Fermi energy is approximately halfway between the conduction and valence bands and, above 0 K, a finite number of electrons are able to transfer to the conduction band. Extrinsic semiconductors have extra energy levels added by impurities or dopants. Whether structural or compositional, these impurities can be treated as localized defect sites or deviations from an ideal lattice and approached with perturbation theory (Ashcroft and Mermin, 1976).

Electron transport in disordered materials, which forms the fundamental basis of the present study, requires an entirely different approach and formalism than the concepts of periodicity and Bloch's theorem for crystalline solids. Localized states are inherent in disordered solids rather than limited to structural or compositional impurities and defects in the lattice. Unlike extrinsic semiconductors, insulators contain significantly larger densities of defects and deviations from an ideal lattice, which greatly limits the applicability of a perturbation approach. Although degenerate molecular orbitals of the successive monomers in polymers form extended electronic states, any impurities, anomalies, and branches disrupt these bands and act to truncate these extended states. It then becomes necessary to develop methods to understand charge transport involving these localized states without utilizing the formalism of band theory.

2.1 Conductivity and Charge Carriers

The traditional definition of conductivity as a macroscopic, mean-field behavior can be written as the ratio of current density, J , and electric field, E , resulting in $J = \sigma E$. In its simplest form, Ohm's Law represents a linear relationship between current density and electric field. This simple expression allows direct substitution of accessible laboratory parameters; current, I , and potential difference, V . When conductivity becomes a question of microscopic behavior, a new definition involving the charge carriers is required. Conductivity, in an equally simplistic form,

can be written as a product of carrier charge, q_c , carrier density, n_c , and carrier mobility, μ_c .

$$\sigma = q_c n_c \mu_c. \quad (1)$$

The separation of carrier density and mobility is artificial; carrier movement and mobility are strongly correlated and may depend on the spatial and energy distribution of the charge carriers. A broad grouping of charge transport mechanisms depends on the time evolution of carrier density rather than motion of individual carriers, including dispersive transport, transient currents, and polarization, etc. The conduction mechanisms available to the carriers fall naturally into two categories: time independent transport determined by the motion of single carriers, expressed through the mobility μ_c , and time-dependent transport determined by the density of the carriers, n_c . Conduction mechanisms that rely on carrier mobility and ability to move between localized states, and the change of that mobility under an applied field or change of temperature, are the primary focus in this study. This kind of transport is known as hopping conductivity.

Multiple trapping is defined as a series of jumps between localized states, resulting in low levels of conduction. It is considered to be the primary charge transport mechanism in a wide variety of disordered and amorphous materials (Böttger and Bryksin, 1985; Dissado and Fothergill, 1992; Zallen, 1983). In extended-state hopping, escape from a trap occurs when a carrier gains enough energy, for example, through phonon interaction in thermally assisted hopping, to overcome the potential barrier of a shallow, localized state and enter an extended state. An illustration of a carrier hop is shown in Fig. 2.2. A carrier may also move via phonon assisted tunneling through a potential barrier between deeper traps where extended states may not be available, also illustrated in Fig. 2.2. In general, these two mechanisms differ in their sensitivity to temperature, applied electric field, and other experimental conditions (Arkhipov *et al.*, 2001; Boudou and Guastavino, 2000; Ieda, 1980; Wintle, 1999). It is prudent to be clear that additional means of energy gain are available, including interaction with photons and other forms of radiation, referred to as radiation induced conductivity. The interested reader is directed to the

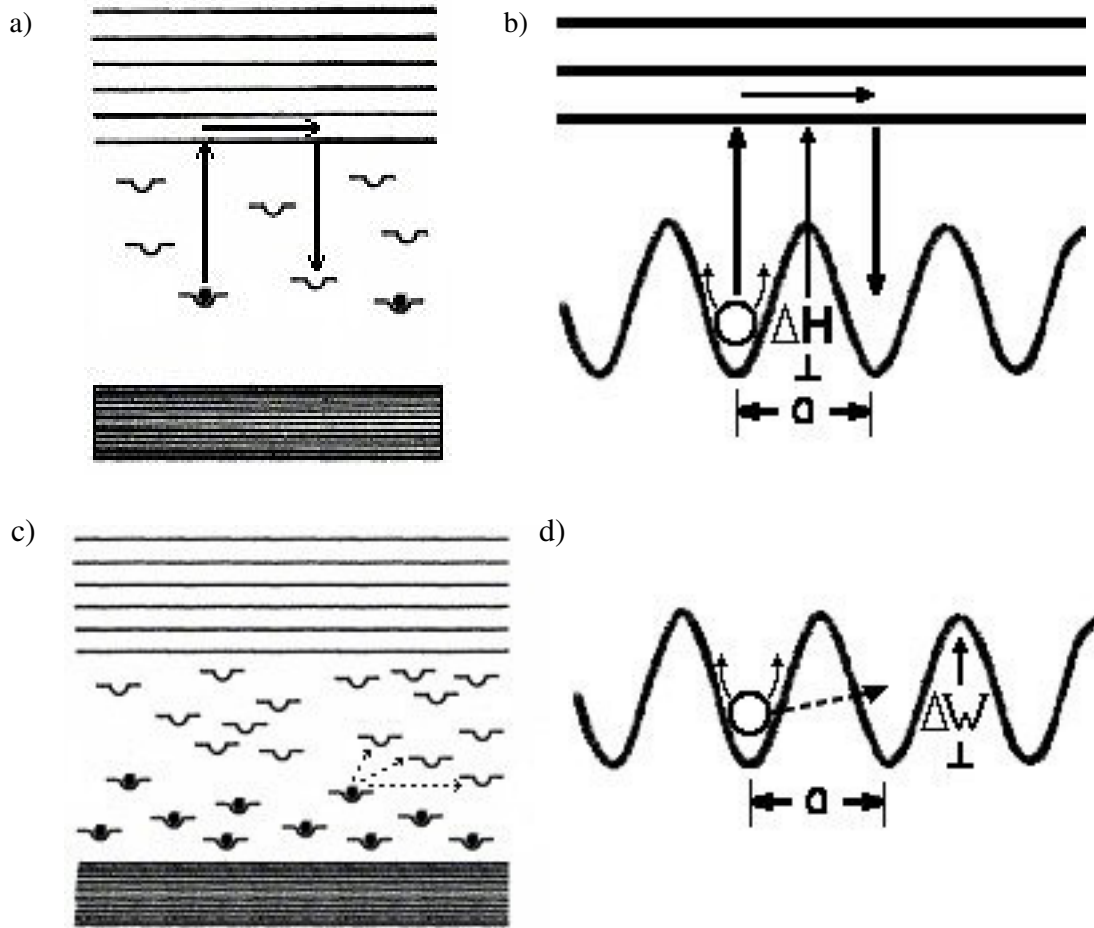


FIG. 2.2. Illustration of hopping conduction. Via carrier trapping a) a single hop is considered to be the escape of a carrier from a shallow, localized state just below the conduction band, movement via an extended state, and recapture in a secondary localized state (a trap). b) The parameter, ΔH , is the average trap depth below the conduction band edge and can be correlated to the activation energy of the material. Illustration of hopping conduction based on quantum mechanical tunneling. c) A carrier may moved from one localized state to another via direct tunneling where there are deep traps well beneath the conduction band. d) The parameter, ΔW , is the difference in trap depths between the first and second localized states.

work of Rose, Campbell, and the USU Materials Physics Group for additional information on radiation induced conductivity (Campbell, 1983; Denmsion *et al.*, 2007, 2009; Rose, 1951).

Much of the groundbreaking work in determining the electronic structure of disordered materials was done by Mott, Anderson, and colleagues (Anderson, 1958; Mott, 1969; Mott and Davis, 1979). For their contributions, the 1977 Nobel Prize in Physics was jointly awarded to Sir

Neville Mott, Phillip Anderson, and John Hasbrouck Van Vleck. This work forms the foundation of modern theory of charge transport in disordered materials, including hopping conductivity. As the study of hopping conduction expanded from fundamental theory provided by Mott, Anderson, and Van Vleck, two distinct types of hopping emerged to describe the movement of the carriers: trapping and tunneling. Due to conflicting nomenclature within the literature, it is often difficult to determine which mechanism is being discussed; unfortunately the terms hopping and tunneling are frequently and incorrectly used interchangeably. Many additional terms are used inconsistently, such as dispersion, space charge, hopping, and trapping, and may have different meanings according to their particular use. The interdisciplinary nature of polymer research increases this confusion by drawing nomenclature from physics, chemistry, and engineering. It is not uncommon for the same, or similar, terms to have different meanings within each individual field. Every attempt will be made in this study to be clear about the nature of the mechanism and to consistently use the terms trapping and tunneling, rather than the use of the more general term, hopping.

Further complicating the investigation into electrical properties of polymers is that many possible charge transport mechanisms manifest with similar behavior, making it difficult to determine which mechanism (or mechanisms) is active. It is also necessary to establish ways of separating the response of the instrumentation from the response of the material being measured, a requirement that is not easily met when the level of currents being measured can be 10^{-14} A or smaller. Although none of the parameters are truly separable, control of experimental conditions allows targeting of specific mechanisms that may be dominant under those conditions.

2.1.1 Identification of Charge Carriers

It is apparent that a wide variety of mechanisms have been theorized during the exploration of polymer behavior, borrowing heavily from the study of ionic conduction in

covalent and ionic crystals as well as modifications of electronic band theory. Many excellent reviews of past work in disordered materials are available (Arkhipov *et al.*, 2001; Dissado and Fothergill, 1992; Whitehead, 1953). Electronic conduction, including holes, is assumed to be the primary mode of conduction in LDPE and electrons are commonly identified as the charge carrier (Crine, 2005; Rose, 1951; Wintle, 1999). However, the identity of the carrier may vary according to experimental and environmental conditions, and lingering controversy remains over the source of the carriers (Lewis, 2002; Wintle, 1999). Polymers with increasing concentrations of plasticizers favor ionic conduction and doped polymers are typically injected with electronically rich functional groups (Dang *et al.*, 2003; Hong *et al.*, 2004; Raju, 2003; Salamone, 1996; Tjong and Liang, 2005). Each polymer must be considered according to its unique structure and functional groups, and also with respect to the specific experimental method used.

The type of electrode also becomes significant. Evaporated aluminum electrodes have been shown to result in transfer of aluminum atoms into the polymer material under certain experimental conditions (Parpal *et al.*, 1997). Impurities in the electrode materials may also provide a source of atoms for ionic conductivity. For solid electrodes in physical contact with the polymer, the energy barrier may be dramatically influenced by the choice of metal and any oxide layer that may develop on the electrode. The metal-polymer interface is complex (Bussac *et al.*, 1998; Lewis, 1986), with surface currents and surface fields that influence bulk behavior and are strongly coupled to the geometry of the electrodes and the experimental apparatus. Much work remains to be done on the behavior of charges with respect to the metal-polymer interface. Aluminum, copper, and high purity gold electrodes have been investigated for the CVC system, but the choice of electrode material will not be considered in the present study. It is reasonable to assume that ionic conduction is unlikely to be favored in undoped LDPE, which has been baked out and chemically cleaned to limit surface contaminants, placed in a parallel plate capacitor configuration with high purity solid OFHC copper electrodes in direct contact with the samples.

Furthermore, the relatively moderate experimental conditions are unlikely to provide the higher energies needed for ionic conduction; temperatures were kept below the melting point and most applied fields were much less than the measured ESD field strength for LDPE. The charge carriers in this study of LDPE are most likely to be electronic in nature (Adamec and Calderwood, 1981; Davies, 1972; Khalil and Gastli, 1999; Lewis, 1986; McCubbin, 1970; Rose, 1951).

Electronic carriers include electrons and holes, and much of the available research does not attempt to distinguish between them. This may stem from the historical practice of extending theory that is applicable to semi-conductors to conduction in polymers, including the identity of the charge carrier. Additionally, electrons move more easily through crystalline and amorphous regions, with the interfacial regions acting as primary trapping centers. There is, however, a reasonable argument for the selection of electrons, rather than holes, as the charge carrier (Rose, 1951). In the case of insulators with wide band gaps, such as LDPE, the filled valence band is energetically deep. An electron leaving the valence band via hopping would leave the hole behind in an extremely deep trap. This effectively immobilizes the hole and prevents it from acting as the charge carrier in a conduction process. A slightly different approach is to consider an asymmetrical trap distribution where the traps for holes are deeper than the traps for electrons due to a shift in the Fermi energy toward the conduction band. This shift also lowers the chances of recombination and again serves to immobilize the holes in deep traps. A shift in the Fermi energy from the center of the band gap is not unexpected and is, in fact, typical of a system with significant lattice defects. The interested reader is directed to the work of Rose (1951) or Broser and Waminsky (1950) for details and mathematical analysis of the mobility of holes.

The individual localized states available to a carrier can be approximately characterized by a potential well with a mean energy barrier of ΔH and an average trap separation of a (see Fig. 2.2) (Dennison and Brunson, 2008; Dennison *et al.*, 2009; Fowler, 1956). This corresponds,

respectively, to the average amount of energy required for a trapped carrier to escape its localized state and the average distance it will travel before being trapped in the next localized state. If enough energy is acquired to avoid immediate recapture, the electron may enter an extended state of overlapping molecular orbitals analogous to a conduction band.

Time spent in extended states before recapture is usually quite small (Fowler, 1956; Mott and Stoneham, 1977), with a typical conduction lifetime of $\tau_c \sim 10^{-14}$ s, which is much less than the time required for true band conduction to be viable. This small capture cross section combined with a large density of traps results in multiple trapping behavior. Even in chemically pure samples of LDPE with low concentrations of impurities and compositional defects, there is expected to be 10^{15} to 10^{18} traps per cm^3 (Rose, 1951). This large concentration of traps means that carriers are likely to be quickly recaptured and there is, comparatively, a much smaller concentration of available carriers, n_f , than available states.

A carrier hop, through phonon interaction, may result in movement that is energetically upward into an extended state or into another localized state. It is also possible for a carrier to hop in a way that is energetically downward through phonon emission, allowing the carrier to become trapped in an available deeper state that requires more energy to escape (Arkhipov *et al.*, 2001; Böttger and Bryksin, 1985; Dissado and Fothergill, 1992; Lewis, 1986). This encourages charge storage and low effective carrier mobility (Apsley and Hughes, 1975; Fowler, 1956; Lewis, 1986; Wintle, 1971). The mean time spent moving from one trap to another is the conduction lifetime of the carrier, τ_c , which, along with a , the average nearest neighbor trap separation, factors into the carrier mobility, μ_c . This is defined as the mean drift velocity, $v_d = a/\tau_c$, divided by the electric field, E .

Physical fluctuations in the polymer chains may create, alter, or destroy localized states and release or trap available charge carriers (Boudou and Gustavino, 2000; Lewis, 2002). The influence of temperature and an applied electric field also affects the ability of a carrier to escape

from a localized state in the direction of E . While there is no localized state with an energy minimum such that there does not remain a finite possibility of escape (Apsley and Hughes, 1975), deeper trap sites have longer trapping times and smaller release rates, which reduces carrier mobility. The potential barrier of a localized state is lowered by an applied electric field, E , which increases the likelihood that a carrier may escape (Mott and Davis, 1979; Poole, 1917). This implies both temperature and electric field dependence for a conduction mechanism utilizing multiple trapping. Typically, the release and the subsequent recapture of the carrier are considered a single carrier jump. Trap controlled charge transport also assumes a negligible conductivity contribution of direct quantum mechanical tunneling of carriers between localized states (Böttger and Bryksin, 1985). Deeper traps and a distribution of traps more complicated than a single, uniform level encourage charge storage rather than charge transport (Apsley and Hughes, 1975; Fowler, 1956; Lewis, 1986; Wintle, 1971, 1999).

The origin of electronic charge carriers remains a subject of controversy; carriers may be available within the polymer or they may be injected at the electrodes and the answer can depend significantly on the type of polymer and experimental conditions (Crine, 2005; Reiser, 1969; Wintle, 1999).

2.1.2 Charge Injection

The chemistry of the metal-polymer interface is quite complex, with different interactions commonly seen between the metal and polymer lamellae, individual polymer chains, impurities, and voids (Dissado and Fothergill, 1992; Lewis, 2002). In an ideal electrode-insulator system, the available carriers are assumed to be injected from the electrode into the material (Wintle, 1999), but the validity of this assumption and the nature of the injection process remain controversial. Many of the theories developed to explain deviations from hopping and multiple trapping models observed in polymers rely on injected charges. It is reasonable to assume that

carrier injection should be proportional to the applied field (Lewis, 2002; Many and Rakavy, 1962), and this assumption will be further investigated in Section 4.3.

A primary model of carrier injection is Schottky injection, which can be customized in many ways and can produce a variety of Schottky-type behaviors, depending on the desired modifications (Bussac *et al.*, 1998; Dissado and Fothergill, 1992; Schug *et al.*, 1907). It is important to be clear at this point that Schottky behavior is not conduction through the bulk of the material; rather, it is an interaction of the metal and polymer at the interface that leads to a current of injected electrons from the electrode into the polymer. The electrons may then move through the material via any conduction mechanism that is available to them. Although Schottky injection does not provide information about which mechanism (or mechanisms) is active, many of the prominent and frequently applied conduction mechanisms rely on the injection of the carriers by the electrode. This provides motivation to determine if, and to what extent, the electrons are injected into the material.

The derivation of Schottky injection is quite involved and will not be reproduced here. An interested reader is directed to Dissado and Fothergill (1992) for the details. It is assumed that some electrons within the electrode arrive at the metal-polymer interface with enough energy to leave the metal surface. These electrons are then injected into the polymer through a thermionic process. The current density due to these injected electrons can be written as

$$J = AT^2 \exp \left[-\frac{\phi - \beta_{sc} E^{1/2}}{kT} \right], \quad (2)$$

where ϕ is the work function of the metal, β_{sc} is the Schottky coefficient, and the pre-exponential term, A , is

$$A = \frac{4\pi q_e m_e k_B^2 (1-R)}{h^3}, \quad (3)$$

where R is the reflection coefficient of the electron at the boundary. This term is typically quite

small and is believed to be sensitive to oxide layers that may develop on the electrode surface (Lewis, 1955). There are two parameters in Schottky injection that need to correspond to physical values in order for it to be verified as a possible charge injection mechanism. The dielectric constant of LDPE can be obtained from the Schottky coefficient, β_{SC} , which can be written as

$$\beta_{SC} = \left(e^3 / 4\pi\epsilon_r\epsilon_o \right)^{1/2}, \quad (4)$$

and the intercept of the linear fit can be used to determine the work function of the electrode metal. Reasonable agreement with accepted values reported in the literature of these two parameters would indicate that Schottky injection is a valid mechanism for LDPE.

Another injection mechanism commonly used is Fowler-Nordheim injection. Schottky injection is a process where an electron gains enough energy to escape the barrier between metal and polymer; Fowler-Nordheim injection builds on the probability that an electron with insufficient energy may tunnel through the barrier. Rather than utilizing a reflection coefficient for the electron, the transmission coefficient, T , is applied to the barrier to determine a tunneling probability, and

$$T = \exp \left\{ - \frac{4}{3} \left(\frac{2m_e}{\eta^2} \right)^{1/2} \frac{(\Phi - E)^{3/2}}{eE} \right\}. \quad (5)$$

The tunneling current density due to injected electrons is then found to be

$$J = \frac{q_e^3 E^2}{8\pi\hbar\phi} \exp \left\{ - \frac{4}{3} \left(\frac{2m_e}{\eta^2} \right)^{1/2} \frac{\phi^{3/2}}{q_e E} \right\}, \quad (6)$$

where ϕ is the work function of the metal, q_e is the charge of the electron, and m_e is the electron mass. Again, the full details of the derivation of Fowler-Nordheim injection are quite involved and will not be reproduced here. The interested reader is directed to Dissado and Fothergill (1992) for details. Unlike Schottky injection, there is no simple plot or relation that can be used

to easily verify Fowler-Nordheim injection. However, this type of carrier injection is expected only to occur at very high fields ($>10^9$ V/m) where the potential barrier at the interface is severely distorted and becomes thin enough to allow tunneling. The applied fields required for Fowler-Nordheim injection would then be well above the observed breakdown strength of LDPE in the range of 10^8 V/m (Dissado and Fothergill, 1992). This discourages further pursuit of this carrier injection mechanism in the present study.

2.2 Conduction Mechanisms of Individual Carriers

Once a charge carrier leaves a trap, regardless of how, there are two primary approaches to the movement of the carrier through disordered solids, which can be represented by percolation theory and dispersive transport. These two mechanisms are related, in a very complex way, to two types of transitions that occur in disordered materials; polymers, in general, exhibit a combination of percolation and dispersive transport. Percolation theory takes advantage of structural disorder, exploiting the idea that a transition occurs that enables long-range connectivity within a material with no long-range order (Zallen, 1983). When percolation is applied to polymers, it typically takes the form of a spatially random resistor network with each link of the network corresponding to the probability of a carrier hop between localized states (Das-Gupta, 1997; Hunt, 1994; Scher and Wu, 1961). Figure 2.3 illustrates a schematic example of a current path through a hopping system corresponding to a random resistor solution. The important feature of any percolation model is the sudden appearance of long-range connectivity at a critical value, typically a critical temperature, T_c (Zallen, 1983). This transition point can often be linked to a physical transition point, such as the glass transition temperature.



FIG. 2.3. Illustration of a random resistor network percolation. This model is most commonly applied to polymer materials. At a critical temperature, T_c , long range connectivity appears along a series of localized states each treated as nodes with a specified resistance between them.

Additional transitions relevant to polymers are localized state to extended state transitions: the Mott transition describes a spatially random distribution of localized states around periodic lattice sites (Mott, 1975; Mott and Davis, 1979) and the Anderson transition describes an energetically random distribution of localized states around a mean energy or trap depth (Anderson, 1958; Böttger and Bryksin, 1985). These transitions would indicate a change in carrier mobility and, in turn, conductivity. Below a temperature, T_c , carriers are restricted to intrachain movement; above T_c the carriers can gain enough energy through phonon interaction for long-range, interchain movement. In theory, this transition should be quite sudden, even first order, but in practice, the wide variety of chain lengths and variability in interconnectivity between crystalline and amorphous regions produces a continuous transition that is difficult to observe (Dissado and Fothergill, 1992; Zallen, 1983).

Both transport mechanisms investigated in the current study can be modeled using percolation theory. Thermally assisted hopping (multiple trapping) can be modeled as spatially random percolation (r-percolation) and variable range hopping (tunneling) can be modeled as spatially and energetically random percolation (r- ϵ -percolation) (Arkhipov *et al.*, 2001; Böttger and Bryksin, 1985; Hunt, 1994).

2.2.1 Poole-Frenkel Conduction

Electric field dependent conduction is of particular interest, where the affects of an applied field would be strong enough to distort the potential well and lower the energy barrier of the trap, effectively decreasing the depth of the trap. An illustration of this effect is seen in Fig. 2.4. One prominent field dependent mechanism often applied to semiconductors and doped polymers is Poole-Frenkel conduction (Das-Gupta, 1997; Poole, 1917; Rakhmanova and Conwell, 2000; Wintle, 1971, 1999). A full derivation will not be reproduced here and the interested reader is directed to Dissado and Fothergill (1992) for a complete treatment.

Formulation of Poole-Frenkel conduction begins with the approximation of localized

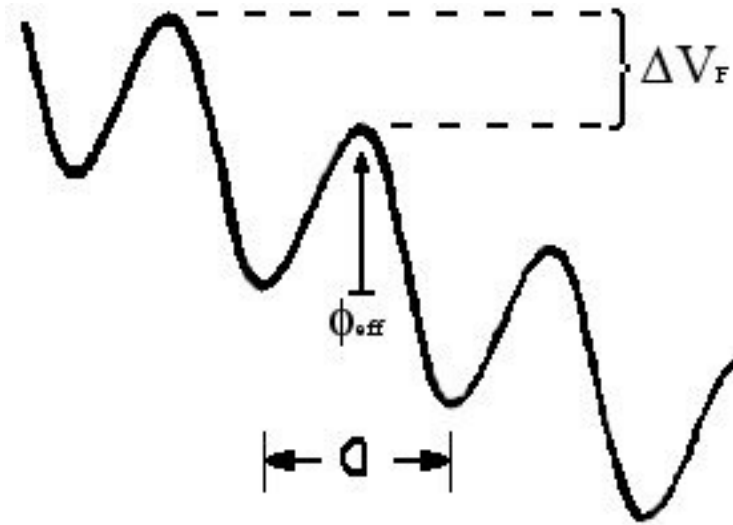


FIG. 2.4. Localized states with distorted potential barriers. The parameter, ΔV_F , represents the change in energy associated with the potential barrier due to the applied electric field.

states as potential wells with average separation, a . Electrons are thermally excited above the barrier of their localized state and into an extended state. The rate of escape of the electron is a function of the density of the occupied localized states (donor states), n_D , the frequency of escape attempts, ν_o , and the effective barrier height, ϕ_{eff} . When an electric field is applied, the barrier height of the potential well is decreased in the field direction, effectively decreasing the trap depth such that

$$\phi_{eff} = \Delta H - \Delta V_F, \quad (7)$$

where the maximum reduction of the barrier height is given by

$$\Delta V_F = -2 \left(\frac{q_e^3 E}{4\pi\epsilon_e\epsilon_r} \right)^{1/2}. \quad (8)$$

The rate of escape of a carrier from a trap is then

$$R_{esc} = n_D \nu_o \exp\left(-\frac{\phi_{eff}}{k_B T}\right), \quad (9)$$

where k_B is the Boltzmann constant. For an equilibrium state, the escape attempt frequency is

$$\nu_o = \frac{k_B^3 T^3}{d h^3 \nu^2}, \quad (10)$$

where d is the number of spatial coordinates available for an electron to move (1, 2, or 3) and ν is the vibrational frequency around the localized state of the electron. The density of empty localized states (empty donor states), N_D , will be much greater than the density of occupied localized states (occupied donor states), n_D , and the density of the conduction electrons is the difference in those densities,

$$n_c = N_D - n_D. \quad (11)$$

The rate of capture will depend on the density of the conduction states, n_c , the density of the unoccupied states, n_D , cross section of the unoccupied localized states, s , and the thermal velocity

of an electron, v ,

$$R_{cap} = n_c(N_D - n_D)v_s = n_c^2 v_s. \quad (12)$$

At equilibrium, the rate of capture will equal the rate of escape and a single expression for the density of free electrons available for conduction can be written as

$$n_c = \left(\frac{n_D v_o}{v_s} \right)^{1/2} \exp\left(-\frac{\phi_{eff}}{2k_B T} \right). \quad (13)$$

Remembering Eq. (1), which gives conductivity in terms of mobility, carrier density, and carrier charge, and expanding the ϕ_{eff} term gives the expected Poole-Frenkel expression for conductivity proportional the electric field,

$$\sigma = \sigma_o \exp\left(\frac{\beta_{PF} E^{1/2}}{kT} \right), \quad (14)$$

where σ_o is the steady state equilibrium conductivity in the absence of an applied field and β_{PF} is the Poole-Frenkel coefficient. The test of its validity is a plot of $\log_e \sigma$ versus $E^{1/2}$, which should produce a straight line with a slope containing β_{PF} if Poole-Frenkel is a viable conduction mechanism. This can be written in terms of the permittivity, ϵ_r , and allows for comparison to the accepted value of the dielectric constant, using

$$\beta_{PF} = \left(\frac{q_e^3}{4\pi\epsilon_o\epsilon_r} \right)^{1/2}, \quad (15)$$

where q_e is the charge of the electron and ϵ_r is the permittivity of free space. Poole-Frenkel conduction is one electric field dependent conduction mechanism that will be investigated in this study.

Poole-Frenkel conduction produces a behavior that is very similar to Schottky charge injection (compare Eq. 4 and 6 with Eq. 14 and Eq. 15), and the two mechanisms are often found to occur simultaneously (Raju, 2003; Wintle, 1999). These two mechanisms are an excellent

example of electrical behaviors that can be very difficult to distinguish experimentally even though they are fundamentally different behaviors. Schottky injection is an interaction between the electrode metal and the polymer that is aided by the lowering of the potential barrier at the interface between electrode and polymer; it is not a true conduction mechanism. Poole-Frenkel conduction is based on thermally released carriers within the polymer aided by the lowering of the potential barrier of a localized state, which is a bulk conduction mechanism. Fundamental assumptions of both Poole-Frenkel conduction and Schottky charge injection immediately limit their applicability to disordered systems and their observation would be unexpected. However, since they are two of the most common conduction mechanisms utilized in both semi-conductors and doped polymers, the extension of these models to an undoped polymer such as LDPE is a necessary step.

With these weaknesses and expectations, particularly the lack of unique behavior that would distinguish Poole-Frenkel conduction from other mechanisms, an alternative field dependent conduction model is necessary. A prominent alternative theory of electric field dependent conduction is space charge limited current.

2.2.2 Space Charge Limited Current Conduction

Space charge limited current (SCLC) behavior can be applied to both low and high fields (Lida *et al.*, 1992; Mott and Gurney, 1940; Qi and Boggs, 2002). To begin determination of space charge limited current behavior, the charges must be injected into the thin film material and uniformly distributed throughout. A cloud of space charge develops as carriers are injected into the polymer and create a localized electric field within the material, preferentially near the electrodes (Montanari *et al.*, 2001; Neagu and Marat-Mendes, 2003). This buildup of space charge diffuses into the bulk as the carriers move away from the electrode, making SCLC sensitive to sample thickness (Das-Gupta, 2002; Dissado and Fothergill, 1992; Wintle, 1983). A

current density equation is written to describe the movement of the carriers, assumed to be electrons, through the material, with three components of carrier motion: conduction, diffusion, and displacement.

$$J = n_c q_e \mu_c E - q_e D_n \frac{dn_c}{dx} + \epsilon_o \epsilon_r \frac{dE}{dt}, \quad (16)$$

where n_c and μ_c are the density and mobility of the electrons, q_e is the charge of an electron, D_n is typically Fick's diffusion coefficient for electrons, and ϵ_o and ϵ_r are the standard permittivity of free space and relative permittivity of the insulator, respectively. Setting $x = 0$ at the cathode and $x = d$ at the anode, where d is the sample thickness; the sample can be treated as an infinite thin film dielectric between two infinite parallel plates. Since the primary focus of this study is the steady-state equilibrium conductivity, the time dependent term can be set to zero, leaving

$$J = n_c q_e \mu_c E - q_e D_n \frac{dn_c}{dx}. \quad (17)$$

Using Poisson's equation

$$\frac{dE}{dx} = \frac{n_c q_e}{\epsilon_o \epsilon_r} \quad (18)$$

gives

$$J = \epsilon_o \epsilon_r \mu_c E \frac{dE}{dx} - \epsilon_o \epsilon_r D_n \frac{d^2 E}{dx^2}. \quad (19)$$

Using the assumption that the carriers uniformly distribute through the bulk in the steady state limit, the diffusion term can be neglected and a constant electric field throughout the dielectric is assumed. This leads to a steady-state approximation for the current density

$$J \cong \epsilon_o \epsilon_r \mu_c E \frac{dE}{dx}. \quad (20)$$

Integrating for electric field, E , with respect to x gives

$$E(x) = \left[\frac{2J}{\epsilon_o \epsilon_r} (x + x_o) \right]^{1/2}, \quad (21)$$

where x_o is a constant of integration assumed to be much less than the thickness of the sample, d . A second integration of the electric field, $E(x)$, with respect to x gives a relationship between the experimental voltage and current density, J .

$$J = \frac{9\epsilon_o \epsilon_r \mu_c V^2}{8d^3}, \text{ for } x_o \ll d. \quad (22)$$

There are two components of the carrier density, n_c ; the electrons intrinsic to the insulator, n_o , and the electrons assumed to be injected from the electrodes, n_i . This leads to two components of the current density

$$J = n_o q_e \mu_c \frac{V}{d} + \frac{9\epsilon_o \epsilon_r \mu_c V^2}{8d^2}, \quad (23)$$

which gives the characteristic regions of SCLC behavior seen in Fig. 2.5.

The first region, labeled region 1 in Fig. 2.5, is linear in E (Ohmic) given by Eq. (1) with the current primarily due to the motion of thermally activated electrons within the bulk. Region 2 transitions to a square law behavior, given by Eq. (22), where the density of the injected electrons is greater than the density of intrinsic electrons and trap-limited SCLC becomes the dominant behavior. As the injected electron density approaches the density of traps, all traps are effectively filled and this allows excess electrons to travel unimpeded. This sharp increase in the current density is shown as region 3, although the distinction between regions 2 and 3 is difficult to observe experimentally. Once all traps are filled, the current density should return to a square law behavior similar to region 2. In practice, electrostatic breakdown in polymers occurs well before this theoretical trap-filled limit is reached, making SCLC difficult to confirm in polymers (Dissado and Fothergill, 1992). SCLC assumes that the free carriers are injected by the electrodes, which leads to conduction that is controlled by the metal-polymer interface. This is in

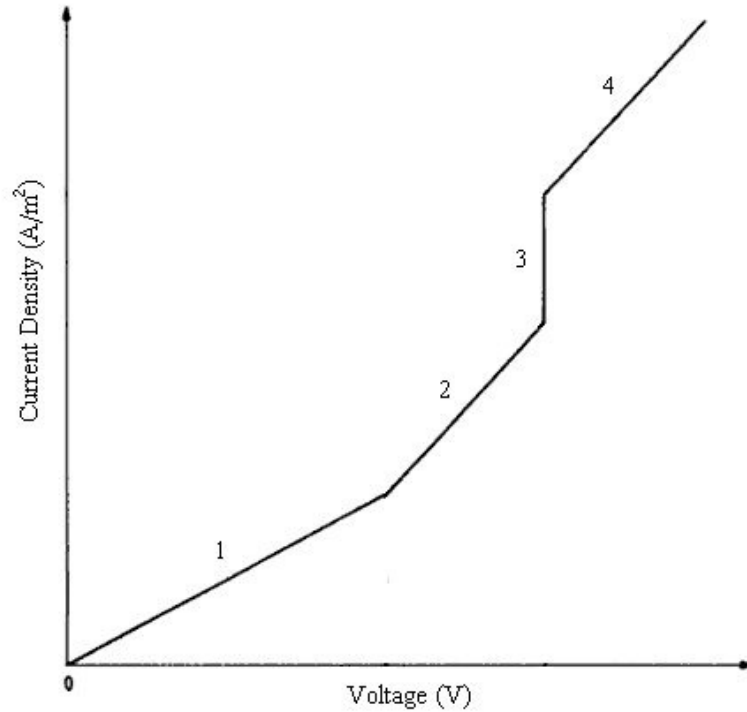


FIG. 2.5. Ideal space charge limited current behavior. Based on a thin film dielectric approximation, SCLC predicts four regions of behavior. Region 1 is Ohmic conduction due to thermally generated carriers. Region 2 is trap limited space charge limited conduction with a square law behavior. Region 3 indicates that all traps at an energy level, E_t , have been filled and there is a sharp increase in conductivity. Region 4 is trap-free space-charge limited conduction with square law behavior.

contrast to Poole-Frenkel conduction, which assumes that the free, excess carriers are already present in the bulk.

2.2.3 Thermally Assisted Hopping Conduction

A promising model of field dependent conduction is thermally assisted conductivity, σ_{TAH} , which can be applied to both low and high fields (Bartnikas, 1983; Böttger and Bryksin, 1985). Like Poole-Frenkel conduction, it is a bulk mechanism that models the movement of individual carriers, assumed to be electrons, through the material. The carriers gain energy through random thermal fluctuations and phonon interaction to escape their localized state and travel in an extended state for a small amount of time before being recaptured by another

localized state. For a complete treatment of the derivation, the interested reader is directed to Bartnikas (1983). Beginning with the expression for the current density involving three components: conduction, diffusion, and displacement, the current density can be written as

$$J = \sigma E + q_e D_o \frac{\partial n_c}{\partial x} + \frac{\partial D}{\partial t}, \quad (24)$$

where D_o is a diffusion coefficient and q_e is the charge of an electron. Again, the assumption for steady state conditions is made, which sets the time derivative term to zero. In addition, the material is assumed to be overall charge neutral, with no net space charge, and the density of electrons remains constant across the thickness of the sample. This reduces the current density expression to the familiar equation,

$$J = \sigma E = n_e q_e \mu_e E. \quad (25)$$

In the absence of an applied electric field, an electron can gain energy through random thermal fluctuations to escape the localized state into an extended state. The probability of escape can be written as

$$\Gamma_o = \nu \exp\left(-\frac{\Delta H}{kT}\right), \quad (26)$$

where ν is a frequency factor and ΔH is the average trap depth.

In a manner similar to the Poole-Frenkel model, the application of an applied field introduces a change in barrier height of the localized state. The energy required to escape the barrier is reduced in the field direction, $-q_e E a$, and increased in the direction against the applied field, $+q_e E a$. The probability of escape of an electron is then the sum of the probabilities of escape in both directions, with the field and against the field,

$$\Gamma(E) = \nu \exp\left(-\frac{\Delta H}{kT}\right) \left[\exp\left(\frac{q_e E a}{2k_B T}\right) - \exp\left(-\frac{q_e E a}{2k_B T}\right) \right], \quad (27)$$

which can be simplified and written as

$$\Gamma(E) = \Gamma_o \left(2 \sinh \left(\frac{q_e E a}{2 k_B T} \right) \right). \quad (28)$$

The term Γ_o is related to the drift velocity and mobility of the electrons, which in turn can be used to obtain an expression for conductivity. Using

$$v_D = \Gamma_o a \quad (29)$$

and

$$\mu_o = \frac{v_D}{E} \quad (30)$$

in combination with the now familiar expression for conductivity, gives an equation for thermally assisted hopping conductivity with electric field dependence that incorporates the physical parameters of average trap depth, ΔH , and average trap separation, a .

$$\sigma_{TAH} = \frac{n_c 2 v_{TAH} a q_e}{E} \exp \left(- \frac{\Delta H}{k_B T} \right) \sinh \left(\frac{q_e E a}{2 k_B T} \right). \quad (31)$$

This expression is neither as simple nor as easily verifiable as either Poole-Frenkel conduction or SCLC. Isolating the electric field dependence and the temperature dependence allows prediction of expected σ_{TAH} behavior for LDPE, shown in Fig. 2.6, where n_c is assumed constant. This assumption of the independence of carrier density on experimental values will be revisited in Section 4.3. Further investigation of thermally assisted hopping conduction is found in Sections 4.1 and 4.2.

2.2.4 Variable Range Hopping Conduction

At low temperatures and for deeper traps, the contribution of thermally assisted hopping conduction model is not expected to be appreciable. Variable range hopping conductivity is a tunneling mechanism that can be applied to a distribution of deeper states where a carrier is unlikely to gain enough energy to leave a trap and promotion to a local extended state is unlikely.

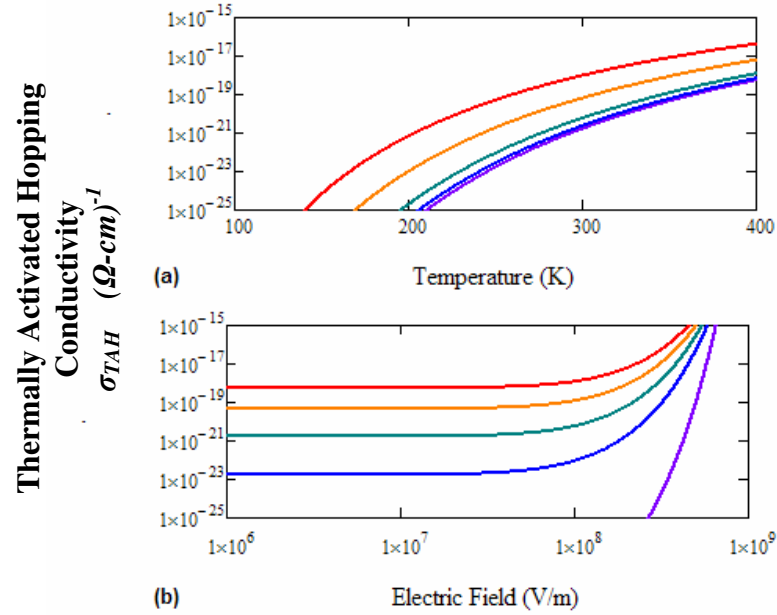


FIG. 2.6. Temperature and field dependence of thermally assisted hopping conductivity. a) Temperature dependence with electric fields of 1×10^7 V/m (purple), 5×10^7 V/m (blue), 1×10^8 V/m (green), 2×10^8 V/m (orange), and 3×10^8 V/m (red). b) Electric field dependence with temperatures of 150 K (purple), 250 K (blue), 300 K (green), 350 K (orange), and 400 K (red). Curves are based on Eq. (32).

σ_{VRH} utilizes these deeper localized states, which contribute less to the overall conductivity of the material but can dominate charge transport at low temperatures. Initially formulated by Mott and Davis (1979), variable range hopping allows for the possibility that a carrier at the Fermi energy level can tunnel to a more distant localized state with a larger energy difference than those of the nearest neighbor states.

A modified mathematical approach from Apsley and Hughes (1974, 1975) allows for a generalized model¹ that results in the same, characteristic $T^{-1/4}$ behavior without the weaknesses of the Mott and Davis derivation. Development of an expression for variable range hopping conductivity, σ_{VRH} , is significantly more difficult than for thermally assisted hopping. Utilizing

¹ Apsley and Hughes use the term hopping to describe the movement of the carrier via quantum mechanical tunneling. This ambiguity will be avoided here as much as possible by using the term tunneling unless referring directly to variable range hopping as a conduction mechanism.

the probabilities of hopping between localized states in three spatial coordinates and one energy coordinate, an average probability of tunneling can be determined for an electron.

Regardless of which formulation is used, Mott and Davis or Apsley and Hughes, a complete derivation of σ_{VRH} is nontrivial and will not be reproduced here. The Apsley and Hughes derivation, which is mathematically preferred, begins by describing the probability of tunneling in a four dimensional space. For a complete treatment of the derivation, the interested reader is directed to the excellent works of Apsley and Hughes (1974, 1975). Conductivity will depend on an average of the probabilities of sequential tunneling events. Using the geometric mean to obtain the probability of this sequence gives

$$\langle P \rangle = \lim_{n \rightarrow \infty} \left[\prod_i^n P_i \right]^{1/n} = \exp \left[\lim_{n \rightarrow \infty} \frac{1}{n} \sum_i^n P_i \right], \quad (32)$$

where P_i is the probability of an individual tunneling event. Apsley and Hughes choose to define a range of the tunneling event, essentially representing the distance traveled in the four dimensional space with equal ranges having equal probabilities. The conductivity is then proportional to a function of the average range traveled by a carrier. Introducing reasonable restrictions on carrier movement can simplify this complex problem, such as the most probable tunneling event occurring between nearest neighbors and in the down field direction in the case of an applied field. This allows the carrier movement to be expressed as mobility rather than a probability. Mobility is a factor of the differences in trap depths between the initial and final localized states, ΔW , the trap separation, $1/r$, as well as a tunneling probability, $\exp(2\alpha\alpha)$, tunneling frequency, ν_{VRH} , and a wave function decay length, α . The problem is then to correlate mobility with distributions of carrier density and energy levels.

After a considerable amount of mathematics, the following expression can be written for variable range hopping conductivity,

$$\sigma(\beta, T) \cong \frac{NkTq_{ph}}{2\alpha E} \left[1 + \frac{P+Q}{P+1} \right] \left[\frac{2}{K(P+Q)} \right]^{\frac{1}{4}} \times \left[\frac{3+\beta}{24(1+\beta)^3} - \frac{1}{8} - \frac{\beta}{3} \right] \exp \left[- \left(\frac{2}{K(P+Q)} \right)^{\frac{1}{4}} \right], \quad (33)$$

where β is the ratio of the energy gained over a tunneling distance to the thermal energy,

$$\beta(E, T, \alpha) \equiv \frac{q_e E}{2\alpha k_B T}, \quad (34)$$

and P, Q, and K are intermediate thermal functions introduced to simplify the notation.

Isolating the electric field dependence and the temperature dependence allows prediction of expected σ_{VRH} behavior for LDPE, shown in Fig. 2.7. Further investigation of variable range hopping conduction is found in Section 4.2. Thermally assisted hopping and variable range hopping are two prominent conduction mechanisms that have been applied to charge transport in

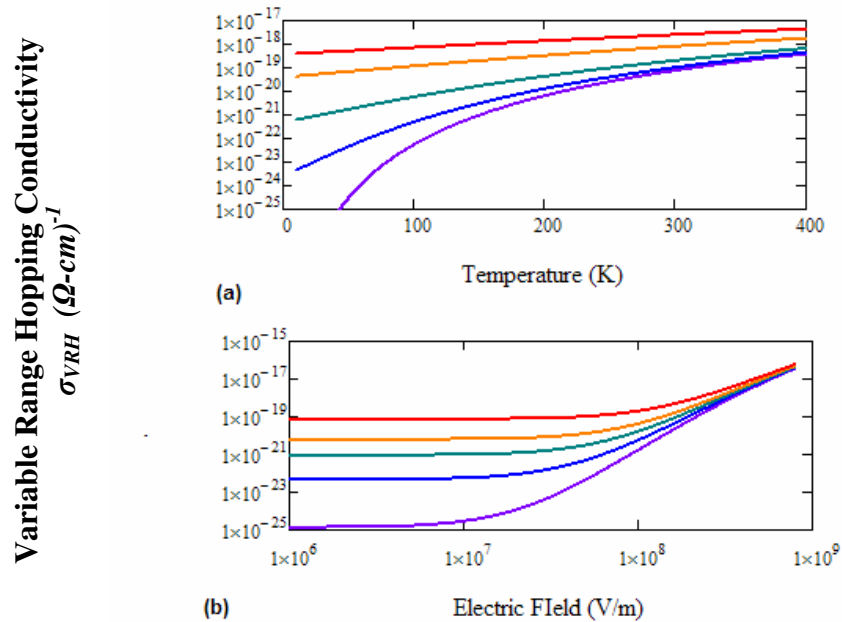


FIG. 2.7. Temperature and field dependence of variable range hopping conductivity. a) Temperature dependence with electric fields of 1×10^7 V/m (purple), 5×10^7 V/m (blue), 1×10^8 V/m (green), 2×10^8 V/m (orange), and 3×10^8 V/m. b) Electric field dependence with temperatures of 50 K (purple), 100 K (blue), 150 K (green), 200 K (orange), and 300 K (red). Curves are based on Eq. (34).

semiconductors and doped polymers with success. Determining if these are viable transport mechanisms in LDPE is the primary focus of this study.

2.3 Conduction Mechanisms of Distributions of Carriers

While the mechanisms by which individual carriers move through a polymer are of primary interest, there are charge transport mechanisms involving the time-dependent propagation or redistribution of spatial inhomogeneities in the charge distribution. This aspect of electrical behavior in polymers has been the subject of much study and debate, particularly with respect to the so-called aging process in high voltage cables (Dang *et al.*, 1996; Griffiths *et al.*, 1998). Unlike many solid materials, i.e. metals and semiconductors, the physical structure of a polymer can change under the influence of an applied field or temperature change and result in a change of mechanical, thermal, and electrical properties. This change can be significant, such as altering the shear modulus of the material (Peacock, 2000), or it may be gradual, such as slow changes in the electrical properties over time. Variation of electrical properties over time remains one of the most elusive polymer behaviors and is not well understood.

A transient conduction mechanism, driven by spatial gradients in the charge distribution, is the diffusion conductivity, σ_{diff} , given by

$$\sigma_{diff}(t) = (q_c D_o / E) \frac{\partial p(t)}{\partial z}, \quad (35)$$

where D_o is a carrier diffusion coefficient, z is the depth of the sample, and $p(t)$ is the time-dependent spatial charge carrier density. For insulators, diffusion can often describe the spread of injected carriers into trapped states within the material. Space charge effects can be significant as traps are filled with injected charge and inhibit further motion of the carriers. Diffusion of particles to lattice sites often leads to a power law model of the time dependence of measured leakage current. This type of conduction often coexists with other acting conduction mechanisms and can make it difficult to accurately determine which mechanisms are present; even normal

transport is not free of diffusive effects.

2.3.1 Dispersive Transport

Another kind of transient conduction, referred to as dispersive transport, is most simply explained as a transition from diffusive transport to equilibrium transport. In normal transport, a pulse or grouping of charge is injected into the material, or existed charges are mobilized, and drift across the sample under the influence of an electric field (Zallen, 1983). This drifting charge creates an observed current through the material and arrives at the receiving electrode with a defined transit time, t_{transit} . Diffusion spreads out the mean position of the pulse or charge group as it travels through the material. In general, shallow traps with a smaller energy difference between the initial localized state and the extended state will release their carriers more quickly than deep traps. This introduces time dependence into the dispersive transport mechanism. The observed behavior of dispersive transport is a continuously decreasing current that extends for long periods of time.

Dispersive transport occurs because of two primary factors: reduction in mobility and reduction in carrier number. As the charges begin to move through the material, the high degree of disorder creates a vast range of microscopic events, each with time dependence, that inhibit the mobility of the individual carriers. The now familiar multiple trapping and tunneling mechanisms are two such types of microscopic events. At very long times, the charges arrive at the receiving electrode and are reabsorbed or immobilized, decreasing the number of available carriers and changing the spatial and energy distribution of the carriers. Dispersive transport is characterized by a distinct transition at the point where carriers begin to arrive at the receiving electrode. At this point, the observed leakage current transitions from the general form of

$$I(t) \approx t^{-(1-\eta)}, \text{ for } t < t_{\text{transit}} \quad (36)$$

to

$$I(t) \approx t^{-(1+\eta)}, \text{ for } t > t_{\text{transit}} \quad (37)$$

with $0 < \eta$. This time-dependent transition was not observed in the LDPE data used for this study and dispersive transport will not be considered as a dominant conduction mechanism at this point. Dispersive transport is commonly observed in complex polymers such as Hytrel™ (Hart *et al.*, 2006).

Both tunneling and multiple trapping can produce dispersive transport behavior, but for different reasons (Zallen, 1983). Hopping, in the case of dispersive transport, refers to direct quantum mechanical tunneling between localized states and is a function of hopping probability; it is enabled by the presence of nearby localized states. Multiple trapping requires a carrier to leave a localized state, move via an extended state, and then be trapped by a second localized state. The time spent in traps is significantly longer than time spent in an extended state and since multiple trapping behavior is a function of trapping time, the nearby trap sites impede carrier mobility.

2.3.2 Polarization

The observation of diffusive behavior may also be attributed to a bulk dielectric response of the polymer material, with a function of relaxation times for the molecules driving the slowly decaying current (Jonscher, 1999; Mort and Scher, 1971). This is commonly attributed to the polarization of the material. At the long time scales of DC measurements, polarization is due to the movement of carriers through the material (Anderson *et al.*, 1990), which creates an internal field that reduces the effects of the applied field. Comparison of the conductivities over repeated charging and discharging cycles is one method of determining the strength and decay time of the polarization response and will be investigated in Section 4.3.3.

Short time currents seen immediately after the applied electric field is introduced can be orders of magnitude larger than final, long time currents. These currents may include a transient

displacement current indicative of free charges moving through the material, the reorientation of molecular dipoles, and the movement of ionic charge from one part of the sample to another. Motion of polarized groups or segments of a polymer chain containing a dipole moment happens quickly after an electric field is applied, with the possibility of releasing charge carriers from nearby localized states as molecules shift. Polymers such as LDPE are considered non-polar, since they lack polar pendant groups or additives, but they still possess a finite dipole moment due to the presence of methyl end groups and double bonds (Amos and Crispin, 1975; Peacock, 2000). The exact origin of dipole moments in LDPE remains unspecified (Peacock, 2000).

In a simple relaxation time model of this charge displacement due to polarization, the conductivity in a parallel plate geometry for a constant applied voltage can be expressed as a time-dependent effective polarization conductivity, σ_p ,

$$\sigma_p(t) = [\epsilon_o(\epsilon_r^\infty - \epsilon_r^o) / \tau_p] e^{-t/\tau_p}, \quad (38)$$

where ϵ_r is the relative dielectric constant of the material and τ_p is the material polarization decay time for the polarization current to decay to 1/e of its initial value. The polarization current, I_p , is then given by

$$I_p(t) = \frac{V_{CV} A \epsilon_o}{d} \left(\frac{\epsilon_r^\infty - \epsilon_r^o}{\tau_p} \right) e^{-t/\tau_p} = I_p^o e^{-t/\tau_p}, \quad (39)$$

where A is the area of the sample, V_{CV} is the applied voltage, d is sample thickness, and the free air capacitance of the sample is $C_o = \epsilon_o A / d$.

The total current as a function of time can then be written as the sum of three components: polarization current, diffusion current, and dark (leakage) current,

$$I_{CV}(t) = I_p(t) + I_{diff}(t) + I_{Leak} = \left[\frac{V_{CV} A \epsilon_o}{d} \left(\frac{\epsilon_r^\infty - \epsilon_r^o}{\tau_p} \right) e^{-t/\tau_p} + q_c D_o A \frac{\partial p(t)}{\partial z} + \frac{V_{CV} A}{d} \sigma_{DC} \right], \quad (40)$$

where

$$I_{DC} = \left(\frac{V_{CV} A}{d} \right) \sigma_{DC} . \quad (41)$$

Here, the dark current conductivity, σ_{DC} , is assumed to be a constant and independent of time, and the applied field E_{CV} (or more conveniently V_{CV}). In the short time limit, the current exhibits exponential decay following

$$I_{CV}(t; \epsilon_r^o, \epsilon_r^\infty, \tau_p) \rightarrow I_p^o(t) e^{-t/\tau_p} , \quad (42)$$

while the diffusive power law behavior dominates at intermediate time scales. In the long time limit, with $t \gg \tau_p$, the current approaches an asymptotic limit equal to the equilibrium dark (leakage) current

$$I_{CV}^\infty(t; \epsilon_r^o, \rho_{CV}) \rightarrow I_{DC} . \quad (43)$$

The latter case is a primary motivation for moving away from the standard ASTM method of determining conductivity. Traditional measurement methods apply an electric field and record a value of current at a set time, typically 1 min. This arbitrary choice of time interval does not take into account any long time behavior, whether due to polarization, dielectric or structural modification, accumulation of space charge, or carrier trapping. Since many high resistance materials commonly used in the space environment are highly polarizable and time is required for a sample to adjust to an applied electric field, conductivity measurements will often continue to change for times well in excess of the standard 1 min settling time period recommended in ASTM D 257-99. The time for the sample to become fully polarized and the so-called absorption current or polarization current to damp toward zero is often tens of minutes, but can exceed hours or even days. Because handbook values are measured using the ASTM standard method, they will have been measured at 1 min and will overestimate the conductivity. The more polarizable the material and the longer the decay time constant for the polarization current, the greater the difference will be between the ASTM D 257-99 measurements and the

long-term limit (Dennison *et al.*, 2006; Frederickson and Benson, 2001). An expression of the ratio of the constant-voltage mode current measured at some time t to the asymptotic limit at long times, I_{DC} , is given by:

$$\frac{\sigma_{CV}(t=T)}{\sigma_{CV}(t \rightarrow \infty)} = \left[\frac{\tau_{DC}}{\tau_p} e^{-T/\tau_p} + 1 \right]. \quad (44)$$

While this discrepancy is more pronounced for materials that are highly polarizable or have long polarization decay times, it cannot be ignored in slightly polar or even non-polar polymers. The influence of even the smallest dipole moment in a non-polar polymer can effect the life cycle and performance of sensitive spacecraft electronics.

For conduction mechanisms involving the redistribution of charge densities, the introduction or injection of charge can be critical. The interface of the polymer and the experimental apparatus has proven to be very important in the distribution and concentration of available charge carriers (Dissado and Fothergill, 1992; Wintle, 1999). A great deal of work has been done to investigate the differences in charge injection that result between electrodes evaporated on the surface of the polymers, solid electrodes pressed against a polymer film, and electrodes with a thin air gap between the metal and polymer surfaces, with inconclusive results.

CHAPTER 3

EXPERIMENTAL DETAILS

To achieve a greater applicability to the electrical behavior of LDPE in the space environment, a high vacuum chamber was developed using commercially available and customized equipment. Experiments were conducted to measure the leakage current through a thin film sample of LDPE under constant temperature and variable applied electric field conditions, as well as constant applied field and variable temperature conditions. Measuring highly resistive materials such as LDPE and other polymers using the constant voltage method requires the ability to measure extremely small currents. This necessitates careful attention to electronic components, interaction between components, noise sources, and laboratory conditions. An overview of the experimental apparatus and of the data that was obtained is contained in the following sections.

Appendices A and B provide more detail on the instrumentation, with additional information found in relevant references (Dennison *et al.*, 2003a, 2003b, 2005a, 2005b, 2006, 2007; Dennison and Brunson, 2008; Swaminathan, 2004). Appendix D catalogues the extensive set of LDPE measurements made by the USU Materials Physics Group, many of which are used in this study.

3.1 Samples and Sample Characterization

Commercial samples of LDPE (Goodfellow, ASTM type I) were obtained with a thickness of $27.4(\pm 0.2)$ μm , a density of 0.92 g/cm^3 , and a crystallinity of 50% (Goodfellow, 2006). Goodfellow also reports an electrostatic breakdown value of $2.7 \times 10^7 \text{ V/m}$ and a resistivity range of 10^{15} - $10^{18} \Omega\text{-cm}$, for $27.4(\pm 0.2)$ μm LDPE. The same mechanism that controls density also controls crystallinity; with the estimated density of 100% crystalline LDPE and 100% amorphous LDPE used to calculate the crystallinity according to the relation in Eq. (45),

$$X_c = \frac{p_c(p - p_a)}{p(p_c - p_a)}. \quad (45)$$

Direct comparison of the conductivity of the LDPE samples obtained from Goodfellow is of limited use, since the Goodfellow values were obtained using the standard ASTM method. This method has been shown to improperly represent the complicated electrical behavior of many polymer materials (Dennison *et al.*, 2003a; Frederickson and Benson, 2001), particularly with respect to spacecraft charging. However, the conductivity range of LDPE reported by Goodfellow is comparable to values commonly found in the literature (Peacock, 2000) and was used to establish an expected range of conductivities. Care must always be taken to evaluate the method and experimental conditions before comparing results from the literature, since the practical limitations of available methods can vary quite significantly.

Samples were cut to size using scissors or razorblades and were not polished, wiped, or ion sputtered prior to any measurements, to avoid damage to the thin-layered structure of the sample. Samples were chemically cleaned with spectral grade methanol to remove contaminants prior to a vacuum bakeout typically conducted at $337(\pm 1)$ K under a pressure of <0.1 mTorr using a cold trapped diffusion pump. The bakeout time was typically longer than 90 hrs and designed to eliminate absorbed water and volatile contaminants that can significantly affect conduction properties. Fig. 3.1 shows details of a typical LDPE bakeout temperature profile. Samples conditioned in this manner were considered dry, as they had a measured outgassing rate of $<0.05\%$ mass loss per 24 hrs at the end of bakeout, as determined with a modified ASTM D 495 test procedure (ASTM D 495). Determination of bakeout time and temperature required to fully condition the samples was obtained using outgassing rate tests performed at the USU Space Dynamics Lab: time to reach the appropriate dryness threshold was found to be ~ 58 hr. Thickness of the samples was verified with a Mitutoyo digital micrometer with a resolution of ± 3 μm . The measured thickness was taken over a surface area of ~ 0.8 cm^2 and the average,

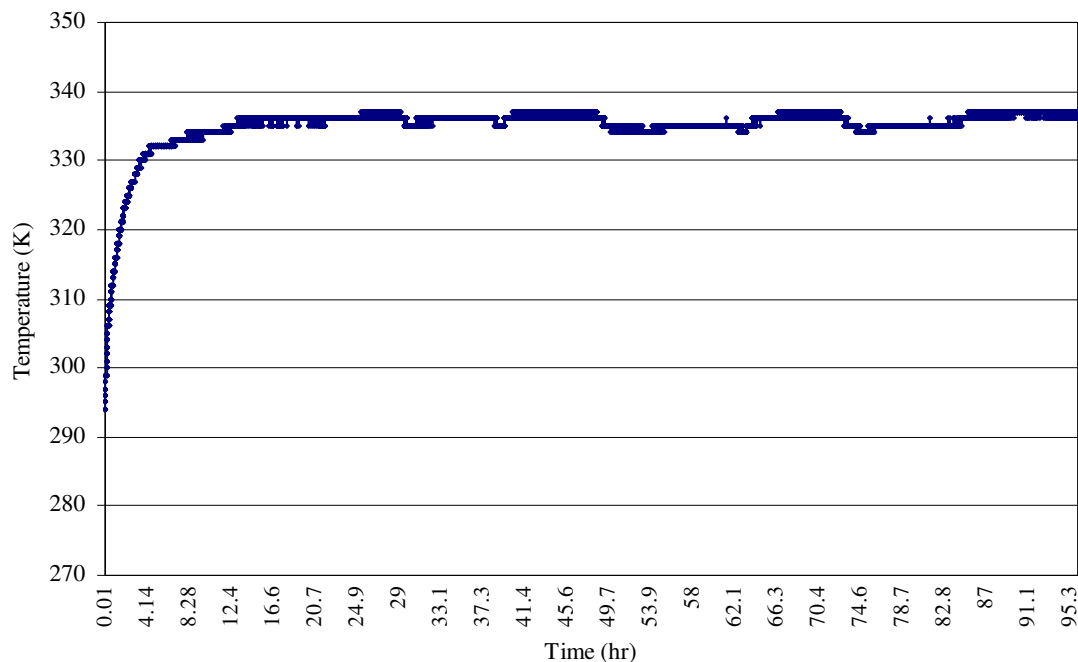


FIG. 3.1. Bakeout profile for LDPE. A typical bakeout profile with a duration of ~93 hrs at $337(\pm 1)$ K. Test criteria for bakeout was a mass loss of 0.05% per 24 hrs, which was found to be reached after ~58 hrs for LDPE. $27.4(\pm 0.2)$ μm .

$27.4(\pm 0.2)$ μm , is used in all calculations and analysis.

Measured sample thickness and mass of a 2.54 cm square sample allowed the calculation of the density to be $0.92(\pm 0.01)$ g/cm^3 , which is in excellent agreement with the manufacturer reported value of 0.92 g/cm^3 . Optical microscopy measurements were taken to study surface roughness, texture, and film imperfections, although the transparency of the samples made it difficult to determine any distinctive features on the LDPE sample surface and impractical to add to a printed document. Over a surface area of approximately 1 mm^2 , the average surface roughness was estimated to be <0.1 μm .

Optical reflectance measurements were taken over the range of photon wavelengths from ~200 nm to 1100 nm (~1.1 eV to 6.2 eV). Uncoated $27.4(\pm 0.2)$ μm LDPE samples were mounted on a bulk colloidal graphite substrate, which absorbs most of the incident light reflected by the

LDPE material. Measurements were made using a grating spectrometer (Ocean Optics, Model HR4000) with a resolution of 0.6 meV (0.75 nm) and 0.2 meV (0.25 nm) data increments. A deuterium/tungsten halogen dual light source was used and the spectrometer wavelength was calibrated using a standard plasma discharge source (Ocean Optics, Model HG-1 Mercury Argon Calibration Source) that produces first order mercury and argon spectral lines from 253-922 nm and second order argon lines to 1700 nm. An aluminum high reflectance specular reflectance standard (Ocean Optics, Model STAN-SSH) was used with a UV-enhanced fiber optic reflectance probe (Ocean Optics, Model R400-7-UV-VIS). Four or more separate spectra were taken at different locations on each sample surface and averaged; a typical example is shown in Fig. 3.2a. These multiple spectra were averaged with no appreciable variations observed between each spectra; a typical residual curve is shown in Fig. 3.2b. Dark current spectra were subtracted from both the average sample spectra and the reflectance standard spectra; the reflectance was determined as the ratio of these differences. The spectra were also adjusted for the known reflectance as a function of wavelength of the specular reflectance standard. Reflectance as a function of wavelength is calculated point wise as

$$R = \frac{[I_{sample} - I_{dark}]}{[I_{stdrd} - I_{dark}] \cdot R_{stdrd}}, \quad (46)$$

with an estimated uncertainty in reflectance of $\pm 5\%$.

The reflectance spectra of LDPE remained approximately constant at 10% over the full wavelength range. This lack of prominent features limits the usefulness of reflectance measurements, which can often be associated with the band gap in the density of states for disordered polymers. Subtle oscillations are seen between approximately 550 nm and 800 nm, which can be explained as a thin film interference pattern. Light is reflected from the air-LDPE interface at the sample surface while light is also reflected from the LDPE-colloidal graphite interface. The two reflected beams interfere constructively or destructively depending on

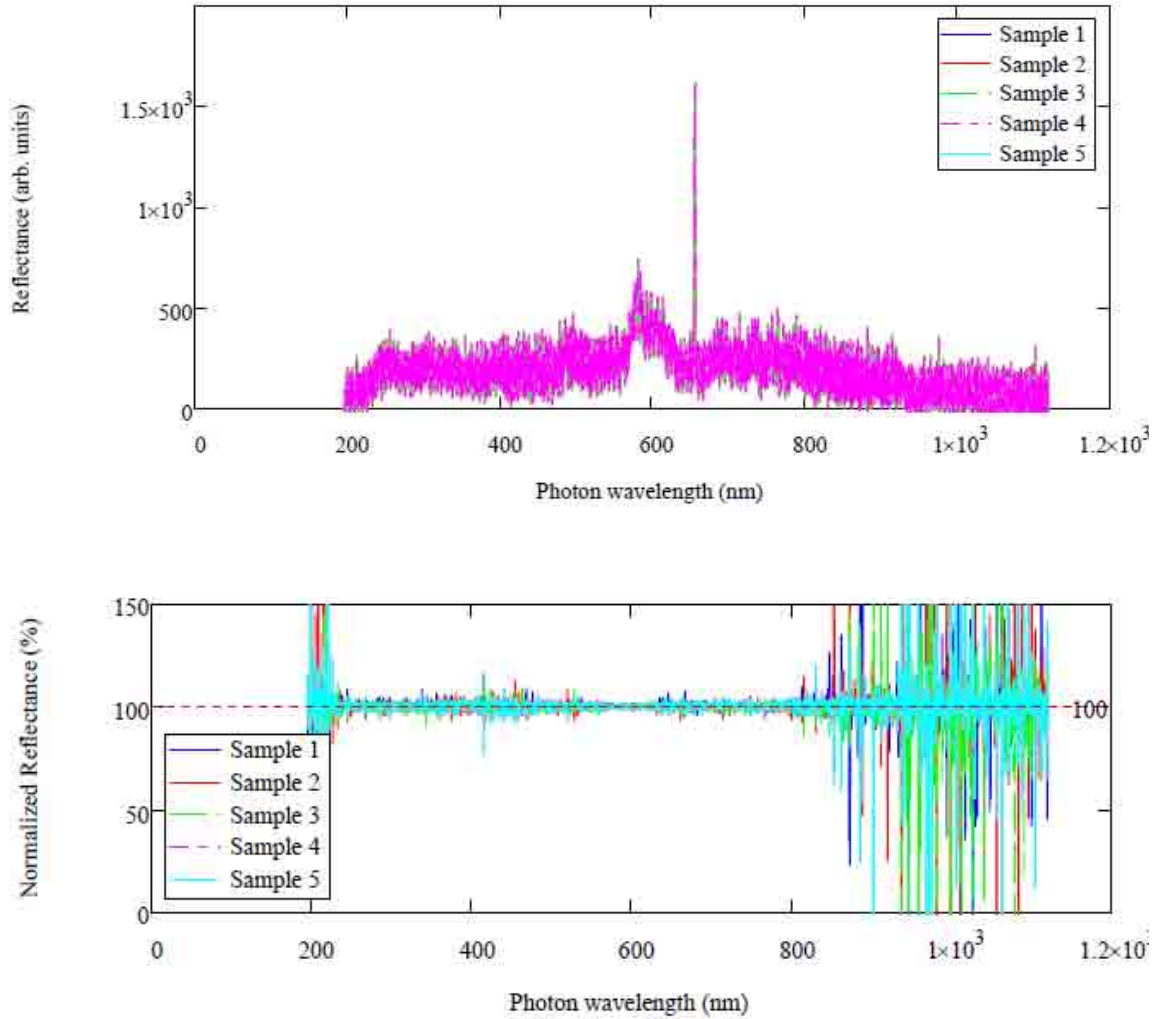


FIG. 3.2. Reflectance spectra of LDPE and residuals. a) Reflectance spectra obtained for 5 samples of LDPE, all $27.4(\pm 0.2)$ μm thick were averaged and b) a typical residual curve of an individual spectrum compared to the average of all curves.

wavelength and film thickness. However, the oscillations are too small and irregular for accurate calculation of the index of refraction of LDPE from the reflectance data. The index of refraction, n_r , given by the manufacturer is 1.51, is in good agreement with values reported in the literature (Peacock, 2000). Fig. 3.3 shows a typical sample reflectance spectrum with both photon energy and wavelength, in both standard axis and semi-log plots.

In addition to reflectance, the transmission spectra of LDPE were also measured with

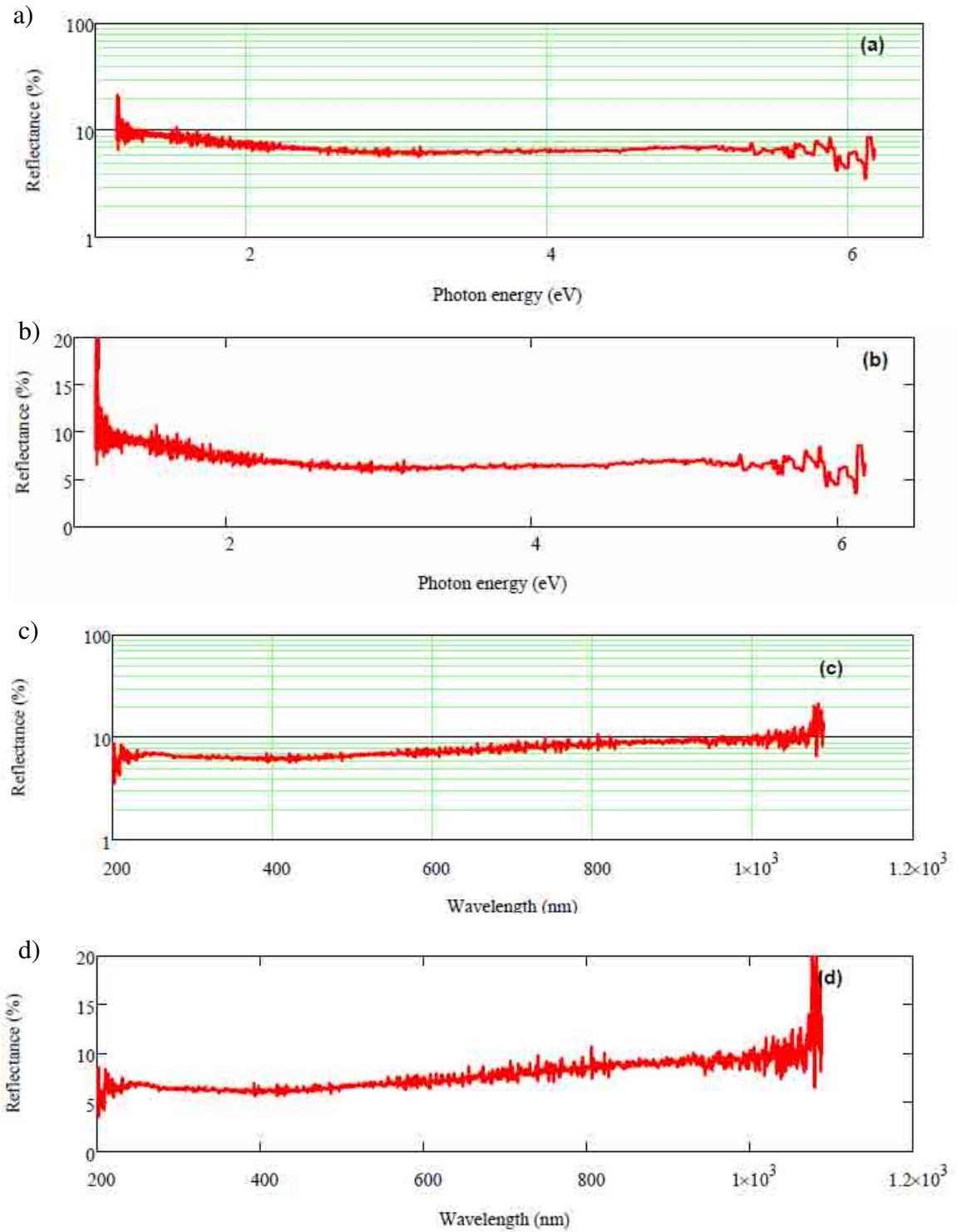


FIG. 3.3. Reflectance of LDPE as a function of photon energy and wavelength. a) Semi-log plot and b) standard axis plot of reflectance of $27.4(\pm 0.2) \mu\text{m}$ LDPE as a function photon energy and c) semi-log plot and d) standard axis plot of reflectance of $27.4(\pm 0.2) \mu\text{m}$ LDPE as a function of wavelength.

results near 100% through the visible spectrum range, which is expected for a very transparent material. Multiple samples were used and the transmission spectra averaged, with the average spectra shown in Fig. 3.4a and a typical residual curve in Fig. 3.4b. These tests all served to characterize the samples and provide more information about the properties of the material, e.g. the lack of an absorption edge implies a band gap energy of > 6 eV.

Electrical parameters are of particular interest, specifically the parameters involved in exposure to an electric field. Every insulator has a limit to the electrical stress that it can withstand, called the electrostatic or dielectric breakdown strength. Electrostatic breakdown field

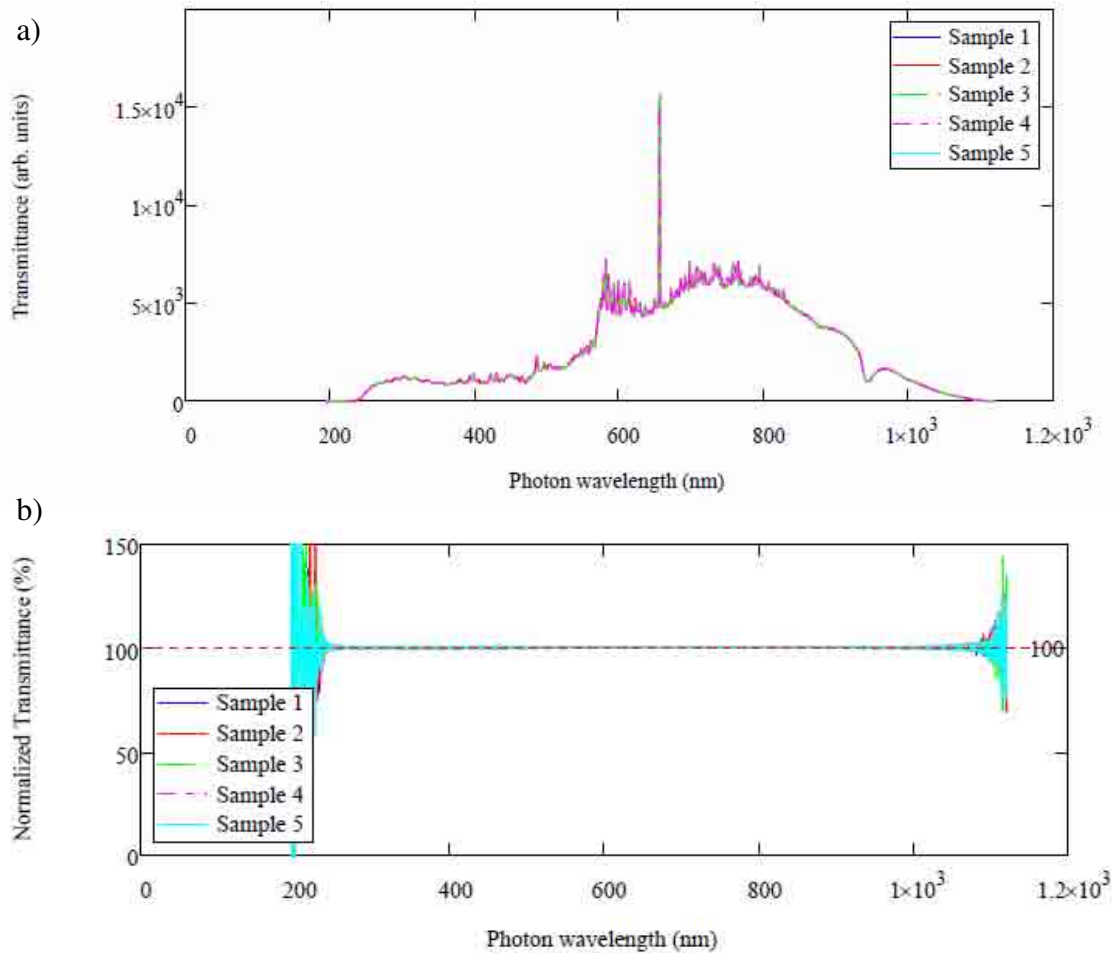


FIG. 3.4. Transmission spectra for LDPE and residuals. a) Transmission spectra for five samples of 27.4(±0.2) μm LDPE were taken and averaged with a b) typical residual curve of an individual sample spectra compared to the average of all the curves.

strength of conditioned $27.4(\pm 0.2)$ μm thick LDPE samples was measured in a separate test chamber to be $2.9(\pm 0.3) \times 10^8$ V/m, using a modified ASTM D 3755 test procedure at room temperature under $<10^{-2}$ Pa vacuum with a voltage ramp rate of a 20 V increase each four seconds (ASTM 3755). A photograph of the ESD chamber developed by the USU Materials Physics Group is shown in Fig. 3.5. A similar test conducted in the constant voltage chamber at a voltage ramp rate of 50 V steps each second found electrostatic breakdown field strength of $2.6(\pm 0.3) \times 10^8$ V/m, which is in good agreement with the more extensive tests in the ESD chamber. The difference between the breakdown strength determined by Goodfellow and the breakdown strength determined using the ESD chamber is attributed to the bakeout process, which eliminates water molecules that could influence conduction and initiate breakdown, and to a difference in voltage ramping rates. Standard ASTM test procedure (ASTM D 257-99) for measuring dielectric breakdown prescribes a ramping rate of 500 V/s, a significantly more rapid rate.

A common parameter in evaluating conduction models in LDPE is the relative dielectric

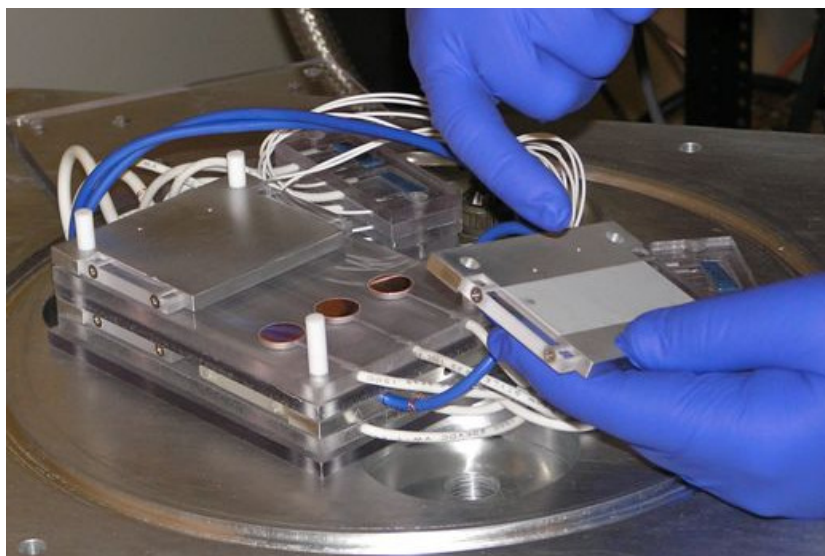


FIG. 3.5. Photograph of inside of ESD chamber. Developed by the USU Materials Physics Group at USU, it uses the same voltage half-plates and sample sizes as the CVC. The ESD chamber is also a vacuum chamber with a temperature range from cryogenic to high temperatures and can test eight samples simultaneously.

constant, ϵ_r . It is more accurately called the relative permittivity, either static or frequency dependent, and serves as a ratio of stored electrical energy. Goodfellow reports a range of 2.25 to 2.35 F/m for the dielectric constant of their LDPE samples at 1 MHz and has been shown to remain approximately constant over a wide range of frequencies, including low frequency measurements (Anderson *et al.*, 1990; Tanaka *et al.*, 1991). This is in agreement with values of the dielectric constant reported for LDPE in the literature (Peacock 2000). The dielectric constant is sensitive to contaminants; in high voltage transmission lines, the LDPE insulation is doped to carefully control the dielectric constant, which also controls the refractive index and optical modes of transmission (Yin *et al.*, 2005). This dependence provides additional motivation for the vacuum bakeout conditioning process and careful sample handling. Additionally, the dielectric constant of LDPE has been shown to be temperature dependent, but the reported values typically remain within the expected range and tend toward a constant after repeated temperature cycles (Tanaka *et al.*, 1991).

3.2 Constant Voltage Chamber

Accurate measurement of the conductivity of highly insulating polymer samples using a constant voltage method with simple parallel plate geometry requires a dedicated, stand alone test chamber. There are basic requirements for such a chamber to obtain adequate measurements. Extremely low currents, down to the femtoamp level, must be measurable, with a highly stable voltage supply capable of the 5 kV range or higher, and a well-controlled sample environment. In this study, the sample environment included high-vacuum conditions, temperature control over the range of 100 K to 375 K, and vibration isolation. Great care must be taken to lower electrical noise and create a sample mount that is easily characterized and reproducible. These technical requirements enable a wealth of data to be taken and, for the sake of practicality, the monitoring and recording of this data and the sample environment must be computer controlled.

3.2.1 Instrumentation Overview

The first incarnation of the constant voltage chamber (Crapo and Dennison, 2002; Takahashi and Dennison, 2005) was a simple metal box containing a stack of copper plates with isolated, copper electrodes that rested against the thin film samples, a voltage input, and ports to attach the chamber to a vacuum system, see Fig. 3.6. This primitive apparatus quickly proved to be catastrophically damaging to the fragile, thin film samples during the course of handling, making accurate measurements impossible to obtain.

Higher precision measurements required development of an entirely new test chamber, which can be seen in Fig. 3.7. Utilizing the stainless steel housing of an electron microscope already equipped with vacuum compatible ports, the copper plate stack from the first CVC was modified and placed inside the chamber; this is shown in Fig. 3.8. The purpose of the plate stack is to provide a versatile, reproducible, and stable configuration to hold samples and make

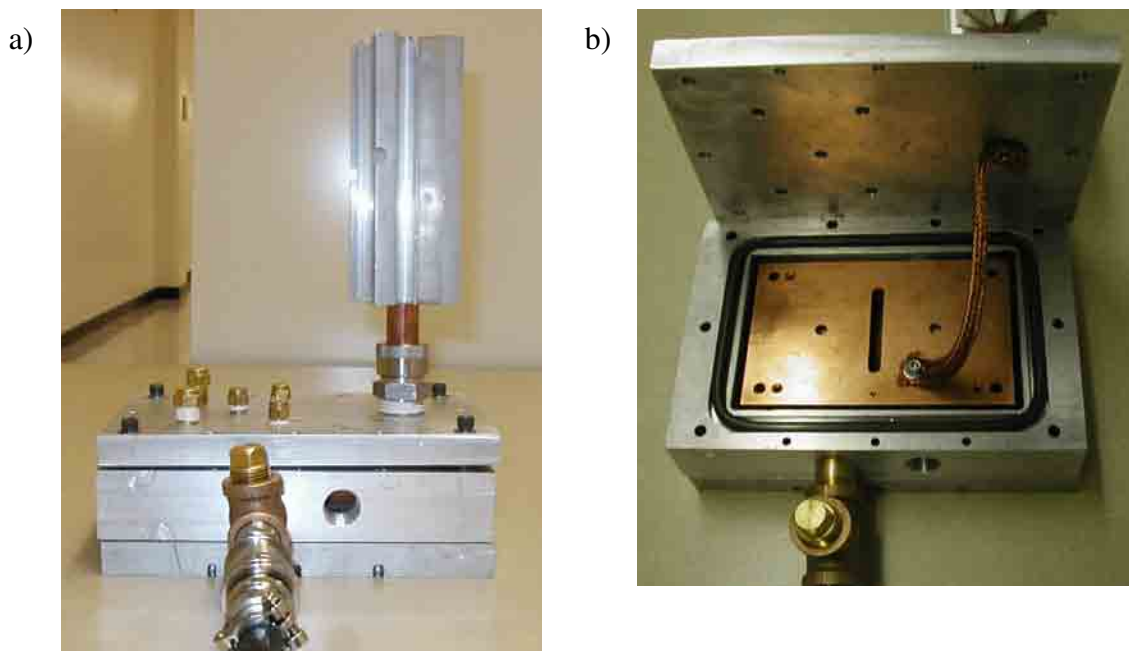


FIG. 3.6. First constant voltage apparatus. a) External closed view with heat sink fin and vacuum valve port attached. b) Inside view with grounding copper braid attached to original copper plate assembly.



FIG. 3.7. Constant voltage chamber. Shown with temperature monitor and one signal triaxial cable attached with vibrational stabilization. For complete details and schematics, see Appendices A, B, and C.

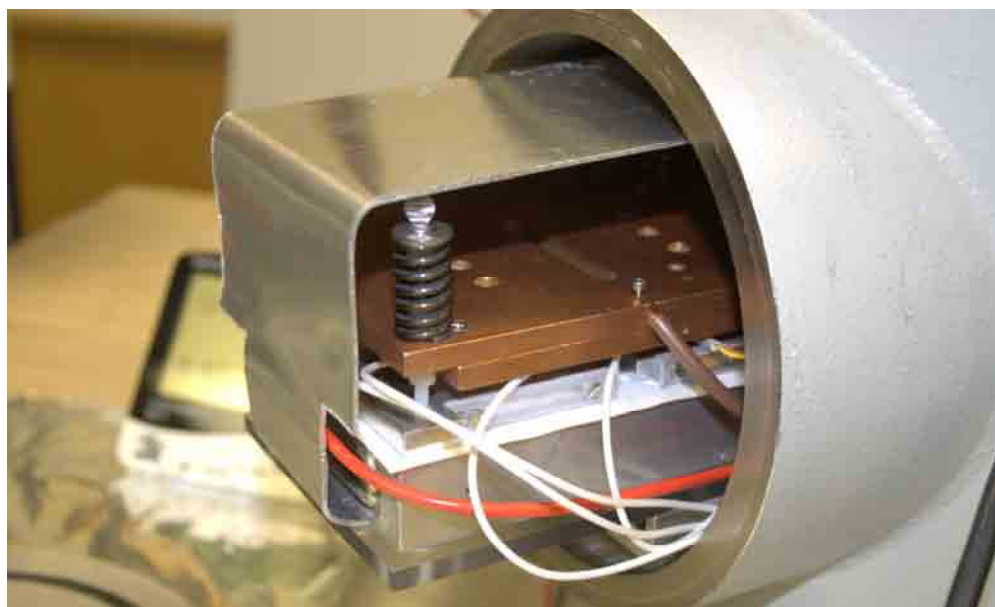


FIG. 3.8. CVC experimental plate stack. Shown with internal radiation shield and spring clamps. Red wires are voltage supply, white wires are coaxial signal wires attached to electrodes. For complete details and schematics, see Appendices A, B, and C.

electrical contacts that limits electrical noise and controls the sample temperature. A polycarbonate base plate electrically isolates the temperature reservoir from the chamber with four polycarbonate posts aligning the stack relative to the polycarbonate base plate. The solid copper voltage plate originally used to hold the samples was replaced with two voltage half-plates, each with polycarbonate clamps to hold the thin film samples in place; an example is shown in Fig. 3.9. Fabricated in both copper and aluminum, the voltage half-plates enabled greater ease in the transfer and rotation of new samples, and allowed for samples of differing thickness to be placed in the chamber at the same time. Each half-plate is attached to a voltage input, with additional holes drilled to accommodate thermocouples for temperature measurements. The cylindrical copper sample electrode disks are isolated from the grounded, copper electrode plate assembly, and are held in place with Teflon bushings and nylon set screws. The electrode plate assembly, shown in Fig. 3.10, surrounds the electrodes with an electrically



FIG. 3.9. CVC voltage half-plate with sample. An aluminum half-plate with corner holes to anchor half-plate to the plate stack, set screw holes to anchor a voltage supply wire and a thermocouple, and polycarbonate side clamps. Shown with a Kapton™ sample for clarity.

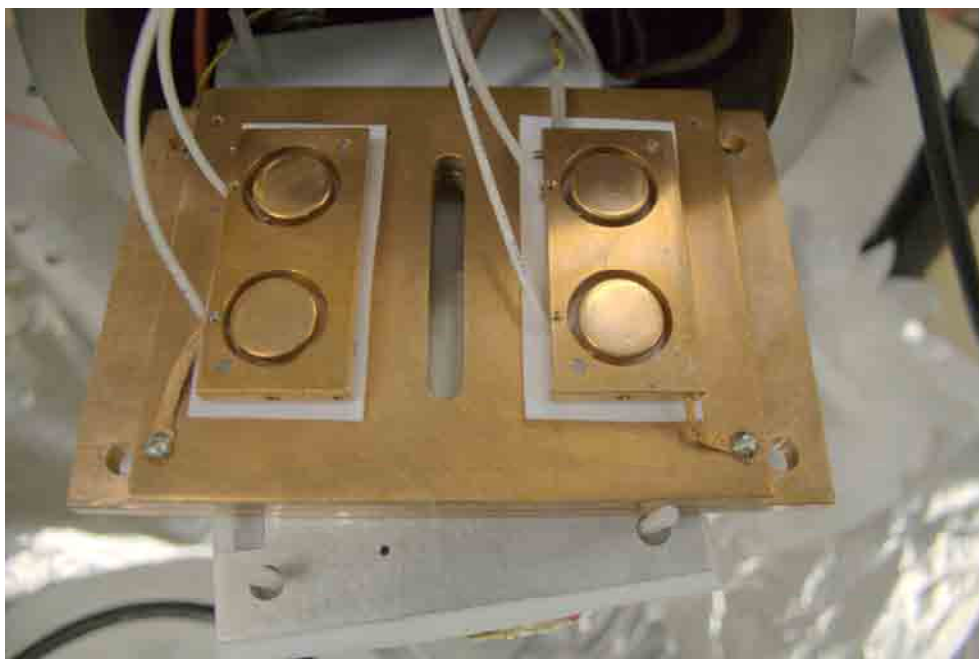


FIG. 3.10. CVC copper electrode plate assembly. The electrode disks are electrically isolated from electrode guard plates and copper anchor plates by a thin layer of Teflon™ and nylon screws. White wires are coaxial signal wires.

isolated guard plate that also stabilizes the delicate, shielded coaxial cables (Belden #83265 009) that carry the signal from the electrodes. The addition of spring clamp mechanisms, seen in Fig. 11, maintains equal pressure of $380(\pm 100)$ kPa of the electrodes against the samples. Details of the electrode spring clamp assembly are found in Appendix A. Two chamber doors were available, one made of stainless steel and another made of polycarbonate. The polycarbonate door was used when visual observation of the plate stack was desirable, particularly when attempting to determine the location of electrostatic discharge events within the chamber.

To achieve greater applicability to the space environment and to limit the effects of the laboratory environment, the CVC was adapted to reach and maintain stable pressures of <0.1 mTorr using a rotary vane mechanical pump (General Electric 5KC36PN435 GX) and a turbomolecular pump (Pfeiffer Balzers TPU-040). A MDC (Model# KMST-152) organic filter was attached to the mechanical pump to prevent pump oil from entering the ultra high vacuum

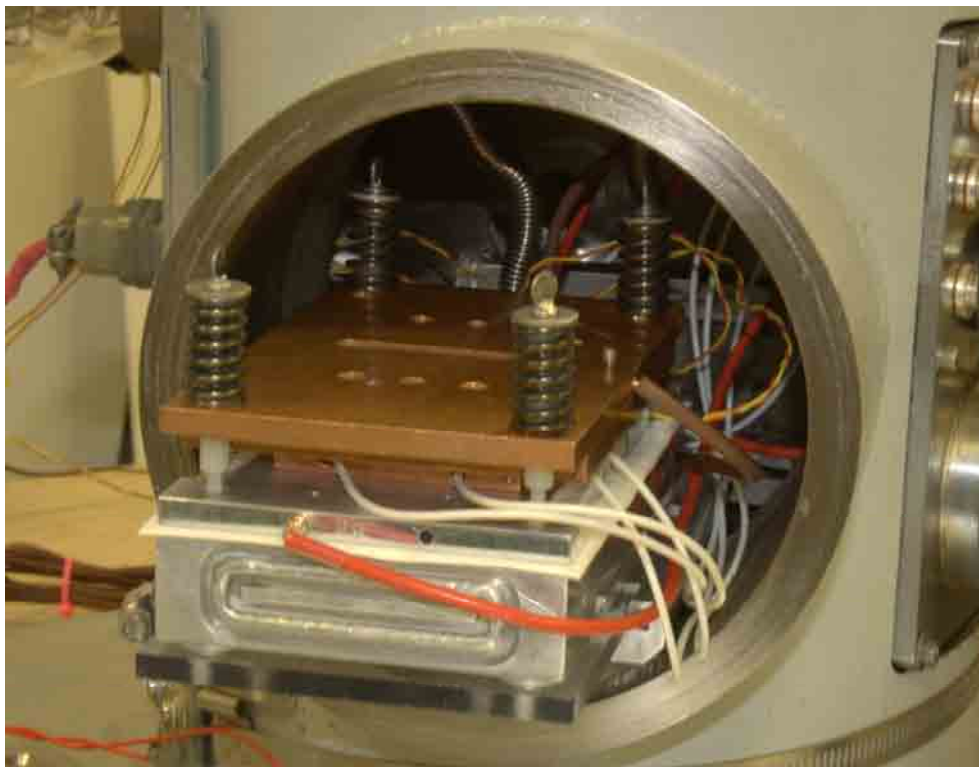


FIG. 3.11. CVC experimental plate stack without radiation shield. Aluminum temperature reservoir is shown at bottom, isolated from the aluminum voltage half-plates by a thin layer of Teflon™. Four spring clamps at each corner maintain consistent pressure on LDPE samples, which are difficult to see due to their transparency. Yellow and red wires attach to ceramic thermocouples in contact with temperature reservoir, a voltage half-plate and an electrode guard plate.

clean pump line and CVC. The pump line was isolated from the CVC with a helium leak tested, high-vacuum valve (Ultek), allowing low pressures to be maintained within the chamber while the pumps were not running. An automatic shut off valve (MKS Vacuum Sentry) was added to prevent loss of vacuum in the event of a power loss. The pump line consisted of 1.5 inch flexible tubing and 2.75 inch Conflat flanges. A vacuum gauge (Granville-Phillips Convectron 275) and controller were attached to the chamber, with a range of 10^3 Torr to 10^{-4} Torr. An additional Bayard-Albert ion gauge and controller have been added with a range of 10^{-4} Torr to 10^{-8} Torr, but were not yet fully functional when this document was written. Copper gasket Conflat seals were used at flange joints and periodically checked for integrity. Joints requiring vacuum

compatible rubber o-rings were periodically checked and greased with vacuum compatible lubricant, including the o-rings for each input port of the CVC. A block diagram of the CVC vacuum chamber and vacuum system is found in Appendix B. All components of the pump line and removable components of the CVC were cleaned prior to use, and as needed, following a prescribed sequence of dichloromethane, acetone, and methanol baths. This eliminated organic contaminants that could prevent high vacuum levels from being reached. The CVC itself was too large and heavy to be placed in a bath, so it was cleaned in place with both acetone and methanol. Another useful addition was a valve port near the vacuum gauge that allowed rapid venting to atmosphere or introduction of another gas, such as dry nitrogen.

Great care was taken to minimize noise in the sample current signal. The vacuum compatible coaxial signal cables attached the sample electrode to BNC vacuum feedthroughs, as shown in Fig. 3.12. Current limiting, thin film metal resistors with a rated value of $10 (\pm 5\%) \text{ M}\Omega$ and 2 mA fuses (Newark #28F060) were added internally, in series, to prevent damage to the external electrometers from surges in voltage or current. Such potentially damaging voltage and current increases are not uncommon during electrostatic breakdown. A shielded metal box provided a transition from the BNC coaxial feedthroughs to triaxial connectors. Shielded triax cables carried the current signal to the electrometers. All cables between the CVC and electrometers were physically stabilized to reduce triboelectric noise caused by movement or vibrations in the laboratory. Extreme care was taken to use proper grounding techniques, avoid ground loops, and route grounds to a central grounding bus. Details of the CVC wiring and grounding are shown schematically in Appendix B. Current is measured over a range of 10^{-6} A to 10^{-15} A using very sensitive electrometers (Keithley, 1975). Manual adjustments were made in the electrometer range and sensitivity during the experiments to optimize the instrument. This adjustment was necessary to record both transient and long time current behavior, which may differ by many orders of magnitude. The electrometers read the leakage current and output a



FIG. 3.12. Coaxial signal wire interface at CVC face plate. The ends of the signal wires are wrapped with heatshrink Teflon™ tubing to protect them from the set screws that anchor them to grounded aluminum caps attached to the faceplate. The wire braid of the wires is grounded through contact with the aluminum caps.

proportional voltage signal that was fed into an analog input channel of a 16-bit data acquisition card (DAQ) (National Instruments), where it is monitored and recorded by a LabVIEW program developed by members of the USU Materials Science Group. A detailed analysis of instrumental errors is given in Appendix C.

Several different power sources were used to provide the applied voltage to the high-voltage plates. These included: (i) a low-voltage 100 V battery source designed to provide a very stable, fixed voltage source, (ii) a medium-voltage supply (Bertan 230-01R) designed to provide stable, variable range voltage, and (iii) one of two high-voltage supplies designed to provide stable, variable range voltage (Acopian P020HA1.5; H.V.T. 25 kV). Both medium-voltage and

high-voltage supplies were set using a programmable input with a low-voltage signal from a 16-bit DAQ analog output. The power supplies output voltages and currents were monitored using DAQ analog input channels and were also recorded by the LabVIEW program. A digital signal from the DAQ controlled by the LabVIEW program was used to enable the output of the supplies and a digital control relay is scheduled to be added to better isolate the line from the analog input signal ground. Schematics of the voltage supply and DAQ wiring are found in Appendix B.

The addition of a temperature reservoir and ceramic encased thermocouples allowed for monitoring of heating and cryogenic conditions during experiment. An aluminum reservoir was built with holes at each corner so that it could be consistently anchored to the plate stack with the polycarbonate rods. Smaller holes were added to accommodate thermocouples. Vacuum compatible flexible metal hoses attach the reservoir to an ultrahigh vacuum feedthrough that allows for fluid to be cycled through the reservoir. Flexible plastic tubing connects to the feedthrough outside the chamber and may be left open to vent to atmosphere. Heavy-duty polycarbonate pipe provides structural strength, protection, and isolation of the temperature feedthrough and tubing. Liquid nitrogen was pumped from a dewar, through insulated tubing, and through the temperature reservoir while a low pressure, ~10 Torr, of nitrogen gas was maintained inside the chamber. The nitrogen gas enhances the thermal transfer from the plate stack to the temperature reservoir. This process was capable of cooling the samples to near liquid nitrogen temperatures of ~90 K. Since the grounded temperature reservoir must be electrically isolated from the high-voltage plate, a Teflon™ film layer was placed between them. Once the low-temperature limit was reached, the nitrogen gas was removed and the voltage was applied to the samples for the duration of the measurements. Control of the temperature within the chamber was obtained by controlling the flow of liquid nitrogen into the reservoir using an Omega temperature controller (iSeries PID) that was connected to the thermocouples within the chamber. This controlled a valve on the liquid nitrogen dewar, turning the flow of liquid nitrogen on and

off as needed to control the temperature. For high-temperature measurements, heating strips capable of reaching 375 K were mounted to the outside of the chamber. Greater technical detail of the apparatus and electronic diagrams can be found in Appendices A, B, and C.

The simplicity of the geometry of the parallel plate capacitor system makes it the standard for electrical measurements and allows for a wide variety of measurements. Primarily limited by the ability of the instrumentation to measure extremely small currents, on the order of 10^{-15} A, it is vital to characterize and minimize electrical noise introduced by electronic components of the system. Even small deviations in the applied electric field produced by fluctuations in the voltage supply can strongly influence the measured current. Physical vibration of the signal cables and thermal fluctuations of the polymer chains can also be read as electrical noise, making it difficult to obtain accurate results (Dissado and Fothergill, 1992). Extreme care was taken in evaluating the interaction of electrical components, including the DAQ used to record the measurements taken by the Keithley 616 electrometers. Careful characterization determined that the entire system, including the chamber and all electrical components, had a total system error in the current measurements of $\pm 5 \times 10^{-15}$ A. This corresponds to an uncertainty in conductivity, at 100(± 1) V, of $\pm 7 \times 10^{-20}$ $\Omega\text{-cm}^{-1}$. A significant portion of this study was the continuing development of instrumentation, including modifications of the chamber and electronic components to improve instrumental resolution. Earlier measurements with greater uncertainty are noted and will be specified when significantly different from these values. Additional improvements have been made recently to further increase the instrumental resolution and the interested reader is directed to Appendix C for details of current error analysis for the CVC.

A National Instruments LabVIEW program was developed to handle data acquisition and automate much of the measurement process, including duration of applied electric fields and measurement of temperature reference points throughout the chamber. During the acquisition of

a single current data point, the LabVIEW program typically acquired and averaged 1000 measurements of the current from the electrometer at a rate of 5 kHz. The LabVIEW program also collected physical information about the sample and the nature of the measurements being taken, such as changes in voltage and duration of measurements. A screenshot of the user interface for the LabVIEW CVC program is shown in Fig. 3.13, and further details of the LabVIEW programs are found in Appendix A.

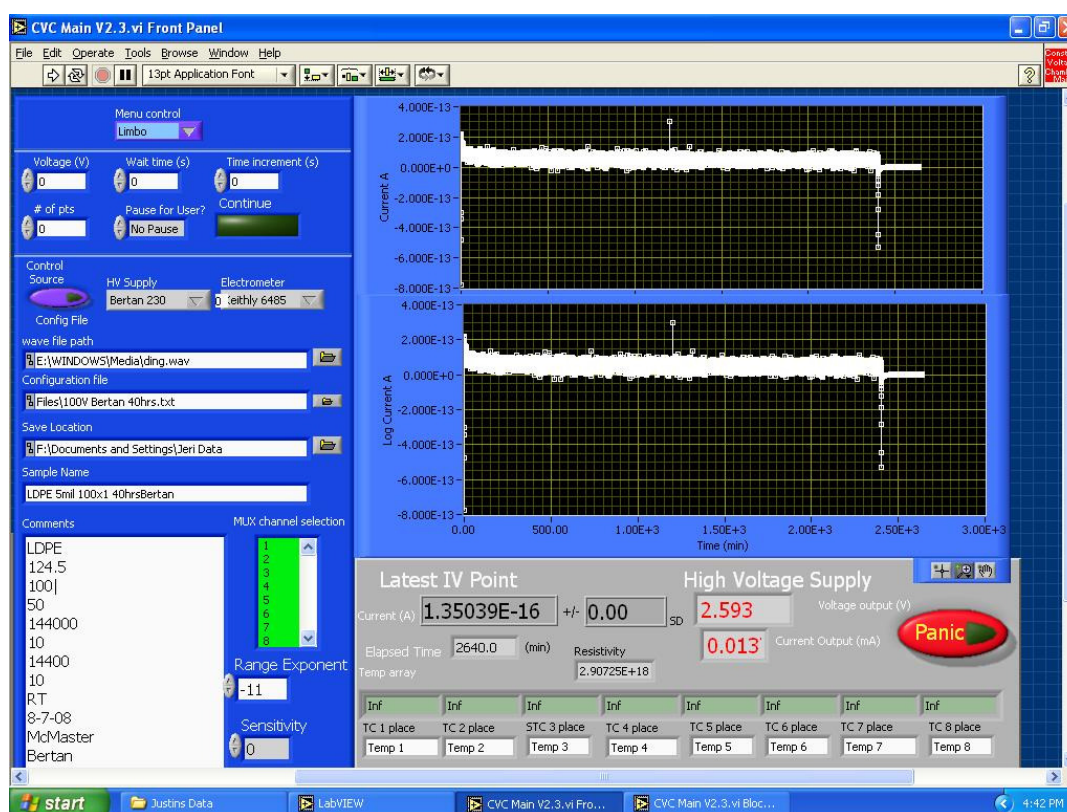


FIG. 3.13. Screenshot of user interface of the LabVIEW program. Real time plots show measured currents versus time. Information recorded includes date, sample type and source, sample thickness, temperature range, voltage ranges, power supply, and additional notes as needed. A panic button immediately turns off any power supply in use.

3.2.2. Applied Field Dependence Measurements

Maintaining the CVC at room temperature and under a pressure of $<10^{-5}$ Torr, many

samples of $27.4(\pm 0.2)$ μm , baked, and chemically cleaned LDPE were subjected to multiple series of applied electric fields and the leakage current through the thin film samples was measured. Samples were subjected to an applied field to determine field dependence of the measured current, typically for one hour, with an equal or greater amount of time following with the applied field removed and the sample grounded. The discharge current following the removal of the applied field was also recorded, although this behavior is not addressed in detail in this study. Behavior of the leakage current was then examined in the short time and long time limits. Additional measurements were taken to focus on the initial response of the material. Samples were exposed to a broad range of electric fields, from less than 1% of estimated breakdown to near breakdown, or in some cases, when breakdown occurred.

Polymers have a significantly different and more complicated electrical response than a conductor or semi-conductor and, due to the dynamic nature of the material, the measured current exhibits several distinct behaviors over time. A single current value will not be obtained. This is one of the challenges in determining the electrical properties of a polymer material.

Typical current measurements can be divided into distinct regions with a sharp initial rise in current followed by an exponential decay of the general form $I = Ae^{-\alpha t}$ that transitions into a power law of the general form $I = Bt^n$. Illustrations of these behavior regions are shown in Fig. 3.14. Each current range setting of the electrometer has a given response time before an accurate measurement can be taken, but even the lowest range used has a response time within the typical range of 1 to 5 sec interval of data acquisition. Response times are listed in Table 3.1. The first 0.5 s of the initial rise in current is assumed to be due to the time required for the voltage supply to the set voltage. Transient behavior is expected due to polarization and reorientation of the polymer chains, but may also be explained using displacement currents and release of carriers from traps. The initial current behavior, often called anomalous current in the literature has been the subject of much debate and is important in understanding polymer behavior (Lindmayer,

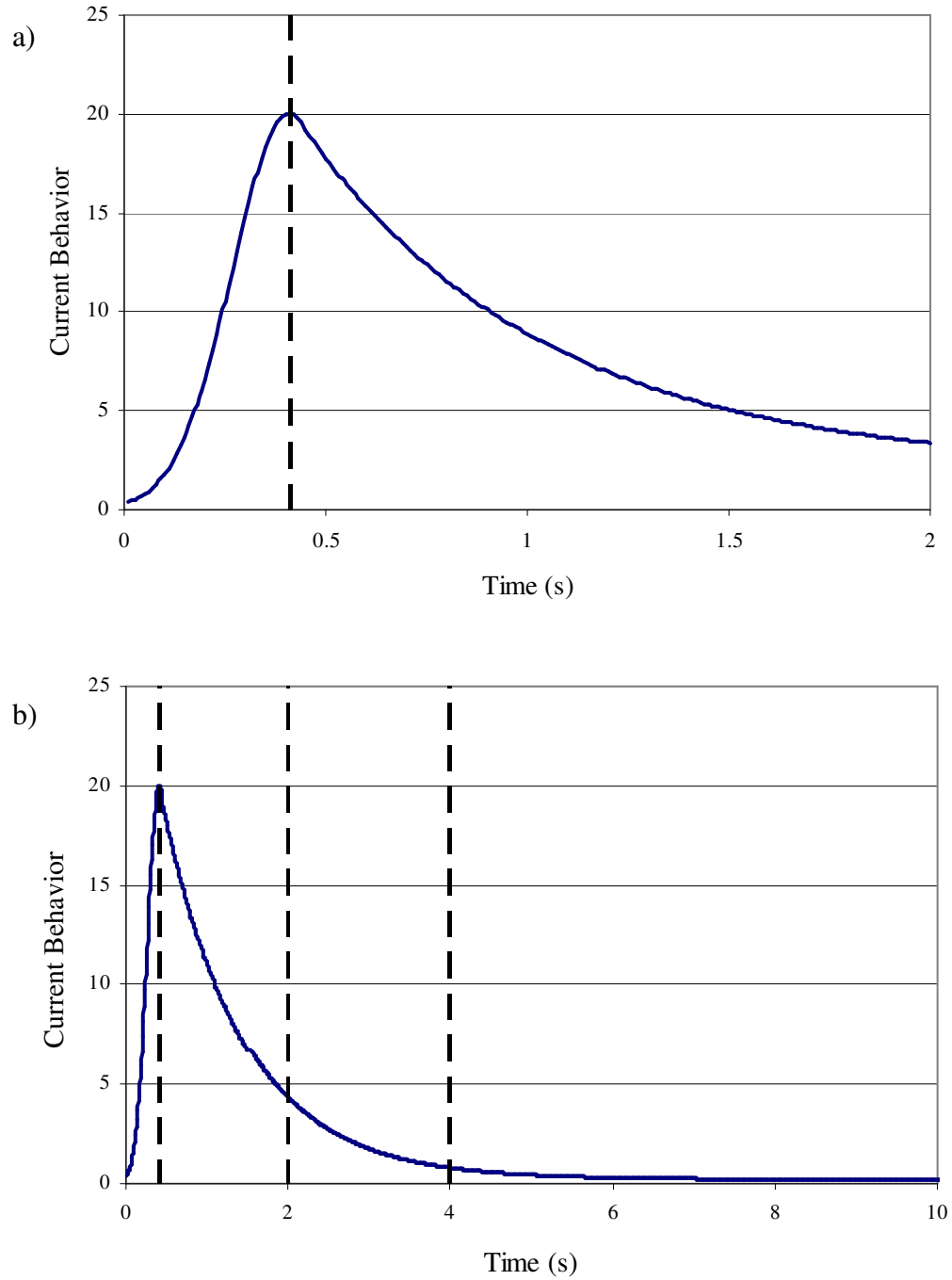


FIG. 3.14. Illustration of regions of observed current behavior. There are four regions of current behavior in a typical measurement of leakage current. a) First two regions are the initial current response of the voltage supply and the material, with a peak current that can be orders of magnitude greater than long time currents. This initial rise is followed by an exponential decay. b) In order from left to right and divided by vertical dashed lines, initial rise and exponential decay followed by a transition region of a blended exponential and power law behavior. The final, long time region is a power law decay behavior.

Table 3.1. Current error and sensitivity of Keithley 616 electrometer. The error in current for the Keithley 616 electrometer is a function of the measured current, I ; the range setting, R ; and the display sensitivity, S . The error for a single current measurement is given by the expression

$$I_{err}(I,R,S)=\{I\cdot\Delta F_{elec}+ \Delta I_{meter}+ \Delta I_{DAC}\}=I\cdot\Delta F_{elec}+R\cdot\{\Delta I_{elec}[1.4-0.4\cdot(3-S)]+ \Delta I_{DAC}\}.$$

Full Scale Current (A)	Mode	Range Setting, R	Sensitivity		Response Time, T _R	Reading, ΔF_{elec}	Errors			
			Setting, S	Voltage			Meter, ΔI_{meter}	Range, ΔI_{elec}	Sensitivity, ΔI_{sens}	Zero drift, $\Delta I_{zero\ drift}$
$<0.0199 \times 10^{-11}$	Fast	10^{-11}	0	10 mV	3 s	5%	$\sim 3 \cdot 10^{-15}$	0.1%	$1 \cdot 10^{-15}$	$2 \cdot 10^{-15}$
$<0.1999 \times 10^{-11}$	Fast	10^{-11}	1	100 mV	3 s	5%	$\sim 6 \cdot 10^{-15}$	0.1%	$4 \cdot 10^{-15}$	$2 \cdot 10^{-15}$
$<1.9999 \times 10^{-11}$	Fast	10^{-11}	2	1 V	3 s	5%	$1 \cdot 10^{-14}$	0.1%	$8 \cdot 10^{-15}$	$2 \cdot 10^{-15}$
$<1.9999 \times 10^{-10}$	Fast	10^{-10}	2	1 V	300 ms	5%	$1 \cdot 10^{-13}$	0.1%	$8 \cdot 10^{-14}$	$2 \cdot 10^{-14}$
$<1.9999 \times 10^{-9}$	Fast	10^{-9}	2	1 V	60 ms	5%	$1 \cdot 10^{-12}$	0.1%	$8 \cdot 10^{-13}$	$2 \cdot 10^{-13}$
$<1.9999 \times 10^{-8}$	Fast	10^{-8}	2	1 V	10 ms	2%	$1 \cdot 10^{-11}$	0.1%	$8 \cdot 10^{-12}$	$2 \cdot 10^{-12}$
$<1.9999 \times 10^{-7}$	Fast	10^{-7}	2	1 V	2 ms	0.5%	$1 \cdot 10^{-10}$	0.1%	$8 \cdot 10^{-11}$	$2 \cdot 10^{-11}$
$.9999 \times 10^{-6}$	Fast	10^{-6}	2	1 V	300 μ s	0.5%	$1 \cdot 10^{-9}$	0.1%	$8 \cdot 10^{-10}$	$2 \cdot 10^{-10}$
$<1.9999 \times 10^{-5}$	Slow	10^{-5}	2	1 V	50 μ s	0.5%	$1 \cdot 10^{-8}$	0.1%	$8 \cdot 10^{-9}$	$2 \cdot 10^{-9}$
$<1.9999 \times 10^{-4}$	Slow	10^{-4}	2	1 V	$<10 \mu$ s	0.5%	$1 \cdot 10^{-7}$	0.1%	$8 \cdot 10^{-8}$	$2 \cdot 10^{-8}$
$<1.9999 \times 10^{-3}$	Slow	10^{-3}	2	1 V	$<10 \mu$ s	0.5%	$1 \cdot 10^{-6}$	0.1%	$8 \cdot 10^{-7}$	$2 \cdot 10^{-7}$
$<1.9999 \times 10^{-2}$	Slow	10^{-2}	2	1 V	$<10 \mu$ s	0.5%	$1 \cdot 10^{-5}$	0.1%	$8 \cdot 10^{-6}$	$2 \cdot 10^{-6}$
$<1.9999 \times 10^{-1}$	Slow	10^{-1}	2	1 V	$<10 \mu$ s	0.5%	$1 \cdot 10^{-4}$	0.1%	$8 \cdot 10^{-5}$	$2 \cdot 10^{-5}$

1965; Lowell, 1990; Scher and Montroll, 1975; Tahira and Kao, 1985; Zallen, 1983). However, the primary focus of this study is the equilibrium conductivity as determined by the long time asymptotic limit of the current.

For long time measurements, the limitations of the experimental equipment become more pronounced, with increasingly small currents leading to measured currents more indicative of the uncertainty of the instrumentation than the true behavior of the sample. Extensive error analysis must be undertaken to separate the instrumental limit from the data. Details of this effort for the CVC and electronic components can be found in Appendix C. The average of the final currents, taken over the last ~10 min, for measurement durations of one hour or more is believed to be an adequate approximation of equilibrium current.

Most measurements were taken in cycles of applied fields with time between each run with no applied field and effective grounding of the samples. These cycles consisted of either increasing (decreasing) applied fields in sequence or as a repeated application of the same applied field. An example of the second case, a repeated application of $500(\pm 1)$ V, is shown in Fig. 3.15.

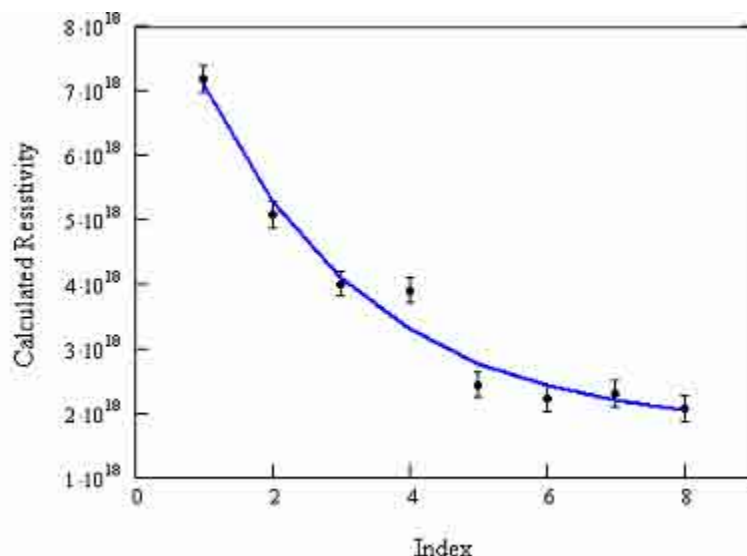


FIG. 3.15. Example of repeated applied field runs. A sequence of eight cycles of applying $500(\pm 1)$ V to a $27.4(\pm 0.2)$ μm LDPE for 1 hr with 1 hr of no applied field with the sample grounded between each run. Note that values shown in figure are resistivity rather than conductivity, which is a more common parameter in spacecraft charging than conductivity.

Ramping rates were typically 50 V/s or smaller. Variable duration measurements were taken with applied field durations ranging from 15 min to 12 hrs. The long time runs were primarily used to establish a cutoff point at which the currents could be considered to have reached equilibrium. This cutoff point is influenced by the applied field, but for the range of applied fields used in the CVC, 30 V to 4300 V, the estimated time of 1 hr was deemed to be sufficient.

3.2.3 Temperature Dependence Measurements

To determine temperature dependence of conduction in LDPE, two phases of measurements were obtained. The temperature range of conductivity measurements for LDPE considered in this study was limited the working range as giving by Goodfellow (2006), which is approximately 210 K to 360 K. Although low-temperature measurements were taken down to approximately 150 K, only the data obtained above the lower bound of the working temperature range was considered here. This restriction avoided anomalous behavior due to structural or phase transitions, including the glass transition,, which occurs between 140 K and 160 K for LDPE, as reported in the literature (Goodfellow, 2006; Peacock, 2000). Upper limit working temperatures for LDPE according to available literature, where typical behavior can be reasonably expected, range from 320 K to 360 K. Above this temperature range, behavior can be unpredictable and approaches the melting point of the polymer at approximately 380 K.

For low-temperature measurements, a significant amount of time was required to cool the samples and chamber and allow them to come to equilibrium. While the liquid nitrogen was being pumped into the temperature reservoir within the chamber, the physical movement of the reservoir made it impossible to record accurate data. Once the samples and chamber reached steady equilibrium at the desired temperature, the liquid nitrogen was shut off and an electric field was applied. The leakage current was measured as the sample and chamber returned to room temperature without intervention or artificial heating. The average rate of heating for the chamber and sample returning to room temperature over the relevant temperature range was ~0.1

K/min. A plot of the measured temperatures during the gradual heating process is shown in Fig. 3.16.

High temperature measurements were taken using the resistance heating strips attached to the chamber to slowly increase the temperature of the chamber and samples. Once the desired temperature was reached, approximately 360 K, the chamber and sample were then allowed to return to room temperature without aid, with an average rate of temperature change over the heating cycle of $\sim 0.10(\pm 0.05)$ K/m. A plot of the measured temperatures during the gradual heating process is shown in Fig. 3.17 and a plot of the rate of temperature change over the entire range of temperatures is shown in Fig. 3.18.

Leakage currents were extremely sensitive to heating and cooling rates, which were most difficult to control at the high- and low-temperature limits and points of transition between high- and low-temperature measurements. Charge carriers are released by increasing thermal energy,

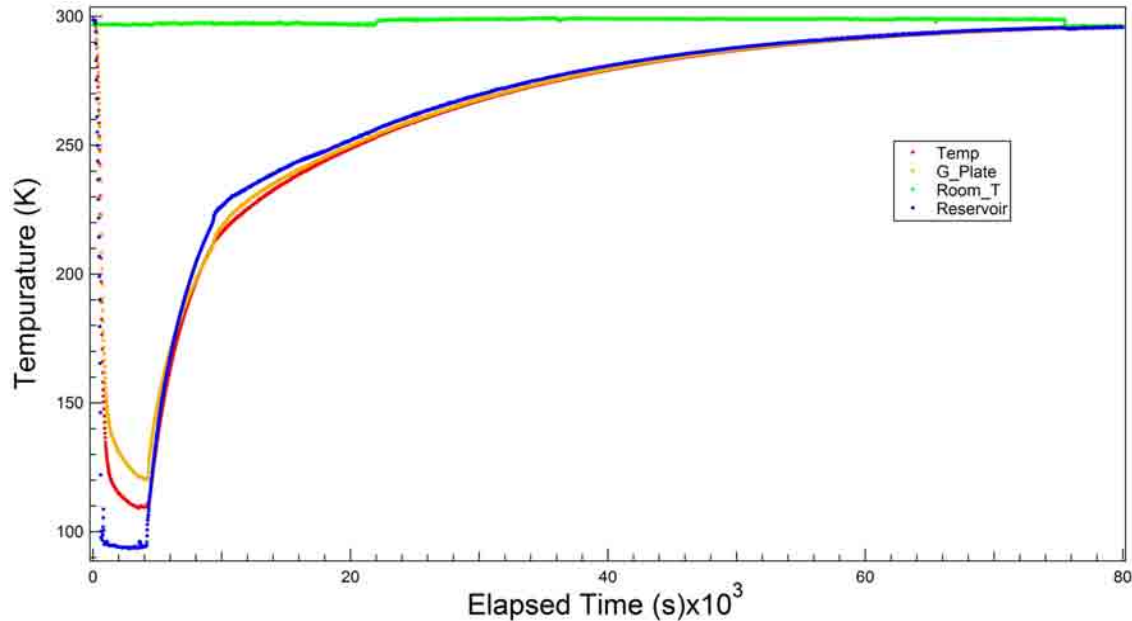


FIG. 3.16. Temperature vs time plot for cryogenic region. Room temperature in the laboratory is shown in green. Time duration was ~ 22 hrs for CVC and samples to rise from low-temperature equilibrium to room temperature.

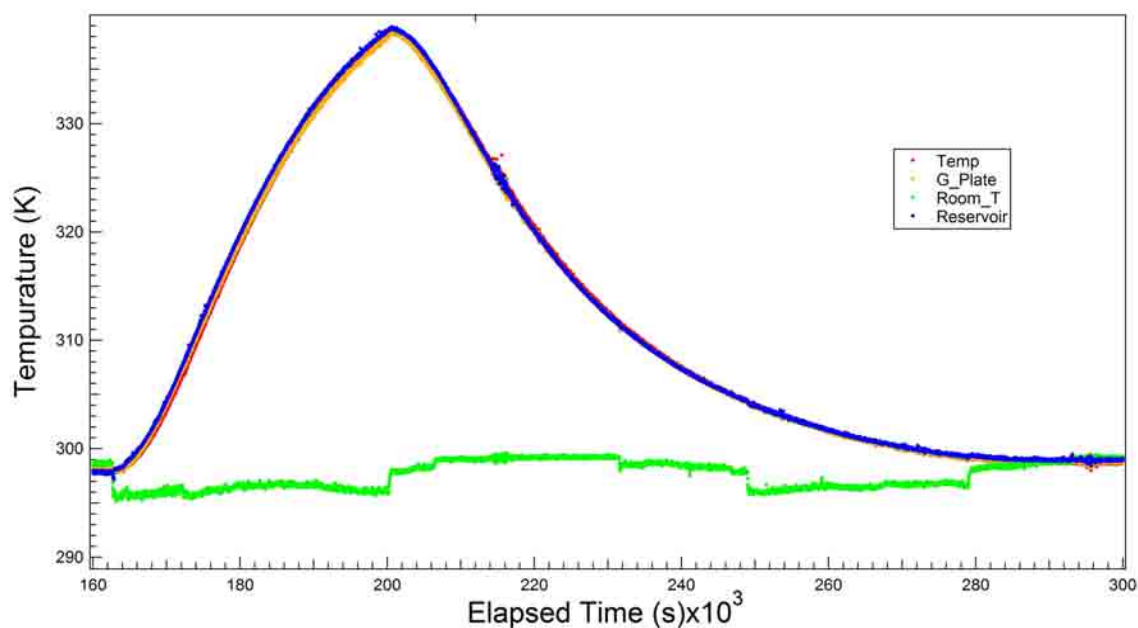


FIG. 3.17. Temperature vs time plot for high-temperature region. Room temperature in the laboratory is shown in green. Time duration was ~83 hrs for CVC and samples to rise to peak temperature and return to room temperature.

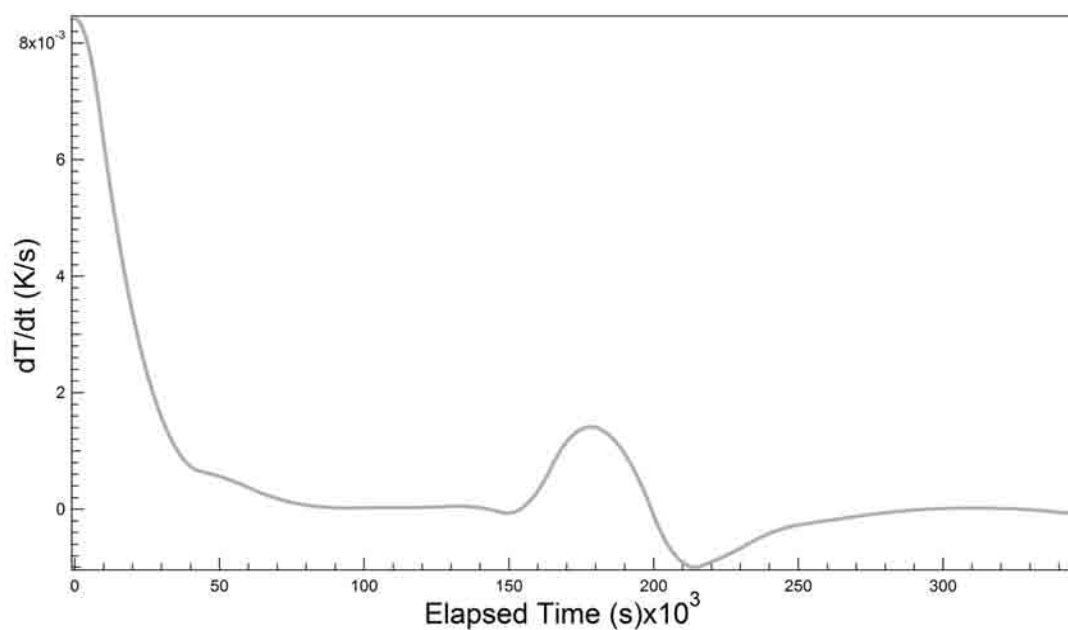


FIG. 3.18. Change in temperature rates over full temperature range. Regions of primary interest are those with the lowest rates of temperature. Time duration for cryogenic and high temperature runs is typically three to four days.

either through the release of stored space charge or relaxation of polymer molecules, in a way that is difficult to predict and quantify. Changing temperatures have also been linked to structural changes of the polymer molecules beyond the expected phase transitions. These structural transitions cannot be avoided even with well-controlled heating rates and can be difficult to positively identify. However, with a suitably slow rate of temperature change, it can be reasonably assumed that leakage currents approach equilibrium and allow calculation of steady state conductivity. Evaluation of temperature dependent conductivity then must also include an inspection of heating rates. Very little work has been done to investigate the influence of the rate of temperature change on conductivity and the rate of temperature change is often unspecified. The reported rates available in the literature range from 18 K/min to 2 K/m (Aranguren *et al.*, 2003; Boudou and Guastavino, 2000; 2002; Dang *et al.*, 2003). The average rates of change in this study were typically $<0.10(\pm 0.05)$ K/min, which represents a significant improvement in reducing the influence of the temperature change rate, and were deemed acceptable for the assumption of equilibrium currents.

3.3 Summary of Measured Data

Each data set taken was carefully evaluated to determine whether or not it could be used to further analysis of the LDPE samples. Any data sets with known technical difficulties or user error were not used in this analysis. The data determined to be viable for analysis is summarized in the following sections.

3.3.1 Summary of Electric Field Dependence Data

Over the course of this research, more than 500 hours of data were obtained under constant temperature and constant voltage conditions. A set of 81 constant temperature measurements for $27.4(\pm 0.2)$ μm LDPE are used in this study, spanning the range of applied voltages from $30(\pm 1)$ V to $4500(\pm 1)$ V. This represents less than a third of the more than 300

data sets taken by the USU Materials Physics Group over the past five years. Many of the unused data sets were discarded due to technical and experimental problems with the CVC or electronic components. These problems include significant interference in the measured signal from a voltage supply or other electronic source, premature electrostatic breakdown, vacuum gasket failure, disconnected cables, difficulty with the LabVIEW data acquisition and control program, and more. More than one dozen samples were used in the process of acquiring the data sets used in analysis. Since the overall behavior of LDPE as a polymer is the goal of this work, results from individual samples are not treated separately. Where there were significant differences between samples, it will be noted with possible explanation. A summary of the measured data used in this analysis is shown in Table 3.2. For a complete summary of LDPE data taken by the USU Materials Physics Group, the reader is directed to Appendix D.

3.3.2 Summary of Temperature Dependence Data

With a greater degree of technical difficulty and much longer times required for temperature dependent measurements, fewer data sets were obtained. Out of more than a half dozen temperature runs, only three sets of complete measurements are used in this analysis: 100(\pm 1) V, 1000(\pm 1) V, and 2500(\pm 1) V. The runs selected were those with the lowest amount of experimental error, the most consistent rates of temperature change over the relevant range of temperatures, and those that could serve as a broad representation of applied electric field. A summary of the measured data used in this analysis is shown in Table 3.3. For a complete summary of LDPE data taken by the USU Materials Physics Group, the reader is directed to Appendix D.

3.3.3 Summary of Electrostatic Discharge Measurements

The ESD chamber uses parallel plate capacitor geometry, much like the CVC, but was designed to reach much higher applied fields, measure much higher currents, and test multiple

Table 3.2. Summary of applied field data used in analysis. Data sets are indexed by voltage and were taken using more than one dozen samples. Conductivity is calculated over final ~10 min of each data set.

Index	Voltage	Electric Field (V/m)	Repeated	Eq. Conductivity
1	30	1.18×10^4	1x	3.67×10^{-19}
2	70	2.76×10^4	1x	2.41×10^{-19}
3	100	3.94×10^4	2x	1.04×10^{-18}
4	140	5.51×10^4	1x	2.14×10^{-19}
5	200	7.87×10^4	2x	1.14×10^{-18}
6	250	9.84×10^4	1x	4.27×10^{-19}
7	280	1.10×10^5	1x	6.23×10^{-19}
8	300	1.18×10^5	1x	3.22×10^{-18}
9	340	1.34×10^5	1x	6.04×10^{-19}
10	400	1.57×10^5	1x	4.60×10^{-19}
11	410	1.61×10^5	1x	6.06×10^{-19}
12	480	1.89×10^5	1x	6.64×10^{-19}
13	500	1.97×10^5	15x	1.09×10^{-18}
14	550	2.17×10^5	1x	7.13×10^{-19}
15	600	2.36×10^5	1x	9.62×10^{-19}
16	620	2.44×10^5	1x	7.31×10^{-19}
17	690	2.72×10^5	1x	7.37×10^{-19}
18	700	2.76×10^5	2x	9.99×10^{-19}
19	750	2.95×10^5	1x	1.01×10^{-18}
20	760	2.99×10^5	1x	7.56×10^{-19}
21	800	3.15×10^5	1x	1.27×10^{-18}
22	830	3.27×10^5	1x	7.61×10^{-19}
23	900	3.54×10^5	2x	9.94×10^{-19}
24	1000	3.94×10^5	7x	1.41×10^{-18}
25	1200	4.72×10^5	1x	1.34×10^{-18}
26	1250	4.92×10^5	1x	1.09×10^{-18}
27	1300	5.12×10^5	1x	1.89×10^{-18}
28	1500	5.91×10^5	2x	2.00×10^{-18}
29	1700	6.69×10^5	1x	1.31×10^{-18}
30	1750	6.89×10^5	1x	3.63×10^{-18}
31	1900	7.48×10^5	1x	2.53×10^{-18}
32	2000	7.87×10^5	1x	1.94×10^{-18}
33	2100	8.27×10^5	1x	2.77×10^{-18}
34	2250	8.86×10^5	2x	3.88×10^{-18}
35	2300	9.06×10^5	1x	3.15×10^{-18}
36	2500	9.84×10^5	3x	4.26×10^{-18}
37	2700	1.06×10^6	1x	4.59×10^{-18}
38	2750	1.08×10^6	2x	6.13×10^{-18}

39	2900	1.14×10^6	1x	5.31×10^{-18}
40	3000	1.18×10^6	2x	8.39×10^{-18}
41	3100	1.22×10^6	1x	6.84×10^{-18}
42	3250	1.28×10^6	1x	2.38×10^{-17}
43	3300	1.30×10^6	1x	9.23×10^{-18}
44	3500	1.38×10^6	2x	2.40×10^{-17}
45	3700	1.46×10^6	1x	1.66×10^{-17}
46	3900	1.54×10^6	1x	2.25×10^{-17}
47	4100	1.61×10^6	1x	2.88×10^{-17}
48	4300	1.69×10^6	1x	2.96×10^{-17}
49	4500	1.77×10^6	1x	5.85×10^{-17}

Table 3.3. Summary of temperature data used in this analysis. Time duration for a typical temperature run was three to four days.

Voltage	Electric Field (V/m)	Temperature Range	Ave. ΔT (K/min)
100	3.94×10^4	107 K - 338 K	0.05
1000	5.91×10^5	180 K – 288 K	0.01
2500	9.84×10^5	110 K – 348 K	0.12

samples at a time. It is maintained at a pressure of $<10^{-5}$ Torr and is capable of temperature ranges from 120 K to 375 K. The breakdown values obtained were at a ramping rate of 20 V over approximately 4 seconds, taking into account an experiment lag time in the voltage supply control. The observed breakdown values according to applied electric field for $27.4(\pm 0.2)$ μm LDPE are shown in Fig. 3.19a. The temperature dependence of LDPE breakdown was also explored; a plot of temperature and breakdown data is also shown in Fig. 3.19b, with an uncertainty of 13% at each temperature. As seen in the plot, the electrostatic breakdown of $27.4(\pm 0.2)$ μm LDPE is independent of temperature. Table 3.4 and Table 3.5 provide a numerical summary of the electrostatic breakdown of LDPE over the range of temperatures.

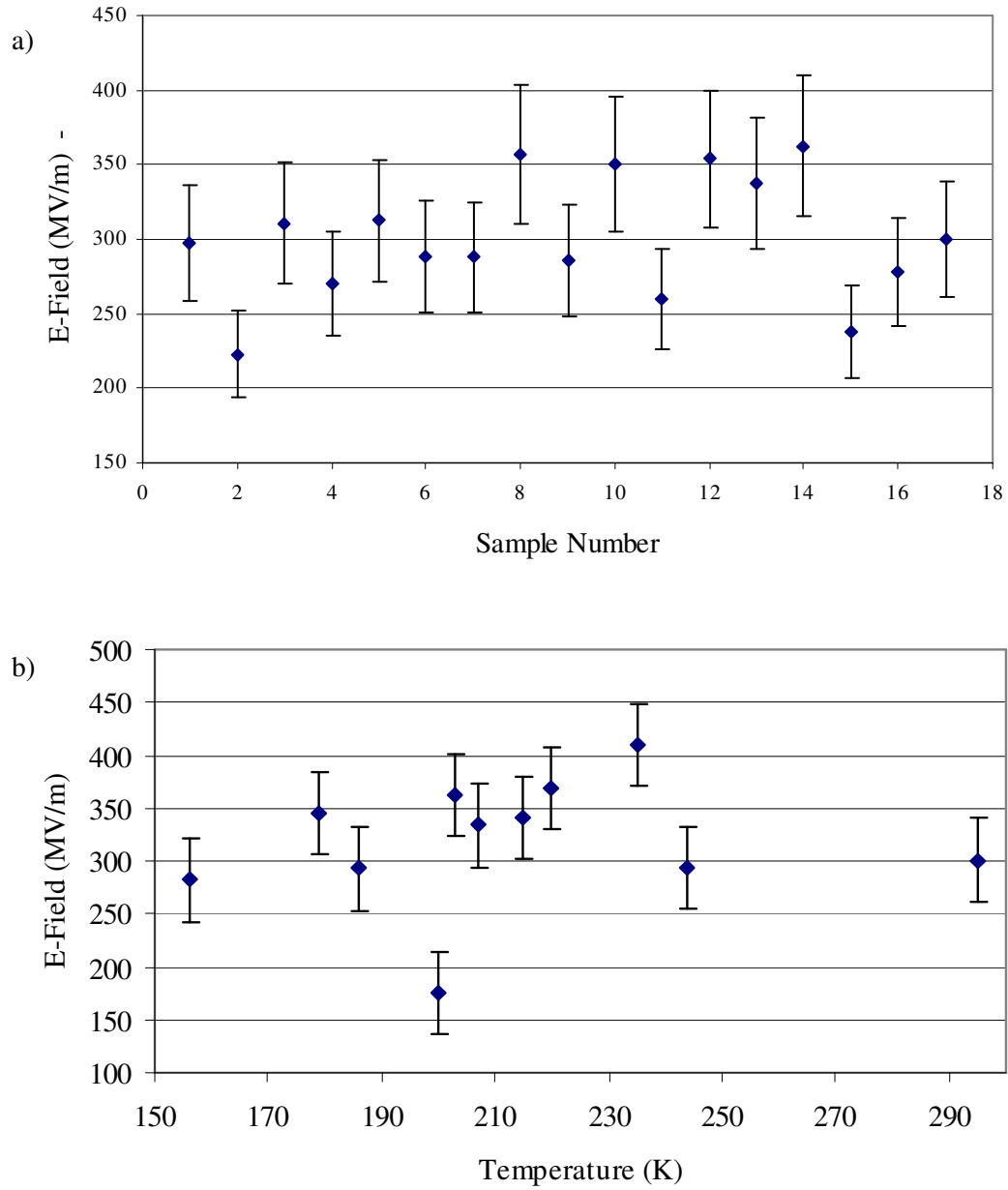


FIG. 3.19. Measured electrostatic field strength of LDPE. a) Each measurement has an uncertainty of 13% and the average field strength was $2.9(\pm 0.3) \times 10^8$ V/m. b) Temperature dependence of electrostatic breakdown values with an uncertainty of 13% in each measurement. No temperature dependence was found in the breakdown strength of $27.4(\pm 0.2)$ μm LDPE.

Table 3.4. Measured* electrostatic breakdown values. For 27.4(\pm 0.2) μm LDPE with an uncertainty of 13% for each measurement.

LDPE Sample Number	ESD Voltage (V)	ESD Electric Field (V/m)
1	7568	2.76×10^6
2	5661	2.07×10^6
3	7897	2.88×10^6
4	6871	2.51×10^6
5	7942	2.90×10^6
6	7339	2.68×10^6
7	7309	2.67×10^6
8	9059	3.31×10^6
9	7260	2.65×10^6
10	8897	3.25×10^6
11	6610	2.41×10^6
12	8989	3.28×10^6
13	8564	3.13×10^6
14	9200	3.36×10^6
15	6043	2.21×10^6
16	7049	2.57×10^6
17	7611	2.78×10^6

* Data obtained using the USU Materials Physics Group ESD chamber (Dennison *et al.*, 2009).

Table 3.5. Measured electrostatic breakdown values with temperature. Temperature dependent measurements* of electrostatic breakdown values of 27.4(\pm 0.2) μm LDPE., no temperature dependence was observed.

LDPE Sample Number	ESD Voltage (V)	ESD Electric Field (V/m)	Temperature (K)
1	7161	2.61×10^6	156
2	8769	3.20×10^6	179
3	7429	2.71×10^6	186
4	9203	3.36×10^6	203
5	4449	1.62×10^6	200
6	8472	3.09×10^6	207
7	8673	3.17×10^6	215
8	9351	3.41×10^6	220
9	10420	3.80×10^6	235
10	7462	2.72×10^6	244
11	7639	2.79×10^6	295

* Data obtained using the USU Materials Physics Group ESD chamber (Dennison *et al.*, 2009).

CHAPTER 4

ELECTRICAL PROPERTIES OF LOW DENSITY POLYETHYLENE

With the data taken and summarized in Section 3.3, the field and temperature dependence of LDPE can be investigated. Tackling the field dependence first, the data sets were examined for obvious behavior trends. The data were then fit with the standard Poole-Frenkel conduction model, the standard space charge limited current model, and the thermally assisted hopping conduction model. Results of these fits will be discussed in Section 4.1. Additionally, the data were fit with the standard Schottky injection model to determine whether or not that is a viable charge injection mechanism for LDPE, as discussed in Section 4.1.2.

Temperature data were evaluated in two ways. The standard approach of determining temperature dependence is to take a discrete number of current measurements at regularly spaced temperature intervals and use an Arrhenius Law to determine the activation energy. This requires only a few points and the experiment can be done relatively quickly. The temperature data summarized in Section 3.3 will be treated in this manner in Section 4.2.1. Results of the standard method will be used to compare values of activation energies to those reported in the literature. However, the ability of the CVC to take continuous measurements over a wide range of temperatures allows a greater amount of information to be obtained about the temperature dependence of the conductivity. It also allows greater control over the rate of temperature change, a significant factor that is typically ignored in the standard method. The temperature data will then be fit with the thermally assisted hopping conductivity and variable range hopping conductivity models to determine their viability as conduction mechanism in LDPE.

Finally, the results of the time-dependent behavior observed in LDPE will be discussed in Section 4.3, including charging and discharging cycles, polarization, and a brief qualitative discussion of endurance time dependence of electrostatic breakdown strength.

4.1 Influence of Applied Electric Field on Conductivity

Determination of field dependence offers more than insight into general charge transport behavior; it also allows for quantitative calculations of physical parameters that can be compared to accepted values for LDPE. It has been established that the application of an electric field introduces strain forces on the polymer chains, distorting the morphology in a variety of ways (Crine, 2005; Ieda, 1980; Lewis, 2002; Lida *et al.*, 1992). This distortion can be significant; experiments indicate that exposure to electrical stress can even alter the mechanical properties of a polymer (Peacock, 2000). The most important effect of this distortion is that the electrical history of the sample becomes a significant factor; repeated exposure to even low electric fields enables charge transport and contributes to the aging of the polymer (Griffiths *et al.*, 1998; Jones *et al.*, 2005; Parpal *et al.*, 1997).

To explore the influence of an applied electric field on LDPE, samples were placed in the CVC under constant temperature and subjected to a wide range of applied electric fields. Typical measurements were taken for a minimum of one hour and, in some cases, up to several hours, with no special care taken to record the transient, short time currents within the initial seconds of the applied field. High field behavior was very difficult to measure due to the onset of discharge events and electrostatic breakdown. Low ramping rates were used, 20 V/s to 50 V/s, to lessen the chance of electrostatic breakdown. Using the average of the final measured currents, the conductivity of LDPE was calculated using the relation,

$$\sigma = \frac{I \cdot d}{V \cdot \alpha}, \quad (47)$$

where d is the thickness of the LDPE sample, α is the effective area of the copper electrode, V is the experimental applied voltage, and I is the average measured current.

At room temperature, mean breakdown voltage observed by the USU Materials Physics Group using the ESD chamber was 7824($\pm 13\%$) V for 27.4(± 0.2) μm thick LDPE samples using

a ramp rate of 20 V increments over ~ 4 s steps. This value was used to determine the range of voltages that would be used in field dependent measurements. A plot of calculated conductivities for the full range of applied fields used, including all data sets listed in Table 3.2, is shown in Fig. 4.1. The full collection of data was taken using multiple samples and the variation from sample to sample can be seen clearly, particularly at higher fields where the history of the sample becomes more important. At high fields, the two distinct curves seen in Fig. 4.1 correspond to measurements taken on different LDPE samples. Complete details for the full data collection, including chronological order and sample information, are found in Appendix D.

For applied fields of $1000(\pm 1)$ V and lower, the conductivity shows no clear dependence on electric field. This corresponds to a low field region up to approximately 13% of breakdown, as shown in Fig. 4.2. For several experimental voltages within this low field range, multiple data sets were taken with multiple samples to determine the consistency of the current measurements over several samples. At $500(\pm 1)$ V (Index # 13 in Table 3.2), the average leakage current was $3.76(\pm 0.05) \times 10^{-13}$ A with a standard deviation of $0.97(\pm 0.05) \times 10^{-13}$ A. This corresponds to an

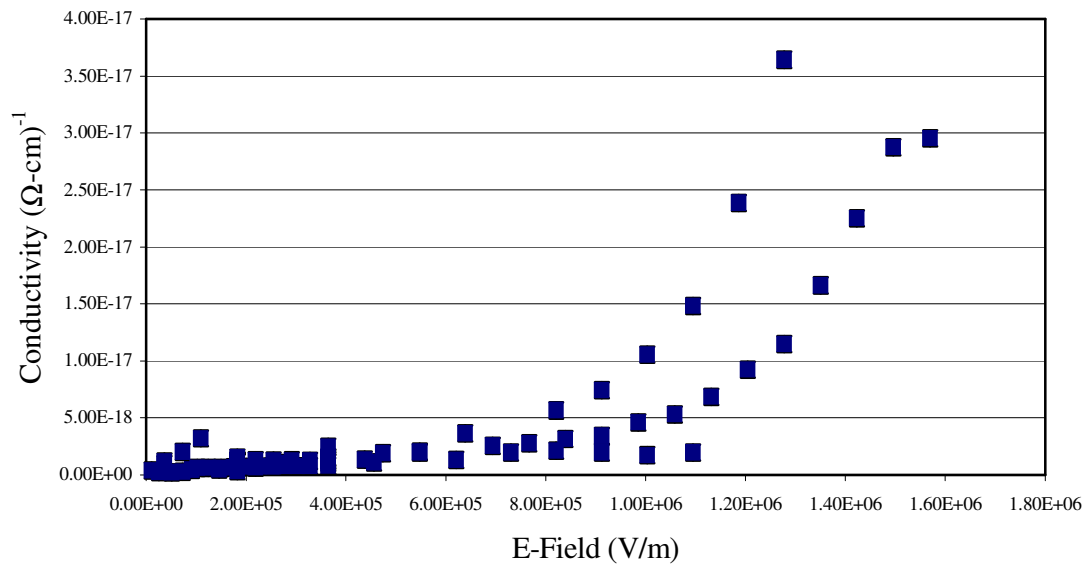


FIG. 4.1. Conductivities for applied field data sets. To approximate equilibrium, the conductivity was calculated from the average current over the final ~ 10 min of each set of the data.

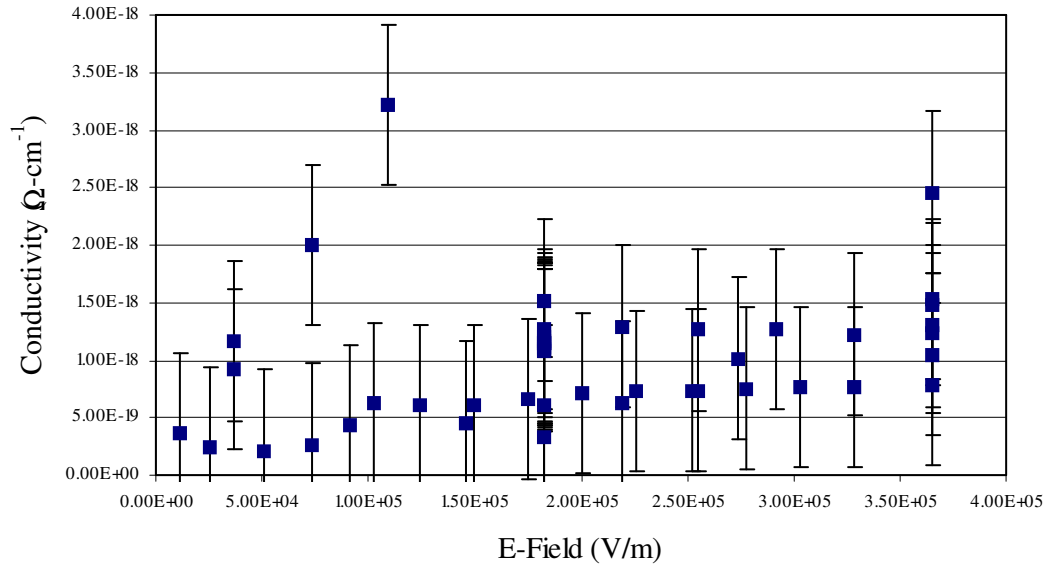


FIG. 4.2. Conductivities for applied field data sets at or below 3.6×10^5 V/m. To approximate equilibrium, the conductivity was calculated from the average current over the final ~10 min of the data. For this field range, the conductivity was determined to be field independent.

average conductivity, at 500 (± 1) V, of $1.09(\pm 0.07) \times 10^{-18} \Omega\text{-cm}^{-1}$ with a standard deviation of $0.28(\pm 0.07) \times 10^{-18} \Omega\text{-cm}^{-1}$. At 1000(± 1) V (see Index # 24 in Table 3.2), the average leakage current is $9.76(\pm 0.05) \times 10^{-13}$ A with a standard deviation at that voltage of $0.37(\pm 0.05) \times 10^{-13}$ A. This corresponds to a conductivity of $1.41(\pm 0.07) \times 10^{-18} \Omega\text{-cm}^{-1}$ with a standard deviation of $0.53(\pm 0.07) \times 10^{-18} \Omega\text{-cm}^{-1}$. Even with the high purity, well-characterized samples obtained for this research, the variability at low experimental voltages over multiple samples and with repeated measurements on the same sample was between 25% (at 500 V) and 31% (at 1000 V). This is an excellent illustration of the difficulty in obtaining consistently reproducible data for the electrical properties of a highly resistive polymer.

At experimental voltages higher than 4000(± 1) V, it was difficult to measure leakage currents with the CVC and an onset voltage for high field behavior could not be accurately determined. The point at which breakdown occurred in the CVC was frequently much less than the breakdown measured with the USU ESD chamber, frequently occurring near half or two-

thirds of the measured mean dielectric strength. This is due to the strong influence of sample history and time duration of measurements and will be discussed qualitatively in Section 4.3. Modeling high field conduction behavior can be complex and problematic, as the interface between polymer and electrode becomes even more important in the understanding of charge transport at high fields. Two primary models of field dependent behavior are Poole-Frenkel conduction and space charge limited current (SCLC).

4.1.1 Electric Field Dependent Conduction Mechanisms

4.1.1.1 Poole-Frenkel Conduction

On standard axes, the Poole-Frenkel model appears to be a good fit of conductivity versus $E^{1/2}$ for low and moderate fields, as shown in Fig. 4.3. Using Eq. (14) and (15), the test of its validity is a plot of $\log_e \sigma$ versus $E^{1/2}$, which produces a straight line with a slope equal β_{PF}/kT . Calculating β_{PF} and then ϵ_r from the slope obtained in Fig. 4.3b gives a value of $14.2(\pm 0.2)$ F/m, which is ~6 times larger than the accepted range of 2.25–2.35 F/m for LDPE. Many modifications have been attempted to achieve better agreement with the dielectric constant, but unfortunately, the Poole-Frenkel model is a poor fit even for heavily doped polymers and is narrowly suited for semi-conductors only (Das-Gupta, 1997; Qi and Boggs; 2002; Wintle, 1999; Yin *et al.*, 2005). While the concept of an applied field lowering the energy required for a carrier to escape its localized state is sound, it is apparent that the Poole-Frenkel model does not adequately describe this effect in LDPE. However, the poor fit of the model is the desired result and confirms that it is not a viable conduction model for LDPE. It is also difficult to distinguish Poole-Frenkel behavior from other mechanisms that fit the same data equally well, but have different meanings and fundamental assumptions, e.g. Schottky injection. Furthermore, at high fields where the applied field where Poole-Frenkel conduction is expected to be most applicable to the conductivity behavior of the material, the fit to the LDPE data is poor. Deviation at high

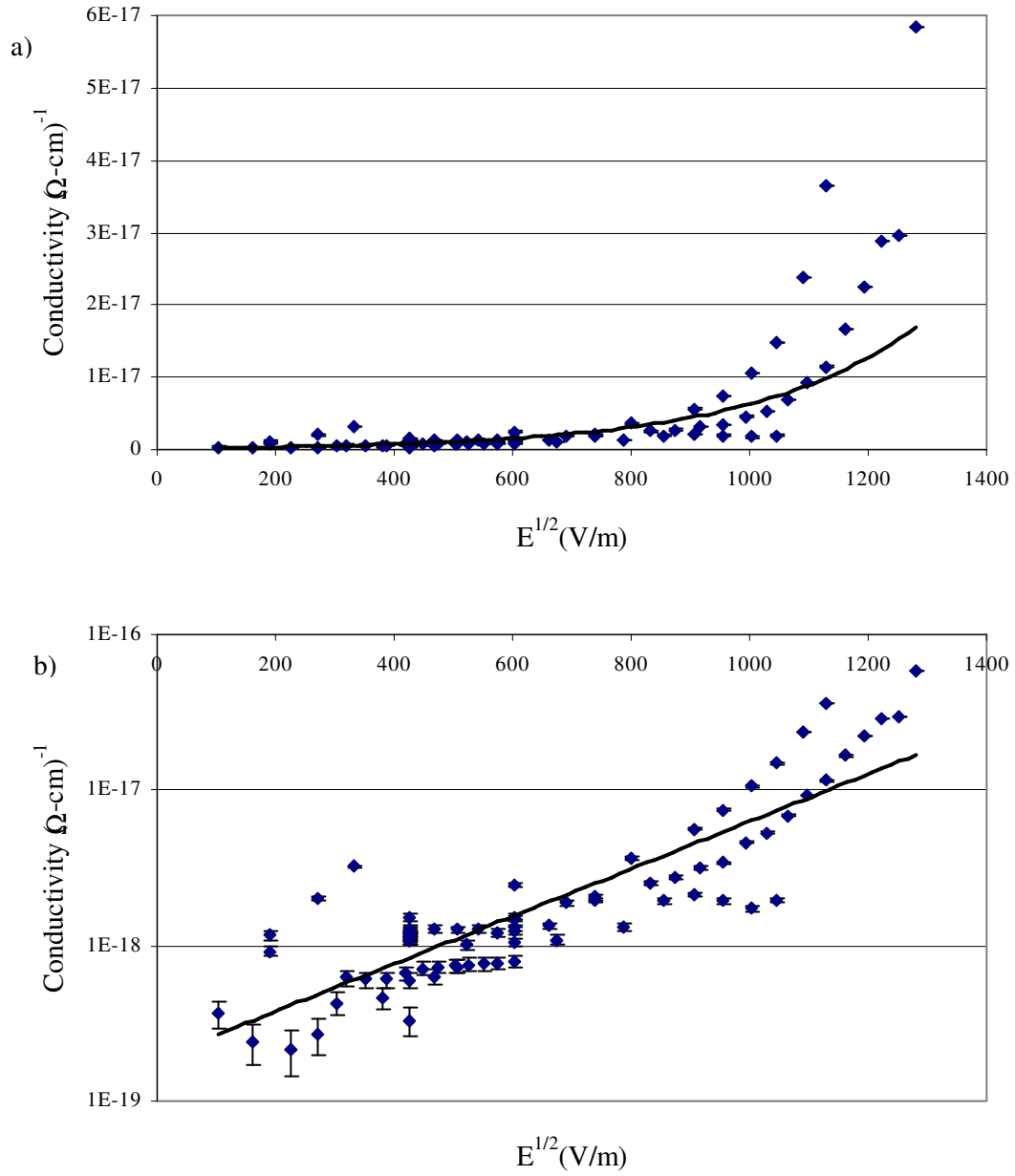


FIG. 4.3. Poole-Frenkel conduction plots for electric field dependence of measured current. a) Applied field data fit with Poole-Frenkel conduction model on standard axes and b) a semi-log plot of the applied field data with Poole-Frenkel conduction model. The slope of the fit in the semi-log plot is used to calculate the dielectric constant of LDPE to verify the model.

fields is not unexpected, since the sample history will begin to play an increasingly significant role. With these weaknesses, particularly the lack of unique behavior that would distinguish Poole-Frenkel conduction from other mechanisms, an alternative field dependent conduction model is necessary.

4.1.1.2 Space Charge Limited Current Conductivity

Considering the current densities for LDPE over the full range of obtained electric field data, a transition is observed at approximately 2500 V and two regions of field dependence are clearly seen in the log-log plot of Fig. 4.4. This roughly corresponds to the first two regions of SCLC behavior, based on Eq. (23). The exponents however, which would be V^1 and V^2 for ideal SCLC behavior, are found to be $V^{3/2}$ and $V^{5/3}$, approximately. These differences indicate that while SCLC may be a charge transport mechanism, the response of LDPE is far from the ideal SCLC behavior. This may be due to the high density of traps, which would also make it very

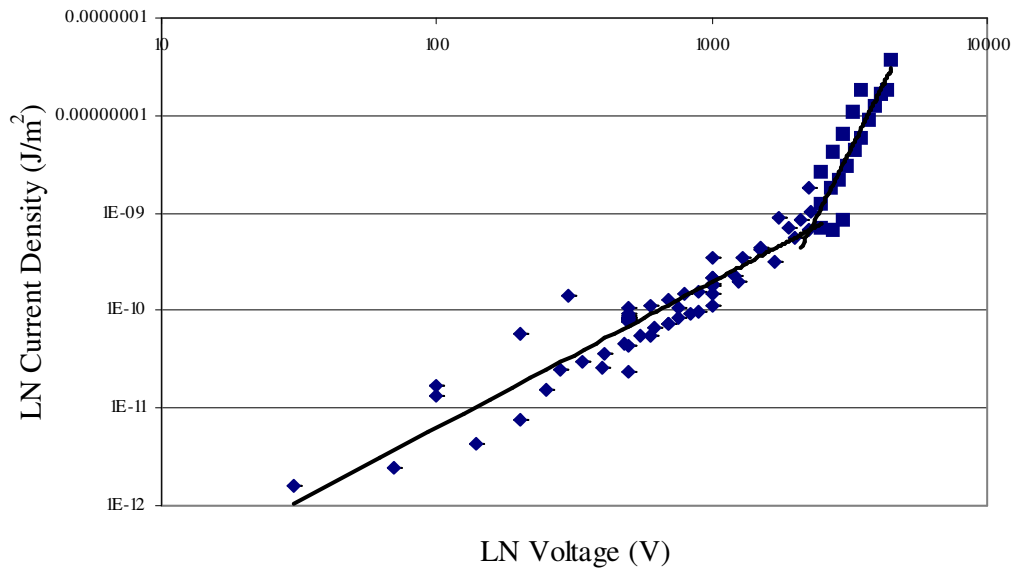


FIG. 4.4. Space charge limited current plot for electric field dependence of current density. There is a clear transition in the slope of the $\log_e J$ versus $\log_e V$ behavior near 2500 V. However, the exponents of the two slopes do not match the values predicted by the SCLC.

difficult to observe regions 3 and 4 where all traps are filled. Filling all traps available in LDPE would require the number of electrons injected by the electrodes to be on the order of 10^{18} per cm^3 , a requirement that is not only difficult to meet, but would certainly be catastrophically damaging to the sample. The onset of electrostatic breakdown from the internal field produced by the space charge would mask the transition between regions 2 and 3, and would prevent region 4 from occurring. In the lower regions 1 and 2, the disagreement in exponents could also be due to the assumptions made in determining the steady state current density, such as neglecting the influence of diffusive transport and assuming a uniform electric field throughout the material. The high degree of disorder of LDPE, with both trapped and free charges contributing to space charge and localized electric fields, makes it difficult for a uniform electric field to be established throughout the material. Without this uniform field, the diffusive transport of electrons will not be negligible. In addition, the assumption for Eq. (22) that $x_o \ll d$ is only valid for electrode-polymer interfaces with good charge injection properties. This once again raises the question of determining if charge injection occurs with LDPE and to what extent the charges are injected. In fact, the criteria for an interface with good charge injection properties are controversial as well (Crine, 2005; Wintle, 1983).

The Poole-Frenkel conduction model produces an unrealistic and significantly higher value of the dielectric constant, which can indicate the development of space charge at the electrodes and electrode polarization (Adamec and Calderwood, 1978) and supports the concept of SCLC. Although Poole-Frenkel is not expected to be seen in LDPE, the SCLC model has been applied with mixed results (Adamec and Calderwood, 1981; Marat-Mendes *et al.*, 2004; Montanari *et al.*, 2001). The data obtained in this study does not follow ideal SCLC behavior and this deviation may be explained by the influence of trapping. Since a fundamental assumption of the SCLC model is the injection of charges from the electrodes, it is necessary to determine if and to what extent the electrons are injected into the LDPE sample; this will be further discussed in

Section 4.2. With the unlikelihood of charge injection given the experimental conditions and choice of polymer of this study, it is also prudent to investigate conduction mechanisms that do not rely on charge injection, such as thermally assisted hopping conductivity.

4.1.1.3 Thermally Assisted Hopping Conductivity

For constant temperature, taking the expansion of the field dependent term in Eq. (32) in the limit that the ratio, β_A , of the energy gained from the field over the trap separation distance, a , to the thermal energy of the carrier gets small; where the energy ratio can be written as

$$\beta_A(E, T, a) = \frac{q_e E a}{k_B T} \quad (48)$$

and in the expansion,

$$\frac{1}{\beta_A} \sinh(\beta_A) \rightarrow \left[1 + \frac{1}{6} (\beta_A)^2 + \frac{1}{120} (\beta_A)^4 + O(\beta_A)^6 + K \right], \quad (49)$$

which yields a field independent limit for small applied fields. Additional details of this expansion and derivation of σ_{TAH} are found in the relevant references (Bartnikas, 1983; Dennison and Brunson, 2008; Dennison *et al.*, 2009). The result of the expansion is consistent with the field independence observed in the data up to approximately 13% of the average electrostatic breakdown strength of LDPE. A fit over the low field range with the constant temperature σ_{TAH} model where conductivity is believed to be independent of the field produces an average trap depth, ΔH , of $0.55(\pm 0.09)$ eV at room temperature, which is within the expected range of activation energies for LDPE at low applied fields and room temperature (Bambery and Fleming, 2003; Boudou and Guastavino, 2000; Fleming *et al.*, 2008; Mizutani *et al.*, 2003; Montanari *et al.*, 2001). The σ_{TAH} fit also gives a trap separation of ~ 0.9 nm, which is in reasonable agreement with values reported in the literature (Boudou and Guastavino, 2002).

Expanding the fit over the full range of the data obtained for LDPE, the σ_{TAH} model

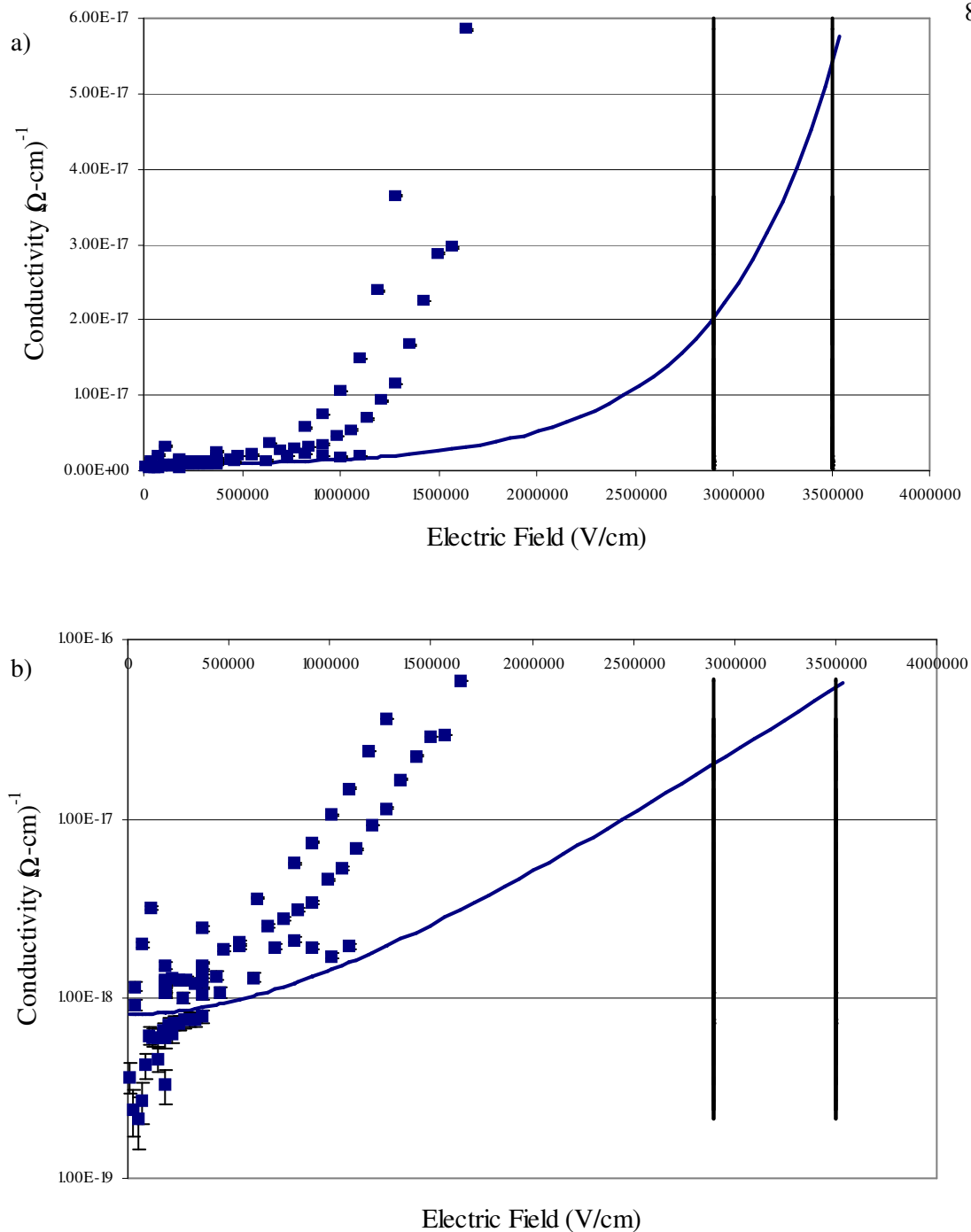


FIG. 4.5. Thermally assisted hopping model fit for electric field data. Shown on standard axis in a) and a log-log plot in b), with vertical bars indicated range of breakdown voltages seen in ESD chambers. The model predicts field independence at low fields and the correct order of magnitude of currents for the expected range of breakdown fields. Breakdown was seen much earlier in the CVC than the ESD chamber, suggesting that the endurance time of the polymer must be taken into account.

produces several interesting results. The full electric field data set with the constant temperature σ_{TAH} fit is shown in Fig. 4.5, in both standard axes and semi-log plots. At the range of fields where breakdown is expected to occur, the conductivity predicted by the σ_{TAH} model diverges. This divergence of the σ_{TAH} model corresponds remarkably well with the range of ESD values found for LDPE using the ESD chamber developed by the USU Materials Physics Group, indicated in Fig. 4.5 by the solid vertical bars. It has already been noted that breakdown was seen much earlier in the CVC than in the ESD chamber, due to the influence of sample history and endurance time on electrostatic breakdown. The influence of endurance time with respect to the LDPE data and the σ_{TAH} model will be addressed in Section 4.3. However, it is worth noting here that the overall behavior of the data and the σ_{TAH} model are consistent, which was not observed with the Poole-Frenkel model. It is also worth stating explicitly that σ_{TAH} does not rely on charge injection of electrons as the source of the carriers; instead, it is meant to model the movement of electrons trapped within the localized states of the material itself. In summary, σ_{TAH} provides reasonable agreement with values of physical parameters at low fields and it does not rely on the unlikely mechanism of charge injection; this makes it a more viable model of conduction than either Poole-Frenkel conduction or SCLC.

Thermally assisted hopping conductivity also contains temperature dependence, both directly and indirectly through a weak temperature dependence of the density of states. It will be revisited in the following section as the temperature dependence of conductivity in LDPE is investigated.

4.1.2 Charge Injection

Schottky behavior can be verified by plotting $\log(J/T^2)$ against $E^{1/2}$, which, from Eq. (2), should be linear if Schottky injection is the primary mechanism of carrier injection from the electrodes to the material. From Eq. (4), the coefficient, β_{SC} , can be seen to be very similar to the Poole-Frenkel coefficient, β_{PF} , which, from Eq. (15), belies the fundamental connection of

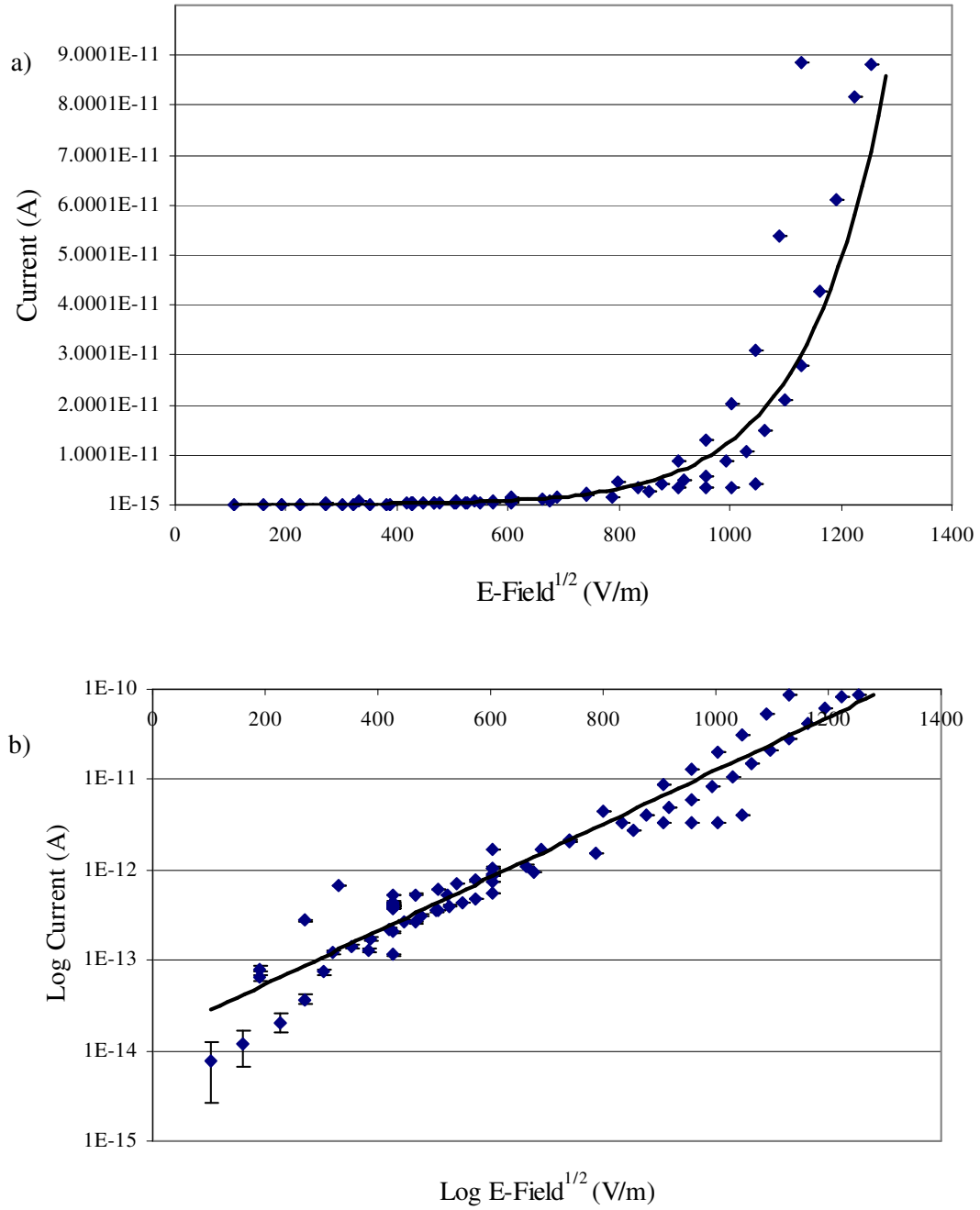


FIG. 4.6. Schottky charge injection plots for electric field dependence of current density. a) Schottky fit on standard axis and b) the log-log plot with a linear fit that allows determination of the dielectric constant using the slope of the fit and the Schottky coefficient. The intercept of the linear fit can be used to determine the work function of the electrode model, another check for the validity of the model.

distortion of a localized state due to an applied electric field. In the case of Schottky injection, it is a distortion and lowering of the barrier between electrode and polymer. The test of its validity is in the log-log plot shown in fig. 4.6b, with a linear fit applied to the full range of obtained electric field data. However using the slope of the Schottky fit to determine the relative permittivity of LDPE, ϵ_r , a value of $4.6(\pm 0.2)$ F/m is obtained. Once again, this is not in agreement with the commonly accepted permittivity of LDPE, being a factor of 2 times larger than the accepted range of 2.25-2.35 F/m. A second point of verification is if the correct work function for the electrode metal is obtained using the intercept of the Schottky fit. The fit of the data produces a work function of $1.3(\pm 0.2)$ eV, which is not in agreement with the accepted value for copper of 4.7 eV. It is possible that this difference in value is due to space charge build up that modifies the nature of the potential barrier at the interface; this underscores the complexity of determining what information may be obtained from the data. Modifications can be made to Schottky injection, but agreement with accepted values of relative permittivity remains elusive. This discrepancy has been theorized to be due in part to the formation of an oxide layer on the metal electrodes (Lewis, 1955; Taylor and Lewis, 1971) and the difficulty separating Schottky injection from Poole-Frenkel conduction. It is reasonable to assume that injection of electrons from the electrodes is neither the primary source of carriers nor does it control the conduction behavior seen in this study.

4.2 Influence of Temperature on Conductivity

The influence of temperature on the conductivity of LDPE is a nontrivial and multifaceted problem, with two distinct types of temperature-dependent behavior. Changes in temperature, and the available thermal energy, can affect the mobility of individual carriers by increasing the hopping rates. This increase in mobility of the carriers is a reversible process and a decrease in temperature will subsequently decrease the mobility of the carriers by decreasing the hopping rate. However, temperature changes also affect the morphological structure of the

polymer, leading to changes in trap density and trap distribution (Boudou and Guastavino, 2000; 2002; Dang *et al.*, 2003; Ding *et al.*, 2000; Griffiths *et al.*, 1998; Ieda *et al.*, 1980). This effect of temperature change can be irreversible.

Annealing processes have been shown to inhibit the development of space charge in polymers (Lida *et al.*, 1992) and the effect of thermal cycling in high voltage cable insulation is a thriving area of study (Griffiths *et al.*, 1998). It can be difficult to determine the influence of irreversible changes under moderate experimental conditions, but a morphological change will be closely tied to the rate of temperature change (Ieda *et al.*, 1980). This sensitivity to heating and cooling rates is exploited in the quenching processes for polymers, where the rate of cooling is adjusted to determine the percent of crystallinity and other physical properties. A consistent, slow rate of temperature change is necessary to approximate equilibrium conditions and identify temperature dependent behavior, such as the release of trapped space charges due to increased motion of the polymer chains.

A set of measurements were taken at $1000(\pm 1)$ V where the CVC and sample were heated at an average rate of $\sim 0.10(\pm 0.05)$ K/min to approximately 338 K and then allowed to return to room temperature at an equivalent rate. Equivalent heating and cooling rates minimized the possibility that electrons were excited into higher energy traps as the temperature increased with the cooling process happening too quickly to allow them to return their previous equilibrium energy distribution as the temperature decreased. This effect would cause a hysteresis-like behavior over a thermal cycle without any change to the polymer morphology and make it extremely difficult to determine if any such modification had occurred. The measured leakage current plotted against temperature is shown in Fig. 4.7. Behavior of the heating and cooling segments of the leakage current served as a test of both the experimental apparatus and any irreversible changes in morphology of the LDPE sample at higher temperatures. By heating the chamber as well as the samples, the thick stainless steel of the CVC served as an excellent

regulator that prevented the samples from heating or cooling too quickly. Minimizing and carefully regulating the heating and cooling rates allowed investigation of what irreversible changes, if any, occurred in LDPE over the course of a temperature cycle. It can be clearly seen in Fig. 4.7 that the conductivity approximately follows the same path during the heating and cooling segments of the thermal cycle, indicating that the increase of conductivity is largely due to a reversible process. The maximum width of the hysteresis loop is ± 1 K and the current remains within $\pm 5\%$ of the initial value at room temperature.

When the thermal cycle was repeated with a higher applied voltage, $2500(\pm 1)$ V, the conductivity during cooling deviates significantly from the conductivity during heating. The maximum width of the hysteresis loop is ± 7 K and the current does not return to the initial value at room temperature, within $\pm 5\%$. This may indicate that an irreversible change in the polymer morphology occurred (e.g temperatures as low as 343 K can alter the unit cell configuration of the crystalline regions (Peacock, 2000)). It may also indicate that the increase in applied field allowed the electrons to be excited into higher energy traps, with fewer electrons returning to the

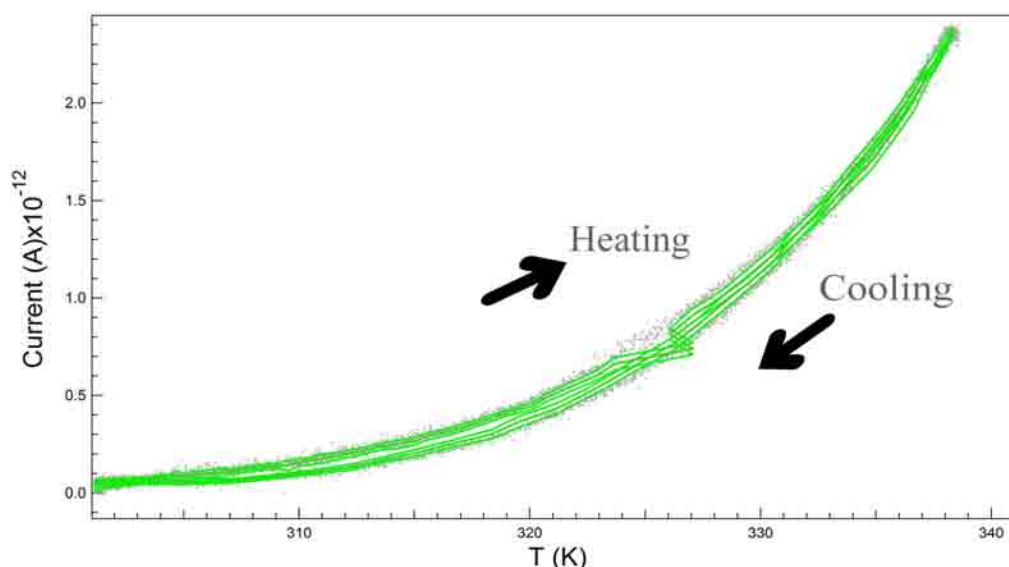


FIG. 4.7. Measured current over one thermal cycle at 1000 V. No significant differences are seen between the measured current of the heating region and the measured region of the cooling region of the thermal cycle.

previous equilibrium energy distribution once the temperature began to decrease. Fig. 4.8 shows the thermal cycle at $2500(\pm 1)$ V. Additional work is needed to determine the compounding effect of the applied electric field and the cumulative effects of multiple thermal cycles on conductivity.

The dynamic response of polymers to temperature change places an important emphasis on understanding how charge transport is influenced by temperature. Multiple structural transition points, including the glass transition and other phase transitions, corresponding to motion of the polymer molecules have been observed in measurements of thermally stimulated currents and thermo luminescence (Ieda *et al.*, 1980). These structural transitions influence the ability of carriers to move through the material and may aid in identifying transitions between dominant charge transport mechanisms. Although the lack of a significant dipole moment in LDPE makes these transitions very difficult to observe electrically, it is still possible to pursue these transition points through indirect methods. The majority of temperature dependent

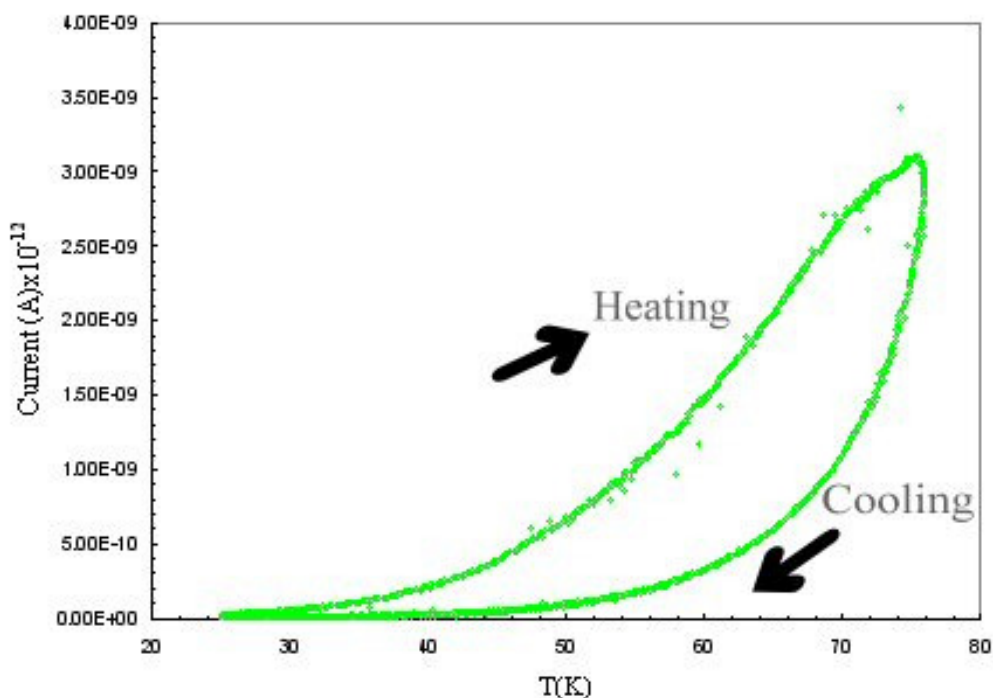


FIG. 4.8. Measured current over one thermal cycle at 2500 V. Significant differences are seen between the measured current of the heating region and the measured region of the cooling region of the thermal cycle.

measurements available from previous studies for comparison are at room temperature and above, including conductivity measurements of molten LDPE (Lida *et al.*, 1992), with relatively little work available at low temperatures (Griffiths *et al.*, 1998; Wintle, 1999). Low temperature work that is available is of variable quality and most often specific to the behavior of high-voltage transmission cables in winter conditions.

Two stages were needed to achieve a wide temperature range; a cryogenic stage for temperatures as low as 120 K and a second, high temperature stage reaching temperatures of 353 K. Anomalous behavior was expected below 213 K, the lower working temperature of the material, and approaching the glass transition temperature at approximately 193 K. Changes in conductivity below the working temperature and through the glass transition are potentially ill defined and unpredictable. The limit of instrumental resolution is also quickly reached as currents decrease with decreasing temperature, adding to the difficulty in extending measurements into the low temperature region. It was difficult to control heating rates during the physical transition from the cryogenic measurements to heating measurements, which often required equipment modifications and, in some cases, opening the CVC to adjust the thermocouple connections.

Careful examination of the measured leakage currents, even at low applied fields, once again confirms the sensitivity of conductivity in LDPE to a change in heating rates. Regions of distinct current behavior in the temperature data were checked for correlation to a change in average heating rate before being used in analysis. Typically, the heating rate was most stable from roughly 213 K to near room temperature. Between 293 K and 303 K, the heating rate fluctuated as the heating strips were turned on and began to heat the chamber. Significant fluctuations in the rate were seen when the CVC needed to be opened to check the samples and the thermocouple connections. These issues with instrumentation create an artificial region in several of the temperature-current measurements, from approximately 293 K and 303 K, which

should only be used with extreme caution. The heating rate typically stabilized once again at approximately 313 K. Fig. 3.18 is an example of typical heating and cooling rates; where the regions of consistent heating or cooling rates are seen where dT/dt is small. Since the effects of changing heating rates are not well characterized and the primary focus of this study is the conductivity at equilibrium, it is sensible to focus on regions of behavior where the rates of temperature change remain approximately constant.

4.2.1 Activation Energies

The usual means of determining temperature in polymers utilizes rate equations and Arrhenius plots to relate measured leakage currents and conductivity with activation energies. Trap depth, ΔH , can be then be approximated as the activation energy, allowing for comparison to a physical parameter of LDPE that serves as a test of the validity of a proposed transport mechanism. The activation energy has both field and temperature dependence and can be found using the slope of an Arrhenius plot with a simple exponential fitting function such as

$$\sigma(T) \approx \sigma_o \exp\left(-\frac{\Delta H}{k_B T}\right). \quad (50)$$

Drawing from the measurements of leakage current taken over a range of temperatures allows the determination of a range of activation energies, E_a , for LDPE. A good place to begin is with a low experimental voltage, 100(\pm 1) V, where conductivity in LDPE was found in Section 4.1 to be approximately independent of electric field. Fig. 4.9a shows the Arrhenius semi-log plot at 100(\pm 1) V; two distinct regions of behavior can be clearly seen. Two more continuous temperature-current measurements were taken at 1000(\pm 1) V and 2500(\pm 1) V. A semi-log plot of all three temperature-current measurements is shown in Fig. 4.9b; each of them showing two distinct regions of behavior. Focusing on the higher temperature region, the data was fit with a simple exponential and the slope was used to calculate the activation energy for that temperature and applied field. This produced activation energies of 0.95(\pm 0.09) eV, 1.18(\pm 0.09) eV, and

0.86(±0.09) eV, for 100(±1) V, 1000(±1) V, and 2500(±1) V, respectively. These values are within range of the expected activation energies for these temperatures and applied fields. However, it is clear from Fig. 4.9 that the simple exponential fit is a poor match to the data. The non-linear, changing slope of the \log_e of conductivity would not be seen in a plot with a limited number of discrete measurements.

In the low temperature region, from room temperature to approximately 213 K, the conductivity shows a significant decrease. An Arrhenius semi-log plot of the high- and low-temperature behavior for 100(±1) V, 1000(±1) V, and 2500(±1) V is shown in Fig. 4.10. The conductivities at low temperatures are close in magnitude and are offset for clarity in the figure.

The conductivity decrease at low temperatures is seen even at the highest applied field and it is clear that there is a transition occurring between 273 K and 263K. Below this point, the activation energies are found to be 0.10(±0.09) eV, 0.06(±0.09) eV, and 0.08(±0.09) eV for 100(±1) V, 1000(±1) V, and 2500(±1) V, respectively. Table 4.1 provides a complete summary of determined activation energies and a selection of comparable values available in the literature.

Temperature dependence of the activation energy can be regarded as a measure of the charge transport process and the depth of traps available to take part in hopping conduction. For a density of localized states, the activation energy, E_a , is the weighted average of the depths of the traps below E_c that are accessible for hopping. At low temperatures, the states with energies proportional to αk_B can be thermally excited in an extended state, with

$$E_a = \frac{1}{2} (E_f' + \alpha k_B T_L) \quad (51)$$

where E_f' is the Fermi energy and T_L is a low temperature limit. Increasing the temperature allows deeper states to participate in hopping conduction and the energy density of states $N(E)$ can be assumed to change step-wise at T_L . The temperature dependence of the density of states means that this assumption is not rigorously acceptable, but it is quite useful to simplify the

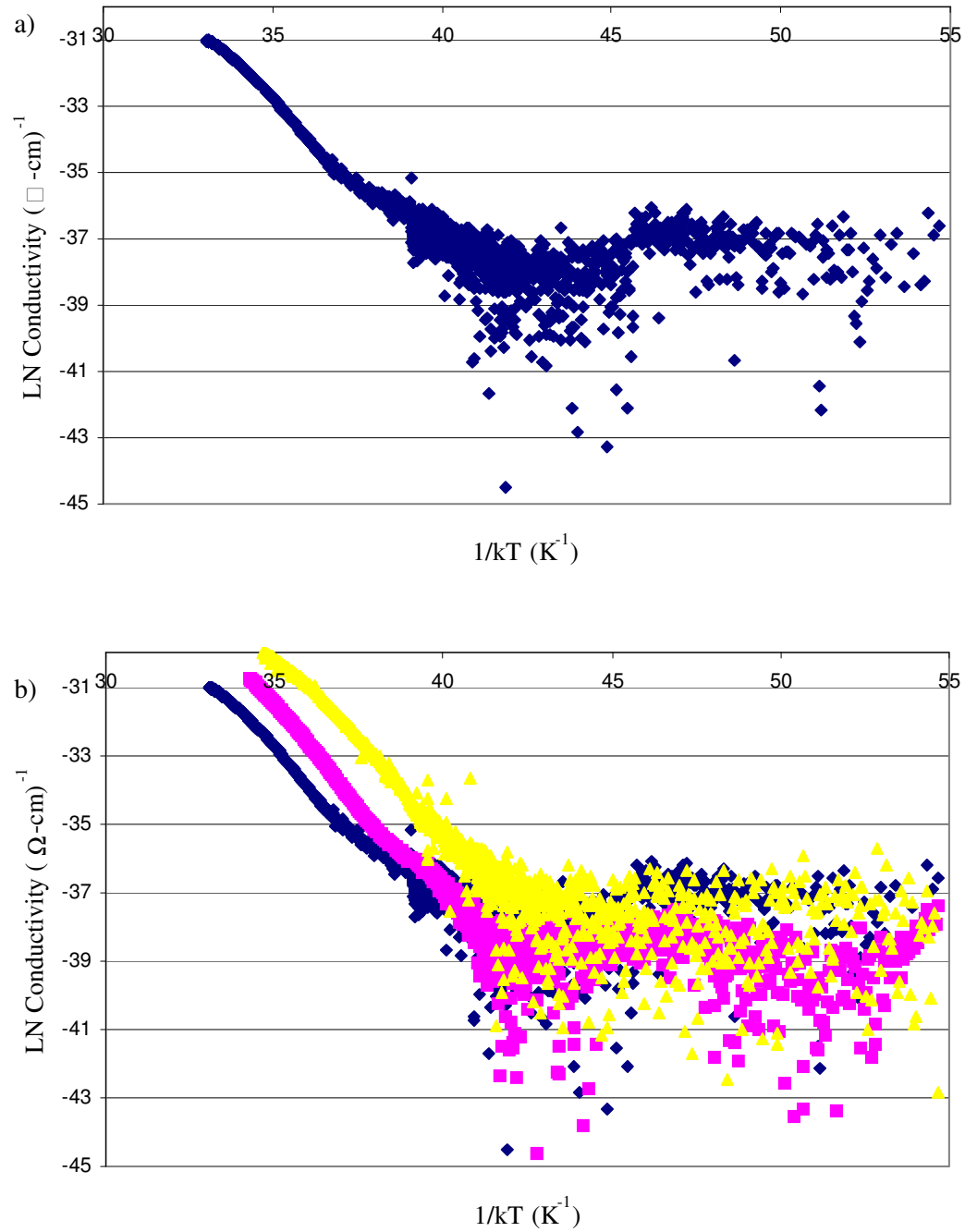


FIG. 4.9. Arrhenius plot for conductivity at 100 V, 1000 V, and 2500 V. a) Arrhenius plot for 100 V alone and b) Arrhenius plot for all three voltages. At 100 V, where the conductivity is considered field independent, there are two regions of the behavior that cannot be fit with the same slope. This behavior is also seen at the higher voltages where the conductivity is not expected to be field independent.

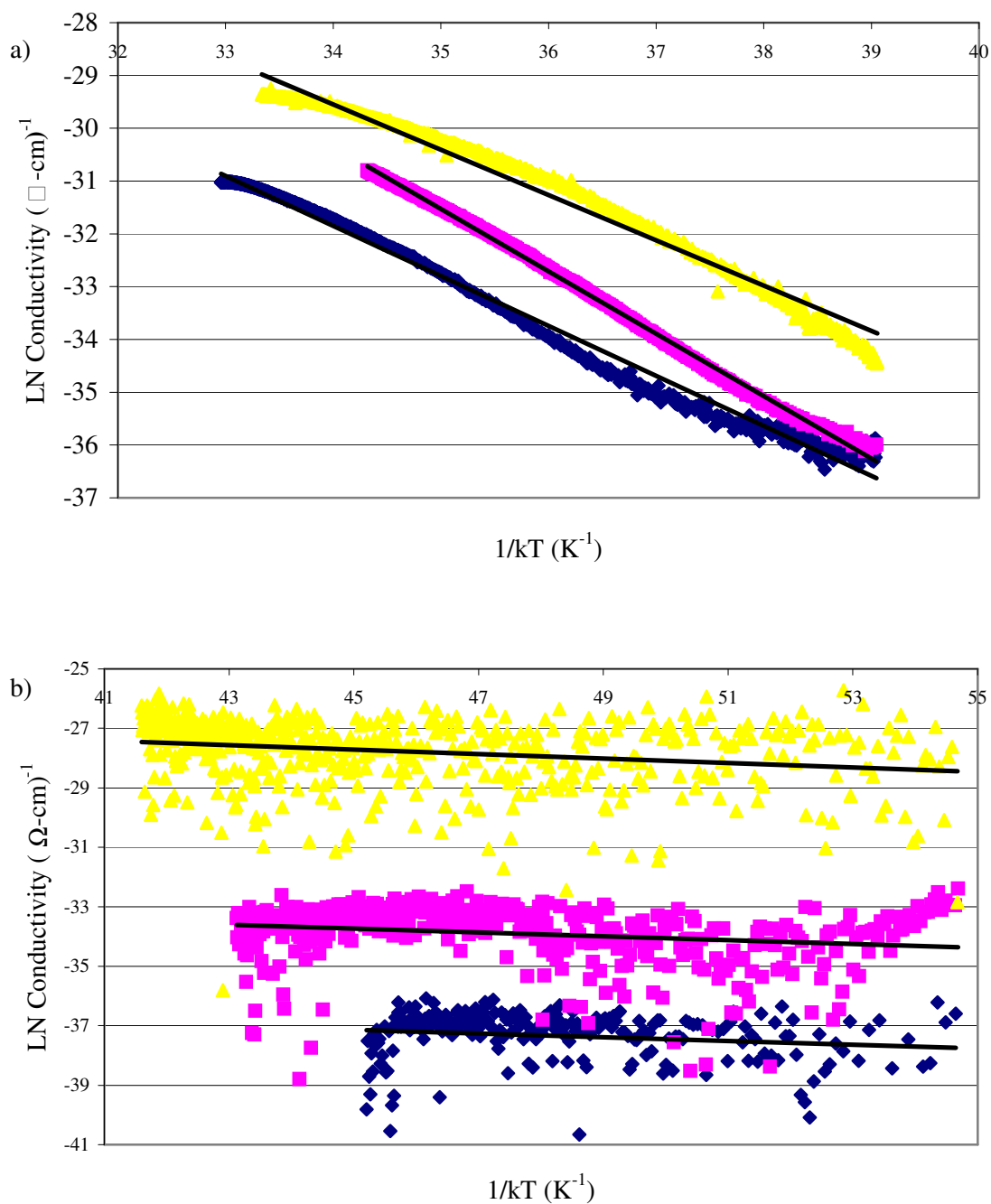


FIG. 4.10. Arrhenius plots for conductivity at 100 V (blue), 1000 V (purple), and 2500 V (yellow) at high and low temperatures. a) High-temperature range plot and b) low-temperature range plot. Data sets are offset for clarity in b).

Table 4.1. Comparison of determined activation energies with values of activation energy reported in literature. Every attempt was made to select comparable values where data was obtained using similar experimental methods and conditions, as well as values obtained through a variety of other methods. Activation energy values obtained using the data in this study are shown by applied field and temperature range on the left side of the table. Comparison activation energy values from the literature are listed in the right side of the table.

Determined Activation Energies			Comparison Activation Energies			
E-Field (kV/m)	T Range	E _a (eV)	E-Field	T Range	E _a (eV)	Reference
3.6×10^5 - 1.6×10^7	293 K	0.55 [†]	1-150 kV/mm	293 K	0.80 - 0.83	Montanari, 2001
3.6×10^5	213 K - 338 K	0.1 - 0.95	5×10^6 , 1×10^6 , 2×10^7 kV/m	293 K - 333 K	0.55 - 1.40, 0.09	Bambery, 2003
3.6×10^6	213 K - 338 K	0.06 - 1.18	10 - 20 kV/mm	303 K - 343 K	0.9 - 1.5	Fleming, 2008
9.1×10^7	213 K - 338 K	0.08 - 0.86	6 kV/mm, 20 kV/mm	298 K - 353 K	0.68 - 0.94	Boudou, 2000
3.6×10^5 - 9.1×10^7	213 K - 338 K	0.57 [‡]	50 MV/m	293 K - 313 K	0.3 - 0.5	Mizutani, 2003
			Not specified	293 K - 373 K	0.4 - 1.5	Fowler, 1956
			Not specified	Not specified	1.5	Fowler, 1953
			7.75×10^2 V/cm	Not specified	0.5	Ramsey, 1953
			Not specified	Not specified	0.54	Stannett, 1957
			10^5 - 10^6 V/cm	Not specified	1.96	Lengyel, 1966
			2.6×10^4 V/cm - 1.3×10^5 V/cm	Not specified	1.11 - 1.45	Taylor, 1971
			70 kV/mm - 1000 kV/mm	303 K - 383 K	0.058 - 0.086	Cho, 1997
			Not specified	Not specified	0.4 - 1.1	Lewis, 2002
			2×10^5 V/cm	308 K - 358 K	0.3 - 1.17	Nath, 1989
			Not specified	Not specified	0.71 - 0.92	Davies, 1972

[†] Determined using σ_{TAH} best fit over low applied field range only.

[‡] Determined using σ_{TAH} and σ_{VRH} best fits over entire temperature and applied field range.

discussion of the temperature dependence of E_a . For the deeper states that become accessible as the temperature increases, the activation energy is then

$$E_a = \frac{1}{2}(E'_f + \alpha k_B T_H) \quad (52)$$

where

$$\frac{1}{2}(E'_f + \alpha k_B T_H) > \frac{1}{2}(E'_f + \alpha k_B T_L). \quad (53)$$

Using Eq. (52), and a fit of the activation energies determined from the Arrhenius plots, produces intercepts of $2.8(\pm 0.3)$ eV, $3.8(\pm 0.3)$ eV, and $2.6(\pm 0.3)$ eV, for $100(\pm 1)$ V, $1000(\pm 1)$ V, and $2500(\pm 1)$ V, respectively. The band gap of LDPE is reported to be in the range of 7.0 – 9.0 eV (Dissado and Fothergill, 1992; Peacock, 2000), which gives a Fermi energy of 3.5 eV – 4.5 eV, if E_f is assumed to be at the center of the band gap. Acknowledging that the presence of lattice defects and disorder frequently moves E_f away from the center of the band gap (Rose, 1951), the values obtained from the temperature dependence of E_a are reasonable.

Although investigation of the activation energies can provide insight into the depths of traps accessible to a hopping conduction mechanism, it is also clear that the behavior is more complicated than the simple exponential fit of the Arrhenius Law. Since the CVC was built to allow continuous measurements of leakage currents over the range over temperatures, it is possible to directly investigate the temperature dependent conductivity. This allows more complex charge transport mechanisms to be investigated with the same relative ease as calculating activation energies with a selection of discrete measurements. Two prominent mechanisms are thermally assisted hopping (multiple trapping) and variable range hopping (tunneling).

4.2.2 Thermally Assisted Hopping Conductivity

Random thermal fluctuations allow carriers to escape from a trap and hop to a

neighboring trap; an increase in thermal energy increases the ability of a carrier to escape. At room temperature, thermally assisted hopping is believed to be the dominant charge transport mechanism, with conductivity proportional to $T^{-1}\exp(T^{-1})$. It is vital to be clear about the nature of the hops, since both trapping and tunneling are referred to as hopping in the literature. Thermally assisted hopping is most accurately viewed as a process of energy gain (or loss) that results in charge carrier leaving a trap and traveling a small distance in an extended state before being once again trapped in a localized state, rather than direct movement via quantum mechanical tunneling between localized states. As a trapping mechanism, thermally assisted hopping is closely tied to the frequency of hops, ν_{TAH} , requiring statistical estimations of trapping and detrapping times. It is usually assumed that trapping times are symmetrical, meaning that the trapping time is equal to the detrapping time (Butcher, 1972; 1974; Hunt, 1994; Movaghar and Schirmacher, 1980). Temperature dependence appears primarily in the energy density of the charge carriers, $N(T)$, with increasing temperature increasing the number of available carriers (Böttger and Bryksin, 1985; Dissado and Fothergill, 1992). A single layer density of shallow states, with a depth of ΔH , is typically assumed, but this is motivated by the existence of an analytic solution for a single layer distribution, rather than a measured distribution of states. There are alternative distributions to be explored and new experimental methods have provided information on the actual distribution of traps in many polymers (Fowler, 1956; Wysocki *et al.*, 1995). Using an exponential distribution of traps rather than a single layer provides better agreement with the distributions measured by pulse radiation experiments. The familiar parameters for trap depth and trap spacing, ΔH and a , directly tie the conductivity to morphological features of LDPE.

Returning once again to thermally assisted hopping, which was introduced field dependence in Section 2.2.3, the expression for the conductivity was found to be

$$\sigma_{TAH}(E, T) = \left[\frac{2N(T)v_{TAH}aq_e}{E} \right] \exp\left[\frac{-\Delta H}{k_B T} \right] \sinh\left[\frac{aq_e E}{k_B T} \right], \quad (32)$$

where the frequency v_{TAH} is typically a phonon frequency on the order of 10^{13} Hz (Bartnikas, 1983). It is then left to determine whether or not this model serves to fit the temperature dependent conductivity data. Again, this is not as mathematically simple as using the Arrhenius Law to investigate the activation energy. To accommodate easier analysis of the data, it is useful to introduce a set of reduced variables, including a ratio of field energy to thermal energy. This allows significant reduction in the number of free parameters needed for curve fitting. Eq. (32) can be expressed in terms of a temperature scaling factor, T_A , an electric field scaling factor, E_A , and a conductivity scaling factor, σ_{TAH_0} ,

$$T_A \equiv \frac{\Delta H}{k_B}, \quad (54)$$

$$E_A \equiv \frac{4\Delta H}{3q_e a}, \quad (55)$$

and

$$\sigma_{TAH_0} \equiv 2N(T)v_{TAH}q_e^2 a^2, \quad (56)$$

which is proportional to the frequency of hops, v_{TAH} . The density of the carriers, $N(T)$, can have a weak temperature dependence, but this influence is assumed to be much smaller than the overall temperature dependence of the conductivity. The ratio of field energy to thermal energy is given as

$$\beta_A \equiv \frac{4ET_A}{3E_A T} = \frac{q_e E a}{k_B T} \quad (57)$$

and

$$Z_A(\beta_A) \equiv 1/\beta_A \sinh(\beta_A). \quad (58)$$

Combining these reduced terms, β_A , and Z_A , gives σ_{TAH} as

$$\sigma_{TAH} = \sigma_{TAH_o}(T) \left(\frac{T_A}{T} \right) Z_A(\beta_A) \exp\left(-\frac{T_A}{T} \right). \quad (59)$$

Since σ_{TAH} is expected to be the dominant mechanism at higher temperatures, the measured currents at room temperature and above are the primary focus. Under a low applied field, the behavior of σ_{TAH} is dominated by the exponential term with an expected $T^{-1}\exp(T^{-1})$ dependence. The fit of the conductivity behavior with the reduced thermally assisted hopping equation is shown, in Fig. 4.11, in both standard axes and semi-log plots. At high temperatures, the σ_{TAH} model fit improves with increasing temperature, as expected, and the semi-log plot reveals that the σ_{TAH} model is a poor fit below 280 K. From the fitting parameters of the σ_{TAH} model, the activation energy is found to be 0.95(±0.09) eV, which is within the range of accepted values for LDPE (see Table 4.1). Between 306 K and 325 K, it is difficult to fit the data with a single set of fitting parameters. This could be due to the temperature dependence of the density of states, which would influence the distribution and depth of traps available for hopping conduction. It could also be due in part to the influence of the instrumentation and a variation in heating rates. Another possibility that must be considered is the interaction of a secondary transport mechanism. The presence of a secondary, and even a tertiary, conduction mechanism is not unexpected. However, identifying a competing mechanism is only possible if the mechanism has a unique current behavior to distinguish it from other mechanisms.

The temperature measurements at 1000(±1) V and 2500(±1) V were also fit with the σ_{TAH} model; these fits can be seen in Fig. 4.12 and Fig. 4.13 in both standard axes and semi-log plots. At 1000(±1) V, the σ_{TAH} model is an excellent fit within the experimental uncertainty of the data at high temperatures. Using the fitting parameters for the σ_{TAH} model, the activation energy is determined to be 1.01(±0.09) eV, which is within the range of accepted values for LDPE (see Table 4.1). For the temperature measurements at 2500(±1) V, the σ_{TAH} model is a reasonable fit within the experimental uncertainty of the data, with a deviation greater of more than one

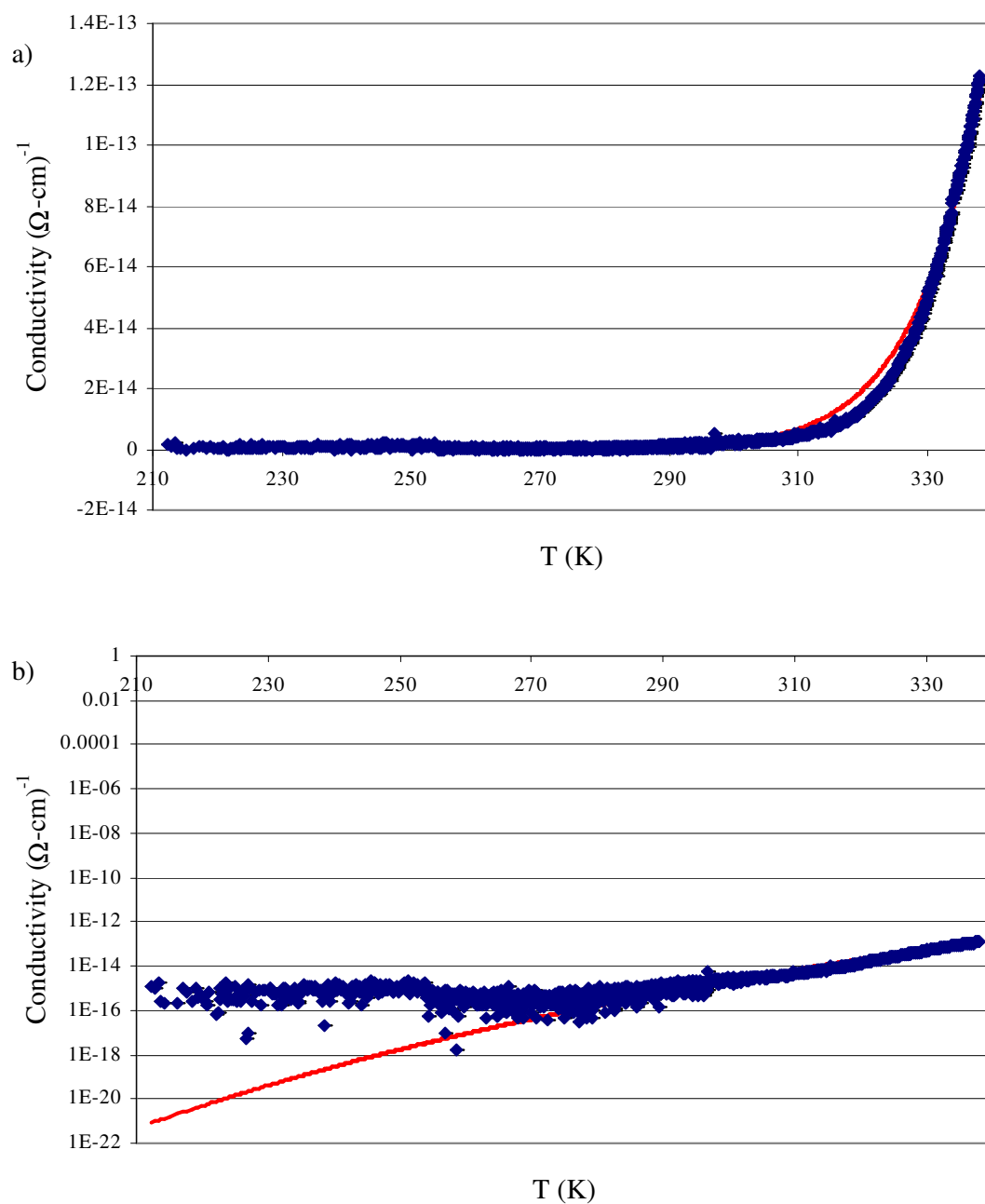


FIG. 4.11. Temperature dependent conductivity at 100 V with thermally assisted hopping model fit (red). a) Data with fit on standard axis and b) data with fit in a semi-log plot.

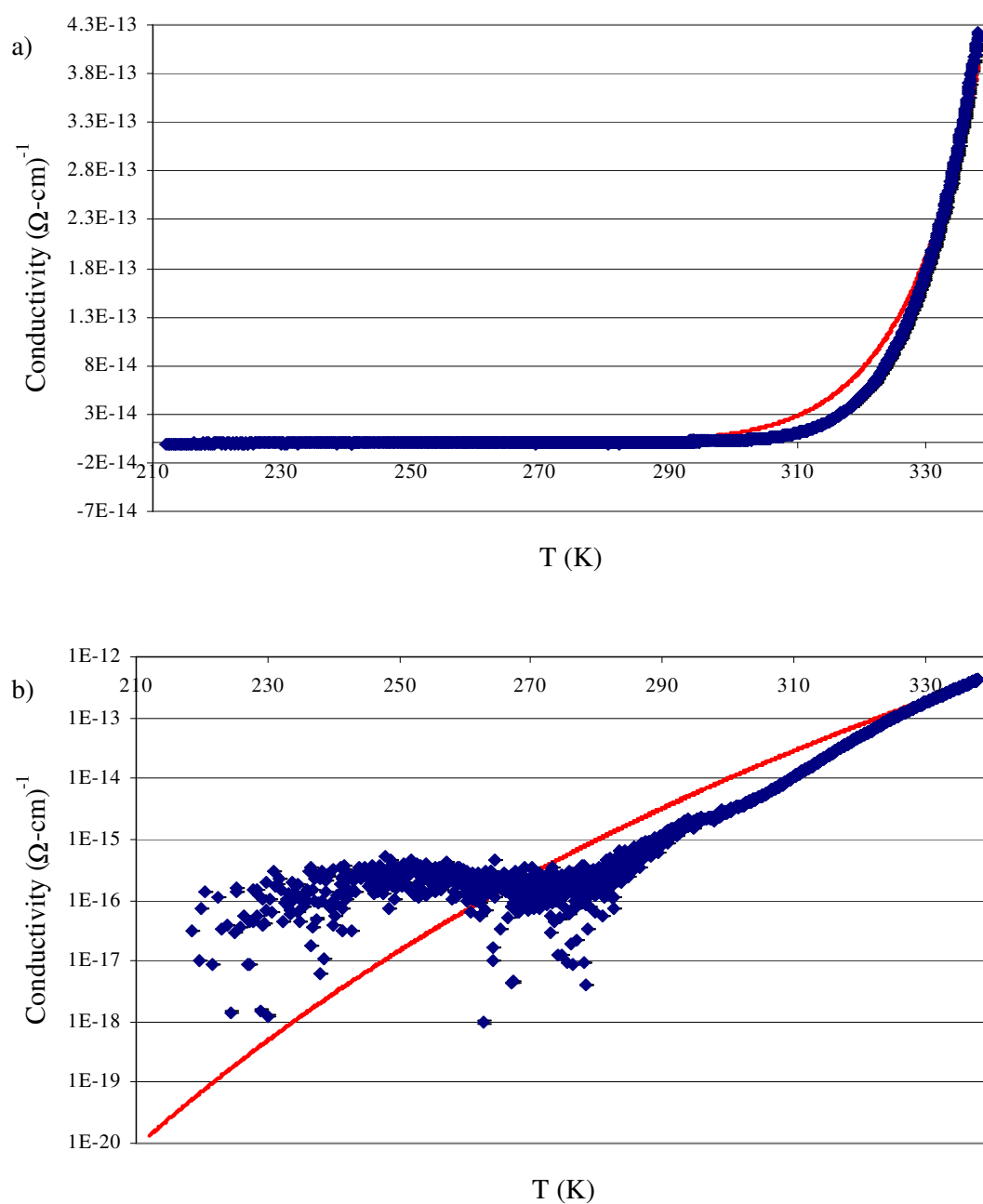


FIG. 4.12. Temperature dependent conductivity at 1000 V with thermally assisted hopping model fit (red). a) Data with fit on standard axis and b) data with fit in a semi-log plot.

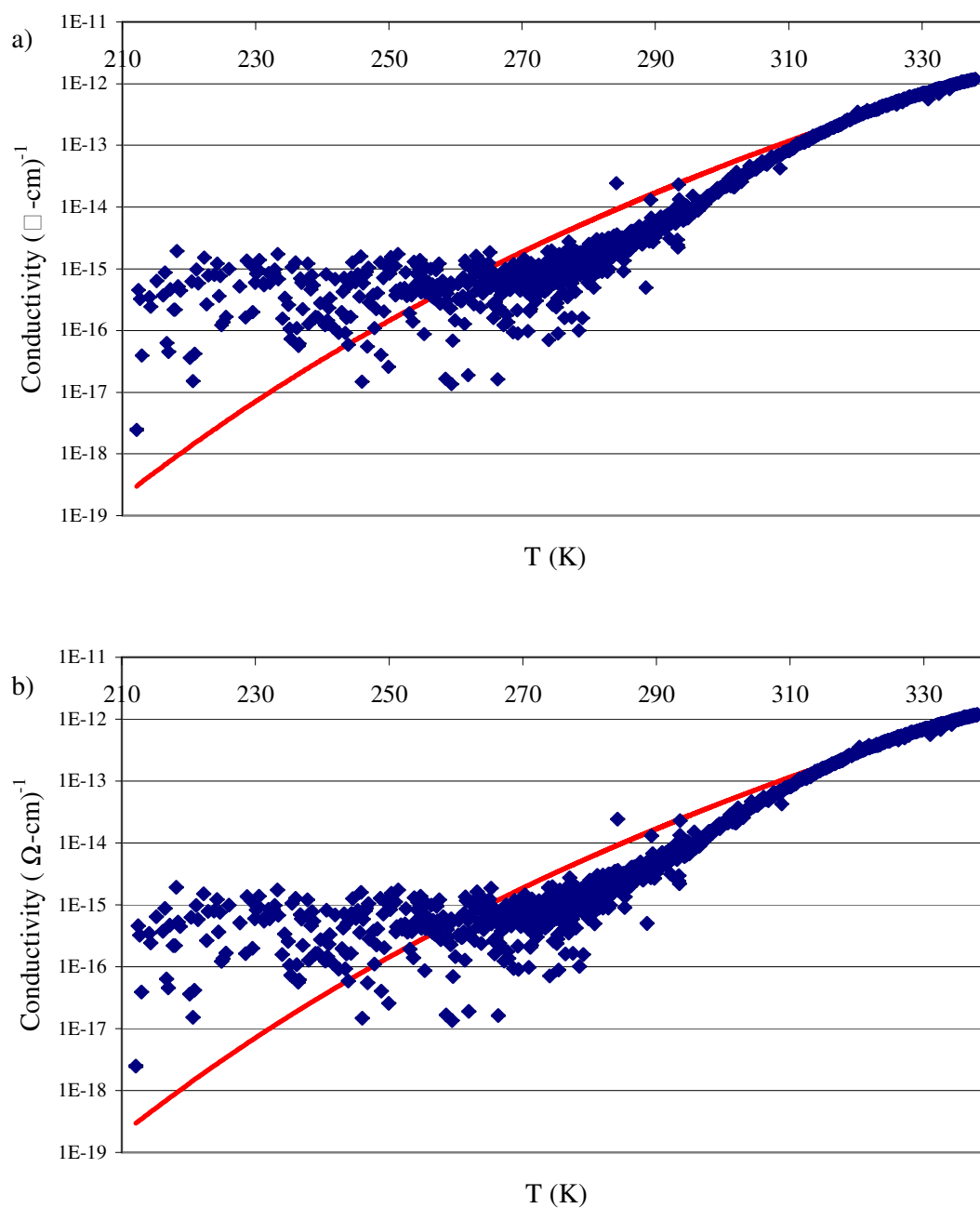


FIG. 4.13. Temperature dependent conductivity at 2500 V with thermally assisted hopping model fit (red). a) Data with fit on standard axis and b) data with fit in a semi-log_e plot.

standard deviation over a small range of temperatures near room temperature. The activation energy at 2500(± 1) V for the best fit of the data was found to be 1.17(± 0.09) eV, which is within the expected range for LDPE.

In each of the three temperature data sets, the σ_{TAH} model fits show deviation over a small range of temperatures near room temperature. Unfortunately, there is no conclusive indication of a unique behavior that would allow identification of a secondary mechanism. Additional data needs to be taken over the temperature range of 280 K to 320 K to eliminate instrumentation effects and changes in heating rates as the cause of disagreement between the fit and the data at those temperatures.

At low applied fields, the model predicts field independence with a $T^{-1}\exp(T^{-1})$ dependence and is a remarkably good fit within the experimental uncertainty of the data over a wide range of temperatures. The lower temperature behavior shows that the contribution to the conductivity from thermally assisted hopping decreases significantly. Lower temperatures mean the energy available to the electrons decreases and it becomes increasingly difficult for a carrier to move via multiple trapping. A sudden change in the conductivity of the sample was observed near 255 K and the σ_{TAH} model is a very poor fit below 255 K. A similar change in conductivity occurs near 255 K at 1000(± 1) V and since the temperature change was typically very consistent from 213 K to near room temperature, this change in conductivity is not due to a change in heating rate. Since the σ_{TAH} model is unable to provide a satisfactory fit of the data and the influence of the instrumentation can be disregarded, this change is a unique current behavior indicating the presence of a different conduction mechanism. At 2500(± 1) V, the change in conductivity behavior at low temperatures is not seen until roughly 205 K, which is below the temperature range selected for investigation in this study.

4.2.3 Variable Range Hopping Conductivity

Taking limits of very small and very large β can greatly simplify the expression for

variable range hopping conduction, Eq. (34). It is also advantageous to develop reduced variables, as was done for thermally assisted hopping. This gives σ_{VRH} in a simplified form,

$$\sigma_{VRH}(E, T) = \left\{ \sigma_{VRH_o}(T) \left(\frac{T_v}{T} \right)^{\frac{1}{4}} Z_{V1}(\beta_v) \exp \left[\left(-\frac{T_v}{T} \right)^{\frac{1}{4}} Z_{V2}(\beta_v) \right] \right\}, \quad (60)$$

where

$$\sigma_{VRH_o}(T) = \frac{2N_{E_F} v_{VRH} q_e^2}{(2\alpha)^2}, \quad (61)$$

$$T_v \equiv \frac{3(2\alpha)^3}{N_{E_F} \pi k_B}, \quad (62)$$

and

$$E_v \equiv \frac{4(2\alpha)^4}{N_{E_F} \pi q_e}. \quad (63)$$

The mean energy density of localized states can be written as

$$N_{E_F} = \left[\left(\frac{3}{\pi} \right) \left(\frac{\Delta H}{(2\alpha)^{-3}} \right) \right] \quad (64)$$

at energy E_F and mean trap separation of $(2\alpha)^{-1}$. The functions Z_{V1} and Z_{V2} seen in Eq. (60) are complex polynomial functions of β_v , both of which go to unity at low electric fields. The forms of these functions are not shown here but they are easily obtained using expansions of β_v and additional information about these functions can be found in the relevant references (Dennison and Brunson, 2008; Dennison *et al.*, 2009).

At low applied fields, the energy ratio is relatively small and applying the limit of small β to (60) gives a simplified, although not simple, reduced expression for σ_{VRH} ;

$$\sigma_{VRH}(E, T, \sigma_{VRH_o}, E_o, T) = \sigma_{VRH_o} \left(\frac{T_o}{T} \right)^{\frac{1}{4}} \left(1 - \frac{9\beta_{V2}(E, T, E_o, T_o)}{16} \right) \exp \left(- \left(\frac{T_o}{T} \right)^{\frac{1}{4}} \left(1 - \frac{(\beta(E, T, \alpha))^2}{4} \right) \right), \quad (66)$$

where β_{V2} is the energy ratio in reduced variables,

$$\beta_{V_2}(E, T, E_o, T_o) = \frac{4}{3} \left(\frac{T_o}{T} \right) \left(\frac{E}{E_o} \right). \quad (67)$$

With this reduced equation, the σ_{VRH} model can be fit to the low temperature LDPE data over the temperature range 213 K to 260 K for both 100(± 1) V and 1000(± 1) V. At these low temperatures, the increased variability inherent in the data makes curve fitting difficult. The fit for the 100(± 1) V set is quite reasonable given the spread of the data and is shown in Fig. 4.14, in standard axis and semi-log plots. Using the simplified σ_{VRH} model equation for the temperature-current LDPE data at 1000(± 1) V produces only a reasonable fit, which is due to using the limit of small β . Relaxing this limit allows a better fit, shown in Fig. 4.15 in both standard axis and semi-log plots, at the expense of increased difficulty of curve fitting. Since the transition in conductivity behavior was not seen at 2500(± 1) V until 205 K, which is outside the working temperature range of LDPE, it was not included in the analysis.

At low applied fields, the conductivity is independent of applied field and the characteristic $T^{-1/4} \exp(T^{-1/4})$ temperature dependence is seen. Investigation of the field dependence of variable range hopping was not aggressively pursued in this study. Low-temperature measurements, which are required to observe variable range hopping, at higher applied fields proved to be experimentally difficult, with increased susceptibility to electrostatic discharge events. Many of the instrumental obstacles to performing these measurements have been successfully addressed since the collection of the data used in this study.

Thus far, each potential mechanism has been treated separately. In the case of σ_{TAH} , it was originally assumed that carrier movement by direct quantum mechanical tunneling was negligible. This is an unrealistic assumption for a polymer and a better approximation of conductivity would be a combination of thermally assisted multiple trapping and tunneling transport mechanisms. Using the LDPE data at 100(± 1) V, both of the σ_{TAH} and σ_{VRH} model fits are shown on a semi-log plot in Fig. 4.16. The use of both models shows promise in improving

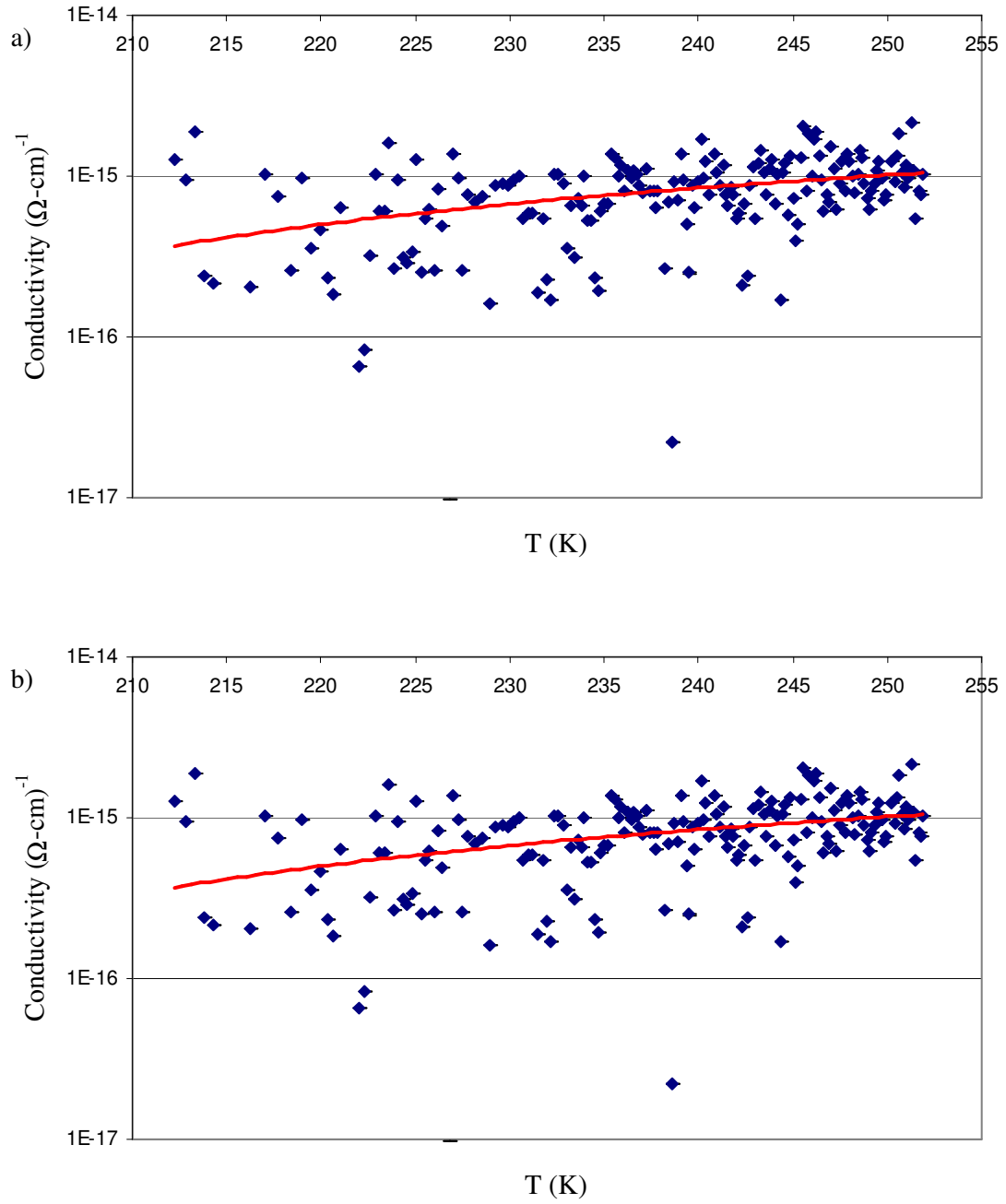


FIG. 4.14. Temperature dependent conductivity at 100 V with variable range hopping model fit (red). a) Data with fit on standard axis and b) data with fit in a semi-log_e plot.

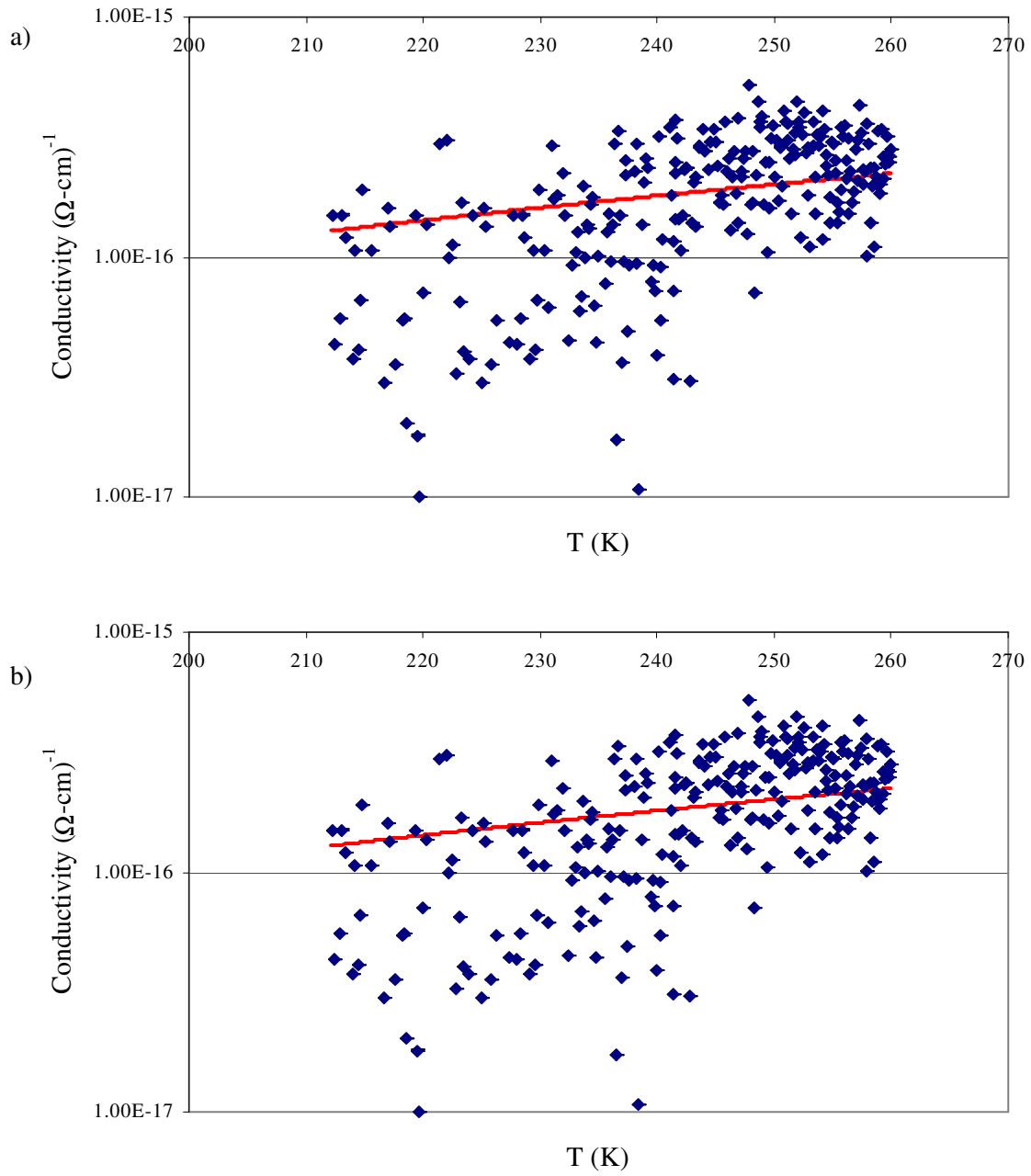


FIG. 4.15. Temperature dependent conductivity at 1000 V with variable range hopping model fit (red). a) Data with fit on standard axis and b) data with fit in a semi-log_e plot.

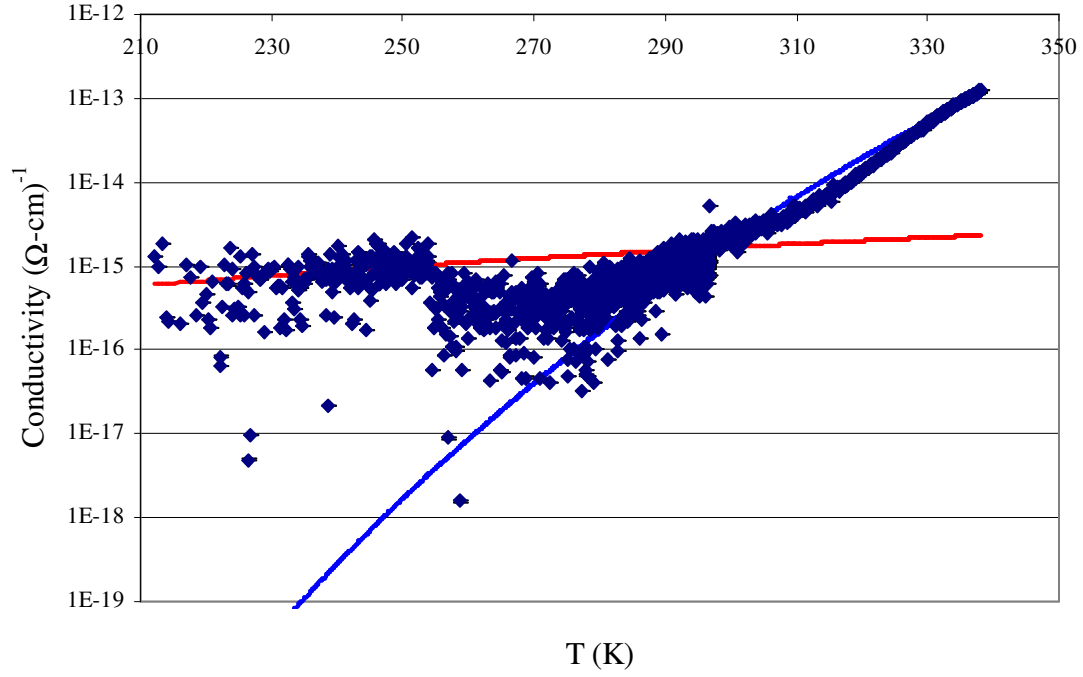


FIG. 4.16. Temperature dependent conductivity at 100 V with thermally assisted hopping conductivity (blue) and variable range hopping conductivity (red) model fits. Both models fit the data well where they are expected to be dominant mechanisms. Regions where neither model produces a good fit may be due to the influence of heating rates or the interaction of the two conduction mechanisms.

the fit over the region near room temperature, where σ_{TAH} was a poor fit to the data. A simple linear combination of the two models verifies this improvement, but does not improve the fit to the data between 260 K and 280 K. The interaction of the two conduction mechanisms is undoubtedly more complicated than a simple linear combination, but resolution of this interaction is left for future research.

It is now apparent that evaluating conductivity is more complicated than the basic function of charge per carrier q_c , carrier density n_c , and carrier mobility μ_c , that results in $\sigma = q_c n_c \mu_c$. Carrier density and mobility fluctuate with changes in the spatial distribution of charge carriers, occupation of charge carrier states, and variation of the localized states due to changes in electric field, temperature, etc., that affect morphology. Even when one transport mechanism may be known to be dominant, the true interdependence of electric field and temperature

behavior remains difficult to separate and quantify. An additional factor in the conductivity of polymers begins to emerge; the time dependence of conduction mechanisms influenced by changes in the distribution of charges or states cannot truly be ignored. This time dependence is briefly discussed in the final section of this chapter.

4.3 Influence of Time of Measurement on Conductivity

4.3.1 Time-Dependent Conduction

Time-dependent decay behavior means that the conductivity calculated for $27.5(\pm 0.02)$ μm LDPE, at 1 min, even for a low applied field of $\sim 3.9 \times 10^5$ V/cm, is typically an order of magnitude greater than the conductivity obtained after applied field duration of an hour or more. For example, the measured leakage current through an LDPE sample at $100(\pm 1)$ V is shown in Fig. 4.17. The conductivity calculated at 1 min is $3.124(\pm 0.007) \times 10^{-17}$, while the conductivity calculated at 1 hr and 5 hrs are $2.26(\pm 0.07) \times 10^{-18}$ $\Omega\text{-cm}^{-1}$ and $1.21(\pm 0.07) \times 10^{-18}$ $\Omega\text{-cm}^{-1}$, respectively.

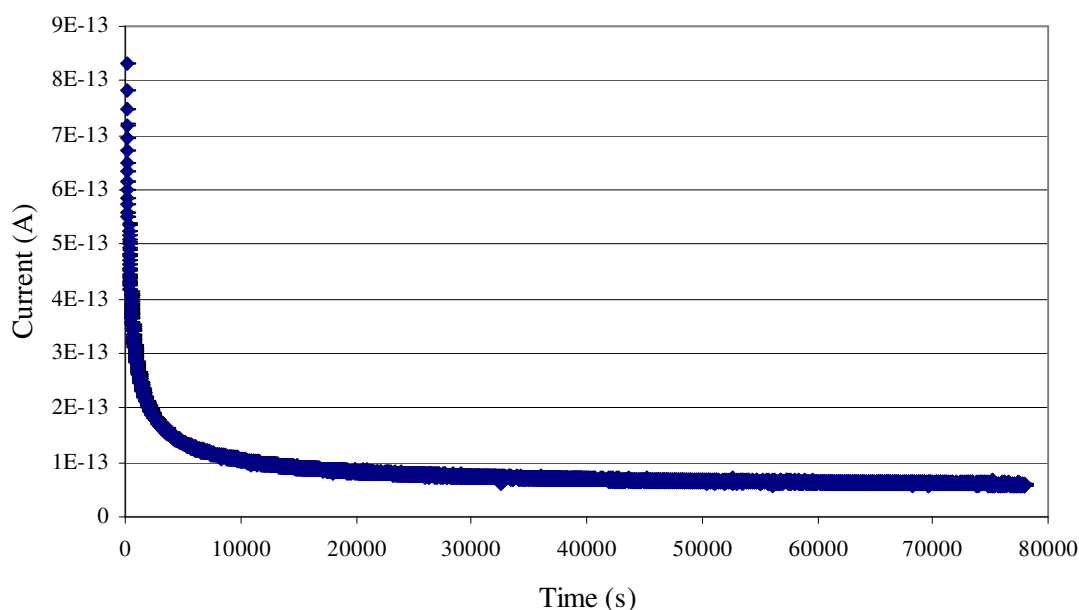


FIG. 4.17. Current decay at 100 V for 22 hrs.

The short time dependence of the current displayed in Fig. 4.18 shows a rapid exponential decrease, typical of a polarization conduction mechanism described by Eq. (37). The initial rise in current before 0.5 sec is attributed to the response time of the voltage supply. All runs exhibited a similar exponential decay with an average polarization decay time $\tau_p = 0.56(\pm 0.04)$ sec, independent of the applied electric field up to 3.6×10^6 V/m.

Such a rapid polarization decay time is consistent with the fact that polyethylene is composed of a non-polar monomer. A limited number of short time measurements were taken to investigate the possible field dependence of the transient initial currents. Although one may expect a correlated increase in peak current with increasing applied field, this behavior is not seen. A plot of the current peak at ~ 0.2 s and ~ 2 s, as a function of applied voltage is shown in Fig. 4.19 and it is apparent there is no correlation beyond the initial influence of the voltage supply. The onset of the exponential decay behavior is remarkably consistent and independent of the applied field. This indicates a stochastic component in the initial behavior, which would show strong field dependence if charge injection was the primary source of charge carriers (Many

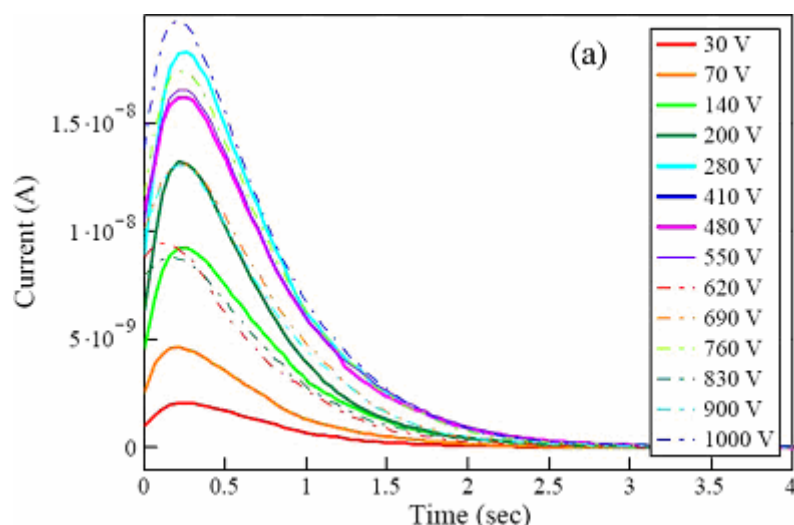


FIG. 4.18. Initial currents at low applied fields. The first 0.5 s rise is attributed to the response time of the voltage supply. a) List of voltages.

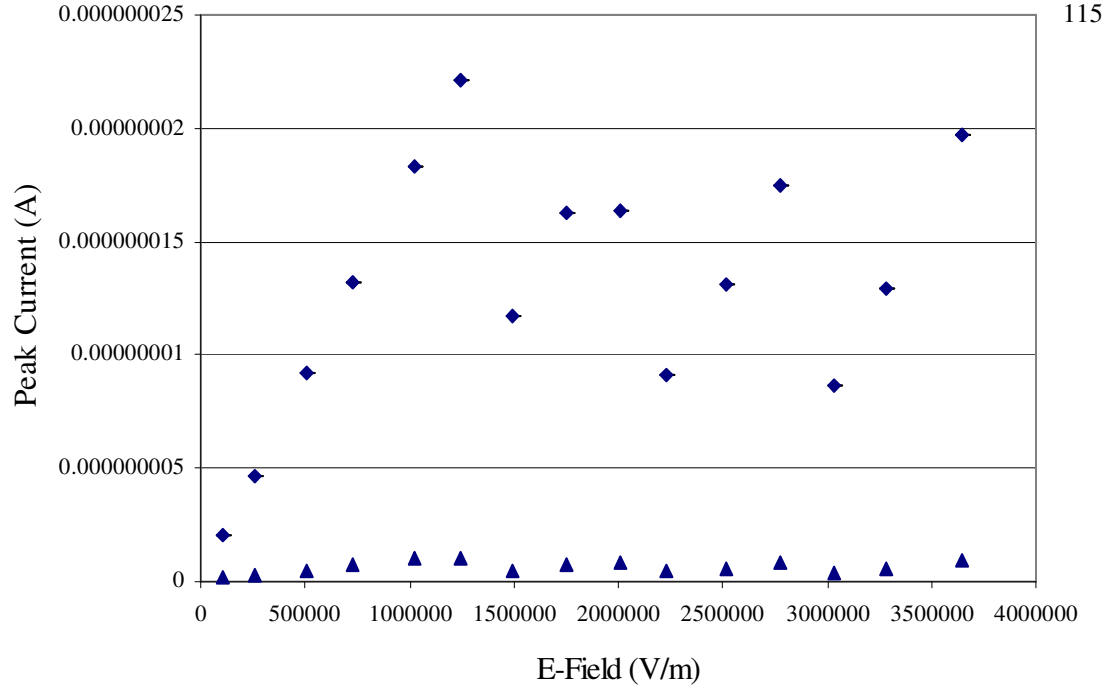


FIG. 4.19. Peak initial current values for 30 V to 1000 V data set. Taken at ~ 0.2 s (diamonds) and ~ 2 s (triangles).

and Rakavy, 1962).

Long time leakage current behavior is best fit with a power law behavior and, in fact, a strict mathematical approach founded on the molecular nature of polymers indicates that power law behavior is the only solution permissible for a relaxation function of the polymer molecules (Weron, 1991; Weron and Jurlewicz, 1993). This result is obtained assuming a wide distribution of dielectric relaxation times as the molecules adapt to the presence of an applied field. However, this behavior may also be adequately explained by a carrier hopping process through localized states, with increasing temperatures leading to a dominant hopping mechanism rather than a relaxation process (Adamec and Calderwood, 1978; Das-Gupta and Brockley, 1978; Lindmayer, 1965; Lowell, 1990). It is also probable that there is a transient dispersive conductivity that contributes to the overall measured currents. Driven by the uneven distribution of localized electric fields within the material, the dispersive component behaves in a similar manner to space charge effects. Traps fill with charge carriers, increasing the distances and energies required for a

carrier to hop into an available localized state. This results in a slowly decaying current.

The decay of the measured leakage current through the thin film LDPE samples shown in Fig. 4.18 can be fit with a decaying power law, $I = I_0 t^{-n}$ typical of diffusion current, shown in Fig. 4.20, in a $\log_e - \log_e$ plot. In the low field region, the exponent is found to be approximately $n=0.33$ and the pre-factor, I_0 , is found to be on the order of 2×10^{-12} A. This value of n is consistent with the process of carriers forming regions trapped space charge, with an exponent of one that would be expected for ohmic conduction of thermally generated carriers and <1 indicating the influence of carrier trapping. Similar power law behavior has been observed by Adamec and Calderwood (1978), with $n<0.4$ at times >10 sec; however, their argument is that the conduction mechanism is due neither to polarization nor to space charge effects, since any internal region of accumulated charge must be so small that its counter-field to the applied field is negligible. In contrast, Montanari and Morshuis (2005) and Marat-Mendes *et al.* (2004) present strong arguments for the presence of space charge trapping mechanisms in LDPE.

While high initial currents are a response of the material to the application of an electric

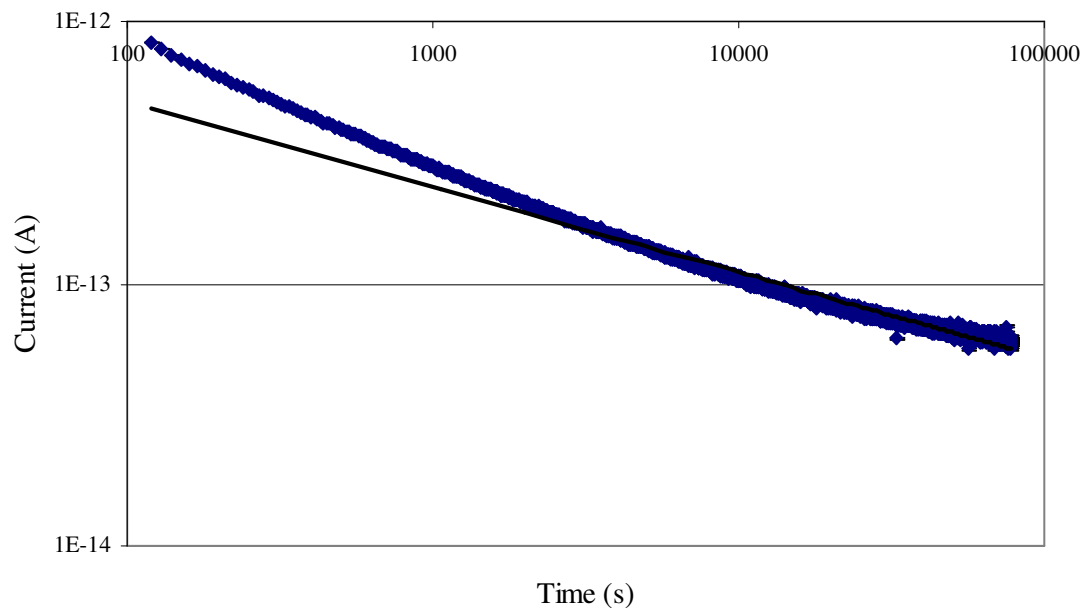


Fig. 4.20. Current decay at 100 V for 22 hours with power law fit.

field and correspond to the release of available carriers that results in a displacement current, the movement and modification of the molecules may continue for a very long time. A long-term, decaying current is observed for PE and many other polymers, with measured currents continuing to decrease over the course of hours or days (Dennison *et al.*, 2003a, 2005b; Frederickson and Benson, 2001; Frederickson and Dennison, 2003). This behavior is often difficult to see and may remain masked at very low currents by instrumental noise. Time-dependent conduction necessitates a method for establishing a reasonable estimation of equilibrium for the polymer being studied. A very long time measurement, with a duration time of 22 hours, at $100(\pm 1)$ V was used to estimate the rate of current change over time. The time of one hour was selected as reasonable for currents in LDPE to reach approximate equilibrium, with an average rate of current decay found to be less than 5% per hour after two hours.

4.3.2 Charging and Discharging Behavior

To gain further insight into the time-dependent behavior of LDPE, the charging and discharging behavior and the effects of repeated charging and discharging cycles were investigated. Steady state conductivity resulting from the motion of charge carriers through the material in direct response to an applied field, often referred to as a dark conductivity within the literature and scientific community, could be found by comparing the time-dependent sample behavior during the application of an applied field to the time-dependent behavior following the removal of the applied field. Several sets of such measurements were taken at $500(\pm 1)$ V, recording both the current under the applied field for one hour and the current after the field was removed for the next hour. Conductivities for these experiments were calculated and shown together in Fig. 4.21, in standard axis and log-log plots.

The differences in behavior between the charging and discharging currents provide insight into both charge transport and the dielectric response arising from the motion and flexibility of the LDPE chains results in the release or transfer of trapped charges. With and

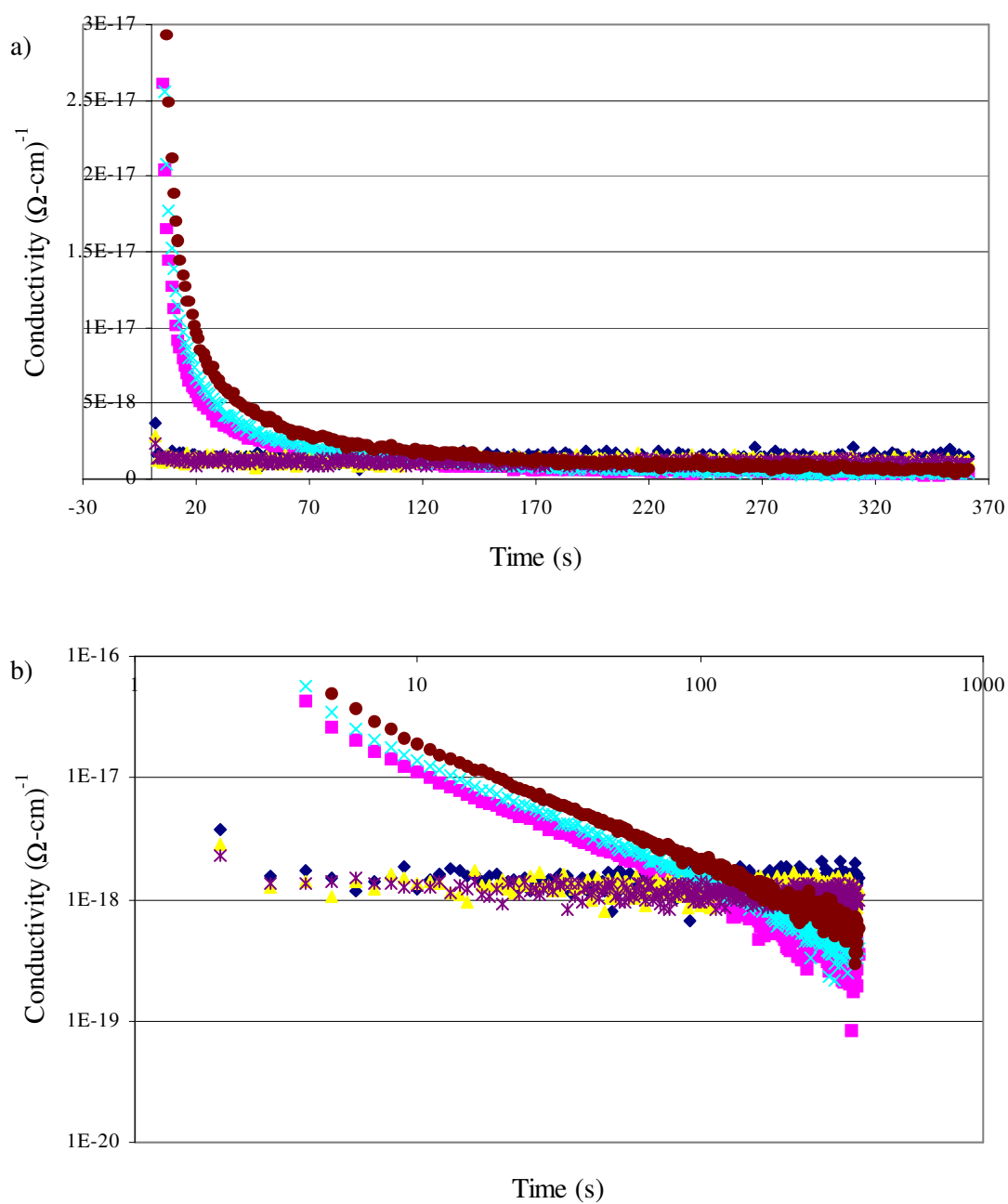


Fig. 4.21. Charging and discharging conductivities. a) Conductivity versus time of three charging (yellow, purple, dark blue) and discharging cycles (pink, light blue, red) at 500 V and b) log-log plot of conductivity versus time of three charging (yellow, purple, dark blue) and discharging cycles.

without the influence of an applied field, the rates of trapping and retrapping will differ and the discharge behavior will not mirror, with reversed polarity, the initial behavior (Adamec and Calderwood, 1978; Das-Gupta and Brockley, 1978). The discharge current should lack a steady state current, or dark conductivity value, although these currents can be very small and extremely difficult to distinguish from the inherent noise of the instrumentation. As shown in Fig. 4.21, the charging and discharging behaviors differ in their decay rate, indicating that multiple trapping, rather than dielectric relaxation, is the dominant mechanism. The discharge currents follow power law decay with an exponent range of $0.76(\pm 0.02)$ to $0.96(\pm 0.02)$, which is significantly larger than the exponent range of $0.32(\pm 0.01)$ to $0.40(\pm 0.01)$ found for the current decay with an applied electric field. The average conductivity value over the final ~10 min of the discharge runs was $4.43(\pm 0.07) \times 10^{-19} \Omega\text{-cm}^{-1}$. This is substantially smaller than the average conductivity obtained when the electric field was applied, which was found to be $1.281(\pm 0.007) \times 10^{-18} \Omega\text{-cm}^{-1}$. This supports the validity of a dark current conductivity, which is proportional to the difference in the absolute value of the charging and discharging currents, although many questions about its nature still remain.

The charging and discharging behaviors add to the rich picture of charge transport in LDPE but neither are useful in establishing a single, experimental conductivity value; rather, they are indicative of a time-dependent response of the material to an applied electric field. The question remains of whether or not the dark conductivity is truly separable from the long time decaying behavior remains. In fact, the presence of time dependent behavior indicates that the very concept of conductivity must be reevaluated for complicated materials such as LDPE and that, with or without a steady state conduction current, charge transport may be deeply connected to a dynamic dielectric response of the material.

Returning to the set of charging and discharging runs at $500(\pm 1)$ V, and expanding to include eight runs, the conductivities calculated from the average over the last ~10 min of the

charging runs are shown in Fig. 3.15. The conductivity can be seen to increase with subsequent cycles by a factor of ~ 5 , confirming that space charge accumulates over repeated applied fields. The conductivities can be fit with an exponential of the form

$$\sigma_{sc}(t) = (\sigma_{sc}^0 - \sigma_{sc}^{\infty})e^{t/\tau_p} + \sigma_{sc}^{\infty},$$

where σ_{sc}^0 and σ_{sc}^{∞} are the zero space charge and full space charge conductivities, with estimated values of $1.10(\pm 0.07) \times 10^{-19} \text{ } \Omega\text{-cm}^{-1}$ and $5.28(\pm 0.01) \times 10^{-19} \text{ } \Omega\text{-cm}^{-1}$, respectively. Assuming that trapped charge does not appreciably dissipate during the discharge times between the successive 1 hr field applications, the space charge decay constant, T_{sc} , is ~ 4 hr. This evidence of cumulative behavior could play a significant role in the evaluation of space charge limited conduction models. It raises the possibility that a conduction mechanism may not accurately depict the movement of individual carriers when there are changes in the time-dependent distribution of charge.

4.3.3 Electrostatic Breakdown

Time evolution becomes particularly important in the investigation of electrostatic discharge behavior, where the onset of breakdown is highly sensitive both to voltage ramping rates and to the duration of previous measurements. This returns to the idea that every applied electric field alters the morphology of the LDPE sample, contributing to charge transport and, by extension, to electrostatic breakdown. Predicting or understanding ESD requires an understanding of LDPE at the molecular level, including bonding energies, cohesive energy densities, and microscopic structural elements. Breaking the strong covalent bonds of the carbon backbone chains is unlikely but the weak van der Waals bonds of interchain bonding have a relatively small energy barrier (Peacock, 2000). It is postulated that there is a critical applied field, E_c , at which breakdown occurs (Dissado and Fothergill, 1992) but, since morphological changes occur even under low and moderate fields, the point at which this critical field is reached

can vary with applied field and sample history. The variation in ESD due to previous exposure and duration of exposure is commonly referred to as an endurance time.

Homogeneous breakdowns occur when a localized field reaches the critical field, internal to the sample, and breakdown is seen as nearly instantaneous (Dissado and Fothergill, 1992; Whitehead, 1953). Frequently these strong localized internal fields occur near the electrodes. Structural changes begin to play a large role; submicrocavities form as the interchain bonds break (Dissado and Fothergill, 1992; Lewis, 2002). These submicrocavities increase the mean-free path of electron charge carriers, enabling them to retain energy gained rather than dissipate the energy through phonon interaction. A runaway or cascade effect is achieved to rapidly increase the rate of bond dissolution. Breakdown may also occur along conduction pathways, without reaching a critical field, as a propagation mechanism. This type of breakdown is most sensitive to impurities and inhomogeneity within the sample. Since inhomogeneity is never completely avoidable in the manufacturing process, this type of breakdown may occur in combination with another type of breakdown.

Aging breakdowns are most strongly tied to sample history, particularly in cases of repeated applications of electric fields or long time durations of an applied field (Dang *et al.*, 1996; Griffiths *et al.*, 1998; Dissado and Fothergill, 1992). The probability of the break of an interchain bond can be correlated to the endurance time, with an increasing probability of bond breaking as time under an applied field increases. This, however, is only one approach in determining the time dependence of electrostatic breakdown and it has proven to be a particularly difficult behavior to quantify. Photographic examples of breakdown in LDPE and other thin-film polymers important in spacecraft charging are shown in Fig. 4.22.

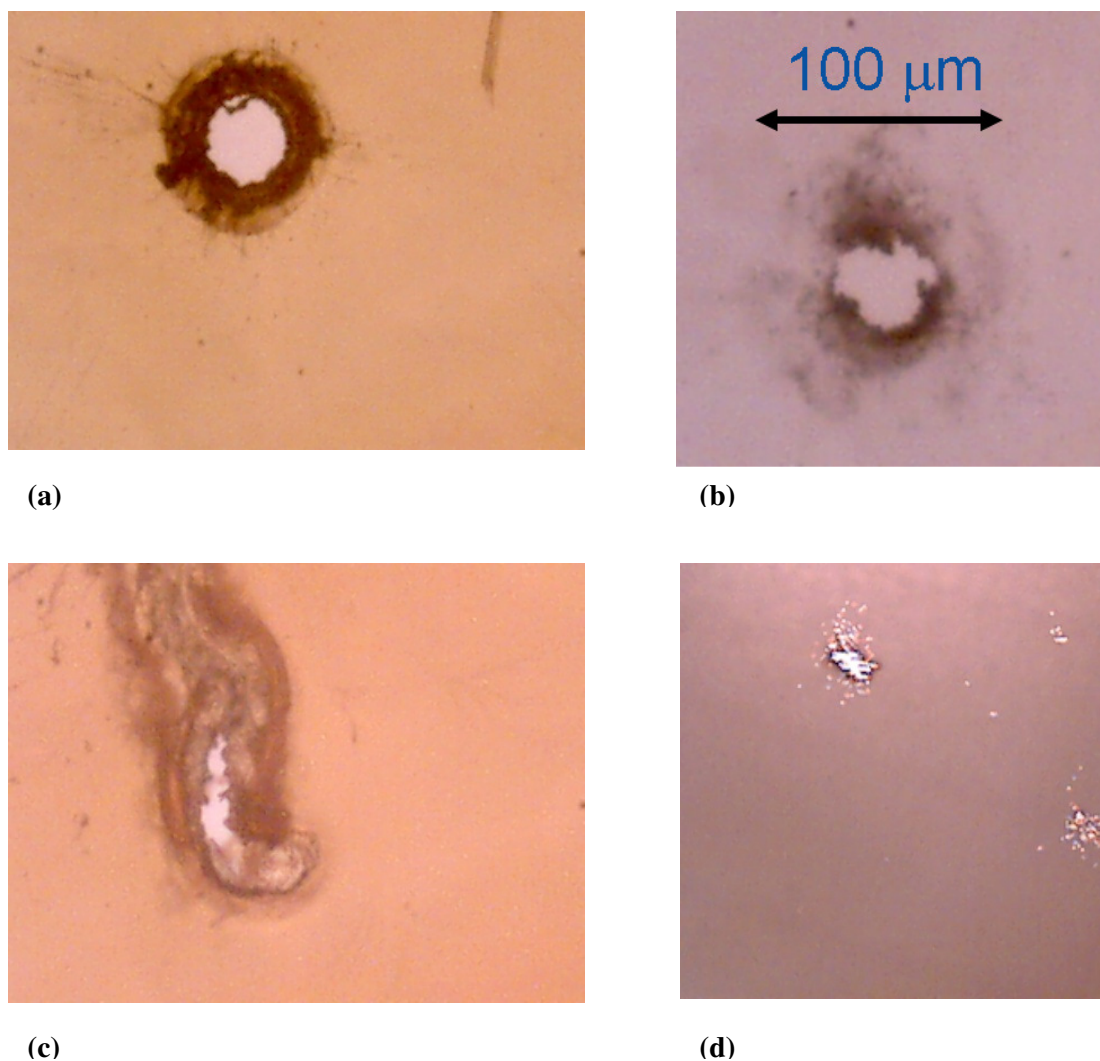


FIG. 4.22. Physical effects of electrostatic breakdown. Optical microscopy images of thin film polymer samples showing physical damage resulting from breakdown in the ESD chamber. Images were chosen to illustrate different types of damage seen for various materials under different breakdown conditions. a) Regular circular damage site of $\sim 25\ \mu\text{m}$ diameter in a Kapton sample taken using the Intel QX3 microscope at 200x magnification showing an approximate image of size of 0.65 mm (h) x 0.95 mm (w). b) Irregular circular damage site in LDPE of $\sim 50\ \mu\text{m}$ diameter for a sample at 6.5 kV. c) Highly irregularly shaped damage site of $\sim 20\ \mu\text{m}$ by $\sim 50\ \mu\text{m}$ in a Kapton sample. d) LDPE sample with multiple points of breakdown. Image was taken using the Intel QX3 microscope at 10x magnification showing an approximate image of size of 15 mm (h) x 23 mm (w).

CHAPTER 5

SUMMARY AND CONCLUSIONS

When investigating complicated and dynamic phenomena like the electrical properties of LDPE, it is necessary to take care in determining what information can be obtained from experiment and what can be inferred from that information. The preferred outcome is direct physical correlation to measured data and any approximations made during analysis, with mathematical consistency throughout. Strong physical correlations are often difficult to make in disordered materials where physical parameters are best represented by statistical averages and there is much debate over which properties of polymers can be considered intrinsic. The significant questions that have been addressed in this study include the properties of the charge carriers, the validity of hopping conduction models, and the influence of time-dependent conduction behavior.

5.1 Charge Carriers and Carrier Mobility

Typical conditions of this study include relatively moderate temperatures and applied electric fields, i.e. well below the melting point of LDPE and typically less than 60% of the average dielectric field strength, with direct contact between high-purity solid OFHC copper electrodes and high-purity samples. All of these factors reduce the likelihood of ionic transport through the sample as the primary conduction mechanism. This is in line with the literature where the identity of the charge carriers in LDPE is widely accepted to be electronic, preferentially electrons with holes assumed to be immobilized in valence bands. Whether or not the free electrons originate in the bulk or are injected by the electrodes remains controversial. This research has provided insight into the origin of charge carriers in LDPE. Initial transient currents are believed to be sensitive to carrier injection but the lack of strong electric field dependence of these transient currents indicates electrode independence for LDPE and a lack of

significant charge injection. This presents a problem because most analytical tools for explaining charge transport in polymers assume that the carriers available for charge transport are injected from the electrodes. The primary mechanism of charge injection found in the literature is Schottky injection, however, the slope obtained utilizing the standard Schottky plot gives an erroneous value of relative permittivity, $4.6(\pm 0.2)$ F/m for LDPE, which is outside the accepted range of 2.25-2.35 F/m. In addition, the field dependent behavior of LDPE has striking differences from an ideal SCLC behavior, which would also be governed by charge injection. The observed behavior is more complicated than a simple SCLC curve, casting further doubt on the validity of charge injection and indicating that space charge limiting currents may only be part of an extremely complex material response. The initial currents must then be due to a transient displacement current arising in response to the applied field with no net transfer of charge in or out of the material. Results of this study confirm that the assumption of electronic conduction is appropriate for LDPE under the given working range of temperatures and a broad range of applied fields. It is most likely that individual materials have different amounts of intrinsic and injected charge, with charge transport in LDPE taking place primarily with intrinsic carriers.

How a charge carrier moves between localized states and the rate of conduction are two of the fundamental questions concerning carrier mobility. Although it is a sound concept that can be directly tied to physical aspects of the material, carrier mobility is difficult to determine and measure experimentally. Standard approaches for crystalline and disordered materials both face limitations in three phase polymers like LDPE where the third, interfacial phase is poorly understood but contributes significantly to carrier trapping.

Conductivity can be related to mobility, $\sigma = q_c n_c \mu_c$, which appears to be simple and straightforward, but direct determination of mobility remains elusive. This is partly due to the existence of two types of conduction mechanisms: time-independent mechanisms involving the mobility of individual carriers and time-dependent mechanisms that depend on the change in

distribution of charges. The primary focus of this study has been investigating the mobility of individual carriers under equilibrium or steady state conditions. Measurements of leakage currents through thin film LDPE samples were used to calculate conductivity at relatively long times, allowing an approximation of steady state, time-independent conditions. This led to evaluation of hopping conductivity models as the primary mechanisms for individual carrier mobility.

5.2 Hopping Conductivity Models

The primary benefit of hopping conductivity models is avoiding the requirement of band structure. Lack of long-range order and periodicity in disordered materials does not lead to good quantum numbers and the standard band theory approach is not valid. Extended states arise along segments of the polymer chains, leading to localized sections of band structure. This leads naturally to hopping from localized state to localized state as the primary conduction mechanism with a wave-function overlap integral serving to determine hopping probabilities between sites. Leaving the details of the quantum mechanics to others (Barrie *et al.*, 1986), it is possible to evaluate hopping models and correlate fitting parameters qualitatively and quantitatively to physical parameters. While there have been many hopping models developed in past decades, two have emerged as the most promising approximations of transport behavior in polymers: thermally assisted hopping and variable range hopping.

Thermally assisted hopping (multiple trapping) was originally formulated for ionic conduction in crystals. It models thermal activation of a carrier from a shallow trap into a conduction band, followed by nearly immediate recapture in a nearby trap. Carrier mobility is then a factor of mean trap depth, ΔH , and the energy gained or lost by the carrier, $aq_c E_a$, as it moves over the distance between traps, a . Two fundamental behaviors are expected if thermally assisted hopping is a conduction mechanism. At low applied fields, σ_{TAH} should be field

independent and show a characteristic $T^{-1}\exp(T^{-1})$ dependence. For a constant temperature, field dependence begins to emerge and near a critical field value, σ_{TAH} diverges, indicating a rapid increase in conductivity leading to dielectric breakdown. A review of the data obtained for LDPE reveals that the conductivity corresponds to the σ_{TAH} model fit at higher temperatures where it is expected to be the dominant mechanism. Low applied fields do not show considerable field dependence and at moderate temperatures the conductivity is proportional to $T^{-1}\exp(T^{-1})$. Calculations of activation energies from the σ_{TAH} model fit are in reasonable agreement with the broad range of values reported in the literature.

The divergent behavior expected from the σ_{TAH} model at high fields is clearly seen in applied field measurements reviewed in Section. 4.1, although the breakdown fields obtained with the CVC were much less than those obtained with the ESD chamber. This reduced breakdown strength is most likely due to the aging response of the polymer, which can be introduced by including an endurance time. The mathematical form of the endurance time as an addition to σ_{TAH} model remains to be determined. Qualitatively, the breakdown values measured with the ESD chamber are considered instantaneous breakdown values and samples are only exposed to the increasing applied fields that lead directly to breakdown. In the CVC, many hours of measurements at lower fields were taken before breakdown occurred and this previous exposure lowered the effective dielectric field strength of the sample. With reasonable agreement in temperature and field dependence and activation energies, thermally assisted hopping was confirmed as a viable option for a charge transport mechanism in LDPE.

The second potential hopping mechanism is variable range hopping (tunneling), with low temperature measurements of particular interest. At room temperature, σ_{VRH} is not expected to play a contributory role in charge transport. As temperature decreases, the temperature dependent behavior shifts to a characteristic $T^{-1/4}\exp(T^{-1/4})$ dependence with a transition point found to be approximately 255 K at 100(\pm 1) V and 1000(\pm 1) V. Evaluation of activation energies reveals a

correlating transition as temperatures decrease and the values obtained at low temperatures are in agreement with values reported in the literature for tunneling behavior. The $T^{-1/4}\exp(T^{-1/4})$ behavior and reasonable agreement of the values of the physical parameters indicated that variable range hopping was a viable conduction mechanism for LDPE. It is also worth noting that a similar transition point has been seen in the radiation induced conductivity of LDPE within this same temperature range (Dennison *et al.*, 2007), possibly indicating a structural or physical transition point.

Field dependence at low temperatures was not pursued due to instrumental difficulties and will need to be examined with additional research. Determination of the effect of the applied field on the transition point at which the temperature dependence changes to $T^{-1/4}\exp(T^{-1/4})$ is of particular interest for future study.

5.3 Time Dependent Phenomena and Electrostatic Discharge in LDPE

Much of the difficulty in measuring electrical properties of a highly resistive polymer like LDPE comes from the dynamic response of the material to the environmental conditions. In this study, every effort was made to reduce the significant variables to easily controllable factors. However, even the best efforts cannot truly isolate single variables in a complex material. Sample history, or aging behavior, is not well understood. This is due to the nature of the polymer, where every applied field has a physical, if subtle, effect on the morphology. Shifting polymer chains alter the distribution and properties of the traps, which changes the ability of the carriers to move through the material. Furthermore, long time exposure to electric fields begins to alter the material significantly enough to lower the dielectric field strength of the material. The concentration and distribution of impurities, physical defects, and submicrocavities formed under mechanical, electrical, or thermal stress also strongly affect the carrier mobility. Diffusive movement of charge carriers, driven by unequal internal electric fields and distribution of charges, also plays a role in conduction. This diffusive behavior may be indistinguishable from

other transport mechanisms or may actively inhibit particular transport mechanisms. Space charge effects, despite theoretical dependence on the injection of charge carriers, cannot be completely disregarded and require much further investigation. All of these factors make it difficult to determine a straightforward conductivity value for LDPE and other polymers.

In addition to the problems inherent in measuring electrical properties of a polymer, there are significant practical difficulties. Highly resistive materials mean that very small currents are measured, often at the level where the physical vibrations of footsteps in the laboratory must be accounted for. The influence of the equipment, from voltage supplies to data acquisition cards and the air conditioning in the laboratory building itself, is often very difficult to determine and may introduce systematic errors. In this study, the Keithley 616 electrometers were capable of measuring currents on the order of 10^{-15} A with a certainty of $\pm 5 \times 10^{-15}$ A. In practice, it was found that the sensitivity of the system, including voltage supplies and the CV chamber itself, was on the order of $\pm 40 \times 10^{-15}$ A. In many cases, experimental results were discarded due to external influences, improper grounding, faulty connections, and a host of other electronic complications.

One final hurdle is that many different conduction models present with identical or very similar behaviors, such as Poole-Frenkel conduction and Schottky charge injection. Multiple charge transport mechanisms may exist simultaneously, either independently or in conjunction with other transport mechanisms. Much additional work is required to determine additional transport mechanisms and the interaction of multiple mechanisms.

5.4 Summary and Future Work

The successes of this study have been to increase the accuracy of measured currents used to determine conductivity and the validation of two hopping conduction mechanisms for LDPE. Investigation of field dependent behavior confirms that Poole-Frenkel conduction produces erroneous values of the dielectric constant, as does the standard Schottky injection model. Space

y charge limited current behavior is seen, but with significant deviations from ideal field behavior that casts doubt on its validity as a conduction mechanism, as well as the underlying assumption of injected charge. Investigation of temperature dependence revealed conductivity behavior in good agreement with thermally assisted hopping (multiple trapping) and variable range hopping (tunneling) models, as well as providing reasonable agreement of activation energies reported in the literature. Both field dependent measurements and thermally assisted hopping theory show a diverging current and conductivity at the onset of breakdown, providing additional confirmation of the thermally assisted hopping model. Time dependent charging and discharging behaviors also indicate that multiple trapping is the predominant transport mechanism at room temperature rather than a bulk dielectric response based on relaxation times of LDPE molecules.

The transition and interaction between conduction mechanisms remains to be investigated and understood, particularly with respect to field dependence. Low-temperature conductivity is extremely difficult to accurately measure and will require additional work and advances in instrumentation. Further work is needed to explore the charging and discharging behavior and other time-dependent conduction mechanisms. Much work remains to be done in quantifying the effect of sample history and the influence of endurance time on the field dependence of the conductivity, particularly with respect to the onset of electrostatic breakdown.

REFERENCES

- Adamec, V. and J. H. Calderwood, 1978, "Electrical Conduction and Polarization Phenomena in Polymeric Dielectrics at Low Fields," *J. Phys. D* **11**, 781-800.
- Adamec, V. and J. H. Calderwood, 1981, "On the Determination of Electrical Conductivity in Polyethylene," *J. Phys. D* **14**, 1487-1494.
- Anderson, J. C., K. D. Leaver, R. D. Rawlings, and J. M. Alexander, 1990, *Materials Science, 4th Edition* (Chapman and Hall, New York).
- Anderson, P. W., 1958, "Absence of Diffusion in Certain Random Lattices," *Phys. Rev.* **109**, 1492.
- Amos, A. T. and R. J. Crispin, 1975, "The Polarizabilities of CH and CC Bonds," *J. Chem. Phys.* **63**, 1890-1899.
- Apsley, N. and P. H. Hughes, 1974, "Temperature and Field-Dependence of Hopping Conduction in Disordered Systems," *Philos. Mag.* **30**, 963-972.
- Apsley, N. and P. H. Hughes, 1975, "Temperature and Field-Dependence of Hopping Conduction in Disordered Systems, II," *Philos. Mag.* **31**, 1327-1339.
- Aranguren, G., E. Hernandez, A. L. Pescador, C. A. D. Rincon, and M. Leon, 2003, "Thermally Stimulated Current and Electrical Resistivity in CuIn_3Se_5 ," *Mater. Lett.* **58**, 573-577.
- Arkhipov, V. I., E. V. Emelianova, and H. Bassler, 2001, "Equilibrium Charge Carrier Mobility in Disordered Hopping Systems," *J. Optoelec. and Adv. Mat.* **3**, 601-608.
- Ashcroft, N. W. and N. D. Mermin, 1976, *Solid State Physics* (W. B. Saunders Company, New York).
- ASTM D 257-99, 1999, *Standard Test Methods for DC Resistance or Conductance of Insulating Materials* (American Society for Testing and Materials, West Conshohocken).
- ASTM D 3755, 2001, *Standard Test Method for Dielectric Breakdown Voltage and Dielectric Strength of Solid Electrical Insulating Materials Under Direct-Voltage Stress* (American Society for Testing and Materials, West Conshohocken).
- ASTM D 495, 2001, *Standard Test Method for High-Voltage, Low-Current, Dry Arc Resistance of Solid Electrical Insulation* (American Society for Testing and Materials, West Conshohocken).
- Bambery, K. R. and R. J. Fleming, 2003, "Activation Energies and Electron Transport in LDPE," in *Annual Report 2003 Conference on Electrical Insulation and Dielectric Phenomena*, Albuquerque, NM, 2003 (IEEE Dielectrics and Electrical Insulation Society, Piscataway, NJ), p.28-31.

Bambery, K. R., R. J. Fleming, and J. T. Holboll, 2001, "Space Charge Profiles in Low Density Polyethylene Samples Containing a Permittivity/Conductivity Gradient," J. Phys. D **34**, 3071-3077.

Barrie, R., P. C. W. Holdsworth, and M. R. A Shegelski, 1986, "Hopping Conductivity for Localized Electronic States," J. Phys. C **20**, 2219-2229.

Bartnikas, R., 1983, *Testing and Materials* (American Society for Testing and Materials, Philadelphia).

Böttger, H. and V. V. Bryksin, 1985, *Hopping Conduction in Solids* (Akademie-Verlag, Berlin).

Boudou, L. and J. Guastavino, 2000, "Influence of Temperature Treatment on the Electrical Properties of Low-Density Polyethylene," J. Phys. D **33**, L129-L131.

Boudou, L. and J. Guastavino, 2002, "Influence of Temperature on Low-Density Polyethylene Films Through Conduction Measurement," J. Phys. D **35**, 1555-1561.

Broser, I. and R. Warminsky, 1950, "Theory of Luminescence and Electrical Conductivity of CdS Crystals," Ann. Der. Phys. **7**, 288.

Brunson, J. and J. R. Dennison, 2006, "E-field Conditioning and Charging Memory in Low-Density Polyethylene," in *Proceedings of the American Physics Society Four Corner Section Meeting*, Logan, UT.

Bussac, M. N., D. Michoud, and L. Zuppiroli, 1998, "Electrode Injection into Conjugated Polymers," Phys. Rev. Lett. **8**, 1678-1681.

Butcher, P. N., 1972, "On the Rate Equation Formulation of the Hopping Conductivity Problem," J. Phys. C **5**, 1817-1829.

Butcher, P. N., 1974, "Stochastic Interpretation of the Rate Equation Formulation of Hopping Transport Theory: III. DC Hopping Analogues and Their Application to Percolative Conductance Networks and Spin Systems," J. Phys. C **7**, 3533-3540.

Campbell, F. W., 1983, in *Engineering Dielectrics—Volume IIA: Electrical Properties of Solid Insulating Materials: Molecular Structure and Electrical Behavior*, American Society for Testing and Materials, edited by R. Bartnikas, Radiation Effects on the Electrical Properties of Solid Insulation (American Society for Testing and Materials, Philadelphia), p. 619.

Cho, K.-S., D.-C. Cho, J.-Y. Shin, S.-W. Lee, and J.-W. Hong, May 25-30, 1997, "Electrical Conduction Properties of Low Density Polyethylene and Cross-Linked Polyethylene Film," in *Proceedings of the 5th International Conference on Properties and Applications of Dielectric Materials*, Seoul, Korea (IEEE, Piscataway, NJ), p.166.

Coelho, R., L. Levy, and D. Sarraill, 1989, "Charge Decay Measurements and Injection in Insulators," J. Phys. D **22**, 1406-1409.

Crapo, E. and J. R. Dennison, 2002, "Spacecraft Charging Analysis," Utah State University Student Showcase, Logan, UT.

Crine, J.-P., 2005, "On the Interpretation of Some Electrical Aging and Relaxation Phenomena in Solid Dielectrics," IEEE Trans. Dielectr. Electr. Insul. **12**, 1089-1107.

Dang, C., J.-L. Parpal, and J.-P. Crine, 1996, "Electrical Aging of Extruded Dielectric Cables," IEEE Trans. Dielectr. Electr. Insul. **3**, 237-247.

Dang, C., L. Fan, Y. Shen, C. Nan, and S. Zhao, 2003, "Study of Thermal and Dielectric Behavior of Low-Density Polyethylene Composites Reinforced With Zinc Oxide Whisker," J. Therm. Anal. Calorim. **71**, 635-641.

Das-Gupta, D. K., 1997, "Conduction Mechanisms and High-Field Effects in Synthetic Insulating Polymers," IEEE Trans. Dielectr. Electr. Insul. **4**, 149-155.

Das-Gupta, D. K., June 21-26 2002, "Space Charge and Dielectric Polarization in Polymers," in *Proceedings of the 5th International Conference on Properties and Applications of Dielectric Materials*, Xi'an, China (IEEE, Piscataway, NJ), p.24.

Das-Gupta, D. K. and R. S. Brockley, 1978, "A Study of 'Absorption Currents' in Low-Density Polyethylene," J. Phys. D **11**, 955-962.

Davies, D. K., 1972, "Carrier Transport in Polythene," J. Phys. D **5**, 162-168.

Dennison, J. R. and J. Brunson, 2008, "Temperature and Electric Field Dependence of Conduction in Low Density Polyethylene," IEEE Trans. Plasma Sci. **36**, 2246-2252.

Dennison, J. R., A. R. Frederickson, N. W. Green, P. V. Swaminathan, and J. Brunson, April 1, 2002 to January 31, 2005b, *Test Protocol for Charge Storage Methods*, NASA Space Environments and Effects Program, Contract No. NAS8-02031, "Measurement of Charge Storage Decay Time and Resistivity of Spacecraft Insulators."

Dennison, J. R., A. R. Frederickson, and P. V. Swaminathan, October 2003a, "Charge Storage, Conductivity and Charge Profiles of Insulators as Related to Spacecraft Charging," in *Proceedings of the 8th Spacecraft Charging Technology Conference*, Huntsville, AL.

Dennison, J. R., J. Gillespie, J. Hodges, R. C. Hoffmann, J. Abbott, A. W. Hunt, and R. Spalding, Jun. 18-21, 2007, "Radiation Induced Conductivity of Highly Insulating Spacecraft Materials," in *Proceedings of the 10th Spacecraft Charging Technology Conference*, Biarritz, France (CNES, Paris, France).

Dennison, J. R., A. Sim, J. Brunson, J. Gillespie, S. Hart, J. Dekany, C. Sim, and D. Arnfield, January 5-8, 2009, "Engineering Tool for Temperature, Electric Field, and Does Rate Dependence of Low Conductivity Spacecraft Materials," in *47th AIAA Aerospace Sciences Meeting*, Orlando, FL (AIAA, Reston, VA), DVD-ROM.

Dennison, J.R., P.V. Swaminathan, R. Jost, J. Brunson, N. Green, and A. R. Frederickson, 2006, "Improved Methods and Analysis for Resistivity Measurements Related to Spacecraft Charging," IEEE Trans. Plasma Sci. **34**, 2191-2203.

Dennison, J. R., P. V. Swaminathan, R. Jost, J. Brunson, N.W. Green, and A. R. Frederickson, April 4-8, 2005a, "Proposed Modifications to Engineering Design Guidelines Related to

Resistivity Measurements and Spacecraft Charging,” in *Proceedings of the 9th Spacecraft Charging Technology Conference*, Epochal Tsukuba, Tsukuba, Japan (Air Force Research Lab, Hanscom AFB, MA), p.98.

Dennison, J. R., C. D. Thomson, J. Kite, V. Zavyalov, and J. Corbridge, October 2003b, “Materials Characterization at Utah State University: Facilities and Knowledgebase of Electronic Properties of Materials Applicable to Spacecraft Charging,” in *Proceedings of the 8th Spacecraft Charging Technology Conference*, Huntsville, AL.

Ding, S., A. Khare, M. T. K. Ling, C. Sandford, and L. Woo, 2000, “Polymer Durability Estimates Based on Apparent Activation Energies for Thermal Oxidative Degradation,” *Thermochimica Acta.* **367-368**, 107-112.

Dissado, L. A. and J. C. Fothergill, 1992, *Electrical Degradation and Breakdown in Polymers*, edited by G. C. Stevens (Peter Peregrinus Ltd., London).

Fleming, R. J., A. Ammala, P. S. Casey, and S. B. Lang, 2008, “Electrical Conductivity in LDPE Containing Nanosized Barium Strontium Titanate Particles,” in *Annual Report: Conference on Electrical Insulation and Dielectric Phenomena* (IEEE, Piscataway, NJ), p. 371-374.

Fowler, J. F., 1956, “X-ray Induced Conductivity in Insulating Materials,” *Proc. Royal Soc. London A* **23**, 464.

Fowler, J. F. and F. J. Farmer, 1953, “Effect of Temperature on the Conductivity Induced in Insulators by X-Rays,” *Nature (London)* **171**, 1020-1021.

Frederickson, A. R. and C. E. Benson, April 2001, “Improved Testing Procedures for Spacecraft Discharge,” in *Proceedings of the 7th Spacecraft Charging Technology Conference*, Noordwijk, The Netherlands (ESA-ESTEC, Noordwijk, The Netherlands) p. 223.

Federickson, A. R. and J. R. Dennison, 2003, “Measurement of Conductivity and Charge Storage in Insulators Related to Spacecraft Charging,” *IEEE Trans. Nucl. Sci.* **50**, 2284-2291.

Goodfellow Cambridge Ltd., Jan. 20, 2006, *Material Information—Polyethylene, Low Density LDPE* (Goodfellow Cambridge Ltd., Devon).

Griffiths, C. L., J. Freestone, and R. N. Hampton, 1998, “Thermoelectric Aging of Cable Grade XLPE,” in *Conference Record of IEEE International Symposium of Electrical Insulators*, Arlington, VA (IEEE, Piscataway, NJ), p. 578.

Hart, S., J. Brunson, and J.R. Dennison, 2006, “Electric Field Induced Hopping Conductivity: An Investigation of Electric Field-Dependent Resistivity in Polymers,” in *Proceedings of the American Physics Society Four Corner Section Meeting*, Logan, UT.

Hastings, D. and H. Garrett, 1996, *Spacecraft-Environment Interactions* (Cambridge Press, New York).

Hong, J. I., P. Winberg, L. S. Schadler, and R. W. Siegel, 2004, “Dielectric Properties of Zinc Oxide/Low Density Polyethylene Nanocomposites,” *Mater. Lett.* **59**, 473-476.

Hunt, A., 1994, "New Developments in the Theory of the Hopping Conductivity of Spatially Random Systems," *J. Phys. Condens. Matter* **6**, 1239-1252.

IEC 505, 1975, *Guide for the Evaluation and Identification of Insulation Systems of Electrical Equipment* (International Electrotechnical Commission, Geneva).

Ieda, M., 1980, "Dielectric Breakdown Process of Polymers," *IEEE Trans. Electr. Insul.* **15**, 206-224.

Ieda, M., T. Mizutani, and Y. Suzuoki, 1980, "TSC and TL Studies of Carrier Trapping in Insulating Polymers," *Mem. Fac. Eng.* **32**, 173-219.

Ieda, M., T. Mizutani, Y. Suzuoki, and Y. Yokota, 1988, "Study of Space Charge Effects in Polyethylene by Thermal Pulse Current Technique," *Proceedings of the 2nd International Conference on Properties and Applications of Dielectric Materials*, Beijing, China (IEEE, Piscataway, NJ), p. 586.

Jones, J. P., J. P. Llewellyn, and T. J. Lewis, 2005, "The Contribution of Field-Induced Morphological Change to the Electrical Aging and Breakdown of Polyethylene," *IEEE Trans. Dielectr. Electr. Insul.* **12**, 951-966.

Jonscher, A. K., 1999, "Dielectric Relaxation in Solids," *J. Phys. D* **32**, R57-R70.

Kiethley Instruments, 1975, *Instruction Manual for 616 Electrometer* (Keithley Instruments Inc., Cleveland).

Kiethley Instruments, 2004, *Lowlevel Measurements Handbook, 6th Edition* (Keithley Instruments Inc., Cleveland).

Khalil, M. S. and A. Gastli, 1999, "Investigation of the Dependence of DC Insulation Resistivity of Ultra-Clean Polyethylene on Temperature and Electric Field," *IEEE Trans. Power Delivery* **14**, 699-704.

Leach, R. D. and M. B. Alexander, 1995, *Failures and Anomalies Attributed to Spacecraft Charging* (NASA Reference Publication, Huntsville).

Lengyel, M. A., 1966, "Schottky Emission and Conduction in Some Organic Insulating Materials," *J. Appl. Phys.* **37**, 807-810.

Lewis, J. T., 1955, "Ionic Configuration Interaction in Some Excited States of the Hydrogen Molecule," *Proc. Phys. Soc.* **68**, 632-636.

Lewis, T. J., 1986, "Electrical Effects at Interfaces and Surfaces," *IEEE Trans. Electr. Insul.* **21**, 289-295.

Lewis, T. J., 2002, "Polyethylene Under Electrical Stress," *IEEE Trans. Electr. Insul.* **9**, 717-729.

Lida, K., J. S. Kim, S. Nakamura, and G. Sawa, 1992, "Effects of Molecular Structure on Electrical Conduction in Low-Density Polyethylene Above its Melting Point," *IEEE Trans. Electr. Insul.* **27**, 391-398.

- Lindmayer, J., 1965, "Current Transients in Insulators," J. Appl. Phys. **36**, 196-201.
- Lowell, J., 1990, "Absorption and Conduction Currents in Polymers: A Unified Model," J. Phys. D **23**, 205-210.
- Many, A. and G. Rakavy, 1962, "Theory of Transient Space-Charge-Limited Currents in Solids in the Presence of Trapping," Phys. Rev. **126**, 1980-1988.
- Marat-Mendes, J. N., R. M. Neagu, and E. R. Neagu, 2004, "Electrical Conduction and Space Charge Trapping in Highly Insulating Materials," J. Phys. D **37**, 343-347.
- McCubbin, W. L., 1970, "Conduction Processes in Polymers," J. Appl. Phys. **46**, 5122-5126.
- Mizutani, T., C. Zhang, and M. Ishioka, 2003, "Space Charge Behavior in LDPE and its Blend Polymers," in *IEEE 11th International Symposium of Electrets*, (IEEE, Piscataway, NJ), p.147.
- Montanari, G. C., C. Laurent, G. Teyssedre, A. Campus, and U. H. Nilsson, 2005, "From LDPE to XLPE: Investigating the Change of Electrical Properties. Part I: Space Charge, Conduction and Lifetime," IEEE Trans. Dielectr. Electr. Insul. **12**, 438-446.
- Montanari, G. C., G. Mazzanti, F. Palmieri, A. Motori, G. Perego, and S. Serra, 2001, "Space-Charge Trapping and Conduction in LDPE, HDPE and XLPE," J. Phys. D **34**, 2902-2911.
- Montanari, G. C. and P. H. F. Morshuis, 2005, "Space Charge Phenomenology in Polymeric Insulating Materials," IEEE Trans. Dielectr. Electr. Insul. **12**, 756-765.
- Mort, J. and H. Scher, 1971, "Transition from Transient to Steady-State Currents in Insulators," J. Appl. Phys. **42**, 3939-3947.
- Mott, N. F., 1969, "Conduction in Non-Crystalline Materials III. Localized States in a Pseudogap and Near Extremities of Conduction and Valence Bands," Phil. Mag. **19**, 835.
- Mott, N. F., 1975, "Coulomb Gap and Low-Temperature Conductivity of Disordered Systems," J. Phys. C **8**, L239-L240.
- Mott, N. F. and E. A. Davis, 1979, *Electronic Processes in Non-Crystalline Materials*, 2nd Edition (Oxford University, Oxford).
- Mott, N. F. and R. W. Gurney, 1940, *Electronic Processes in Ionic Crystals* (Oxford University, Oxford).
- Mott, N. F. and A. M. Stoneham, 1977, "The Lifetime of Electrons, Holes and Excitons Before Self-Trapping," J. Phys. C **10**, 3391-3398.
- Movaghar, B. and W. Schirmacher, 1980, "On the Theory of Hopping Conductivity in Disordered Systems," J. Phys. C **14**, 859-880.
- Nath, R. and M. M. Perlman, 1989, "Steady-State Bulk Trap-Modulated Hopping Conduction in Doped Linear Low-Density Polyethylene," J. Appl. Phys. **65**, 4854-4858.

Neagu, E. R. and J. N. Marat-Mendes, 2003, "Space-Charge-Controlled Conductivity in Low-Density Polyethylene," *Appl. Phys. Lett.* **82**, 1920-1922.

Parpal, J.-L., J.-P. Crine, and C. Dang, 1997, "Electrical Aging of Extruded Dielectric Cables: A Physical Model," *IEEE Trans. Dielectr. Electr. Insul.* **4**, 197-209.

Peacock, A. J., 2000, *Handbook of Polyethylene* (Marcel Dekker Inc., Basel).

Poole, H. N., 1917, "On the Dielectric Constant and Electrical Conductivity of Mica in Intense Fields," *Philos. Mag.* **34**, 195-204.

Oi, X. and S. Boggs, 2002, "Model for High Field Conduction in Doped Polymers," in *IEEE International Symposium of Electrical Insulators*, Boston, MA (IEEE, Piscataway, NJ), CD-ROM.

Raju, G.G., 2003, *Dielectrics in Electric Fields* (Marcel Dekker Inc., New York).

Rakhmanova, S. V. and E. M. Conwell, 2000, "Electric-Field Dependence of Mobility in Conjugated Polymer Films," *Appl. Phys. Lett.* **76**, 3822-3824.

Ramsey, N. W., 1953, "Effect of Temperature on Conductivity Induced in Insulators by X-Rays," *Nature (London)* **172**, 214.

Reiser, A., M. W. B. Lock, and J. Knight, 1969, "Migration and Trapping of Extrinsic Charge Carriers in Polymer Films," *Trans. Faraday Soc.* **65**, 2168-2185.

Rose, A., 1951, "An Outline of Some Photoconductive Processes," *RCA Rev.* **12**, 362-414.

Salamone, J. C., 1996, Ed., *Polymeric Materials Encyclopedia, Volume 9* (CRC Inc., Rochester).

Scher, H. and E. W. Montroll, 1975, "Anomalous Transit-Time Dispersion in Amorphous Solids," *Phys. Rev. B* **12**, 2455-2477.

Scher, H. and C. H. Wu, 1961, "Random Walk Theory of a Trap-Controlled Hopping Transport Process," *Proc. Natl. Acad. Sci.* **78**, 22-26.

Schug, J. C., A. C. Lilly, and D. A. Lowitz, 1907, "Schottky Currents in Dielectric Films," *Phys. Rev. B* **1**, 4811-4818.

Sperati, C. A., W. A. Franta, and H. W. Starkweather, 1953, "The Molecular Structure of Polyethylene. V. The Effect of Chain Branching and Molecular Weight on Physical Properties," *J. Am. Chem. Soc.* **75**, 6127-6133.

Stannet, A. W. and D. A. Schroff, 1957, "Temperature Coefficient of Resistivity of Polyethene and Oil-Impregnated Paper," *Nature (London)* **179**, 94.

Swaminathan, P. V., 2004, "Measurement of Charge Storage Decay Time and Resistivity of Spacecraft Insulators," Master of Science Thesis, (Utah State University).

Tahira, K. and K. C. Kao, 1985, "Anomalous Photocurrent Transient in Polyethylene," J. Phys. D **18**, 2247-2259.

Takahashi, S. and J. R. Dennison, 2001, "Classical Resistivity Method in Atmosphere and Vacuum," Senior Research Project (Utah State University).

Tanaka, Y., N. Ohnuma, K. Katsunami, and Y. Okhi, 1991, "Effects of Crystallinity and Electron Mean-Free-Path on Dielectric Strength of Low-Density Polyethylene," IEEE Trans. Electr. Insul. **26**, 258-265.

Taylor, D. M. and T. J. Lewis, 1971, "Electrical Conduction in Polyethylene Terephthalate and Polyethylene Films," J. Phys. D **4**, 1346-1357.

Tjong, S. C. and G. D. Liang, 2005, "Electrical Properties of Low-Density Polyethylene/ZnO Nanocomposites," Mater. Compos. Phys. **100**, 1-5.

Weron, K., 1991, "A Probabilistic Mechanism Hidden Behind the Universal Power Law for Dielectric Relaxation: General Relaxation Equation," J. Phys. Condens. Matter **3**, 9151-9162.

Weron, K. and A. Jurlewicz, 1993, "Two Forms of Self-Similarity as a Fundamental Feature of the Power-Law Dielectric Response," J. Phys. A **26**, 395-410.

Whitehead, S., 1953, *Dielectric Breakdown of Solids* (Oxford University Press, Oxford).

Wintle, H. J., 1971, "Decay of Excess Charge in Dielectrics Having Shorted Electrodes," J. Appl. Phys. **42**, 4724-4730.

Wintle, H. J., 1983, in *Engineering Dielectrics—Volume IIA: Electrical Properties of Solid Insulating Materials: Molecular Structure and Electrical Behavior*, edited by R. Bartnikas, Conduction Processes in Polymers (American Society for Testing and Materials, Philadelphia), p. 239.

Wintle, H. J., 1999, "Charge Motion and Trapping in Insulators," IEEE Trans. Dielectr. Electr. Insul. **6**, 1-9.

Wysocki, S., S. Karolczak, L. Mazurek, and J. Kroh, 1995, "The Energy Distribution Function of Excess Electrons Trapped in the Pulse Irradiated Low Density Polyethylene," Radiat. Phys. Chem. **45**, 79-85.

Yin, Y., J. Chen, Z. Li, and D. Xiao, June 5-9 2005, "High Field Conduction of the Composites of Low-Density Polyethylene/Nano SiO_x and Low-Density Polyethylene/Micrometer SiO₂," in *Proceedings of the International Symposium of Electrical Insulating Materials*, Kitakyushu, Japan (IEEE, Piscataway, NJ), CD-ROM.

Zallen, R., 1983, *The Physics of Amorphous Solids* (Wiley, New York).

APPENDICES

APPENDIX A

CVC INSTRUMENTATION

Obtaining accurate measurements of extremely small leakage currents required significant creation and adaptation of equipment. This effort can be divided into four areas of instrumentation: sample measurement, reducing electrical noise, chamber adaptations, and managing overall system error. Sample measurement includes the details of the electrode plate assembly, spring clamp assembly, and electrode disks. Reducing electrical noise details the specific steps taken to reduce electrical noise introduced to the chamber or signal from the laboratory environment. Chamber adaptations include descriptions and details of outfitting the CVC chamber for vacuum and temperature measurements. Overall system errors are addressed in Appendix C.

A.1 Sample Measurement

A.1.1 Electrode Plate Assembly

The samples must be well characterized, both in their properties and in the preparation and handling of the samples. This was explained in detail in Section 3.2. Samples must also be able to interact with the CVC chamber in a reproducible, controlled way. This begins with the configuration and construction of the electrode and sample apparatus. The electrode plate assembly includes two types of copper plates, as well as the copper electrode disks. One plate is anchored to the grounded copper plate and also serves as an anchor to the electrodes, with nylon screws attaching each pair of the electrode disks. The electrode guard plates are copper rectangles with holes for the electrode disks; they are screwed into the anchor plates and have small holes for thermocouple contacts and for the signal wires to pass through. Nylon tipped set screws hold the signal wires in position as they pass through the guard plates; this reduces the

strain on the wires, which are delicate and break easily. Additional set screws in the electrode disks ensure good contact between the wire core and the copper of the electrode disk. Between the anchor plate and the electrode guard plates is a layer of 125 μm thick Teflon film from McMaster-Carr. The layers of Teflon were periodically washed with methanol to remove contaminants that may have accumulated during use of the chamber. When needed, the electrode plate assembly was disassembled for cleaning and polishing. Polishing compounds without aluminum oxides and meant for copper were used to polish the plates and electrode disks. The electrode plate assembly was washed with soap and water to remove residue from the polishing compound. Each piece was then chemically cleaned with a sequence of dichloromethane, acetone, and methanol baths in an ultrasonic cleaner.

The electrode disks were machined and sanded to round the edges in contact with the samples, reducing the chance of localized discharge events due to high electric fields developed along sharp metal edges. Each electrode disk has an effective diameter of 1.59 (± 0.03) cm, corresponding to a percent error of $\pm 2\%$, and an effective area of 1.98 (± 0.08) cm^2 , corresponding to a percent error of $\pm 4\%$. Errors in diameter were set at a lower bound by subtraction of half the 50 μm radius of curvature machined on the edges of the electrode disks and at an upper bound by addition of half of a typical sample thickness of approximately 50 μm . The area of the electrode disk is fixed, but the contact area may vary if proper precautions are not taken.

A.1.2 Spring Clamp Assembly

Initially, the polycarbonate plate clamps were used to hold the thin film samples in place on the metal half plates. The weight of the electrode plate stack held the electrode disks in contact with the samples. This proved to be insufficient to obtain consistent contact areas, however, due to natural variations in sample thickness and inconsistent pressures and torques introduced by the cooling reservoir. Firm contact with consistent pressure between the electrode

disks and the samples is necessary for reproducible conduction. The ASTM standard for DC conductivity measurements for insulating materials requires 140-700 kPa pressure applied to the sample. A spring clamp system was developed by J. Dekany and S. Hart of the USU Materials Physics Group to deliver a consistent clamping force between samples and the polished copper electrode disks. The spring clamp assembly is seen in Fig. 3.13. The variability of surface contact area from run to run with the spring clamp assembly is roughly estimated to be less than $\pm 1\%$. Determining the pressure on the samples takes both the mass of the electrode plate assembly and the force exerted by the springs into account.

$$P = \frac{F_{epa} + F_{sp}}{A} = \frac{m_{epa}g + 4(kX_c)}{4(\pi R^2)},$$

where k is the spring constant, given by McMaster-Carr as $4.6 (\pm 0.5) \times 10^4$ N/m. X_c is the spring compression and is measured to be $1.6(\pm 0.2)$ mm of compression after two full rotations. R is the effective radius of the electrode. The mass, m_{epa} , is the mass of the entire electrode plate assembly and was measured to be $1.35(\pm 0.01)$ kg. The constant, g , is the acceleration of gravity. This produces a total pressure exerted on the sample, per electrode, of $380(\pm 100)$ kPa. Since the pressure due to the weight of the electrode plate assembly is significantly less than the uncertainty in the pressure due to the spring clamp assembly, the overall uncertainty in the pressure calculation can be obtained using

$$\frac{\Delta P}{P} = \frac{\Delta k}{k} + \frac{\Delta X_c}{X_c} + 2 \frac{\Delta R}{R},$$

and was found to be $\pm 24\%$. This total clamping pressure of $380(\pm 100)$ kPa is at the center of the required range given by the ASTM standard. The clamp design assures that the clamping pressure is both uniform and reproducible. Washers added to the electrode mount assures that the electrode is parallel to the sample and underlying high voltage plate, which leads to a consistent clamping area.

A.1.3 Reducing Electrical Noise

At the femtoamp level of current measurements, the care taken to eliminate electrical noise is critical. This process is a matter of trial and error and will continue as the CVC chamber remains in use by the USU Materials Physics Group. Electrical noise has many variable sources and can be very difficult to eliminate. Obvious steps are the correct selection of low-noise cabling, including the vacuum-compatible coaxial cables that attach to the electrode disks and the shielded triaxial cables. The BNC to triax connection is made inside a grounded metal box outside the chamber. Each voltage plate inside the chamber, as well as the electrode plate assembly and the CVC chamber itself were kept grounded even when no measurements were being taken. Every effort was made to eliminate and avoid ground loops both within the chamber and between the chamber and the electronic components. All electrometers, voltage supplies, signal control units, and other electronic components were carefully grounded to a central grounding hub on the support cabinet. Ground connections were painstaking tracked and are noted in the diagrams in Appendix B.

A rather sophisticated system of AC power distribution is used for the CVC chamber to minimize electrical noise from the line voltages of the system. Three separate AC systems, with two separate feeds from the building AC power network, are used, one for noisy components and one for the most sensitive electronics. A low noise AC power circuit from the building is connected to a power line filter (Tripp-Lite Isobar AC Power Filter), which has a basic circuit and a low noise circuit. The low noise circuit is used to supply power to the electrometers, signal control units, and power supplies. The temperature control system and computer system are connected to the basic circuit. A standard AC power line is used for the mechanical and turbomolecular pumps, chamber heaters, and other less sensitive electronic components. There are two signal control units: a National Instruments digital and analogue control and a customized

control box that enables automation and control of the Bertan 230 power supply. Electronic diagrams can be found in Appendix B.

The triaxial cables for measured currents travel through a stabilized, shielded, and grounded tube to minimize their movement and the influence of physical vibrations and air currents in the laboratory. Rubber vibration isolation pads approximately 1 cm thick were placed beneath the legs of the support cabinet beneath the CVC chamber that also houses the electronics; additional foam vibration reduction pads were placed beneath the electrometers for further isolation. This reduced the influence of tribostatic currents from physical vibrations carried through the floor from sources outside the laboratory. The turbomolecular pump was isolated from the CVC chamber by a ~1 m long flexible metal bellows hose. Vibrations, and the introduced noise, from the mechanical pump were unavoidable until recent advances were made in stabilizing vacuum levels. This influence was not quantifiable at the time the data in this analysis were taken and is assumed to be a portion of the overall system noise.

Maintaining vacuum levels can also be a source of electrical noise, due to leakage that changes the pressure inside the chamber. Changes in pressure within the chamber can cause movement of the delicate signal cables and increase the noise in the measurements. Ensuring stable vacuum levels required frequent greasing or replacement of the vacuum seal o-rings. The original rubber gaskets in the BNC connectors of the electron microscope shell were replaced with high vacuum compatible nitrile o-rings and provided significant improvement in vacuum stability. This will enable future measurements to be made without the mechanical and turbomolecular pumps running during the measurement, which will decrease the electrical noise even further.

APPENDIX B

ELECTRONIC DIAGRAMS AND SCHEMATICS

Figures are in the following order:

Fig. B.1 CVC computer system block diagram.

Fig. B.2 CVC vacuum chamber block diagram.

Fig. B.3 CVC AC power system wiring diagram.

Fig. B.4 CVC chamber block diagram.

Fig. B.5 CVC LabVIEW VI flowchart.

Fig. B.6 CVC LabVIEW VI flowchart - Configuration Mode.

Fig. B.7 CVC LabVIEW VI flowchart - Manual Mode.

Fig. B.8 CVC temperature control system block diagram.

Fig. B.9 CVC vacuum pumping system block diagram.

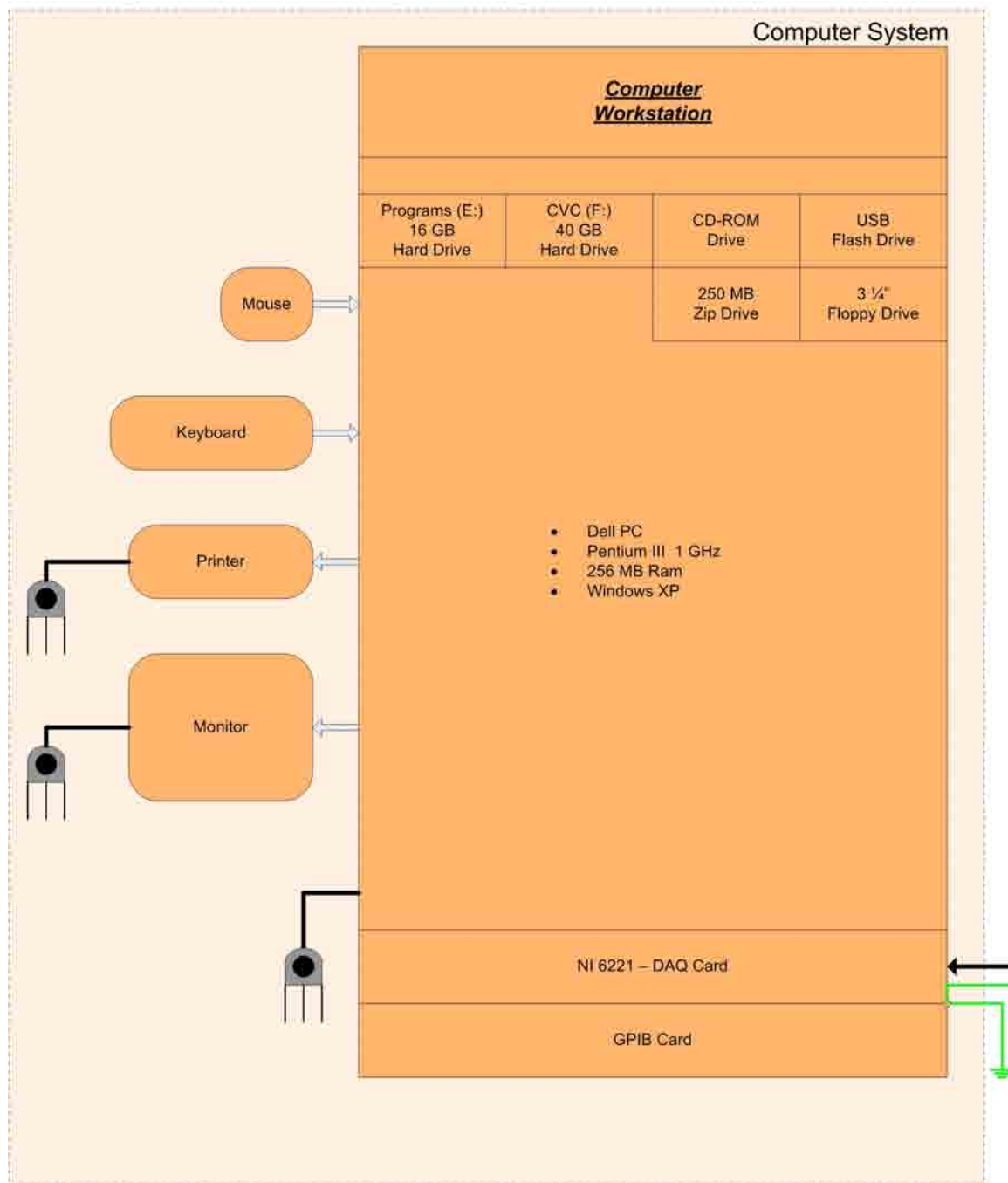


FIG. B.1. CVC computer system block diagram.

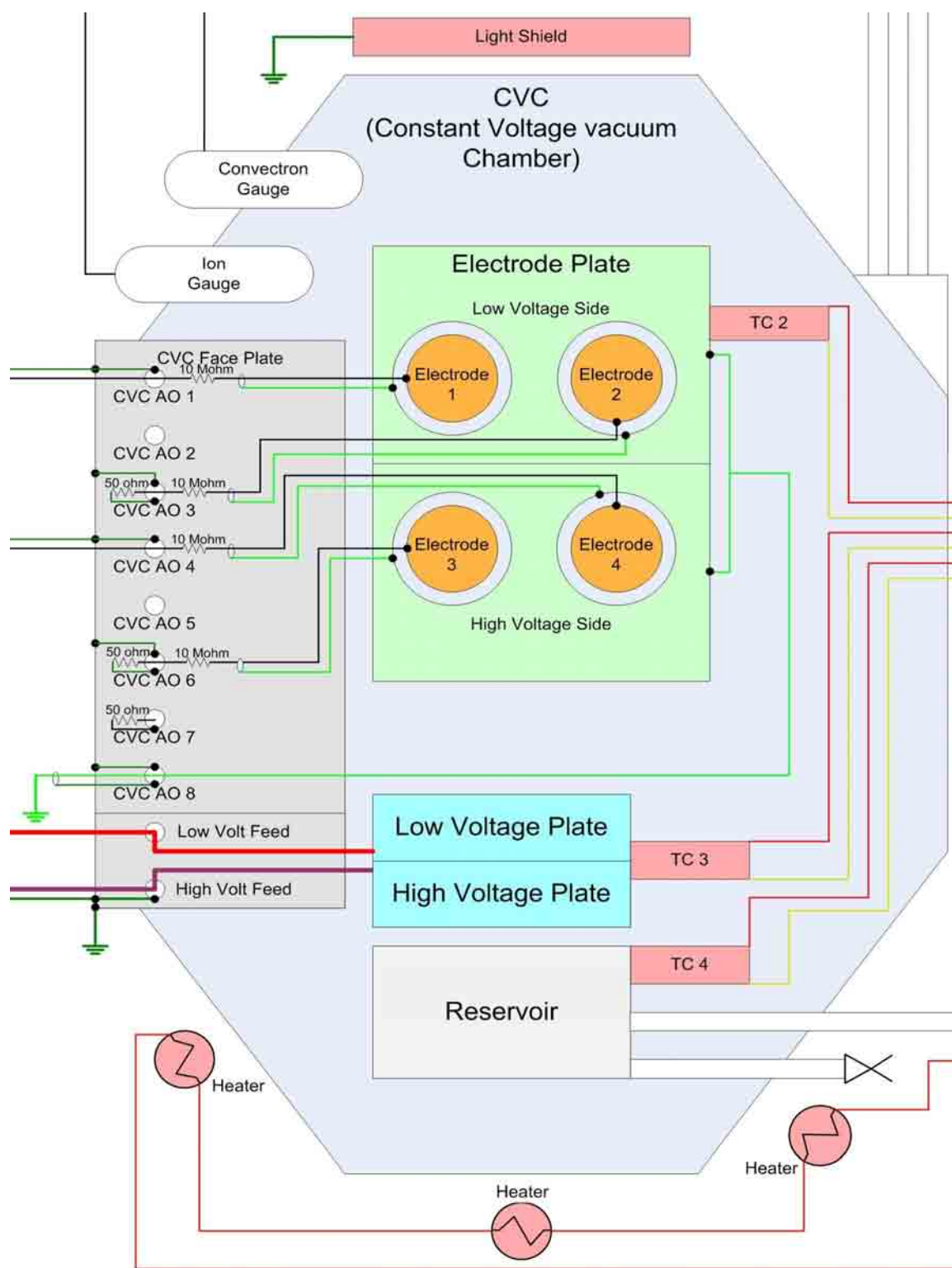


FIG. B.2. CVC vacuum chamber block diagram.

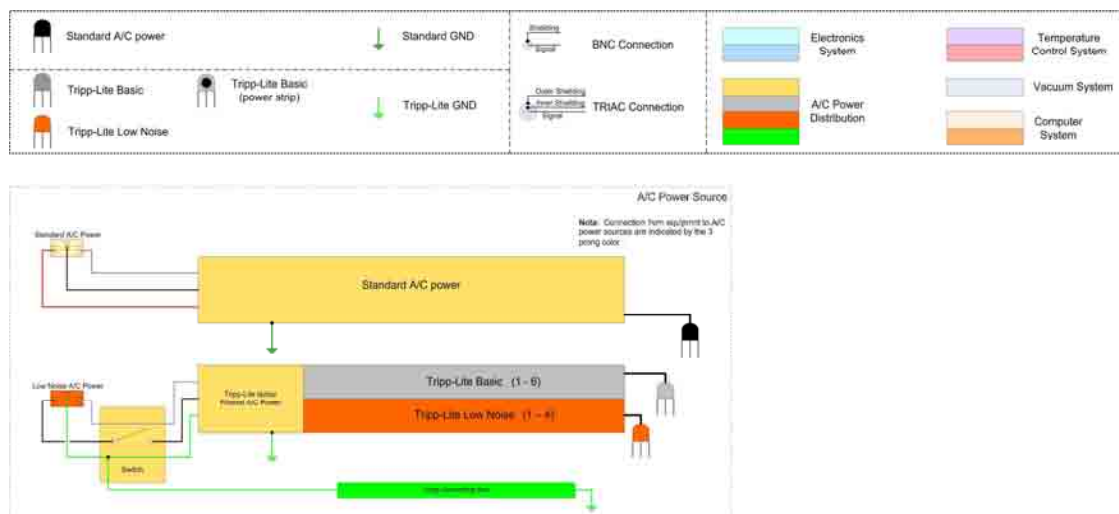


FIG. B.3. CVC AC power system wiring diagram.

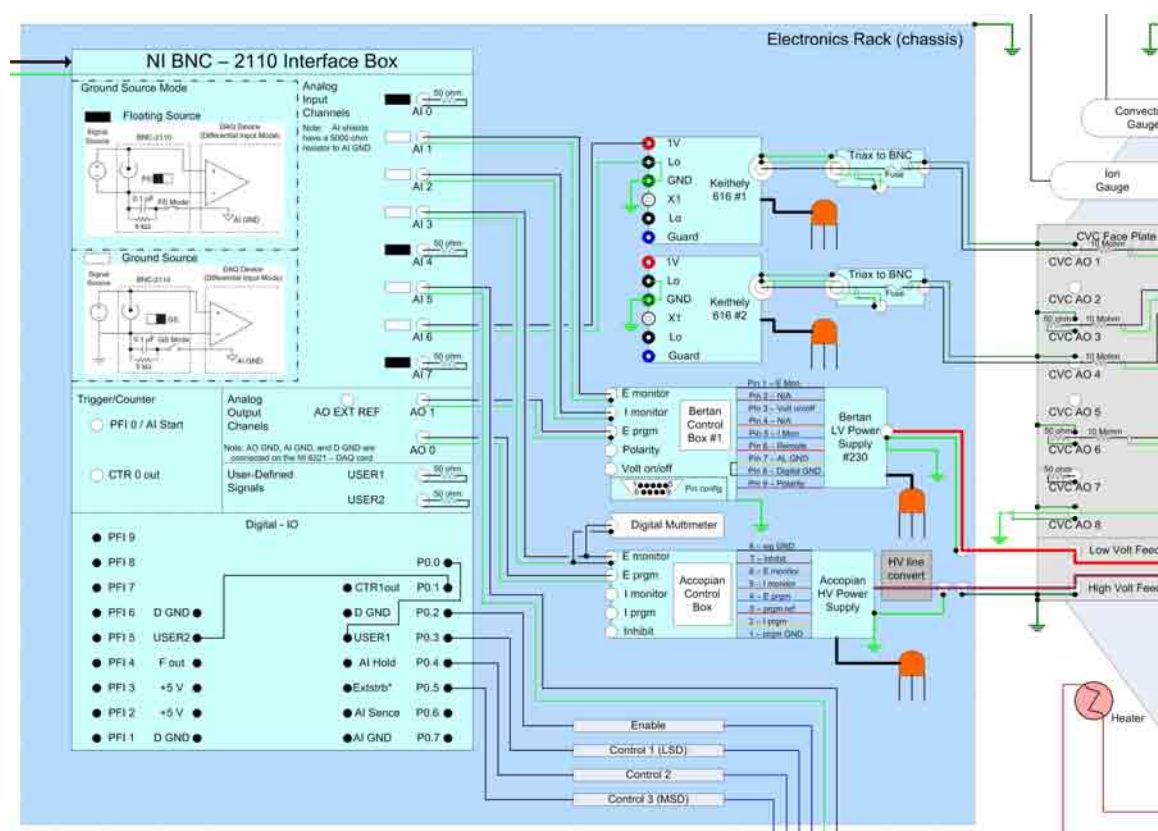


FIG. B.4. CVC chamber block diagram.

Constant Voltage Chamber (CVC)
LabVIEW Data Acquisition VI
Version 2.0c
9/10/2007

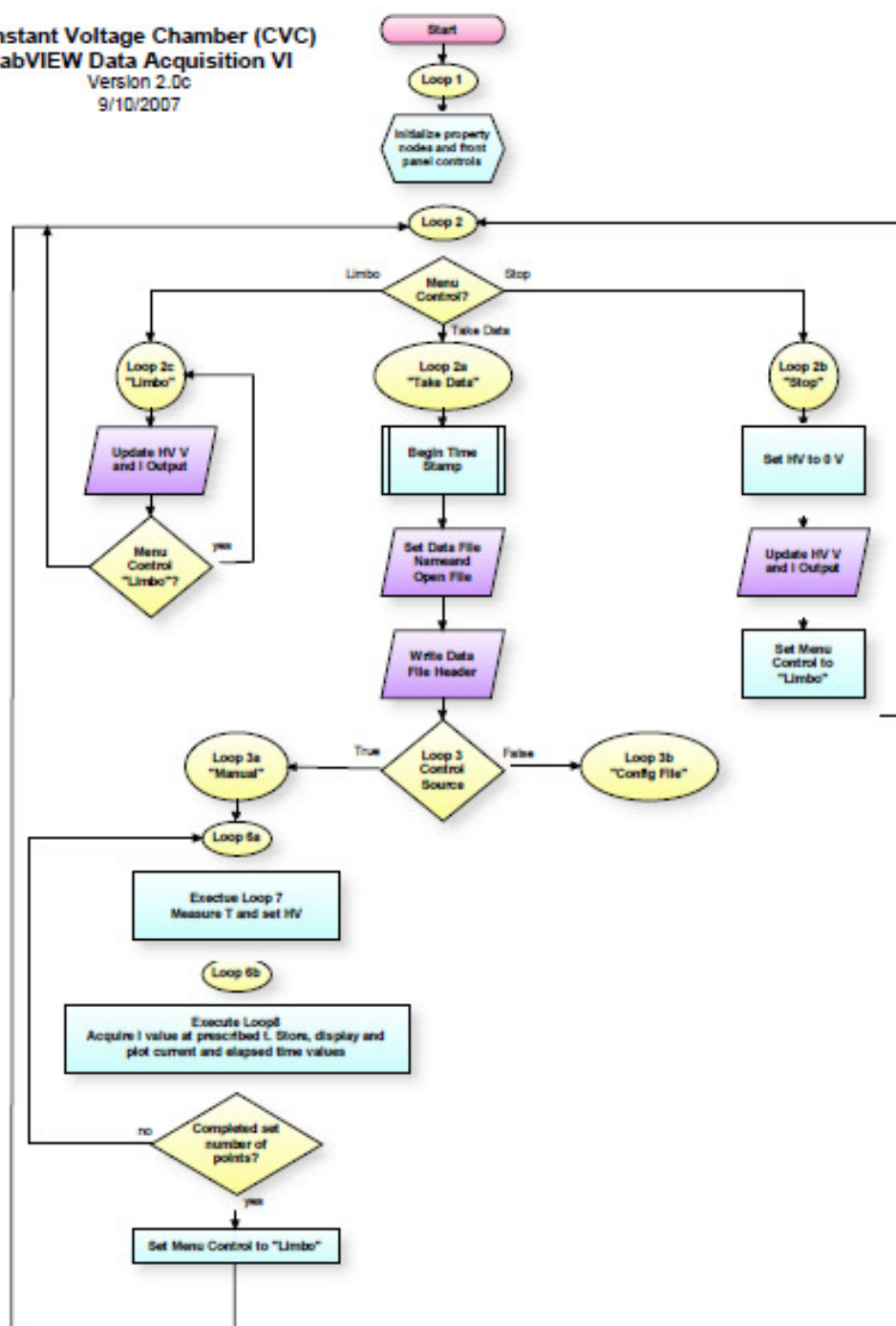


FIG. B.5. CVC LabVIEW VI flowchart.

[illegible]

FIG. B.6. CVC LabVIEW VI flowchart - Configuration Mode.

**Constant Voltage Chamber (CVC)
LabVIEW Data Acquisition VI**
Version 2.0c
9/10/2007

Manual Data Acquisition Mode Loop

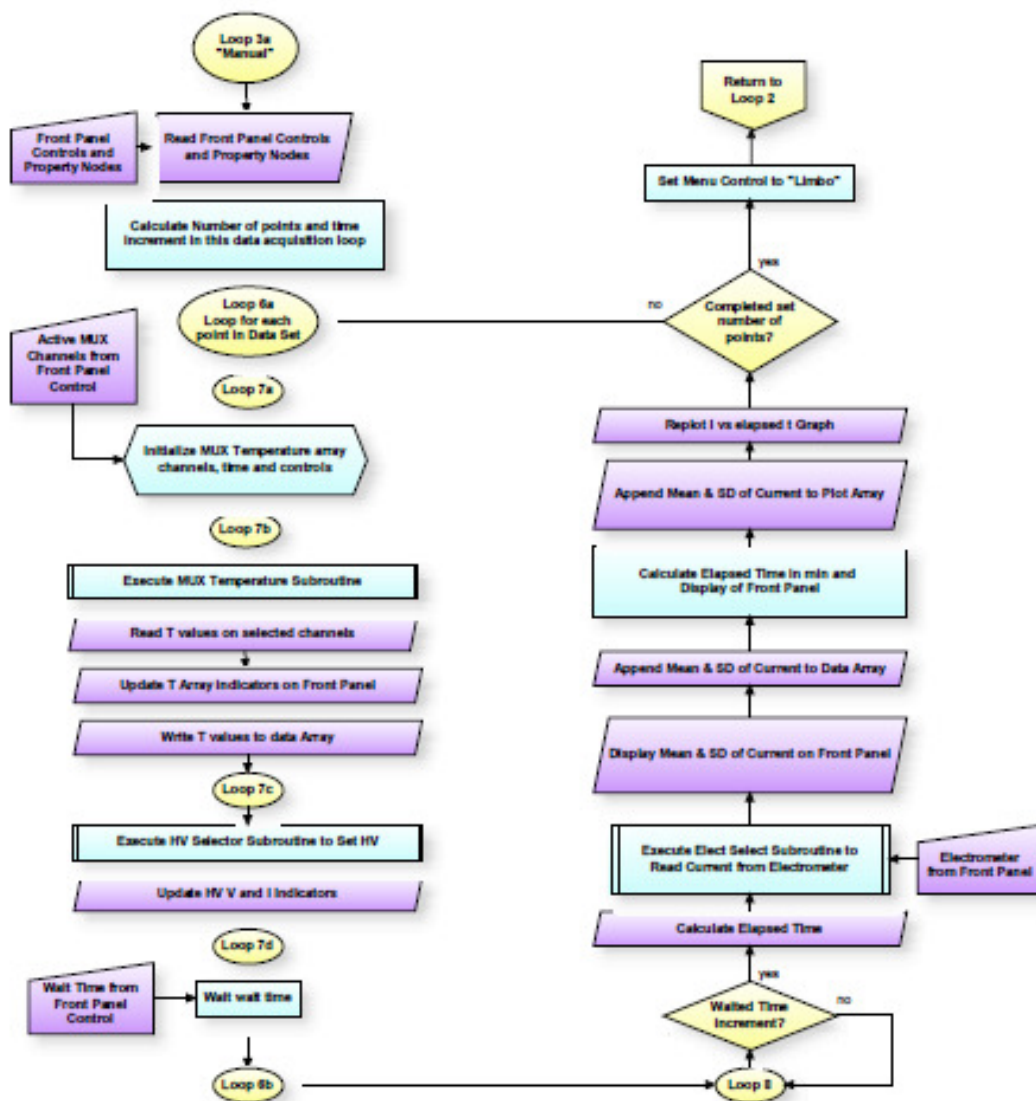


FIG. B.7. CVC LabVIEW VI flowchart - Manual Mode.

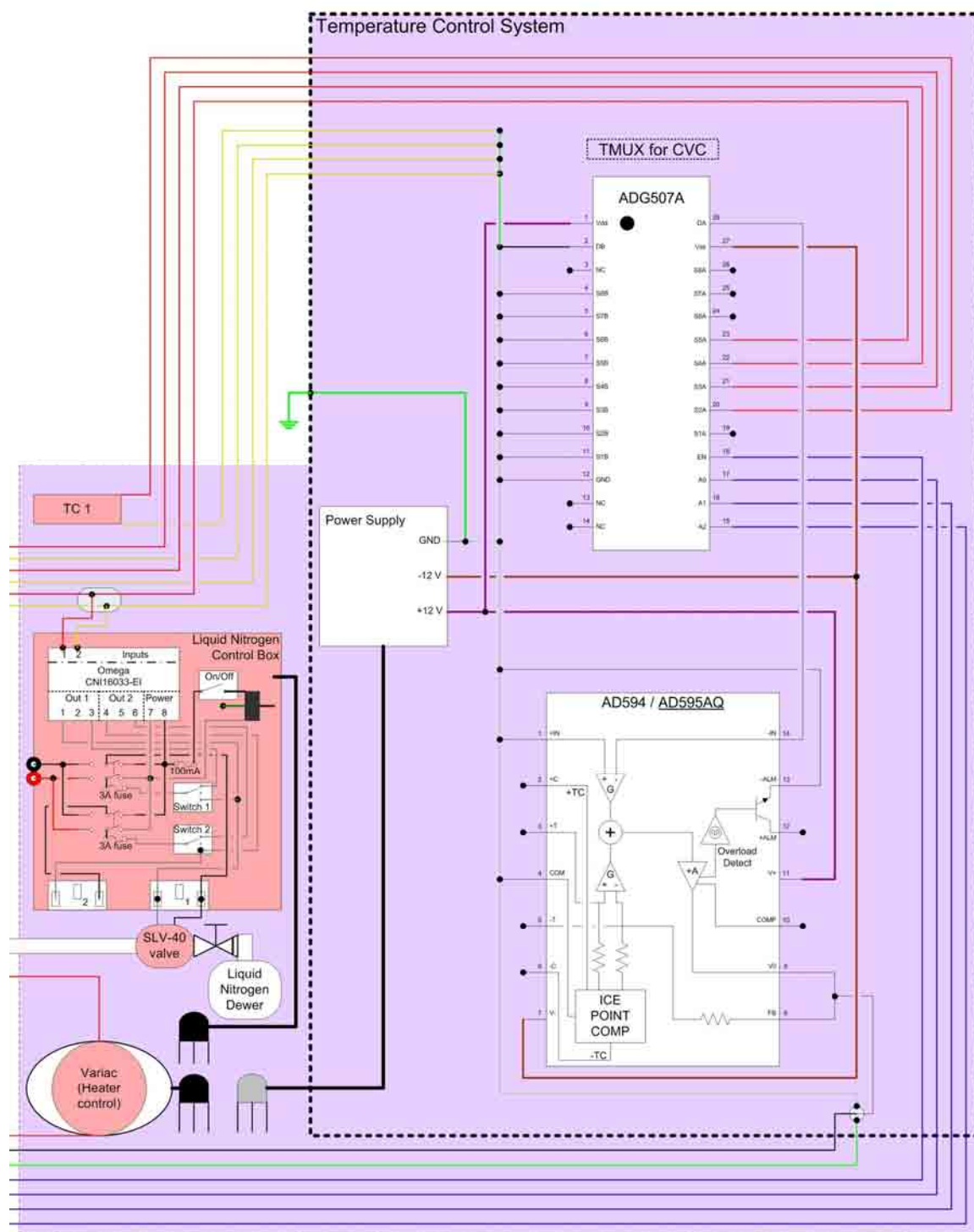


FIG. B.8. CVC temperature control system block diagram.

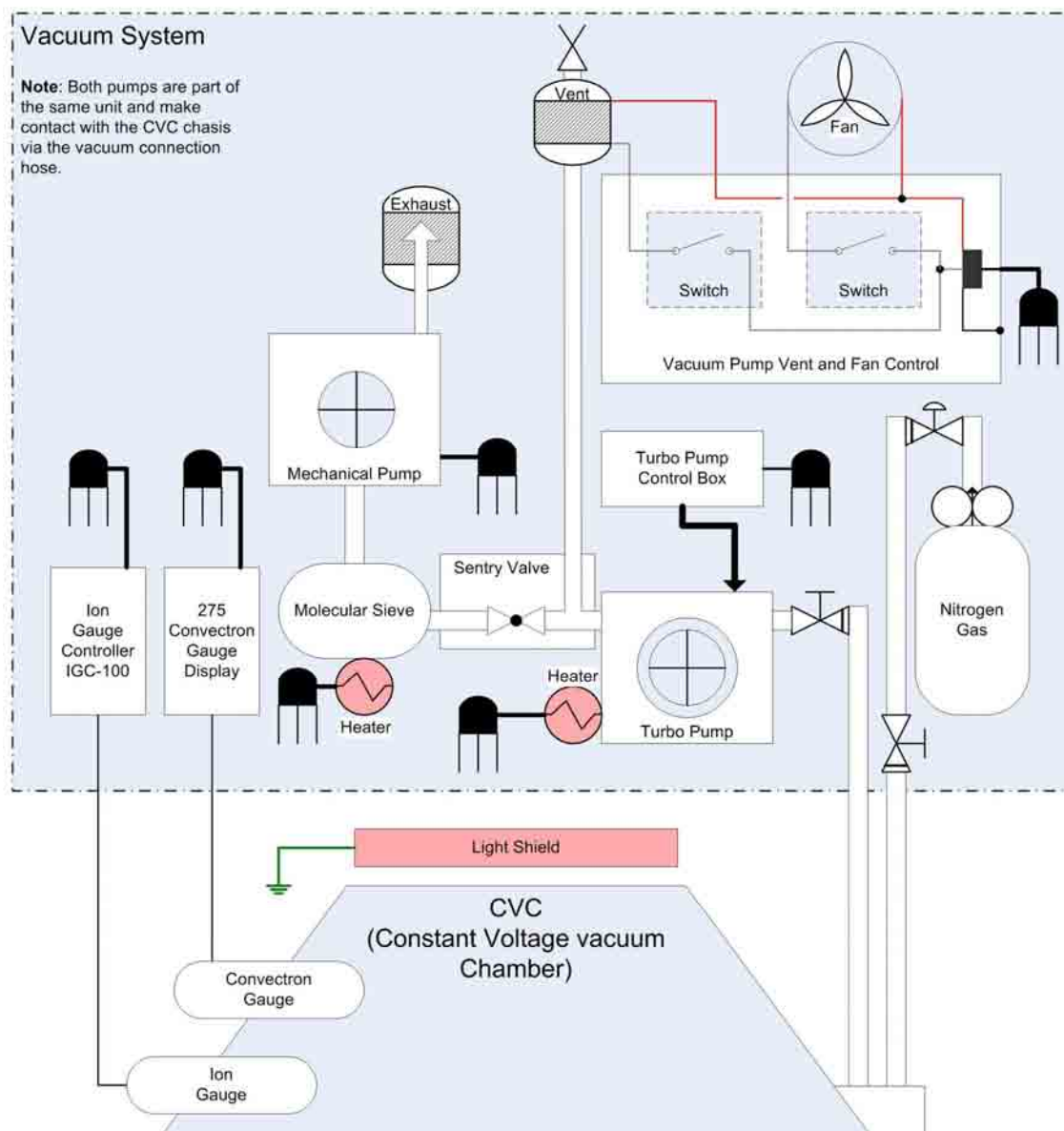


FIG. B.9. CVC vacuum pumping system block diagram.

APPENDIX C

INSTRUMENTAL RESOLUTION

This document provides a detailed description of the mathematics, environmental, and physical settings that determine error analysis of data for the Constant Voltage Chamber (CVC). This is a diagnostic tool that facilitates calibration and validation of the CVC system. Further, it can establish upper and lower bounds on measurable current and conductivity of samples with extremely high resistivity.

Determining resolution is concerned with the estimation of the error in the conductivity, which is calculated as

$$\sigma = \frac{J}{F} = \frac{I d}{A V}, \quad (C1)$$

where I is the measured current, d is the sample thickness, A is the area, and V is the applied voltage. The relative error in conductivity (or resistivity) is the sum of relative errors of these four measured components added in quadrature:

$$\frac{\Delta\sigma}{\sigma} = \sqrt{\left(\frac{\Delta I}{I}\right)^2 + \left(\frac{\Delta V}{V}\right)^2 + \left(\frac{\Delta A}{A}\right)^2 + \left(\frac{\Delta d}{d}\right)^2}, \quad (C2)$$

A discussion of the magnitudes of the components of random and systematic errors and their relative contribution to the total error in conductivity follows, based on standard error analysis methods. Fig. C.1 shows the basic relationship between the CVC system components and the measurement flow.

The precision for a single current measurements, ΔI , using an electrometer (Keithley, 1975) and data acquisition (DAQ) card (National Instruments, Model 6221) over a current range of 10^{-6} A to 10^{-15} A is given by

$$\Delta I = \left\{ I \left| \Delta F_{elec} + \Delta I_{elec} + \Delta I_{DAQ} \right| \right\}. \quad (C3)$$

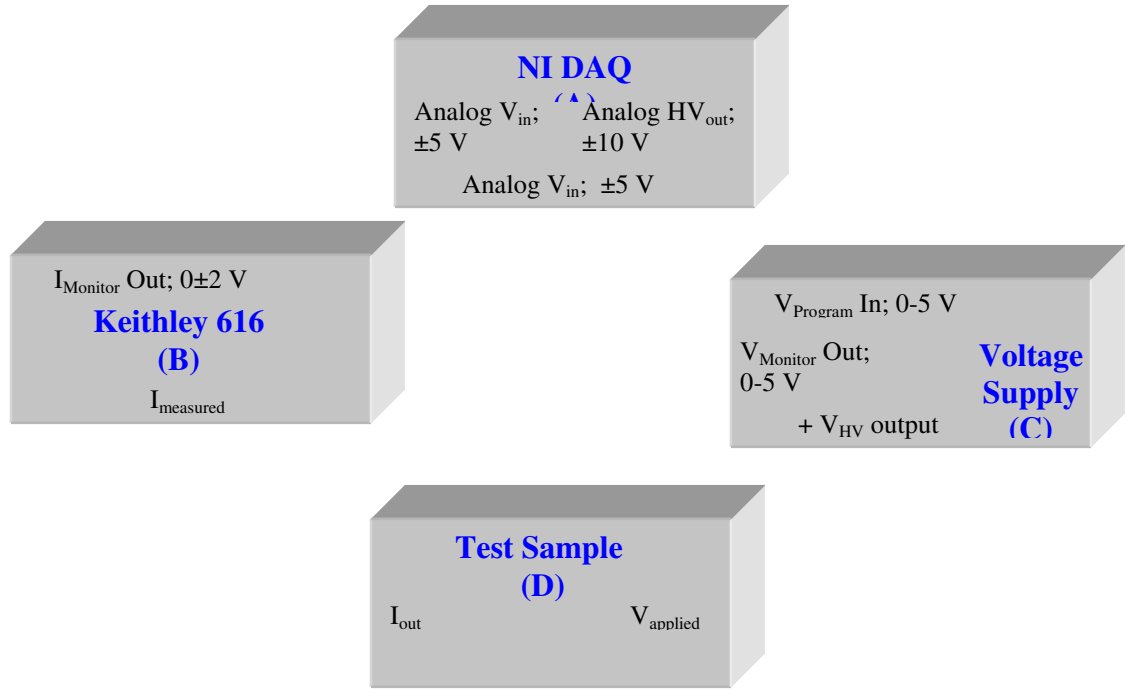


FIG. C.1 Components in the CVC measurement system. Red lines indicate a data flow of control voltages or measured data. Values listed for the Voltage Supply (C) are for the Bertan medium voltage supply; these are different for other supplies.

This uncertainty is shown in Fig. C.2 for the useful range of currents measured by the Keithley electrometer. The relative part of the electrometer error proportional to the measured current, $|I| \cdot \Delta F_{elec}$, is dependant on the range through the proportionality constant, ΔF_{elec} , as listed in Table 3.1. The absolute part of the electrometer error is ΔI_{elec} . The error due to the digital to analog conversion by the DAQ card is ΔI_{DAQ} .

For determination of each mean current measurement from the electrometer, a data set consisting of N_I points (typically 1000) is sampled by the DAQ card at a rate of f_I (typically 5 kHz) over a sampling period N_I / f_I (typically 0.2 seconds). The precision of a set of N_I measurements of the current using the electrometer and DAQ card is given by

$$\Delta I = \left[(N_I - 1) \cdot \text{Min} \left(1, \frac{540}{T_R \cdot f_I} \right) \right]^{-1/2} \left\{ |I| \Delta F_{elec} + [1.4 - 0.4(3 - S)] \Delta I_R \cdot 10^R + F_{DAQ} 10^R \right\}, \quad (C4)$$

where we define the following variables and functions (Keithley, 1975):

- I = Current measured by the electrometer,
- R = Electrometer current range setting,
- S = Electrometer display sensitivity setting,
- ΔF_{elec} = Electrometer range resolution factor at a given range, R ,
- T_R = Rise time (response time of the meter for a current change from 10% to 90% of full scale) at a given range, R ,
- F_{DAQ} = DAQ resolution factor = $\left(\frac{2 \cdot 10 \text{ V}}{2 \cdot 2 \text{ V}} \right) 2^{-16} = 0.02\%$,
- N_I = Number of samples taken for a given current data set,
- f_I = Sampling rate of DAQ card.

For the Keithley 616 electrometer, the values for R , S , F_R , and T_R used in Eq. (C4) are listed in Table 3.1. The absolute part of the electrometer error, $\Delta I_{elec} = \Delta I_{sens} + \Delta I_{zero_drift}$, is proportional to the current range times the range resolution, ΔI_R , and dependant on the display sensitivity through the empirical term in the square brackets of Eq. (C4) (refer to D→B in Fig. C.1).

The DAQ card error is ΔI_{DAQ} , which results from fluctuations of ± 1 in the Least Significant Bit (LSB) of the analog to digital conversion of the current monitor voltage from the electrometer by the DAQ card (B→A in Fig. C1). Numerically, a ± 2 V analog output signal from the Keithley 616 electrometer into the ± 10 V analog input of the DAQ card gives a 16-bit DAQ card resolution, F_{DAQ} , of 0.02% relative uncertainty with a total offset error of $\pm 0.03\%$ of full scale. The DAQ card has a ± 25 ppm/°C thermal error. At the lowest currents, the contributions from uncertainties due to the electrometer and DAQ card are approximately equal.

The initial term in square brackets, in Eq. (C4), accounts for the reduction in the uncertainty of the mean by sampling the electrometer N_I times. The standard deviation of the mean of the current set sampled is reduced by a complex function proportional to $(N_I - 1)^{-1/2}$ that

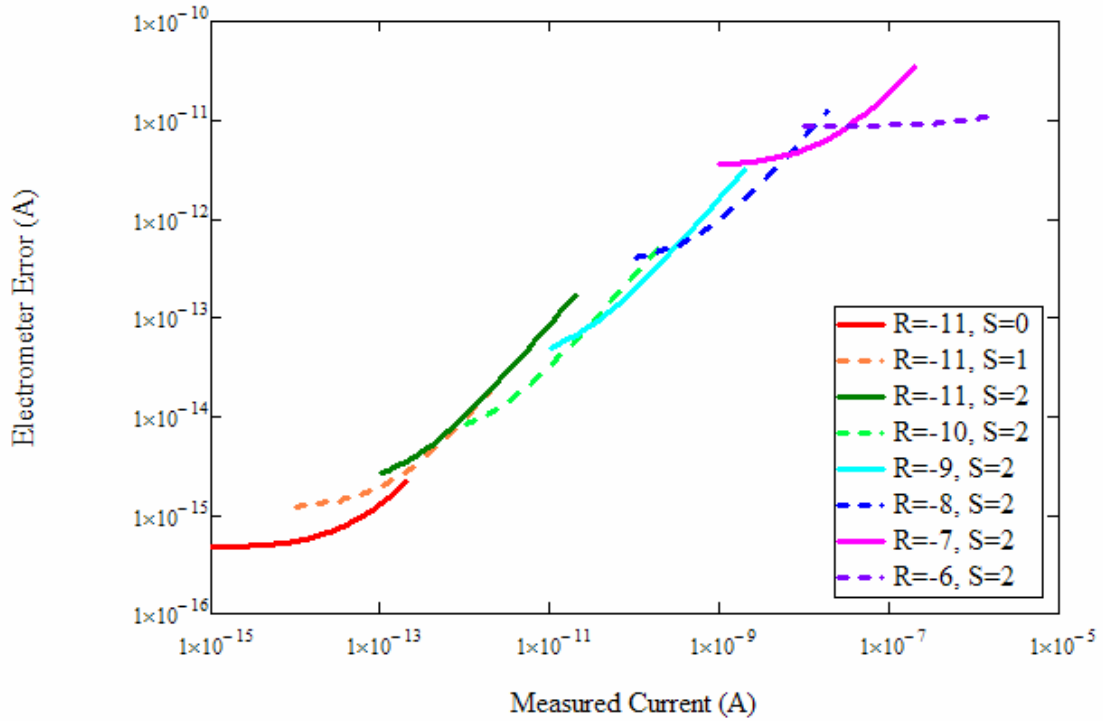


FIG. C.2 Total current error for the Keithley 616 electrometer. Curves show the error over the range of measurable currents for each of 8 range, R , and sensitivity, S , settings.

depends on the number of data points sampled by the DAQ card, the sampling rate of the DAQ card, and the electrometer rise time. The *Min* function returns the minimum value of unity or $(540 T_R f_i)$; this corrects for the limitation that at lower range settings the sampling time $1/f_i$ is less than the response time of the electrometer and oversampling results. The factor of 540 is an empirical scaling factor relating the electrometer response time for small changes in current to the rise time for a current change from 10% to 90% of full scale (Keithley, 1975).

The error in applied voltage depends on the voltage source used. We consider a medium-voltage power supply, a high-voltage power supply, and a low-voltage battery source.

For the programmable medium-voltage supply used (Bertan, Model 230-01R; 1 kV @ 15 mA), the instrumental precision is approximately

$$\Delta V = (N_V - 1)^{-\frac{1}{2}} \left[250 \text{ mV} + 0.1\% \cdot V_{\text{applied}} \right]. \quad (\text{C5})$$

The uncertainties in Eq. (C5) are a combination of uncertainties from the DAQ card (National Instruments) and programmable voltage supply (Bertan) (refer to A, C and D in Fig. C.1). The *voltage dependent term*, 0.1%, in Eq. (C5) is a sum in quadrature of voltage supply uncertainties for:

- the high-voltage output including the stability of the voltage supply (0.02% per 8 hrs), load regulation (0.005%), and AC line regulation (<0.001%) (C→D in Fig. C.1),
- the voltage supply circuit converting the programming voltage from the DAQ card to the high-voltage output (<0.1% for A→C in Fig. C.1), and
- the voltage supply circuit converting the high voltage output to the voltage monitor signal passed to the DAQ card (<0.1% for C→A in Fig. C.1).

The *constant error term*, 250 mV, in Eq. (C5) results from:

- variations of ± 1 LSB in the ± 10 V 16 bit analog output signal of the DAQ card into the 0 V to +5 V programming voltage of the power supply (A→C in Fig. C.1), resulting in a $\left(2 \cdot 10 \text{ V} / 2^{16}\right) \cdot \left(1000 \text{ V} / 5 \text{ V}\right)$ or ± 60 mV uncertainty with a total offset error of ~ 200 mV plus a 0.01% relative uncertainty for the DAQ card. The DAQ card has a ± 25 ppm/ $^{\circ}\text{C}$ thermal error,
- variations of ± 1 LSB in the ± 5 V 16 bit analog signal from the DAQ card derived from the 0 V to +5 V high-voltage monitoring signal of the power supply (C→A in Fig. C.1), resulting in a $\left(2 \cdot 5 \text{ V} / 2^{16}\right) \cdot \left(1000 \text{ V} / 5 \text{ V}\right)$ or ± 30 mV uncertainty with a total offset error of ~ 100 mV plus a 0.01% relative uncertainty for the DAQ card. The DAQ card has a ± 25 ppm/ $^{\circ}\text{C}$ thermal error,
- a ± 10 mV maximum ripple in the high-voltage output of the voltage supply, and

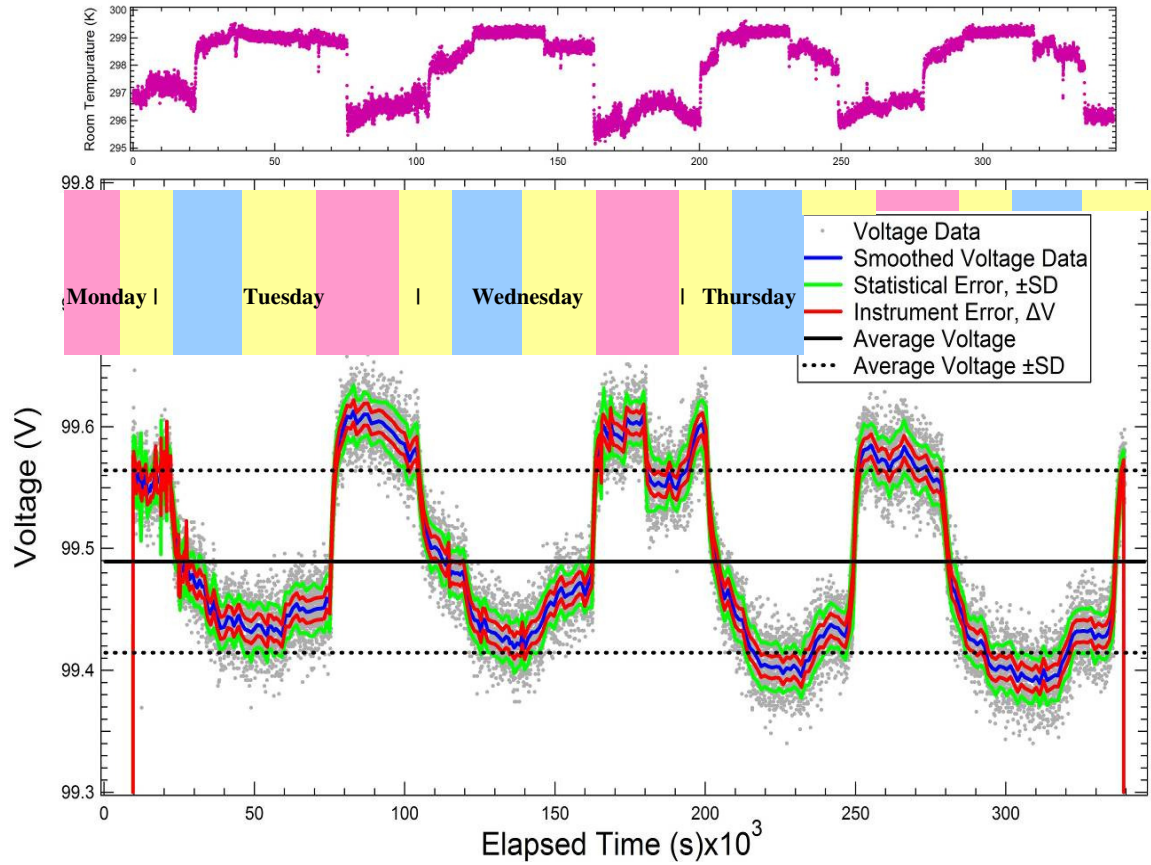


Fig. C3 Voltage as a function of elapsed time for a constant voltage data set. (Test LDPE filter 100V Cryo 96hr 3-30-2009) for 96 hr at variable temperature with a 27.4 μm thick LDPE sample. Data were acquired at 100 V nominal using a filtered medium-voltage Bertan voltage source. Data sets acquired at 20 s intervals are shown as grey dots. Smoothed values from a dynamic binning and averaging algorithm are shown in blue. Green lines show statistical errors for the binned and averaged data at ± 1 standard deviation. The red curves show the estimated instrumental uncertainty based on Eq. (C5). The average voltage for the full duration of the experiment is shown as a horizontal black line, with ± 1 standard deviation of the voltage for the full experiment shown as dashed horizontal black lines. Red, yellow and blue bands at the top of the graph show the daily heating and cooling cycle of the laboratory. The room temperature as a function of elapsed time is shown in the plot above the bands.

- ± 50 mV variations due to random thermal fluctuations in the voltage supply (± 0.5 $^{\circ}\text{C}$ at 100 mV/ $^{\circ}\text{C}$).

A set of N_V (typically 100) measurements of the voltage monitor are made at a rate f_V (typically 1 kHz, which is assumed to be below the response time of the voltage supply monitoring circuit), which reduces the uncertainty of the standard deviation of the mean by a

factor of $(N_V - 1)^{-1/2}$. At voltages below 400 V, the instrumental precision depends primarily on the DAQ card, while above this voltage errors from the voltage supply increase to about twice the DAQ card error.

Variations in the accuracy of the applied voltage from the power supply are directly monitored with the DAQ card and compensated for in calculations of conductivity. Hence, the accuracy of the conductivity is affected only by inaccuracies in the power supply voltage monitoring circuit and the DAQ card digitization of the monitor voltage. Accuracy of the programmable voltage supply is limited to $\pm 1\text{V}$ plus $\pm 0.1\%$ of the measured voltage due to the voltage supply program circuit and a similar error due to the voltage supply monitor circuit. The contribution to the accuracy from the DAQ card is much less, at 100 mV.

Fig. C.3 shows the voltage versus time plot for an experimental data set for LDPE at 100 V for 96 hr at variable temperature. The plot shows the estimated error in applied voltage from Eq. (C5), as well as the average and standard deviation of the voltage for the duration of the measurements. This shows short-term temporal changes in the voltage and the long-term stability simultaneously. Measured voltage sets at 20 s intervals are shown as grey dots. The blue curve is the smoothed data derived from the binned averaging algorithm described in this Appendix. The green lines show the statistical variations for the binned/averaged data at ± 1 standard deviation of the data sets in each bin. The approximately consistent narrow band in the spread of the grey data points bounded by the red curves of about ± 25 mV corresponds to the estimated instrumental precision from the medium-voltage supply and DAQ card, which is estimated for this data set to be ± 20 mV or $\pm 0.03\%$ based on Eq. (C5). The larger, periodic discrete jumps in the voltage of ~ 150 mV with a period of 24 hr are presumably due to daily changes in the room temperature of ~ 1.5 °C. Fig. C.3 has the daily heating and cooling cycle for the laboratory superimposed on the voltage versus elapsed time plot and juxtaposed to the room temperature versus elapsed time plot as confirmation of the temperature effect.

For the programmable high-voltage supply used (Acopian, Model P020HA1.5; 20 kV @ 1.5 mA), the instrumental precision is approximately

$$\Delta V = \left(\frac{N_v}{5} - 1 \right)^{-\frac{1}{2}} \left[4 \text{ V} + 0.7\% \cdot V_{\text{applied}} \right]. \quad (\text{B6})$$

The documentation for the Acopian power supply does not provide full details of the instrumental uncertainties. The uncertainties in Eq. (C6) are a combination of uncertainties from the DAQ card (National Instruments) and programmable voltage supply (Acopian) (refer to A, C and D in Fig. C.1). The *voltage dependent term*, 0.7%, in Eq. (C6) is a sum in quadrature of voltage supply uncertainties for:

- the high-voltage output including the stability of the voltage supply (0.05% per 8 hrs), load regulation (0.05%), and AC line regulation (<0.05%) (C→D in Fig. C.1),
- a ±0.05% ripple in the high-voltage output of the voltage supply (C→D in Fig. C.1),
- the voltage supply circuit converting the programming voltage from the DAQ card to the high-voltage output (estimated as <0.5% for A→C in Fig. C.1),
- the voltage supply circuit converting the high-voltage output to the voltage monitor signal passed to the DAQ card (estimated as <0.5% for C→A in Fig. C.1), and
- ±0.001% variations due to random thermal fluctuations in the voltage supply (±0.5 °C at 0.02%/°C).

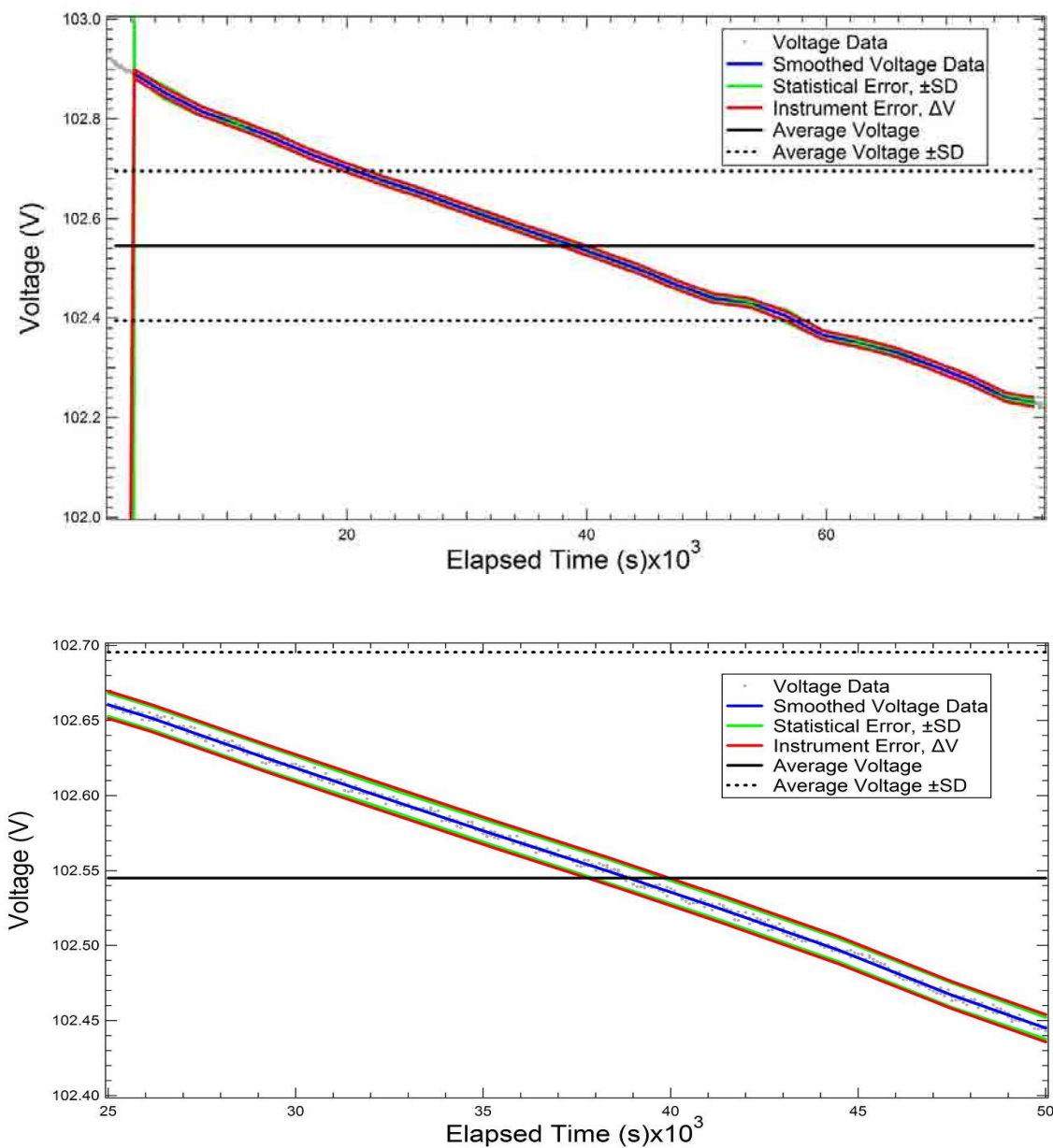


FIG. C.4 Voltage as a function of elapsed time for a constant voltage data set. (LDPE 100V 22hr RT testing 2-5-2009) for 22 hr at room temperature with a 27.4 μm thick LDPE sample. Data were acquired at 100 V nominal using a low-voltage battery source. Data sets acquired at 10 s intervals are shown as grey dots. Smoothed values from a dynamic binning and averaging algorithm are shown in blue. Green lines show statistical errors for the binned and averaged data at ± 1 standard deviation. The red curves show the estimated instrumental uncertainty based on Eq. (C7). The average voltage for the full duration of the experiment is shown as a horizontal black line, with ± 1 standard deviation of the voltage for the full experiment shown as dashed horizontal black lines. (top) Full scan highlighting nonlinearities. (bottom) Detailed scan over approximately 30% of the time highlighting the individual data points and uncertainties.

The *constant error term*, 1.3 V, in Eq. (C6) results from:

- variations of ± 1 LSB in the ± 10 V 16 bit analog output signal of the DAQ card into the 0 V to +5.1 V programming voltage of the power supply (A \rightarrow C in Fig. C.1), resulting in a $\left(2 \cdot 10 \text{ V} / 2^{16}\right) \cdot \left(20000 \text{ V} / 5.1 \text{ V}\right)$ or ± 1.2 V uncertainty with a total offset error of ~ 4 V plus a 0.01% relative uncertainty for the DAQ card. The DAQ card has a ± 25 ppm/ $^{\circ}\text{C}$ thermal error,
- variations of ± 1 LSB in the ± 5 V 16 bit analog signal of the DAQ card derived from the 0 V to +5.1 V high-voltage monitoring signal of the power supply (C \rightarrow A in Fig. C.1), resulting in a $\left(2 \cdot 5 \text{ V} / 2^{16}\right) \cdot \left(20000 \text{ V} / 5.1 \text{ V}\right)$ or ± 0.6 V uncertainty with a total offset error of ~ 2 V plus a 0.01% relative uncertainty for the DAQ card. The DAQ card has a ± 25 ppm/ $^{\circ}\text{C}$ thermal error.

A set of N_{V2} (typically 100) measurements of the voltage monitor are made at a rate f_{V2} (typically 1 kHz, which is ~ 5 times faster than the 5 ms response time of the voltage supply monitoring circuit), which reduces the uncertainty of the standard deviation of the mean by a factor of $((N_{V2}/5) - 1)^{-1/2}$. At voltages below 190 V, the instrumental precision depends primarily on the DAQ card, while above this voltage errors from the voltage supply increase to about 100 times the DAQ card error.

Variations in the accuracy of the applied voltage from the power supply are directly monitored with the DAQ card and compensated for in calculations of conductivity. Hence, the accuracy of the conductivity is affected only by inaccuracies in the power supply voltage monitoring circuit and the DAQ card digitization of the monitor voltage. Accuracy of the programmable voltage supply is limited to $\pm 1\text{V}$ plus $\pm 2\%$ of the measured voltage due to the voltage supply program circuit and a similar error due to the voltage supply monitor circuit. The contribution to the accuracy from the DAQ card is much less, at 1.3 V.

A low-voltage battery source constructed of twelve nine-volt Duracell Professional Alkaline batteries in series, produces an applied voltage of approximately 102.5 V. For the low-voltage battery source, the instrumental precision is approximately

$$\Delta V = (N_{V3} - 1)^{-1/2} \left[16 \text{ mV} + 0.015\% \cdot V_{\text{applied}} \right]. \quad (\text{C7})$$

Uncertainties result largely from the voltage monitoring circuit (C→A in Fig. C.1) which include:

- Variations in ± 1 LSB in the 16 bit 0 V to 1 V signal from the battery source 1:100 voltage divider circuit into the $\pm 2\text{V}$ analog input of the DAQ card, resulting in a $\left(2 \cdot 2\text{V} / 2^{16}\right) \cdot \left(100\text{V} / 1\text{V}\right)$ or $\pm 6 \text{ mV}$ uncertainty with a total offset error of $\sim 16 \text{ mV}$ plus a 0.01% relative uncertainty for the DAQ card. The DAQ card has a $\pm 25 \text{ ppm}/^\circ\text{C}$ thermal error,
- Precision due to instabilities and drift of the components of the 1:100 voltage divider circuit, The circuit uses 1% precision of the thin film metal resistors in the voltage divider, with typical temperature coefficients of $\pm 50 \text{ ppm}/^\circ\text{C}$. Estimated random thermal fluctuations in the temperature of the battery source and DAQ combined for $\pm 0.5^\circ\text{C}$ lead to a $\pm 30 \text{ ppm}$ thermal drift (C→A in Fig. C.1), and
- Calibration of the voltage divider circuit with a standard $4\frac{1}{2}$ -digit volt meter with an accuracy of $\sim 0.01\%$.

A set of N_{V3} (typically 100) measurements of the voltage monitor are made at a rate f_{V3} (typically 1 kHz, which is much slower than the $< 7 \mu\text{s}$ response time of the DAQ card), which reduces the uncertainty of the standard deviation of the mean by a factor of $(N_{V3} - 1)^{-1/2}$. At 100 V, the instrumental precision depends primarily on the voltage divider error.

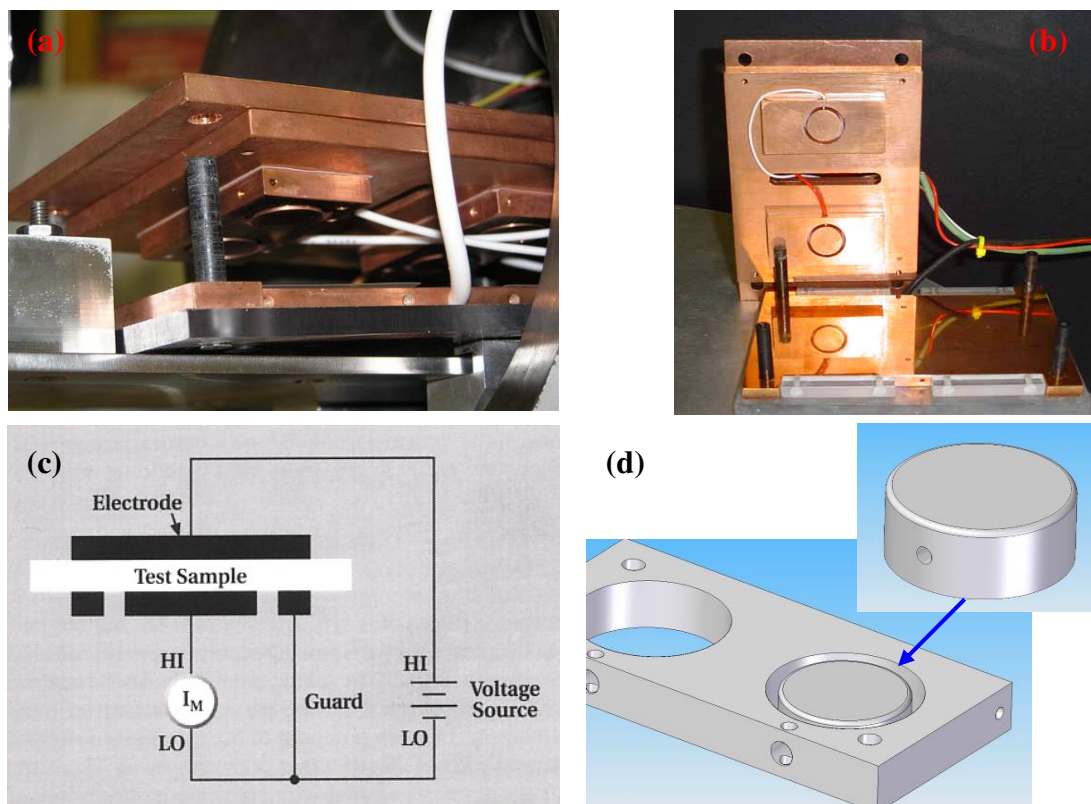


Fig. C5 Constant Voltage Chamber electrode assembly. (a) Electrode stack partially separated. (b) Electrode stack full separated. (c) Schematic of conductivity test circuit. (d) Detailed view of the 15.9 ± 0.3 mm diameter sample electrodes.

Fig. C.4 shows the battery supply voltage as monitored by the DAQ card for ~22 hrs. The data show a long time scale variation with a (30 ± 2) mV/hr decline due to battery discharge and a 0.01% deviation from the linearity resulting largely from the uncertainties in the voltage monitoring and DAQ card (C→A in Fig. C.1). On a short time scale, the voltage data show a 4 mV or 20 ppm deviation from the linear fit to the decay, in very good agreement with Eq. (C7). Again variation in accuracy of the applied voltage (due primarily to drift) are directly monitored with the DAQ card and compensated for in the conductivity calculations.

The area of the Cu electrode (see Fig. C6) is determined to be $1.98(\pm 0.08)$ cm² with an accuracy of $\pm 4\%$. The effective diameter of the electrode is $1.59(\pm 0.03)$ cm $\pm 2\%$. Errors in diameter were set, at a lower bound, by subtraction of half the 50 μ m radius of curvature

machined on the edges of the electrodes to reduce high electric fields from sharp edges and at an upper bound by addition of half of a typical sample thickness of approximately 50 μm .

The area of the electrode is invariant, with the exception of contact area. Contact area has been made more uniform by the addition of the sample clamping capabilities. The accuracy in area is estimated to be 4%. Precision in the surface area from run to run due to variations in the clamping is crudely estimated as $\sim 1\%$.

Sample thicknesses were measured with a standard digital micrometer (Mitutoya) with a resolution of $\pm 3 \mu\text{m}$. The anvil of the micrometer was $\sim 0.5 \text{ cm}$ in diameter, so that each measured thickness was an average over a surface area of $\sim 0.8 \text{ cm}^2$ and was insensitive to smaller area variations. The average sample thickness for a 1 mil LDPE sample is $(27.4 \pm 0.1) \mu\text{m}$ (0.4%). For 5 mil LDPE sample the thickness is $(124.5 \pm 0.3) \mu\text{m}$ or $\pm 0.3\%$. Repeated measurements had a range of values comparable to the instrumental resolution.

To further improve the quality of the data, an adaptive smoothing algorithm has been developed to process the measured current and voltage data. The time scale between acquisition of a data set of N_I (or N_V) points, ΔT , is commonly set to between 0.1 s and 10 s, depending on the nature of the experiment. In regions where these data are varying significantly on a time scale comparable to ΔT no additional smoothing is used. In regions where the current and voltage signals are changing more slowly, the data are smoothed by calculating a simple average \bar{x} and standard deviation of the mean σ_x^{SDOM} over N_{Bin} data sets as

$$\bar{x} = \left[\frac{1}{N_{Bin}} \right] \sum_{i=-\frac{1}{2}N_{Bin}}^{\frac{1}{2}N_{Bin}} (x_i), \quad (\text{C8})$$

and

$$\sigma_x^{SDOM} = \sqrt{\left[\frac{1}{N_{Bin}(N_{Bin}-1)} \right] \sum_{i=-\frac{1}{2}N_{Bin}}^{\frac{1}{2}N_{Bin}} (x_i - \bar{x})^2} \quad (C9)$$

The number of bins—or equivalently the time interval ($N_{Bin} \Delta T$)—to average over is chosen dynamically to optimize the smoothing of the data without sacrificing information about rapidly changing signals. An odd value of $N_{Bin}=(2^n-1)$, where n is an integer, is used so that the data sets are equally spaced on either side of the midpoint in time. There are four cases considered in setting N_{Bin} :

1. For very rapidly changing signals, $N_{Bin}=1$ is used. That is, there is no smoothing.
2. For data sets that change fairly rapidly signals at the beginning of a data set, a static binning can be used. The first N_o points are smoothed using bins with a width $N_{Bin}=L$, the next group of points are binned with a width $N_{Bin}=L+ N_I$ (typically $N_I=5$), the third group binned with width $N_{Bin}=L+ 2N_I$, and so on, until a maximum bin width of $N_{Bin}=N_{max}$ (typically $N_{max}=50$) is reached. All subsequent points are smoothed using a bin width of $N_{Bin}=N_{max}$.
3. For moderately changing signals, a dynamic binning can be used. An average value is calculated for a first bin of minimum width $N_{Bin}=B_{min}$. The average for next test region of points with width $N_{Bin}=R$ immediately beyond the first bin is calculated. If the percent change between these two bins is less than a set threshold, I_{thresh} , a subsequent test bin of the same width $N_{Bin}=R$ beginning a distance ($n R$) from the end of the first bin now with $n=1$ is tested is compared to the first bin average; again, if the change is below I_{thresh} a new bin of width $N_{Bin}=R$ beginning a distance ($2 N_R$) is tested. Tests with successively higher values of n are repeated until the change exceeds I_{thresh} or until the distance between the beginning of the first bin and the start of the test bin reaches B_{max} . The dynamic bin width is set to a bin width from the start of the first bin and the start of the test bin and the process is repeated for the next dynamic bin,

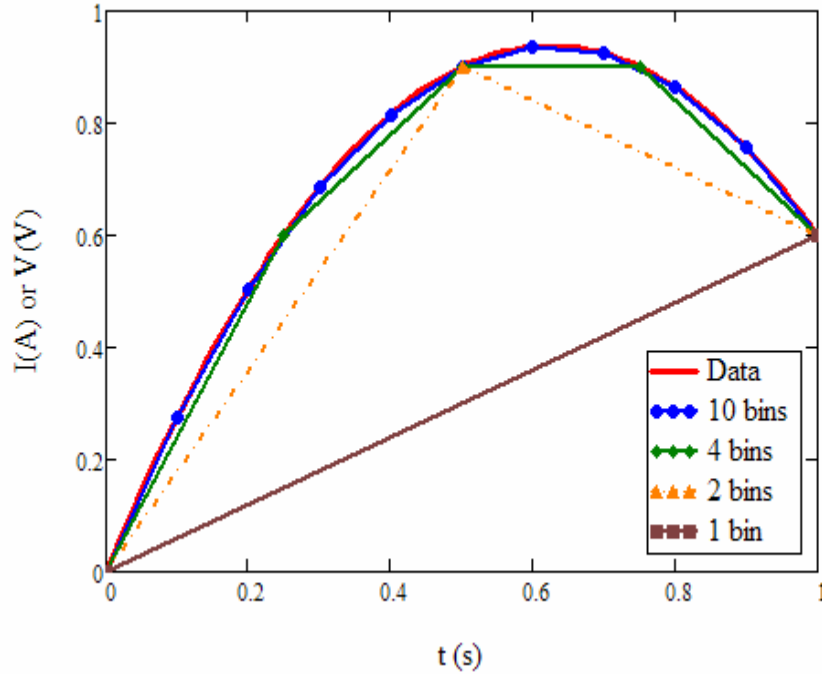


FIG. C.6 Example of errors introduced in binning of time varying data. The signal (red) is fit with progressively fewer bins (10, 4, 2 and 1 bins), producing an increasingly poor fit to the signal.

4. For slowly varying signals, a maximum bin size of $N_{Bin}=N_{max}$ set by the user (typically $N_{max}=50$) is used.

A flow chart of the dynamic bin selection algorithm used is shown in Fig. C.6. Fig. C.7 illustrates the errors introduced in binning of a time varying signal (red) that is fit with progressively fewer bins (10, 4, 2 and 1 bins), producing an increasingly poor fit to the signal.

The detailed analysis of compact errors presented here can be combined to determine the total uncertainty of conductivity using Eq. (C2).

For typical a 27 μm thick LDPE sample at room temperature for a range of applied voltages from the various voltage sources, the errors in current are the dominate source of error for low-voltage measurements, although estimated errors in electrode area and sample thicknesses become dominant above a few kV. For higher resistance materials where currents are reduced at

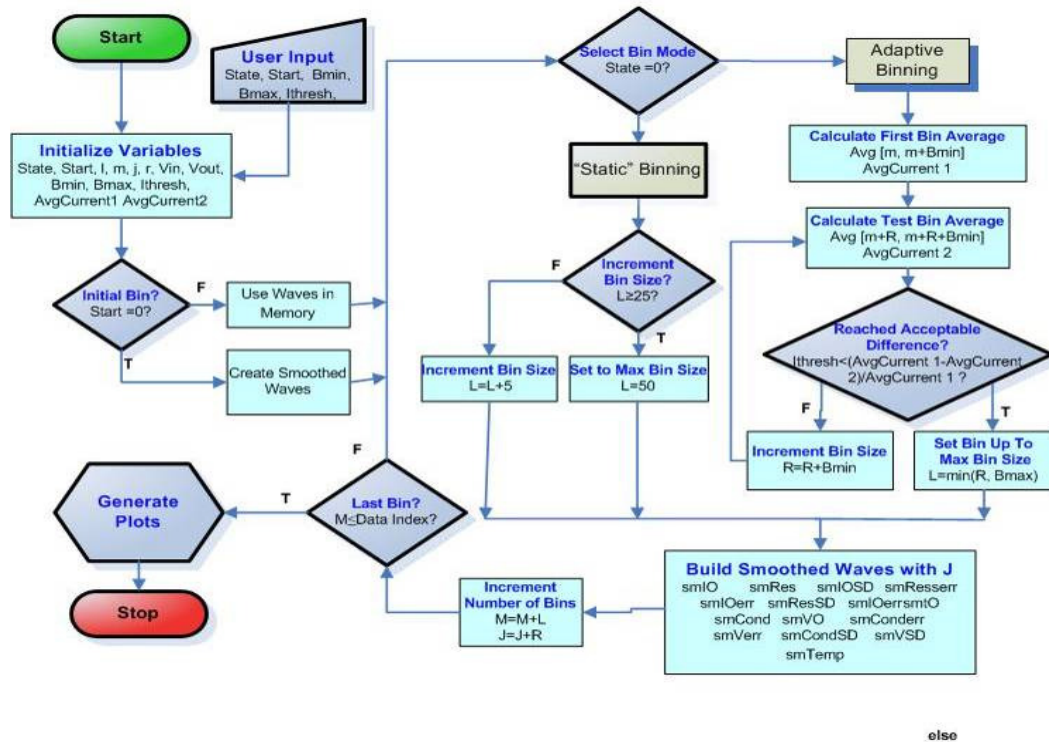


FIG. C.7 Flow chart of the dynamic bin selection algorithm.

comparable voltages, thicknesses and area, the relative current errors will increase and will dominate at all voltages. At present, instrumentation errors from the electrometer and medium or high-voltage supplies are typically somewhat larger than errors associated with the DAQ card. However, for measurements made with low voltages from the medium-voltage power supply or with the low-voltage battery source, errors associated with the DAQ card can be larger.

It may be possible to further reduce the error in current by reducing the multiple sampling factors at low current range. This is accomplished by extending the sampling time by either taking more data points or by decreasing the sampling rate. This, of course, is done at the expense of data acquisition rate and can provide only a factor of two to four reductions in uncertainty before DAQ card errors become dominant. At this point, uncertainties from area and thickness measurements will become comparable to uncertainty due to current measurements.

The detailed error analysis conducted above allows determination of the ultimate

resolution of the CVC chamber. This can be compared to fundamental limits set by the environment. Based on an estimated lowest measurable current of ~ 0.4 fA, the calculated ultimate instrument conductivity resolution is $\sim 7 \cdot 10^{-21} (\Omega\text{-cm})^{-1}$ for a typical 100 V applied voltage and $\sim 8 \cdot 10^{-23} (\Omega\text{-cm})^{-1}$ for a maximum applied voltage of 8200 V at the breakdown voltage for LDPE. It is worth noting that the theoretical noise limits for low-current measurements from Eq. (C4) with current data collection settings is ~ 0.4 fA or ~ 7000 electrons/s.

The fundamental limit to measurement of current or conductivity is the Johnson noise of the source resistance. For any resistance, thermal energy produces motion of the constituent charged particles, which results in what is termed Johnson or thermal noise. Based on a standard formula for peak to peak Johnson current noise (Keithley, 2004):

$$\Delta I_{pp} = 5 \sqrt{\frac{4 k_B T W_{Band}}{R}}, \quad (\text{C10})$$

where W_{Band} is the signal band width approximated as $(0.35/T_{rise})$. T_{rise} is the time for the electrometer to respond to a change in current signal from 10% to 90% of the meter range listed in Table 4.1; for the lowest 10^{-11} A range of the Keithley 616 electrometer this is ~ 3 s and T_{rise} is 0.12 Hz. For a typical LDPE sample at room temperature $\Delta I_{pp} \sim 4 \cdot 10^{-18}$ A with a corresponding $\sigma_{pp} \sim 6 \cdot 10^{-23} (\Omega\text{-cm})^{-1}$ at 100 V. For a typical LDPE sample at ~ 100 K, $\Delta I_{pp} \sim 3 \cdot 10^{-19}$ A with a corresponding $\sigma_{pp} \sim 5 \cdot 10^{-24} (\Omega\text{-cm})^{-1}$ at 100 V. This is $\sim 1\%$ of the ultimate instrument conductivity resolution calculated above.

Another limit to the conductivity results from interaction with the natural background environment. The worldwide average natural background radiation dose for a human being from the cosmic background is about 0.26 millisievert (mSv) per year. This is increased by a factor of about 75% at an altitude of 1400 m in Logan, UT. Radiation from other sources of background radiation including terrestrial sources, such as soil and radon gas, as well as man-made sources are typically not high enough energy to penetrate the CVC vacuum chamber wall, and are hence

shielded and not considered in this calculation. By contrast, cosmic background radiation is of high enough energy to have penetrated the atmosphere and so will not be appreciably attenuated by the building or chamber walls. The calculation also does not take into account any charge deposited by the cosmic radiation or secondary charge emitted by the sample or electrodes in contact with the sample; this conceivably could be a significant term.

Assuming a typical biological radiation weighting factor, r_W of 1 Gy/Sv, this is an annual dose of ~46 mRad and an average dose rate of $1.4 \cdot 10^{-9}$ Rad/s. For a value of $k_{RIC} = 2 \cdot 10^{-16}$ ($\Omega\text{-cm-Rad/s}$)⁻¹ and $\Delta = 0.8$ for LDPE at room T. This corresponds to a background RIC of $\sim 4 \cdot 10^{-23}$ ($\Omega\text{-cm}$)⁻¹, or about 0.5% of the ultimate instrument conductivity resolution at 100 V applied voltage or ~50% of the ultimate instrument conductivity resolution for a maximum applied voltage of 8200 V at the breakdown voltage for LDPE.. At 100 K, $k_{RIC} = 3 \cdot 10^{-18}$ ($\Omega\text{-cm-Rad/s}$)⁻¹ and $\Delta = 1$ for LDPE which corresponds to a background RIC of $\sim 4 \cdot 10^{-27}$ ($\Omega\text{-cm}$)⁻¹, or <1 ppm of the ultimate instrument conductivity resolution at 100 V applied voltage or ~50 ppm of the ultimate instrument conductivity resolution for a maximum applied voltage of 8200 V at the breakdown voltage for LDPE.

Thus, in summary, the fundamental limit of the CVC system is set:

- at low temperatures by thermal noise sets,
- at room temperature and lower voltages by RIC from cosmic background radiation, and
- at room temperature and highest voltages equally by RIC from cosmic background radiation and the ultimate instrument conductivity resolution.

APPENDIX D

DETAILS OF DATA COLLECTION

Each attempt to obtain data on LDPE was recorded in an archive with record of sample information, source, experimental conditions, and any additional information available. If a particular data run was deemed unusable for analysis, it was noted in the archive log and the original data file was kept. Any calibration or testing data sets were also noted as such to ensure they were used appropriately.

Use	Material	Voltage	Type	T. Regime	Total Duration	Run Date	Thick.	Source	PS	Data Filename	Notes
?	LDPE	1500	x1	Cryo	24 hrs	8/19/2007	1 mil	Goodfellow	HVT	LDPE warming 1500 V 8-19-2007.txt	Behavior is different from all other temperature runs. Could be due to HVT. Repeat necessary.
X	LDPE	50 V steps	ESD	RT	9 min	8/17/2007	1 mil	Goodfellow	HVT	LDPE Breakdown 8-17-2007.txt	Broke down at 6000V
X	LDPE	500	x1	Cryo	24 hrs	8/16/2007	1 mil	Goodfellow	Bertan	LDPE Warming 500 V 8-16-2007.txt	
Limited	LDPE	1100	x1	RT	2 hrs	8/16/2007	1 mil	Goodfellow	HVT	LDPE 1100 V 8-16-2007.txt	May be used after care is taken to remove influence of HVT malfunction
Limited	LDPE	1200	x1	RT	2 hrs	8/16/2007	1 mil	Goodfellow	HVT	LDPE 1200 V 8-16-2007.txt	May be used after care is taken to remove influence of HVT malfunction
Limited	LDPE	1300	x1	RT	2 hrs	8/16/2007	1 mil	Goodfellow	HVT	LDPE 1300 V 8-16-2007.txt	May be used after care is taken to remove influence of HVT malfunction
Limited	LDPE	1400	x1	RT	2 hrs	8/16/2007	1 mil	Goodfellow	HVT	LDPE 1400 V 8-16-2007.txt	May be used after care is taken to remove influence of HVT malfunction
Limited	LDPE	1500	x1	RT	2 hrs	8/16/2007	1 mil	Goodfellow	HVT	LDPE 1500 V 8-16-2007.txt	May be used after care is taken to remove influence of HVT malfunction
X	LDPE	700	x1	RT	2 hr	8/15/2007	1 mil	Goodfellow	Bertan	LDPE 700 to 1000 V 8-15-2007.txt	
X	LDPE	800	x1	RT	2 hr	8/15/2007	1 mil	Goodfellow	Bertan	LDPE 700 to 1000 V 8-15-2007.txt	
X	LDPE	900	x1	RT	2 hr	8/15/2007	1 mil	Goodfellow	Bertan	LDPE 700 to 1000 V 8-15-2007.txt	

Use	Material	Voltage	Type	T. Regime	Total Duration	Run Date	Thick.	Source	PS	Data Filename	Notes
X	LDPE	1000	x1	RT	2 hr	8/15/2007	1 mil	Goodfellow	Bertan	LDPE 700 to 1000 V 8-15-2007.txt	
X	LDPE	25	x1	RT	2 hrs	8/14/2007	1 mil	Goodfellow	Bertan	LDPE Up to 1000 V 8-14-2007.txt	
X	LDPE	50	x1	RT	2 hrs	8/14/2007	1 mil	Goodfellow	Bertan	LDPE Up to 1000 V 8-14-2007.txt	
X	LDPE	100	x1	RT	2 hrs	8/14/2007	1 mil	Goodfellow	Bertan	LDPE Up to 1000 V 8-14-2007.txt	
X	LDPE	200	x4	RT	8 hrs	8/14/2007	1 mil	Goodfellow	Bertan	LDPE Up to 1000 V 8-14-2007.txt	
X	LDPE	300	x1	RT	2 hrs	8/14/2007	1 mil	Goodfellow	Bertan	LDPE Up to 1000 V 8-14-2007.txt	
X	LDPE	400	x1	RT	2 hrs	8/14/2007	1 mil	Goodfellow	Bertan	LDPE Up to 1000 V 8-14-2007.txt	
X	LDPE	500	x1	RT	2 hrs	8/14/2007	1 mil	Goodfellow	Bertan	LDPE Up to 1000 V 8-14-2007.txt	
X	LDPE	600	x1	RT	2 hrs	8/14/2007	1 mil	Goodfellow	Bertan	LDPE Up to 1000 V 8-14-2007.txt	
X	LDPE	700	x1	RT	2 hrs	8/14/2007	1 mil	Goodfellow	Bertan	LDPE Up to 1000 V 8-14-2007.txt	
X	LDPE	800	x1	RT	2 hrs	8/14/2007	1 mil	Goodfellow	Bertan	LDPE Up to 1000 V 8-14-2007.txt	
X	LDPE	900	x1	RT	2 hrs	8/14/2007	1 mil	Goodfellow	Bertan	LDPE Up to 1000 V 8-14-2007.txt	
X	LDPE	1000	x1	RT	2 hrs	8/14/2007	1 mil	Goodfellow	Bertan	LDPE Up to 1000 V 8-14-2007.txt	
Partial	LDPE	140	x1	Heating	12 hrs	4/25/2007	1 mil	Goodfellow	Bertan	140 V heating 1 mil LDPE 2 4-25- 2007.txt	

Use	Material	Voltage	Type	T. Regime	Total Duration	Run Date	Thick.	Source	PS	Data Filename	Notes
Partial	LDPE	140	x1	Heating	4 hrs	4/25/2007	1 mil	Goodfellow	Bertan	140 V heating 1 mil LDPE 3 4-25-2007.txt	
Partial	LDPE	140	x1	Heating	8 hrs	4/24/2007	1 mil	Goodfellow	Bertan	140 V heating 1 mil LDPE 4-24-2007.txt	
Partial	LDPE	600	x1	Cryo	1 min	4/24/2007	5 mil	Goodfellow	Bertan	600 V ten hours 5 mil LDPE 2 4-24-2007.txt	Didn't reach room temperature before data collection stopped
Partial	LDPE	600	x1	Cryo	10 hrs	4/24/2007	5 mil	Goodfellow	Bertan	600 V ten hours 5 mil LDPE 4-23-2007.txt	
	LDPE	620	x1	Cryo	<1 min	4/16/2007	1 mil	Goodfellow	Bertan	Warming 2nd half 1 mil LDPE 4-16-2007.txt	Aborted
	LDPE	620	x1	Cryo	2 hrs	4/16/2007	1 mil	Goodfellow	Bertan	Warming 620 V 1 mil LDPE 2 4-16-2007.txt	Thermocouple data not recorded
Partial	LDPE	620	x1	Cryo	10 hrs	4/16/2007	1 mil	Goodfellow	Bertan	Warming 620 V 1 mil LDPE 3 4-16-2007.txt	
X	LDPE	0	x1	Cryo	30 min	4/16/2007	1 mil	Goodfellow	Bertan	Warming 620 V 1 mil LDPE 4-16-2007.txt	Noise Test
	LDPE	620	x1	Cryo	10 hrs	4/16/2007	1 mil	Goodfellow	Bertan	Warming 620 V 1 mil LDPE 4-16-2007.txt	Aborted
	LDPE	620	x1	Cryo	<1 min	4/16/2007	1 mil	Goodfellow	Bertan	Warming 620 V 1 mil LDPE 4 4-16-2007.txt	Aborted

Use	Material	Voltage	Type	T. Regime	Total Duration	Run Date	Thick.	Source	PS	Data Filename	Notes
Partial	LDPE	620	x1	Cryo	10 hrs	4/16/2007	1 mil	Goodfellow	Bertan	Warming 620 V 1 mil LDPE yet again 4-16-2007.txt	
Partial	LDPE	140	x1	Cryo	11 hrs	4/15/2007	1 mil	Goodfellow	Bertan	140 V Warming 1 mil LDPE 4-15-2007.txt	
Partial	LDPE	140	x1	Cryo	4 min	4/13/2007	1 mil	Goodfellow	Bertan	10 C 140 V 1 mil LDPE 4-13-2007.txt	
	LDPE	200	x1	Cryo	59 min	4/13/2007	1 mil	Goodfellow	Bertan	10 C 200 V 1 mil LDPE 4-13-2007.txt	All negative currents
	LDPE	140	x1	Cryo	<1 min	4/13/2007	1 mil	Goodfellow	Bertan	140 ten hour 1 mil LDPE 4-13-2007.txt	Empty data file - nothing recorded
Partial	LDPE	140	x1	Cryo	10 hrs	4/13/2007	1 mil	Goodfellow	Bertan	140 V ten hours 1 mil LDPE 4-13-2007.txt	
Partial	LDPE	140	x1	Cryo	3 hrs	4/13/2007	1 mil	Goodfellow	Bertan	140 V Warming 1 mil LDPE 4-13-2007.txt	
	LDPE	200	x1	Cryo	4 min	4/13/2007	1 mil	Goodfellow	Bertan	200 V Ten Hours 1 mil LDPE 4-13-2007.txt	Out of range
	LDPE	140	x1	Cryo	2 min	4/13/2007	1 mil	Goodfellow	Bertan	Low T 140 V 1 mil LDP 4-13-2007.txt	No temperatures recorded
	LDPE	6300	x1	RT	<1 min	4/12/2007	5 mil	Goodfellow	HVT	6300 V HourHalf Hour 5 mil LDPE 4-12-2007.txt	Aborted
	LDPE	6300	x1	RT	1.5 hr	4/12/2007	5 mil	Goodfellow	HVT	6300 V Hour-Half Hour 5 mil LDPE 4-12-2007.txt	Significant arcing

Use	Material	Voltage	Type	T. Regime	Total Duration	Run Date	Thick.	Source	PS	Data Filename	Notes
	LDPE	6600	x1	RT	<1 min	4/12/2007	5 mil	Goodfellow	HVT	6600 V test 5 mil LDPE 4-12-2007.txt	Aborted
	LDPE	6900	x1	RT	<1 min	4/12/2007	5 mil	Goodfellow	HVT	6900 V test 5 mil LDPE 4-12-2007.txt	Aborted
	LDPE	6900	x2	RT	4 hrs	4/12/2007	5 mil	Goodfellow	HVT	Long runs 5 mil LDPE 4-12-2007.txt	Significant arcing
	LDPE	6600	x1	RT	2 hrs	4/12/2007	5 mil	Goodfellow	HVT	Long runs 5 mil LDPE 4-12-2007.txt	Significant arcing
Limited	LDPE	5000?	x1	RT	1.5 hr	4/11/2007	5 mil	Goodfellow	HVT	5000 V Hour-Half Hour 5 mil LDPE 4-11-2007.txt	Onset of arcing, May be used after care is taken to remove influence of HVT malfunction
Limited	LDPE	5300	x1	RT	1.5 hr	4/11/2007	5 mil	Goodfellow	HVT	5300 V Hour-Half Hour 5 mil LDPE 4-11-2007.txt	Onset of arcing, May be used after care is taken to remove influence of HVT malfunction
Limited	LDPE	5900	x1	RT	1.5 hr	4/11/2007	5 mil	Goodfellow	HVT	5900 V Hour-Half Hour 5 mil LDPE 4-11-2007.txt	Significant arcing
X	LDPE	5300	Char	RT	<10 min	4/11/2007	5 mil	Goodfellow	HVT	5300 V Initial Characterization 5 mil LDPE 4-11-2007.txt	
X	LDPE	5600	Char	RT	2 hrs	4/11/2007	5 mil	Goodfellow	HVT	5600 V Initial Characterization 5 mil LDPE 4-11-2007.txt	

Use	Material	Voltage	Type	T. Regime	Total Duration	Run Date	Thick.	Source	PS	Data Filename	Notes
X	LDPE	5900	Char	RT	<1 min	4/11/2007	5 mil	Goodfellow	HVT	5900 V Initial Characterization 5 mil LDPE 4-11-2007.txt	
Limited	LDPE	3800	x1	RT	1.5 hr	4/10/2007	5 mil	Goodfellow	HVT	3800 V Hour-Half Hour 5 mil LDPE 4-10-2007.txt	Onset of arcing, May be used after care is taken to remove influence of HVT malfunction
Limited	LDPE	4200	x1	RT	1.5 hr	4/10/2007	5 mil	Goodfellow	HVT	4200 V Hour-Half Hour 5 mil LDPE 4-10-2007.txt	Onset of arcing, May be used after care is taken to remove influence of HVT malfunction
Limited	LDPE	4600	x1	RT	1.5 hr	4/10/2007	5 mil	Goodfellow	HVT	4600 V Hour-Half Hour 5 mil LDPE 4-10-2007.txt	Onset of arcing, May be used after care is taken to remove influence of HVT malfunction
Limited	LDPE	5000?	x1	RT	6 hr	4/10/2007	5 mil	Goodfellow	HVT	5000 V with five hour tail 5 mil LDPE 4-10-2007.txt	Onset of arcing, May be used after care is taken to remove influence of HVT malfunction
X	LDPE	3800	Char	RT	<20 min	4/10/2007	5 mil	Goodfellow	HVT	3800 V Initial Characterization 5 mil LDPE 4-10-2007.txt	
X	LDPE	4200	Char	RT	3 hrs	4/10/2007	5 mil	Goodfellow	HVT	4200 V Final Characterization 5 mil LDPE 4-10-2007.txt	

Use	Material	Voltage	Type	T. Regime	Total Duration	Run Date	Thick.	Source	PS	Data Filename	Notes
X	LDPE	4200	Char	RT	3 hrs	4/10/2007	5 mil	Goodfellow	HVT	4200 V Initial Characterization 5 mil LDPE 4-10-2007.txt	
X	LDPE	4600	Char	RT	<1 hr	4/10/2007	5 mil	Goodfellow	HVT	4600 V Final Characterization 5 mil LDPE 4-10-2007.txt	
X	LDPE	4600	Char	RT	<1 hr	4/10/2007	5 mil	Goodfellow	HVT	4600 V Initial Characterization 5 mil LDPE 4-10-2007.txt	
X	LDPE	5000	Char	RT	<10 min	4/10/2007	5 mil	Goodfellow	HVT	5000 V Initial Characterization 5 mil LDPE 4-10-2007.txt	
	LDPE	2800	x1	RT	4 min	4/9/2007	5 mil	Goodfellow	HVT	2800 V Hour-Half Hour 5 mil LDPE 2 4-9-2007.txt	Out of range
Limited	LDPE	2800	x1	RT	1.5 hr	4/9/2007	5 mil	Goodfellow	HVT	2800 V Hour-Half Hour 5 mil LDPE 4-9-2007.txt	Onset of arcing, May be used after care is taken to remove influence of HVT malfunction
Limited	LDPE	1400	x1	RT	2 hrs	4/9/2007	5 mil	Goodfellow	HVT	Make up Set 5 mil LDPE 4-9-2007.txt	May be used after care is taken to remove influence of HVT malfunction
Limited	LDPE	1700	x1	RT	2 hrs	4/9/2007	5 mil	Goodfellow	HVT	Make up Set 5 mil LDPE 4-9-2007.txt	May be used after care is taken to remove influence of HVT malfunction

Use	Material	Voltage	Type	T. Regime	Total Duration	Run Date	Thick.	Source	PS	Data Filename	Notes
Limited	LDPE	2100	x1	RT	2 hrs	4/9/2007	5 mil	Goodfellow	HVT	Make up Set 5 mil LDPE 4-9-2007.txt	May be used after care is taken to remove influence of HVT malfunction
Limited	LDPE	2400	x1	RT	2 hrs	4/9/2007	5 mil	Goodfellow	HVT	Make up Set 5 mil LDPE 4-9-2007.txt	May be used after care is taken to remove influence of HVT malfunction
Limited	LDPE	3100	x1	RT	2 hrs	4/9/2007	5 mil	Goodfellow	HVT	Make up Set 5 mil LDPE 4-9-2007.txt	May be used after care is taken to remove influence of HVT malfunction
Limited	LDPE	3500	x1	RT	2 hrs	4/9/2007	5 mil	Goodfellow	HVT	Make up Set 5 mil LDPE 4-9-2007.txt	May be used after care is taken to remove influence of HVT malfunction
X	LDPE	2800	Char	RT	<10 min	4/9/2007	5 mil	Goodfellow	HVT	2800 V Initial Characterization 5 mil LDPE 4-9-2007.txt	
X	LDPE	2800	Char	RT	11 min	4/9/2007	5 mil	Goodfellow	HVT	2800 V Test Characterization 5 mil LDPE 4-9-2007.txt	
X	LDPE	3500	Char	RT	3 min	4/9/2007	5 mil	Goodfellow	HVT	3500 V Final Characterization 5 mil LDPE 4-9-2007.txt	
X	LDPE	1000	Char	RT	7 min	4/8/2007	5 mil	Goodfellow	Bertan	1000 V Final Characterization 5 mil LDPE 4-8-2007.txt	

Use	Material	Voltage	Type	T. Regime	Total Duration	Run Date	Thick.	Source	PS	Data Filename	Notes
X	LDPE	1400	Char	RT	10 min	4/8/2007	5 mil	Goodfellow	HVT	1400 V Final Characterization 5 mil LDPE 4-8-2007.txt	
X	LDPE	1400	Char	RT	13 min	4/8/2007	5 mil	Goodfellow	HVT	1400 V Initial Characterization 5 mil LDPE 4-8-2007.txt	
X	LDPE	1700	Char	RT	11 min	4/8/2007	5 mil	Goodfellow	HVT	1700 V Final Characterization 5 mil LDPE 4-8-2007.txt	
X	LDPE	1700	Char	RT	10 min	4/8/2007	5 mil	Goodfellow	HVT	1700 V Initial Characterization 5 mil LDPE 4-8-2007.txt	
X	LDPE	2100	Char	RT	6 min	4/8/2007	5 mil	Goodfellow	HVT	2100 V Final Characterization 5 mil LDPE 4-8-2007.txt	
X	LDPE	2100	Char	RT	7 min	4/8/2007	5 mil	Goodfellow	HVT	2100 V Initial Characterization 5 mil LDPE 4-8-2007.txt	
X	LDPE	2400	Char	RT	12 min	4/8/2007	5 mil	Goodfellow	HVT	2400 V Final Characterization 5 mil LDPE 4-8-2007.txt	

Use	Material	Voltage	Type	T. Regime	Total Duration	Run Date	Thick.	Source	PS	Data Filename	Notes
X	LDPE	2400	Char	RT	12 min	4/8/2007	5 mil	Goodfellow	HVT	2400 V Initial Characterization 5 mil LDPE 4-8-2007.txt	
Limited	LDPE	1400	x1	RT	1.5 hr	4/8/2007	5 mil	Goodfellow	HVT	1400 V Hour-Half Hour 5 mil LDPE 4-8-2007.txt	May be used after care is taken to remove influence of HVT malfunction
Limited	LDPE	1700	x1	RT	1.5 hr	4/8/2007	5 mil	Goodfellow	HVT	1700 V Hour-Half Hour 5 mil LDPE 4-8-2007.txt	May be used after care is taken to remove influence of HVT malfunction
Limited	LDPE	2100	x1	RT	1.5 hr	4/8/2007	5 mil	Goodfellow	HVT	2100 V Hour-Half Hour 5 mil LDPE 4-8-2007.txt	May be used after care is taken to remove influence of HVT malfunction
Limited	LDPE	2400	x1	RT	1.5 hr	4/8/2007	5 mil	Goodfellow	HVT	2400 V Hour-Half Hour 5 mil LDPE 4-8-2007.txt	Onset of arcing, May be used after care is taken to remove influence of HVT malfunction
X	LDPE	1000	Char	RT	7 min	4/8/2007	5 mil	Goodfellow	Bertan	1000 V Final Characterization 5 mil LDPE 4-8-2007.txt	
X	LDPE	1400	Char	RT	10 min	4/8/2007	5 mil	Goodfellow	HVT	1400 V Final Characterization 5 mil LDPE 4-8-2007.txt	
X	LDPE	1400	Char	RT	13 min	4/8/2007	5 mil	Goodfellow	HVT	1400 V Initial Characterization 5 mil LDPE 4-8-2007.txt	

Use	Material	Voltage	Type	T. Regime	Total Duration	Run Date	Thick.	Source	PS	Data Filename	Notes
X	LDPE	1700	Char	RT	11 min	4/8/2007	5 mil	Goodfellow	HVT	1700 V Final Characterization 5 mil LDPE 4-8-2007.txt	
X	LDPE	1700	Char	RT	10 min	4/8/2007	5 mil	Goodfellow	HVT	1700 V Initial Characterization 5 mil LDPE 4-8-2007.txt	
X	LDPE	2100	Char	RT	6 min	4/8/2007	5 mil	Goodfellow	HVT	2100 V Final Characterization 5 mil LDPE 4-8-2007.txt	
X	LDPE	2100	Char	RT	23 min	4/8/2007	5 mil	Goodfellow	HVT	2100 V Initial Characterization 5 mil LDPE 4-8-2007.txt	
X	LDPE	2400	Char	RT	12 min	4/8/2007	5 mil	Goodfellow	HVT	2400 V Final Characterization 5 mil LDPE 4-8-2007.txt	
X	LDPE	2400	Char	RT	12 min	4/8/2007	5 mil	Goodfellow	HVT	2400 V Initial Characterization 5 mil LDPE 4-8-2007.txt	
X	LDPE	150	Char	RT	6 min	4/7/2007	5 mil	Goodfellow	Bertan	150 V Final Characterization 5 mil LDPE 4-7-2007.txt	

Use	Material	Voltage	Type	T. Regime	Total Duration	Run Date	Thick.	Source	PS	Data Filename	Notes
X	LDPE	220	Char	RT	32 min	4/7/2007	?	Goodfellow	Bertan	220 V Initial Characterization 4-7-2007.txt	
X	LDPE	350	Char	RT	8 min	4/7/2007	5 mil	Goodfellow	Bertan	350 V Final Characterization 5 mil LDPE 4-7-2007.txt	
X	LDPE	350	Char	RT	8 min	4/7/2007	5 mil	Goodfellow	Bertan	350 V Initial Characterization 5 mil LDPE 4-7-2007.txt	
X	LDPE	700	Char	RT	6 min	4/7/2007	5 mil	Goodfellow	Bertan	700 V Final Characterization 5 mil LDPE 4-7-2007.txt	
X	LDPE	700	Char	RT	9 min	4/7/2007	5 mil	Goodfellow	Bertan	700 V Initial Characterization 5 mil LDPE 4-7-2007.txt	
X	LDPE	1000	Char	RT	9 min	4/7/2007	5 mil	Goodfellow	Bertan	1000 V Initial Characterization 5 mil LDPE 4-7-2007.txt	
X	LDPE	1000	Char	RT	35 min	4/7/2007	1 mil	Goodfellow	Bertan	1000 V Final Characterization 1 mil LDPE 4-7-2007.txt	

Use	Material	Voltage	Type	T. Regime	Total Duration	Run Date	Thick.	Source	PS	Data Filename	Notes
Limited	LDPE	1100	Char	RT	20 min	4/7/2007	1 mil	Goodfellow	HVT	1100 V Initial Characterization 1 mil LDPE 4-7-2007.txt	Sample broke down
	LDPE	1100	x1	RT	<1 min	4/7/2007	1 mil	Goodfellow	HVT	1100 V Hour-Half Hour 1 mil LDPE 4-7-2007.txt	Sample broke down
X	LDPE	150	x1	RT	1.5 hr	4/7/2007	5 mil	Goodfellow	Bertan	150 V Hour-Half Hour 5 mil LDPE 4-7-2007.txt	
X	LDPE	350	x1	RT	1.5 hr	4/7/2007	5 mil	Goodfellow	Bertan	350 V Hour-Half Hour 5 mil LDPE 4-7-2007.txt	
X	LDPE	700	x1	RT	1.5 hr	4/7/2007	5 mil	Goodfellow	Bertan	700 V Hour-Half Hour 5 mil LDPE 4-7-2007.txt	
X	LDPE	150	Char	RT	6 min	4/7/2007	5 mil	Goodfellow	Bertan	150 V Final Characterization 5 mil LDPE 4-7-2007.txt	
X	LDPE	350	Char	RT	8 min	4/7/2007	5 mil	Goodfellow	Bertan	350 V Final Characterization 5 mil LDPE 4-7-2007.txt	
X	LDPE	350	Char	RT	8 min	4/7/2007	5 mil	Goodfellow	Bertan	350 V Initial Characterization 5 mil LDPE 4-7-2007.txt	

Use	Material	Voltage	Type	T. Regime	Total Duration	Run Date	Thick.	Source	PS	Data Filename	Notes
X	LDPE	700	Char	RT	6 min	4/7/2007	5 mil	Goodfellow	Bertan	700 V Final Characterization 5 mil LDPE 4-7-2007.txt	
X	LDPE	700	Char	RT	9 min	4/7/2007	5 mil	Goodfellow	Bertan	700 V Initial Characterization 5 mil LDPE 4-7-2007.txt	
X	LDPE	1000	Char	RT	9 min	4/7/2007	5 mil	Goodfellow	Bertan	1000 V Initial Characterization 5 mil LDPE 4-7-2007.txt	
X	LDPE	690	Char	RT	26 min	4/6/2007	1 mil	Goodfellow	Bertan	690 V Final Characterization 1 mil LDPE 4-6-2007.txt	
X	LDPE	760	Char	RT	33 min	4/6/2007	1 mil	Goodfellow	Bertan	760 V Final Characterization 1 mil LDPE 4-6-2007.txt	
X	LDPE	760	Char	RT	23 min	4/6/2007	1 mil	Goodfellow	Bertan	760 V Initial Characterization 1 mil LDPE 4-6-2007.txt	
X	LDPE	830	Char	RT	47 min	4/6/2007	1 mil	Goodfellow	Bertan	830 V Final Characterization 1 mil LDPE 4-6-2007.txt	

Use	Material	Voltage	Type	T. Regime	Total Duration	Run Date	Thick.	Source	PS	Data Filename	Notes
X	LDPE	830	Char	RT	46 min	4/6/2007	1 mil	Goodfellow	Bertan	830 V Initial Characterization 1 mil LDPE 4-6-2007.txt	
X	LDPE	900	Char	RT	37 min	4/6/2007	1 mil	Goodfellow	Bertan	900 V Final Characterization 1 mil LDPE 4-6-2007.txt	
X	LDPE	900	Char	RT	39 min	4/6/2007	1 mil	Goodfellow	Bertan	900 V Initial Characterization 1 mil LDPE 4-6-2007.txt	
X	LDPE	1000	Char	RT	50 min	4/6/2007	1 mil	Goodfellow	Bertan	1000 V Initial Characterization 1 mil LDPE 4-6-2007.txt	
X	LDPE	760	x1	RT	1.5 hr	4/6/2007	1 mil	Goodfellow	Bertan	760 V Hour-Half Hour 1 mil LDPE 4-6-2007.txt	
X	LDPE	830	x1	RT	1.5 hr	4/6/2007	1 mil	Goodfellow	Bertan	830 V Hour-Half Hour 1 mil LDPE 4-6-2007.txt	
X	LDPE	900	x1	RT	1.5 hr	4/6/2007	1 mil	Goodfellow	Bertan	900 V Hour-Half Hour 1 mil LDPE 4-6-2007.txt	
X	LDPE	1000	x1	RT	1.5 hr	4/6/2007	1 mil	Goodfellow	Bertan	1000 V Hour-Half Hour 1 mil LDPE 4-6-2007.txt	

Use	Material	Voltage	Type	T. Regime	Total Duration	Run Date	Thick.	Source	PS	Data Filename	Notes
X	LDPE	480	Char	RT	38 min	4/5/2007	1 mil	Goodfellow	Bertan	480 V Final Characterization 1 mil LDPE 4-5-2007.txt	
X	LDPE	480	Char	RT	33 min	4/5/2007	1 mil	Goodfellow	Bertan	480 V Initial Characterization 1 mil LDPE 4-4-2007.txt	
X	LDPE	550	Char	RT	39 min	4/5/2007	1 mil	Goodfellow	Bertan	550 V Final Characterization 1 mil LDPE 4-5-2007.txt	
X	LDPE	550	Char	RT	34 min	4/5/2007	1 mil	Goodfellow	Bertan	550 V Initial Characterization 1 mil LDPE 4-5-2007.txt	
X	LDPE	620	Char	RT	48 min	4/5/2007	1 mil	Goodfellow	Bertan	620 V Final Characterization 1 mil LDPE 4-5-2007.txt	
X	LDPE	620	Char	RT	55 min	4/5/2007	1 mil	Goodfellow	Bertan	620 V Initial Characterization 1 mil LDPE 4-5-2007.txt	
	LDPE	690	Char	RT	1 min	4/5/2007	1 mil	Goodfellow	Bertan	690 V Final Characterization 1 mil LDPE 4-5-2007.txt	Out of range

Use	Material	Voltage	Type	T. Regime	Total Duration	Run Date	Thick.	Source	PS	Data Filename	Notes
X	LDPE	690	Char	RT	30 min	4/5/2007	1 mil	Goodfellow	Bertan	690 V Initial Characterization 1 mil LDPE 4-5-2007.txt	
X	LDPE	550	x1	RT	1.5 hr	4/5/2007	1 mil	Goodfellow	Bertan	550 V Hour-Half Hour 1 mil LDPE 4-5-2007.txt	
X	LDPE	620	x1	RT	1.5 hr	4/5/2007	1 mil	Goodfellow	Bertan	620 V Hour- Half Hour 1 mil LDPE 4-5-2007.txt	
X	LDPE	690	x1	RT	1.5 hr	4/5/2007	1 mil	Goodfellow	Bertan	690 V Hour-Half Hour 1 mil LDPE 4-5-2007.txt	
X	LDPE	200	Char	RT	25 min	4/4/2007	1 mil	Goodfellow	Bertan	200 V Final Characterization 1 mil LDPE 4-4-2007.txt	
X	LDPE	280	Char	RT	29 min	4/4/2007	1 mil	Goodfellow	Bertan	280 V Final Characterization 1 mil LDPE 4-4-2007.txt	
X	LDPE	280	Char	RT	28 min	4/4/2007	1 mil	Goodfellow	Bertan	280 V Initial Characterization 1 mil LDPE 4-4-2007.txt	
X	LDPE	340	Char	RT	32 min	4/4/2007	1 mil	Goodfellow	Bertan	340 V Final Characterization 1 mil LDPE 4-4-2007.txt	

Use	Material	Voltage	Type	T. Regime	Total Duration	Run Date	Thick.	Source	PS	Data Filename	Notes
X	LDPE	340	Char	RT	30 min	4/4/2007	1 mil	Goodfellow	Bertan	340 V Initial Characterization 1 mil LDPE 4-4-2007.txt	
X	LDPE	410	Char	RT	37 min	4/4/2007	1 mil	Goodfellow	Bertan	410 V Final Characterization 1 mil LDPE 4-4-2007.txt	
X	LDPE	410	Char	RT	24 min	4/4/2007	1 mil	Goodfellow	Bertan	410 V Initial Characterization 1 mil LDPE 4-4-2007.txt	
X	LDPE	280	x1	RT	1.5 hr	4/4/2007	1 mil	Goodfellow	Bertan	280 V Hour-Half Hour 1 mil LDPE 4-4-2007.txt	
X	LDPE	340	x1	RT	1.5 hr	4/4/2007	1 mil	Goodfellow	Bertan	340 V Hour-Half Hour 1 mil LDPE 4-4-2007.txt	
X	LDPE	410	x1	RT	1.5 hr	4/4/2007	1 mil	Goodfellow	Bertan	410 V Hour-Half Hour 1 mil LDPE 4-4-2007.txt	
X	LDPE	480	x1	RT	1.5 hr	4/4/2007	1 mil	Goodfellow	Bertan	480 V Hour-Half Hour 1 mil LDPE 4-4-2007.txt	
X	LDPE	30	Char	RT	31 min	4/3/2007	1 mil	Goodfellow	Bertan	30 V Final Characterization 1 mil LDPE 4-3-2007.txt	

Use	Material	Voltage	Type	T. Regime	Total Duration	Run Date	Thick.	Source	PS	Data Filename	Notes
X	LDPE	70	Char	RT	36 min	4/3/2007	1 mil	Goodfellow	Bertan	70 V 1 mil LDPE Initial Characterization 4-3-2007.txt	
X	LDPE	70	Char	RT	26 min	4/3/2007	1 mil	Goodfellow	Bertan	70 V Final Characterization 1 mil LDPE 4-3-2007.txt	
X	LDPE	140	Char	RT	30 min	4/3/2007	1 mil	Goodfellow	Bertan	140 V Final Characterization 1 mil LDPE 4-3-2007.txt	
X	LDPE	140	Char	RT	16 min	4/3/2007	1 mil	Goodfellow	Bertan	140 V Initial Characterization 1 mil LDPE 4-3-2007.txt	
X	LDPE	200	Char	RT	34 min	4/3/2007	1 mil	Goodfellow	Bertan	200 V Initial Characterization 1 mil LDPE 4-3-2007.txt	
X	LDPE	30	Char	RT	59 min	4/3/2007	1 mil	Goodfellow	Bertan	Low Voltage 1 mil LDPE Initial Characterization 4-3-2007.txt	
X	LDPE	30	x1	RT	1.5 hr	4/3/2007	1 mil	Goodfellow	Bertan	30 V Hour-Half Hour 1 mil LDPE 4-3-2007.txt	

Use	Material	Voltage	Type	T. Regime	Total Duration	Run Date	Thick.	Source	PS	Data Filename	Notes
X	LDPE	70	x1	RT	1.5 hr	4/3/2007	1 mil	Goodfellow	Bertan	70 V Hour-Half Hour 1 mil LDPE 4-3-2007.txt	
X	LDPE	140	x1	RT	1.5 hr	4/3/2007	1 mil	Goodfellow	Bertan	140 V Hour-Half Hour 1 mil LDPE 4-3-2007.txt	
X	LDPE	200	x1	RT	1.5 hr	4/3/2007	1 mil	Goodfellow	Bertan	200 V Hour-Half Hour 1 mil LDPE 4-3-2007.txt	
	LDPE	30	Char	RT	<1 min	4/2/2007	1 mil	Goodfellow	Bertan	Initial Characterization Low V LDPE 1 mil 4-2-2007.txt	DAQ Error
	LDPE	100	Char	RT	36 min	10/2/2006	5 mil	Goodfellow	Bertan	FC 100 V LDPE 5 mil 10-2-2006.txt	Testing and Calibration
	LDPE	300	Char	RT	<10 min	10/2/2006	5 mil	Goodfellow	Bertan	FC 300 V LDPE 5 mil 10-2-2006.txt	Testing and Calibration
	LDPE	500	Char	RT	46 min	10/2/2006	5 mil	Goodfellow	Bertan	FC 500 V LDPE 5 mil 10-2-2006.txt	Testing and Calibration
	LDPE	600	Char	RT	50 min	10/2/2006	5 mil	Goodfellow	Bertan	FC 600 V LDPE 5 mil 10-2-2006.txt	Testing and Calibration
	LDPE	1000	Char	RT	46 min	10/2/2006	5 mil	Goodfellow	Bertan	FC 1000 V LDPE 5 mil 10-2-2006.txt	Testing and Calibration
	LDPE	100	Char	RT	<10 min	10/2/2006	5 mil	Goodfellow	Bertan	FC 100 V LDPE 5 mil 10-2-2006.txt	Testing and Calibration
	LDPE	300	Char	RT	<10 min	10/2/2006	5 mil	Goodfellow	Bertan	FC 300 V LDPE 5 mil 10-2-2006.txt	Testing and Calibration
	LDPE	500	Char	RT	<10 min	10/2/2006	5 mil	Goodfellow	Bertan	FC 500 V LDPE 5 mil 10-2-2006.txt	Testing and Calibration

Use	Material	Voltage	Type	T. Regime	Total Duration	Run Date	Thick.	Source	PS	Data Filename	Notes
	LDPE	600	Char	RT	<10 min	10/2/2006	5 mil	Goodfellow	Bertan	FC 600 V LDPE 5 mil 10-2-2006.txt	Testing and Calibration
	LDPE	1000	Char	RT	<10 min	10/2/2006	5 mil	Goodfellow	Bertan	FC 1000 V LDPE 5 mil 10-2-2006.txt	Testing and Calibration
X	LDPE	1000	x1	RT	9 hrs	10/1/2006	5 mil	Goodfellow	Bertan	Long 1000 V LDPE 5 mil 10-1-2006.txt	
Limited	LDPE	1000	x1	RT	9 hrs	10/1/2006	5 mil	Goodfellow	Bertan	Long 1000 V LDPE 5 mil 10-1-2006.txt	Range discrepancy
X	LDPE	500	x8	RT	16 hrs	9/30/2006	5 mil	Goodfellow	Bertan	Comprehensive Low V LDPE 5 mil 9-30-2006.txt	
X	LDPE	100	x2	RT	4 hrs	9/30/2006	5 mil	Goodfellow	Bertan	Comprehensive Low V LDPE 5 mil 9-30-2006.txt	
X	LDPE	300	x2	RT	4 hrs	9/30/2006	5 mil	Goodfellow	Bertan	Comprehensive Low V LDPE 5 mil 9-30-2006.txt	
X	LDPE	600	x2	RT	4 hrs	9/30/2006	5 mil	Goodfellow	Bertan	Comprehensive Low V LDPE 5 mil 9-30-2006.txt	
X	LDPE	1000	x2	RT	4 hrs	9/30/2006	5 mil	Goodfellow	Bertan	Comprehensive Low V LDPE 5 mil 9-30-2006.txt	
	LDPE	100	Char	RT	26 min	9/30/2006	5 mil	Goodfellow	Bertan	IC 100 V LDPE 5 mil 9-30-2006.txt	Testing and Calibration
	LDPE	300	Char	RT	<10 min	9/30/2006	5 mil	Goodfellow	Bertan	IC 300 V LDPE 5 mil 9-30-2006.txt	Testing and Calibration
	LDPE	500	Char	RT	32 min	9/30/2006	5 mil	Goodfellow	Bertan	IC 500 V LDPE 5 mil 9-30-2006.txt	Testing and Calibration

Use	Material	Voltage	Type	T. Regime	Total Duration	Run Date	Thick.	Source	PS	Data Filename	Notes
	LDPE	600	Char	RT	32 min	9/30/2006	5 mil	Goodfellow	Bertan	IC 600 V LDPE 5 mil 9-30-2006.txt	Testing and Calibration
	LDPE	1000	Char	RT	40 min	9/30/2006	5 mil	Goodfellow	Bertan	IC 1000 V LDPE 5 mil 9-30-2006.txt	Testing and Calibration
	LDPE	100	Char	RT	<10 min	9/30/2006	5 mil	Goodfellow	Bertan	IC 100 V LDPE 5 mil 9-30-2006.txt	Testing and Calibration
	LDPE	300	Char	RT	<10 min	9/30/2006	5 mil	Goodfellow	Bertan	IC 300 V LDPE 5 mil 9-30-2006.txt	Testing and Calibration
	LDPE	500	Char	RT	<10 min	9/30/2006	5 mil	Goodfellow	Bertan	IC 500 V LDPE 5 mil 9-30-2006.txt	Testing and Calibration
	LDPE	600	Char	RT	<10 min	9/30/2006	5 mil	Goodfellow	Bertan	IC 600 V LDPE 5 mil 9-30-2006.txt	Testing and Calibration
	LDPE	100	Char	RT	<10 min	9/30/2006	5 mil	Goodfellow	Bertan	IC 1000 V LDPE 5 mil 9-30-2006.txt	Testing and Calibration
	LDPE	500	x1	RT	1 hr	9/9/2006	5 mil	Goodfellow	Bertan	Final 500 V 9.txt	Anomalous charging
	LDPE	500	x1	RT	1 hr	9/9/2006	5 mil	Goodfellow	Bertan	Final 500 V 10.txt	Anomalous charging
	LDPE	500	x1	RT	1 hr	9/9/2006	5 mil	Goodfellow	Bertan	Final 500 V 11.txt	Anomalous charging
	LDPE	0	x1	RT	1 hr	9/9/2006	5 mil	Goodfellow	Bertan	Final 500 V Rec 1.txt	Recovery time
	LDPE	0	x1	RT	1 hr	9/9/2006	5 mil	Goodfellow	Bertan	Final 500 V Rec 2.txt	Recovery time
	LDPE	0	x1	RT	1 hr	9/9/2006	5 mil	Goodfellow	Bertan	Final 500 V Rec 3.txt	Recovery time
	LDPE	0	x1	RT	1 hr	9/9/2006	5 mil	Goodfellow	Bertan	Final 500 V Rec 4.txt	Recovery time
	LDPE	0	x1	RT	1 hr	9/9/2006	5 mil	Goodfellow	Bertan	Final 500 V Rec 5.txt	Recovery time
	LDPE	0	x1	RT	1 hr	9/9/2006	5 mil	Goodfellow	Bertan	Final 500 V Rec 6.txt	Recovery time

Use	Material	Voltage	Type	T. Regime	Total Duration	Run Date	Thick.	Source	PS	Data Filename	Notes
	LDPE	0	x1	RT	1 hr	9/9/2006	5 mil	Goodfellow	Bertan	Final 500 V Rec 7.txt	Recovery time
	LDPE	0	x1	RT	1 hr	9/9/2006	5 mil	Goodfellow	Bertan	Final 500 V Rec 8.txt	Recovery time
	LDPE	0	x1	RT	1 hr	9/9/2006	5 mil	Goodfellow	Bertan	Final 500 V Rec 9.txt	Recovery time
	LDPE	0	x1	RT	1 hr	9/9/2006	5 mil	Goodfellow	Bertan	Final 500 V Rec 10.txt	Recovery time
	LDPE	0	x1	RT	1 hr	9/9/2006	5 mil	Goodfellow	Bertan	Final 500 V Rec 11.txt	Recovery time
	LDPE	500	x4	RT	8 hrs	9/8/2006	5 mil	Goodfellow	Bertan	Final Redundancy 5 mil LDPE 9-8-2006.txt	Unknown scaling factor
	LDPE	500	x7	RT	14 hrs	9/8/2006	5 mil	Goodfellow	Bertan	Redundancy 7 5 mil LDPE 9-8-2006.txt	Unknown scaling factor
	LDPE	500	x1	RT	1 hr	9/8/2006	5 mil	Goodfellow	Bertan	Final 500 V 1.txt	Anomalous charging
	LDPE	500	x1	RT	1 hr	9/8/2006	5 mil	Goodfellow	Bertan	Final 500 V 2.txt	Anomalous charging
	LDPE	500	x1	RT	1 hr	9/8/2006	5 mil	Goodfellow	Bertan	Final 500 V 3.txt	Anomalous charging
	LDPE	500	x1	RT	<1 hr	9/8/2006	5 mil	Goodfellow	Bertan	Final 500 V 4.txt	Aborted
	LDPE	500	x1	RT	1 hr	9/8/2006	5 mil	Goodfellow	Bertan	Final 500 V 5.txt	Anomalous charging
	LDPE	500	x1	RT	1 hr	9/8/2006	5 mil	Goodfellow	Bertan	Final 500 V 6.txt	Anomalous charging
	LDPE	500	x1	RT	1 hr	9/8/2006	5 mil	Goodfellow	Bertan	Final 500 V 7.txt	Anomalous charging
	LDPE	500	x1	RT	1 hr	9/8/2006	5 mil	Goodfellow	Bertan	Final 500 V 8.txt	Anomalous charging
	LDPE	1000	x1	RT	2 hr	9/7/2006	5 mil	Goodfellow	Bertan	1000 V run 5 mil LDPE 9-7-2006.txt	Anomalous charging
	LDPE	1000	x1	RT	<1 min	9/7/2006	5 mil	Goodfellow	Bertan	1000 V run 5 mil LDPE 9-7-2006.txt	Disconnected cable

Use	Material	Voltage	Type	T. Regime	Total Duration	Run Date	Thick.	Source	PS	Data Filename	Notes
	LDPE	100	x1	RT	1 hr	9/7/2006	5 mil	Goodfellow	Bertan	100 V 1 Hour 5 mil LDPE 2.txt	Anomalous charging
	LDPE	0	x1	RT	1 hr	9/7/2006	5 mil	Goodfellow	Bertan	100 V 1 Hour Recovery 5 mil LDPE 2.txt	Anomalous charging
	LDPE	300	x1	RT	1 hr	9/7/2006	5 mil	Goodfellow	Bertan	300 V 1 Hour 5 mil LDPE 2.txt	Anomalous charging
	LDPE	300	x1	RT	1 hr	9/7/2006	5 mil	Goodfellow	Bertan	300 V 1 Hour Recovery 5 mil LDPE 2.txt	Aborted
	LDPE	600	x1	RT	1 hr	9/7/2006	5 mil	Goodfellow	Bertan	600 V 1 Hour 5 mil LDPE.txt	Testing and Calibration
	LDPE	0	x1	RT	1 hr	9/7/2006	5 mil	Goodfellow	Bertan	600 V 1 Hour Recovery 5 mil LDPE.txt	Testing and Calibration
	LDPE	1000	x1	RT	1 hr	9/7/2006	5 mil	Goodfellow	Bertan	1000 V 1 Hour 5 mil LDPE.txt	Out of range
	LDPE	0	x1	RT	1 hr	9/7/2006	5 mil	Goodfellow	Bertan	1000 V 1 Hour Recovery 5 mil LDPE.txt	Recovery time
	LDPE	0	x1	RT	1 hr	9/7/2006	5 mil	Goodfellow	Bertan	1000 V Constant Pressure Rec.txt	Testing and Calibration
	LDPE	1000	x1	RT	1 hr	9/7/2006	5 mil	Goodfellow	Bertan	1000 V Constant Pressure.txt	Testing and Calibration
	LDPE	0	x1	RT	<1 min	9/7/2006	5 mil	Goodfellow	Bertan	1000 V Rising Pressure Rec.txt	Aborted
	LDPE	1000	x1	RT	1 hr	9/7/2006	5 mil	Goodfellow	Bertan	1000 V Rising Pressure.txt	Testing and Calibration

Use	Material	Voltage	Type	T. Regime	Total Duration	Run Date	Thick.	Source	PS	Data Filename	Notes
	LDPE	1000	x1	RT	1 hr	9/7/2006	5 mil	Goodfellow	Bertan	1000 V run 5 mil LDPE 2.txt	Testing and Calibration
	LDPE	1000	x1	RT	1 hr	9/7/2006	5 mil	Goodfellow	Bertan	1000 V run 5 mil LDPE 9-7-2006.txt	Testing and Calibration
	LDPE	1000	x1	RT	1 hr	9/7/2006	5 mil	Goodfellow	Bertan	1000 V Run Const P 5 Mil LDPE.txt	Testing and Calibration
	LDPE	5	x1	RT	1 hr	8/31/2006	5 mil	Goodfellow	Bertan	Very Low Ramp Up 5 mil~ LDPE 8-31-2006.txt	DAQ Error
	LDPE	10	x1	RT	1 hr	8/31/2006	5 mil	Goodfellow	Bertan	Very Low Ramp Up 5 mil~ LDPE 8-31-2006.txt	DAQ Error
	LDPE	5	x1	RT	10 min	8/30/2006	5 mil	Goodfellow	Bertan	Very Low Ramp Up 5 mil~ LDPE 8-30-2006.txt	Cable disconnected
	LDPE	100	x1	RT	2 hr	8/29/2006	5 mil	Goodfellow	Bertan	5 mil~ LDPE Low Ramp Up 8-29-2006.txt	Excessive noise
	LDPE	300	x1	RT	2 hr	8/29/2006	5 mil	Goodfellow	Bertan	5 mil~ LDPE Low Ramp Up 8-29-2006.txt	Excessive noise
	LDPE	600	x1	RT	2 hr	8/29/2006	5 mil	Goodfellow	Bertan	5 mil~ LDPE Low Ramp Up 8-29-2006.txt	Excessive noise
	LDPE	1000	x1	RT	2 hr	8/29/2006	5 mil	Goodfellow	Bertan	5 mil~ LDPE Low Ramp Up 8-29-2006.txt	Excessive noise
	LDPE	100	x1	RT	1 hr	8/29/2006	5 mil	Goodfellow	Bertan	100 V 1 Hour 5 mil LDPE.txt	Anomalous charging

Use	Material	Voltage	Type	T. Regime	Total Duration	Run Date	Thick.	Source	PS	Data Filename	Notes
	LDPE	0	x1	RT	1 hr	8/29/2006	5 mil	Goodfellow	Bertan	100 V 1 Hour Recovery 5 mil LDPE.txt	Anomalous charging
	LDPE	300	x1	RT	1 hr	8/29/2006	5 mil	Goodfellow	Bertan	300 V 1 Hour 5 mil LDPE.txt	Anomalous charging
	LDPE	100	Char	RT	<10 min	8/28/2006	5 mil	Goodfellow	Bertan	100 V Characterization 1.txt	Testing and Calibration
	LDPE	100	Char	RT	<10 min	8/28/2006	5 mil	Goodfellow	Bertan	100 V Characterization 2.txt	Testing and Calibration
	LDPE	100	Char	RT	<10 min	8/28/2006	5 mil	Goodfellow	Bertan	100 V Characterization 3.txt	Testing and Calibration
	LDPE	100	Char	RT	<10 min	8/28/2006	5 mil	Goodfellow	Bertan	100 V Characterization 4.txt	Testing and Calibration
	LDPE	300	Char	RT	<10 min	8/28/2006	5 mil	Goodfellow	Bertan	300 V Characterization 1.txt	Testing and Calibration
	LDPE	300	Char	RT	<10 min	8/28/2006	5 mil	Goodfellow	Bertan	300 V Characterization 2.txt	Testing and Calibration
	LDPE	300	Char	RT	<10 min	8/28/2006	5 mil	Goodfellow	Bertan	300 V Characterization 3.txt	Testing and Calibration
	LDPE	300	Char	RT	<10 min	8/28/2006	5 mil	Goodfellow	Bertan	300 V Characterization 4.txt	Testing and Calibration

Use	Material	Voltage	Type	T. Regime	Total Duration	Run Date	Thick.	Source	PS	Data Filename	Notes
	LDPE	300	Char	RT	<10 min	8/28/2006	5 mil	Goodfellow	Bertan	300 V Characterization 5.txt	Testing and Calibration
	LDPE	600	Char	RT	<10 min	8/28/2006	5 mil	Goodfellow	Bertan	600 V Characterization 1.txt	Testing and Calibration
	LDPE	600	Char	RT	<10 min	8/28/2006	5 mil	Goodfellow	Bertan	600 V Characterization 2.txt	Testing and Calibration
	LDPE	600	Char	RT	<10 min	8/28/2006	5 mil	Goodfellow	Bertan	600 V Characterization 3.txt	Testing and Calibration
	LDPE	600	Char	RT	<10 min	8/28/2006	5 mil	Goodfellow	Bertan	600 V Characterization 4.txt	Testing and Calibration
	LDPE	1000	Char	RT	<10 min	8/28/2006	5 mil	Goodfellow	Bertan	1000 V Characterization 1.txt	Testing and Calibration
	LDPE	1000	Char	RT	<10 min	8/28/2006	5 mil	Goodfellow	Bertan	1000 V Characterization 2.txt	Testing and Calibration
	LDPE	1000	Char	RT	<10 min	8/28/2006	5 mil	Goodfellow	Bertan	1000 V Characterization 3.txt	Testing and Calibration
	LDPE	1000	Char	RT	<10 min	8/28/2006	5 mil	Goodfellow	Bertan	1000 V Characterization 4.txt	Testing and Calibration

Use	Material	Voltage	Type	T. Regime	Total Duration	Run Date	Thick.	Source	PS	Data Filename	Notes
	LDPE	100	Char	RT	23 min	8/28/2006	5 mil	Goodfellow	Bertan	100 V Characterization 8-28-2006.txt	Testing and Calibration
	LDPE	300	Char	RT	66 min	8/28/2006	5 mil	Goodfellow	Bertan	300 V Characterization 8-28-2006.txt	Testing and Calibration
	LDPE	600	Char	RT	<1 min	8/28/2006	5 mil	Goodfellow	Bertan	600 V Characterization 8-28-2006.txt	Aborted
	LDPE	1000	Char	RT	34 min	8/28/2006	5 mil	Goodfellow	Bertan	1000 V Characterization 8-28-2006.txt	Testing and Calibration
	LDPE	500	x12	RT	24 hrs	8/22/2006	5 mil	Goodfellow	Bertan	Redundancy Thin LDPE 8-22-2006.txt	Out of range

CURRICULUM VITAE

Jerilyn Brunson
(January 2010)

EDUCATION:

Bachelor of Science
Physics
May 2003

Doctor of Philosophy
Physics
May 2010

SCHOLARSHIPS, FELLOWSHIPS, AND AWARDS:

Presidential Scholarship	Undergraduate
Seely-Hinckley Scholarship	2003 – 2004
Rocky Mountain Space Grant Consortium Fellowship	2004 – 2008
ASUSU Member of the Year	2007 – 2008

TEACHING EXPERIENCE:

Intermediate Laboratory Teaching Assistant	2003 – 2004
Dr. J.R. Dennison	
Dr. Mike Taylor	

RESEARCH EXPERIENCE:

Research Assistant	2004 - 2009
Dr. J.R. Dennison	

PUBLICATIONS:

J.R. Dennison, A. Sim, J. Brunson, J. Gillespie, S. Hart, J. Dekany, C. Sim, and D. Arnfield, "Engineering tool for temperature, electric field, and does rate dependence of low conductivity spacecraft materials," *47th AIAA Aerospace Sciences Meeting*, (Orlando, Fl., January 5-8, 2009).

J.R. i and J. Brunson, "Temperature and electric field dependence of conduction in low density polyethylene," *IEEE Trans. Plasma Sci.*, 36, 2246-2252 (2008).

J.R. Dennsion, J. Brunson, P. Swaminathan, N.W. Green, and A.R. Frederickson, "Methods for High Resistivity Measurements Related to Spacecraft Charging," *IEEE Trans. on Plasma Science*, 34, 2006, (2191 –2203)

J. Brunson, and J.R. Dennison, "E-Field Dependent Conduction in Low-Density Polyethylene," *Proceedings of the 12th Annual Rocky Mountain Space Grant Consortium Fellowship Symposium*, Salt Lake City, Utah, May 8, 2006.

J.R. Dennison, A. R. Frederickson, N.W. Green, P. Swaminathan and J. Brunson, "*Test Protocol for Charge Storage Methods*," NASA Space Environments and Effects Program, Contract No. NAS8-02031, "Measurement of Charge Storage Decay Time and Resistivity of Spacecraft Insulators," April 1, 2002 to January 31, 2005.

J.R. Dennison, P. Swaminathan, R. Jost, J. Brunson, N.W. Green and A. R. Frederickson, "Proposed Modifications To Engineering Design Guidelines Related To Resistivity Measurements And Spacecraft Charging," *Proceedings of the 9th Spacecraft Charging Technology Conference*, Epochal Tsukuba, Tsukuba, Japan, April 4-8, 2005.

J. Brunson and J.R. Dennison, "Measuring Charge Storage Decay Time and Resistivity of Spacecraft Insulators," *Proceedings of the 11th Annual Rocky Mountain Space Grant Consortium Fellowship Symposium*, Salt Lake City, Utah, May 9, 2005.

P. Swaminathan, A.R. Frederickson, J.R. Dennison, A. Sim, J. Brunson and E. Crapo, "Comparison of Classical and Charge Storage Methods for Determining Conductivity of Thin Film Insulators," *Proceedings of the 8th Spacecraft Charging Technology Conference*, NASA Marshall Space Flight Center, Huntsville, Alabama, October 2003.

CONFERENCE PRESENTATIONS:

"Dependence of Resistivity in Low-Density Polyethylene on Space Environment Parameters". 2007, Oral presentation at the 10th Spacecraft Charging Technology Conference, Biarritz, France.

"Measuring Charge Storage Decay Time and Resistivity of Spacecraft Insulators". 2005, Oral presentation at 11th Annual Rocky Mountain Space Grant Consortium Fellowship Symposium, Salt Lake City, Utah.

"Measuring Resistivity of Extreme Insulators". 2005, Oral presentation at APS Four Corners Section Meeting, Boulder, Colorado.

"E-Field Dependent Conduction in Low-Density Polyethylene". 2006, Oral presentation at 12th Annual Rocky Mountain Space Grant Consortium Fellowship Symposium, Salt Lake City, Utah.

"E-Field Conditioning and Charging Memory in Low-Density Polyethylene". 2006, Oral presentation at APS Four Corners Section Meeting, Logan, Utah.

PROFESSIONAL AFFILIATIONS:

Member of the American Physical Society (APS)
Member of the APS: Division of Polymer Physics